DUCTILE CEMENT-BASED COMPOSITES WITH WOOD FIBRES
Material design and experimental approach

Proefschrift

ter verkrijging van de graad van doctor
aan de Technische Universiteit Delft,
op gezag van de Rector Magnificus prof. ir. K.C.A.M. Luyben,
voorzitter van het College voor Promoties,
in het openbaar te verdedigen
op dinsdag 20 december 2011 om 15.00 uur
door

Mercedes Guadalupe SIERRA BELTRÁN

Maestra en Ingeniería
Universidad Nacional Autónoma de México, Mexico
geboren te Mexico Stad, Mexico.

Dit proefschrift is goedgekeurd door de promotor(en):

Prof dr. ir. K. van Breugel

Copromotor   Dr.ir. E. Schlangen

Samenstelling promotiecommissie:

Rector Magnificus,   voorzitter
Prof dr. ir. K. van Breugel,   Technische Universiteit Delft, promotor
Dr. ir. E. Schlangen,   Technische Universiteit Delft, copromotor
Prof. dr. ir. G.P.A.G. van Zijl, Universiteit Stellenbosch, Zuid Afrika
Prof. dr. ir. L. Taerwe,   Universiteit Gent, Belgïe
Prof. ir. A. Beukers,   Technische Universiteit Delft
D. Sc. R.D. Toledo Filho,   Universidade Federal do Rio de Janeiro, Brazilïe
Dr. G. van der Wegen,   SGS Intron
Prof. dr. ir. E.M. Haas,   Technische Universiteit Delft, reservelid

Summary

The use of natural fibres is the oldest form of reinforcing a building material. During the 20th century a wide variety of fibre reinforced cement-based materials (FRC) has been developed for applications that require specific material properties. Different types of man-made materials, such as steel, glass and polyvinyl alcohol are currently used as reinforcement, as well as some natural fibres. Compared to synthetic fibres, natural fibres are more easily available worldwide and they are friendlier to the environment since less energy is needed to produce them. They are also a renewable resource. However, the properties of natural fibres are not as constant as those of synthetic fibres and natural fibres have a lower tensile strength.

Some studies using natural fibres in cement-based materials have shown several benefits: reduction of plastic shrinkage, improvement of the bending behaviour and tensile-hardening with multiple-cracking behaviour in pre-cast, thin elements. However, the use of natural fibres in cement-based materials has been limited to those pre-cast elements [Swamy 1988, Savastano 2000, Silva 2009b], while synthetic fibres are used for both pre-cast and cast-in-place applications. In order to achieve a cast-in-place cement-based material reinforced with natural fibres, this thesis proposes a new approach using discontinuous randomly distributed wood fibres [Sierra and Schlangen 2008].

From a variety of available natural fibres, wood was chosen. Within wood, softwood fibres were selected over hardwood fibres for several reasons. Most importantly, softwood single fibres are bigger and more uniformly distributed through the wood. Additionally, hardwoods are more susceptible to attack of alkalis and cement setting is more inhibited. Fibres were obtained from three different softwood species: larch, spruce and pine. Even tough larch fibres showed promising results regarding the fibre tensile strength and the fibre-matrix interface properties, due to production constraints they no longer considered as possible reinforcement for this research. Further studies continued with pine and spruce fibres.

Cement matrices using partial cement replacement with other binders were studied to achieve a low environmental-impact matrix as well as a matrix with a tensile strength compatible with the chosen wood fibre's strength. The binders used in combination with cement are three residual products from industry: blast furnace slag, fly ash and silica fume. Additionally, limestone powder and river sand with improved particle size distribution were used as fillers to create a denser matrix. For grain sizes below 180 μm the mix design was governed by the desired paste chemical reaction and not by the particle size distribution.

The fibre-matrix interface properties vary according to the fibre type and cement matrix composition. The effects of curing conditions and fibre geometry were evaluated. The natural curving from the fibres increased the mechanical bond. However, excessive curving will lead to fibre rupture when the fibre is pulled out. By treating the fibres the volumetric changes due to humidity were controlled. This leads to improved pullout behaviour for both spruce and pine fibres. Even tough spruce fibres exhibited high pullout stress in combination with cement

matrices with blast furnace slag and limestone powder, due to production constraints, these fibres were not considered for further studies in this research project.

A comparison was made between the slip behaviour during pullout tests of the wood fibres and synthetic fibres using an analytical model proven for synthetic fibres. This model, based on gradual debonding of the fibre followed by fibre slide, is not applicable for wood fibres. A different approach was taken by using a numerical model that assumes volume loss due to internal damage of the wood fibre during pullout. This model fits the laboratory test results.

Preliminary experimental tests results of composites with a high strength cement matrix and a low fibre content percentage (2% volume) were used in a micromechanic-based model, together with information from the fibres and the cement matrix. The model showed the need to lower the cement matrix strength and increase the fibre volume in order to develop multiple cracking prior to failure under bending stress. The fibre content was then increased to 5%.

Proper viscosity of the fresh mix allows the fibres to evenly distribute in 2D or 3D arrangements, depending on the geometry of the samples casted. Fibres do not float even though they are lighter than any other composite ingredient.

A lightweight cement-based composite reinforced with pine fibres was designed to exhibit deflection-hardening behaviour. The material can be pre-cast or cast-in-place. The environmental impact of the composite would be lower compared to standard cement-based materials by partially replacing the cement content with fly ash and silica fume (both industrial by-products) and by employing natural fibres instead of synthetic fibres. This material developed multiple cracking prior to failure under bending stress. The designed material can be considered for applications such as low-budget housing in countries subject to seismic risk, where ductility and low weight are desirable characteristics of the building material.

Samenvatting

Het gebruik van natuurlijke vezels is de oudste vorm van wapening van bouwmaterialen. Gedurende de 20^e eeuw is een grote variatie aan vezelversterkte materialen op cementbasis ontwikkeld voor toepassingen die specifieke materiaaleigenschappen vereisen. Verschillende types kunstmatige materialen zoals staal, glas en polyvinyl alcohol worden tegenwoordig gebruikt als wapening, net als sommige natuurlijke vezels. Vergeleken met synthetische vezels zijn natuurlijke vezels wereldwijd makkelijker beschikbaar en milieuvriendelijker, aangezien minder energie nodig is om ze te produceren. Bovendien zijn ze een hernieuwbare hulpbron. Echter, de eigenschappen van natuurlijke vezels zijn niet zo constant als die van synthetische vezels en natuurlijke vezels hebben een lagere treksterkte.

Sommige studies waarin natuurlijke vezels worden gebruikt in een materiaal op cementbasis laten diverse voordelen zien: reductie van plastische krimp en verbetering van zowel het gedrag onder buiging als de trekversteviging met meervoudige scheuren in dunne prefab elementen. Echter, het gebruik van natuurlijke vezels in materialen op cementbasis is beperkt to prefab elementen [Swamy 1988, Savastano 2000, Silva 2009b] terwijl synthetische vezels worden gebruikt voor zowel prefab als in het werk gestorte toepassingen. Om een in het werk gestort materiaal op cementbasis met natuurlijke vezels te bereiken wordt in deze dissertatie een nieuwe benadering voorgesteld voor het gebruik van discontinue willekeurig verdeelde houtvezels [Sierra en Schlangen 2008].

Uit een variatie van beschikbare natuurlijke vezels is hout gekozen. Binnen hout zijn zachthoutvezels gekozen boven hardhoutvezels om een aantal redenen. Als belangrijkste: zachthoutvezels zijn groter en meer uniform verdeeld in het hout. Bovendien is hardhout gevoeliger voor alkaliën en belemmert het de cementreactie meer. Vezels zijn verkregen uit drie verschillende soorten zachthout: larix, spar en den. Hoewel larix vezels veelbelovende resultaten gaf met betrekking tot zowel de treksterkte van de vezels als de vezel-matrix interface zijn ze in deze studie verder buiten beschouwing gelaten als mogelijke wapening in verband met de productie beperkingen van de vezels. De verdere studie is gedaan met dennen- en sparvezels.

Cement matrices waarin het cement gedeeltelijk is vervangen door andere bindmaterialen zijn bestudeerd om zo een matrix te krijgen met zowel een lage milieubelasting als een matrix met een treksterkte die past bij de sterkte van de gekozen houtvezels. De bindmaterialen die zijn gebruikt in combinatie met cement zijn drie restproducten uit de industrie: hoogovenslak, vliegas en microsilica. Aanvullend zijn kalksteenpoeder en rivierzand met verbeterde korrelverdeling gebruikt als vulmaterialen om een matrix met groter dichtheid te krijgen. Voor korrelgroottes onder 180 μm werd het mixontwerp bepaald door de gewenste chemische reactie in de cementpasta en niet door de korrelverdeling.

De eigenschappen van de vezel-matrix interface variëren met het type vezel en de samenstelling van de cement matrix. Het effect van uithardingscondities en de vezelgeometrie

zijn onderzocht. De natuurlijke kromming van de vezels verhoogt de mechanische binding. Echter, een sterke kromming leidt tot breuk van de vezel tijdens de vezeltrektest. Door de vezels te behandelen zijn de volumeveranderingen ten gevolge van vochtigheid te controleren. Dit leidt tot een verbeterd trektestgedrag voor zowel dennen- als sparvezels. Hoewel sparvezels een hogere treksterkte vertonen in combinatie met cementmatrices met hoogovenslak en kalksteenpoeder, zijn deze vezels door hun productiebeperkingen niet verder beschouwd in dit onderzoeksproject.

Er is een vergelijking gemaakt tussen het slipgedrag van houtvezels en synthetische vezels tijdens de trekproeven middels een analytisch model voor synthetische vezels. Dit model, dat is gebaseerd op een geleidelijk loslaten van de vezel totdat de vezel begint te slippen, is niet toepasbaar voor houtvezels. Een andere aanpak is daarom gekozen met een numeriek model dat uitgaat van volumeverlies door interne beschadiging van de vezel tijdens de trekproef. Dit model geeft resultaten die passen bij de laboratoriumtestresultaten.

Voorlopige experimentele resultaten voor composietmaterialen met een hoge-sterkte cementmatrix en een laag vezelgehalte (2% volume) zijn gebruikt in een op micomechanica gebaseerd model, tesamen met informatie over de vezels en de cementmatrix. Het model toont de noodzaak aan om de sterkte van de cementmatrix te verlagen en het vezelvolume te verhogen om meervoudigepatronen te ontwikkelen voorafgaand aan bezwijken onder buiging. Het vezelvolume is daarom verhoogd tot 5%.

De juiste viscositeit van de verse cementmix staat de vezels toe zich evenredig 2D of 3D te verdelen, afhankelijk van de geometrie van de proefmonsters. De vezels komen niet bovendrijven ondanks hun lagere dichtheid vergeleken met de andere bestanddelen van het composietmateriaal.

Een lichtgewicht composietmateriaal op cementbasis met dennenvezels is ontworpen op verstevigingsgedrag onder buiging. Het materiaal kan prefab worden gemaakt of in het werk worden gestort. De milieubelasting van het composietmateriaal zal lager zijn vergeleken met standaard materialen op cementbasis door gedeeltelijke vervanging van het cement door vliegas en microsilica (beide industriele bijproducten) en door natuurlijke vezels te gebruiken in plaats van synthetische vezels. Dit materiaal vertoont meervoudige scheuren voorafgaand aan bezwijken onder buiging. Het ontworpen materiaal kan worden gebruikt voor toepassingen zoals low-budget huizen in landen met aardbevingsrisico, waar vervormingscapaciteit en een laag gewicht gewenste eigenschappen zijn voor een bouwmateriaal.

Resumen

El uso de fibras naturales es la forma más antigua de reforzar un material de construcción. Durante el siglo XX se desarrollaron una gran variedad de materiales base cemento reforzados con fibras, para aplicaciones que requieren propiedades específicas de materiales. Diferentes tipos de materiales desarrollados por el hombre, tales como acero, vidrio o polivinil alcohol, se usan actualmente como refuerzo, así como también fibras naturales. Comparadas con las fibras sintéticas, las fibras naturales se encuentran disponibles con mayor facilidad alrededor del mundo, además de ser más amigables para el medio ambiente pues se necesita menos energía para producirlas. Sin embargo, las propiedades de las fibras naturales no son constantes como lo son las propiedades de las fibras sintéticas. Además, las fibras naturales tienen una menor capacidad a tensión.

Estudios en los que se utilizaron fibras naturales en materiales base cemento mostraron beneficios tales como: reducción de la contracción, mejoramiento del comportamiento a la flexión, así como también endurecimiento por tracción con múltiple agrietamiento en elementos delgados y prefabricados. Sin embargo, el uso de fibras naturales en materiales base cemento se ha limitado justamente a elementos prefabricados. [Swamy 1988, Savastano 2000, Silva 2009b], mientras que las fibras sintéticas son usadas tanto para elementos colados en sitio, como para elementos prefabricados. A fin de desarrollar un material base cemento reforzado con fibras naturales que pueda ser colado en sitio, esta tesis propone un nuevo enfoque utilizando fibras naturales discontinuas, distribuidas aleatoriamente [Sierra y Schlangen 2008].

De la variedad de fibras naturales disponibles, se eligieron las fibras de madera y entre estas las fibras de madera blanda (coníferas) en lugar de las de madera dura (de árboles de hoja caduca) por diversas razones; siendo la razón más importante que las fibras de madera blanda son más grandes y están distribuidas de manera más uniforme a lo largo de la madera. Adicionalmente, la madera dura es más susceptible al ataque de álcalis y esta madera tiene un mayor efecto inhibidor del fraguado del cemento. Las fibras se obtuvieron de tres diferentes especies de madera blanda: alerce, abeto y pino. A pesar que las fibras de alerce mostraron resultados prometedores en cuanto a su resistencia a la tensión y a las propiedades de la interfaz fibra-matriz, debido a las limitaciones de producción debieron ser descartadas, en esta investigación, como posible refuerzo. Los estudios continuaron con fibras de abeto y de pino.

Se estudiaron así también, matrices cementicias en las que se reemplazó parcialmente el cemento por otros conglomerantes a fin de lograr una matriz que tenga a la vez un bajo impacto ambiental y una resistencia a tensión compatible con el de las fibras de madera seleccionadas. Los conglomerantes utilizados en combinación con el cemento son tres productos residuales de la industria: escoria de alto horno, ceniza volante y humo de sílice. Adicionalmente, se utilizaron como relleno mineral, polvo de caliza y arena de río con una distribución de tamaño de partículas optimizada, a fin de crear una matriz más densa. Para

tamaño de partículas menores a 180 μm el diseño de la mezcla está gobernado por la reacción química deseada de la pasta y no por la distribución de tamaño de partículas.

Las propiedades de la interfaz fibra-matriz varían de acuerdo al tipo de fibra y a la composición de la matriz cementicia. Los efectos de las condiciones de curado y la geometría de la fibra fueron evaluados. La curvatura natural de las fibras incrementó la adhesión mecánica. Sin embargo, la curvatura excesiva puede dar lugar a ruptura de las fibras cuando estas son arrancadas. Los cambios volumétricos de las fibras, debido a la humedad, fueron controlados mediante un tratamiento. Esto generó un comportamiento de arrancamiento mejorado tanto para las fibras de abeto como para las fibras de pino. A pesar que las fibras de abeto exhibieron mayor esfuerzo de arrancamiento en combinación con matrices con escoria de alto horno y polvo de caliza, debido a limitaciones de producción estas fibras no fueron consideradas para los estudios subsiguientes de este proyecto de investigación.

Posteriormente se efectuó una comparación entre el comportamiento deslizante durante las pruebas de arrancamiento (pullout) de las fibras de madera y de fibras sintéticas, utilizando un modelo analítico ya probado con fibras sintéticas. Se concluyó que este modelo, basado en la separación gradual de la fibra y la matriz seguida por el deslizamiento de la fibra, no es aplicable a las fibras de madera. Un enfoque diferente se tomó al usar un modelo numérico que asume pérdida de volumen debido al daño interno en la fibra madera durante el arrancamiento. Este modelo logra ajustarse a los resultados de laboratorio.

Los resultados de pruebas experimentales preliminares de compuestos con una matriz cementicia de alta resistencia y un porcentaje bajo de contenido de fibras (2% en volumen) se utilizaron en un modelo basado en micro mecánica, junto con información sobre las fibras y las matrices cementicias. El modelo muestra la necesidad de disminuir la resistencia de la matriz cementicia e incrementar el volumen de fibras a fin de desarrollar, ante cargas flexionantes, agrietamientamiento múltiple previo a la ocurrencia de la falla. El contenido de fibras fue entonces incrementado al 5%.

Una viscosidad adecuada de la mezcla en estado fresco permite a las fibras distribuirse equitativamente en arreglos bidimensionales y tridimensionales, dependiendo de la geometría de las muestras. Las fibras no flotan a pesar de ser más ligeras que cualquiera de los otros elementos del compuesto.

Se diseño un compuesto base cemento ligero, reforzado con fibras de madera, que exhibe comportamiento de endurecimiento a la deformación. Este material puede ser colado en sitio o prefabricado. El impacto ambiental de este compuesto será menor que el de un material estándar base cemento al haber reemplazado en el, parcialmente, el contenido de cemento con ceniza volante y humo de sílice, que son subproductos industriales, como también al emplear fibras naturales en lugar de fibras sintéticas. Dicho material desarrolla múltiple agrietamiento previo a la falla bajo esfuerzos flexionantes. El material diseñado puede ser considerado para aplicaciones tales como vivienda de interés social en países sujetos a riesgo sísmico, donde la ductilidad y el bajo peso son características deseables en un material de construcción.

Table of Contents

List of Symbols

Roman

c	initial flaw size
d [mm]	diameter
d_f [mm]	fibre diameter
f	Snubbing coefficient
f_d	cumulative percent of particles finer than D
k_{total}	stiffness of machine and sample in micro tension-compression testing device
k_s	stiffness of sample, in micro tension-compression testing device
k_c	stiffness of machine in micro tension-compression testing device
l [mm]	length
l_e [mm]	embedded length
q	adjustment factor for particle size distribution
$p(\phi)$	probability density function of fibre orientation angle
$p(z)$	probability density function of centroidal distance of fibres from crack plane
r [mm]	fibre radius
A_c [mm^2]	fibre cross-section area
C_f [mm]	fibre cross-section contour
D_L [mm]	maximum diameter in particle size distribution
D_S [mm]	minimum diameter
E_f [GPa]	Young's modulus of the fibre
E_m [GPa]	Young's modulus of the cement matrix
F [N]	Tensile load
G_1 [N/mm]	energy released during the first millimetre of pullout test
G_d [N/m]	pullout interfacial chemical bond energy
G_t [N/mm]	energy released during pullout test
J_b' [J/m^2]	Complementary energy
J_{tip} [N/m]	Matrix crack tip toughness
K_m [MPa m]	matrix fracture toughness
L_c [mm]	fibre critical length
L_f [mm]	fibre length
P_{au} [N]	maximum pullout resistance force
P_e [N]	force necessary to break the elastic bond
P_{fr} [N]	pullout frictional force
S_1, S_2, S_3	Sublayers of secondary wall in wood fibres
V_f	fibre volume fraction

Greek

β	slip-hardening coefficient
δ_0 [mm]	crack opening corresponding to σ_0
δ_c [mm]	crack opening when all fibres finish debonding
Δ [mm]	pullout displacement
Δ_n [mm/mm]	normalized pullout displacement
ν	Poisson's ratio
ρ [kg/m^3]	density
$\sigma(\delta)$	fibre-bridging behaviour relation
σ_0 [MPa]	maximum fibre bridging strength
σ_{fc} [MPa]	first crack strength
σ_n [MPa]	normal stress
σ_{ss} [MPa]	steady state crack stress
τ_{au} [MPa]	maximum shear bond stress
τ_{fu} [MPa]	frictional shear bond stress
τ_{max} [MPa]	maximum interface shear stress
ψ [mm]	equivalent circumference of the fibre
φ	angle of internal friction of the soil
ω	water-powder ratio

List of Abbreviations

Al_2O_3	Aluminium oxide
BFS	Blast furnace slag
BSE	Backscattered electron
C_3A	Tricalcium aluminate
C_3S	Tricalcium silicate
CaO	Calcium oxide
$CaCO_3$	Calcium carbonate
CH	Calcium hydroxide
CI	Continuity index
CMOD	crack-mouth-opening displacement
CO_2	Carbon dioxide
CSH	Calcium silicate hydrate
CT	computer tomography
CTMP	Chemo-thermo-mechanical pulping
ECC	Engineered cementitious composite
EDS	Energy dispersive spectroscopy
ESEM	Environmental scanning electron microscope
FA	Fly ash
FCS	First crack strength
FRC	Fibre reinforced cement-based material
FT	Fourier transform
HCl	hydrogen chloride
HPFRCC	High performance fibre-reinforced cement composites
HRWRA	High-range water-reducing admixture
LP	Limestone powder
LVDT	linear variable differential transformer
LT	long treated pine ($l = 25$mm)
LU	long untreated pine ($l = 25$mm)
MIR	Middle Infrared Reflectance
MOR	Modulus of rupture
NaOH	sodium hydroxide
NSSC	neutral sulphite semi chemical procedure
OPC	Ordinary Portland cement
PE	Polyethylene
PP	Polypropylene
PVA	Polyvinyl alcohol
RH	Relative humidity
SAP	Super absorbent polymer

SF	Silica fume
SiO_2	Silicon dioxide
Si	silicon
SP	Superplasticizer
T	treated pine ($l = 10$ mm)
TMP	Thermo-mechanical pulping / pulp
U	untreated pine ($l = 10$ mm)
w/c	water-to-cement ratio
wt%	percentage per weight

General Introduction

1.1   Background

The use of natural fibres is the oldest form of reinforcing a composite: 3500 years ago in Ancient Egypt straw was used to reinforce mud blocks *(Exodus 5:6)*. In North and South America clay bricks reinforced with straw is an ancient, yet still valid building technique (figure 1.1). With the development of other more durable building material such as concrete this use was worldwide forgotten. Concrete is a reliant, fairly durable material. It has a high compressive strength but a low tensile strength that in most cases is compensated by steel reinforcing. However, due to its inherent brittleness concrete is prone to fracture failure. During the 20th century the idea of using fibres as reinforcement was resumed leading to the development of a wide variety of fibre reinforced cement-based materials (FRC) for applications that require specific material properties.

Figure 1.1: Detail of a house in New Mexico, USA [Schlangen].

The fibres are added to the cement composites to enhance material toughness, strength, fatigue life, impact resistance and/or fire resistance. Different types of man-made fibres are currently in use: stiff fibres such as glass or steel and flexible fibres as polyvinyl alcohol [Li et al. 2002] or polypropylene fibres, as well as some natural fibres. Natural fibres can be a low cost replacement for the synthetic fibres, of which the production process is energy intensive [Campbell and Coutts 1980; Silva et al. 2009b]. The production of polyvinyl alcohol (PVA) and polypropylene (PP) needs phenol compounds and amines and the use of these substances is not sustainable. Compared to synthetic fibres, natural fibres are more easily available worldwide as well as friendlier to the environment since less energy is necessary to produce

them. They are also a renewable resource. However, the properties of natural fibres are not as constant as those of synthetic fibres and natural fibres have a lower tensile strength.

Some studies using natural fibres in cement-based materials have shown several benefits. Soroushian and Ravanbakhsh [1998] describe a reduction of plastic shrinkage; Mohr et al. [2005b] mention a reduction of autogenous shrinkage; Savastano et al. [2003] and Tonoli et al. [2007] show an improvement of the bending behaviour of the composite. Silva [2009b] achieved tensile-hardening with multiple-cracking behaviour in precast, thin elements. However, the use of natural fibres in cement-based materials has been limited to pre-cast elements [Swamy 1988; Savastano et al. 2003; 2005] while the synthetic fibres are used for pre-cast as well as cast-in-place applications. In order to achieve a cast-in-place cement-based material reinforced with natural fibres, this thesis proposes a new approach with the use of discontinuous randomly distributed wood fibres [Sierra and Schlangen 2008]. By means of this approach the FRC material with wood fibres will develop a deflection-hardening behaviour. "Deflection-hardening" describes the behaviour of a ductile composite that exhibit multiple cracking in bending.

Under direct tension, conventional FRC usually exhibit strain-softening behaviour, in which cracks open with decreasing tension. A different type of material, high performance fibre reinforced cement composites (HPFRCC) are characterized by a tensile stress-strain response that exhibits strain hardening accompanied by multiple cracking. A good example of these materials is ECC, Engineered Cementitious Composites, a cement-based material reinforced with a small volume fraction (typically 2%) of short discontinuous synthetic fibres (<10 μm long). PVA fibres are the synthetic fibre most frequently used as reinforcement in ECC. ECC shows enhanced ductility achieved by multiple cracking and a strain capacity in the range of 3-7%. Figure 1.2 shows a typical tensile stress-strain curve of ECC and figure 1.3 shows an example of the multiple cracking and high ductility under bending stress. The crack widths of ECC remain below 100 μm even at a strain of 4-5%. Such small crack width may translate into an improvement in structural durability [Li et al. 2002]. The ECC material design based on micromechanics is an inspiration for the design of a wood fibre reinforced cement based material, proposed in this research project.

Nowadays the environmental impact and sustainability of concrete is a major concern. Cement is an energy intensive material, responsible for more than 50% of the CO_2-emission in a concrete mixture [Battelle 2002]. Partially replacing cement by other binders without sacrifying the mechanical properties will have the benefit of saving energy, reducing greenhouse gas release from mining, calcination and grinding of limestone [Kosmatka and Panarese 1998] and producing less waste. Many residual products from industries, such as fly ash, silica fume and blast furnace slag can have a positive influence in the concrete properties [Jiang et al. 2004; Aïtcin 2008]. Therefore these 3 by-products are used in this thesis as partial cement replacements in order to achieve a FRC with a lower environmental impact, not only for the use of natural fibres but also from a sustainable cement matrix point of view.

Low-budget housing in Latin America needs to be structural fulfilling but sustainable and lightweight. A good part of the Latin America is subject to seismic risk; therefore structural elements in houses should be able to sustain alternating tensile and compressive forces during a possible earthquake. The structure could sustain damage but it should not fail, to allow the inhabitants to evacuate, thus ductility is a desirable characteristic for the structure itself, the individual structural elements and ultimately for the building material itself. In Latin America cast-in-place concrete represents a bigger market than prefabricated concrete elements. A material with high ductility but light and low production costs and environmentally friendly can solve this issue.
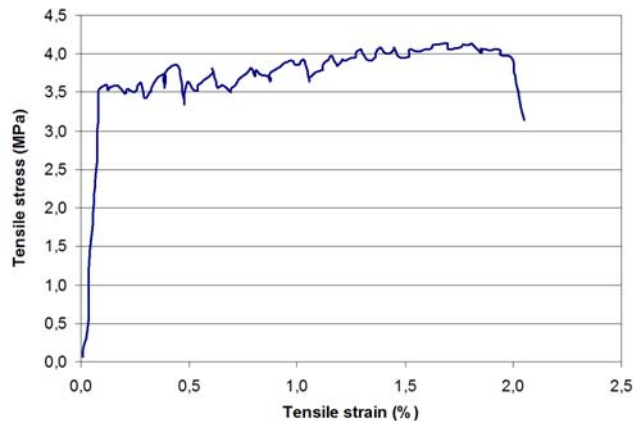
Figure 1.2: Typical tensile stress-strain curve of ECC material.

Figure 1.3: Example of multiple cracking and enhanced ductility of ECC [Boshoff 2007].

1.2   Research objective

The main goal of this project is to develop and mechanically characterize a cement-based composite reinforced with natural fibres from wood that will show an enhanced ductile capacity as well as low environmental impact, weight and production costs when compared with traditional concrete. It should be possible that this new material can be cast-in-place and used in applications such as low-budget housing in Latin America.

1.3   Research strategy and outline

In fibre reinforced concrete the composites´ properties depend on the fibre, the cement matrix and the fibre-matrix interface. To be able to achieve the goal described in the previous section the research was carried out by first studying each of these components and later using this knowledge to design the cement-based material reinforced with wood fibres. The outline of the thesis is presented in figure 1.4.

Chapter 2 is a literature survey on the use of natural fibres as reinforcement in cement-based materials. While other natural fibres such as sisal or hemp have been successfully used as reinforcement, this review makes evident the lack of research regarding wood fibres and therefore the need for the present research project.

In Chapter 3 different wood and other natural fibres are considered as possible reinforcement. The physical and mechanical properties of the available fibres are studied, as well as their durability in an alkaline environment.

The fourth chapter describes the design of a cement matrix with reduced environmental impact and mechanical properties that would match with the fibre properties obtained in the previous chapter.

The fibre-matrix interface is studied in Chapter 5. To be able to determine the bond strength and the fibre pullout behaviour pullout tests were conducted using different cementitious matrices with wood fibres. With the test results and image analysis the effects of curing conditions on pullout behaviour are evaluated, as well as the influence of the cement matrix composition, fibre type and fibre geometry.

The performance of different cement-based materials reinforced with the wood fibres is presented in Chapter 6. The mechanical behaviour of these composites was compared with the behaviour of a new ECC. This new ECC is designed with low cement content, sand particles up to 2 mm and low fibre content (1% or 0.5% volume of PVA fibres). Comparison were made, as well, with samples with hybrid reinforcement of PVA and wood fibres.

Chapter 7 summarizes the results and conclusions of this study, and presents some recommendations for future research. Recommendations for applying the material here developed are also given.
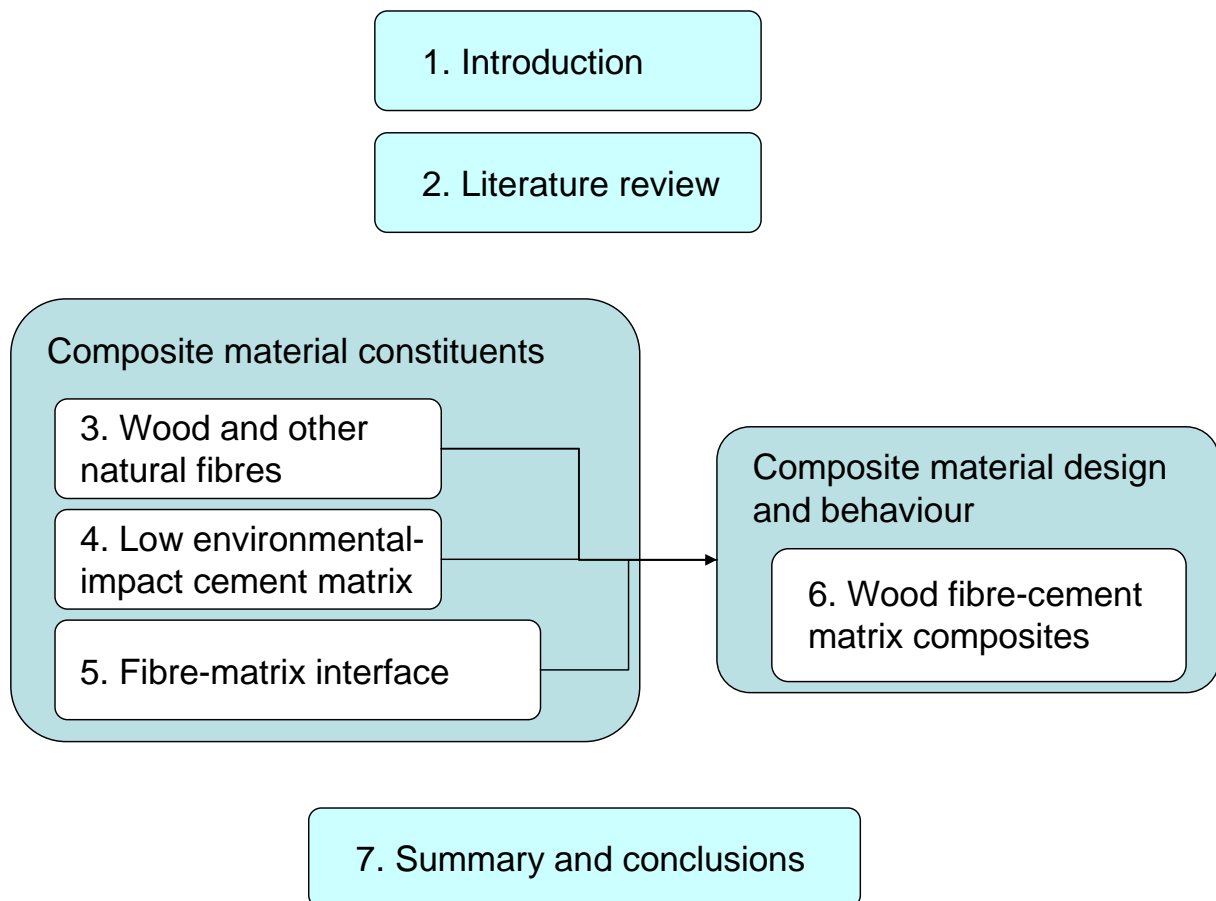
Figure 1.4: Outline of the thesis.

Chapter 2

Natural Fibres in Cement-Based Materials: A Survey of Literature

2.1 Introduction

Natural fibres are an available, renewable and low cost resource for reinforcing materials. Additionally, using natural fibres generates less concern for health and safety during both handling and processing [Reis 2006] than synthetic fibres do. Furthermore, natural fibres are friendlier to the environment since less energy is needed to produce them, as shown in table 2.1.

Table 2.1: Energy associated with the production of fibres

Fibre	Energy to produce	
	(MJ/kg)	(GJ/m^3)
Natural fibres		
Kenaf	3.1	
Wood fibre (TMP)	8.6	4.3
Lignocellulosic	4.0	2.4 - 4.8
Wood : Lumber (not fibres)		1.0 - 6.0
Synthetic fibres		
Glass	13.0	34.0
Carbon	130.0	234.0
PVA	101.0	131.0

Compiled from [Campbell and Coutts 1984; Kavelin 2005; Keoleian et al. 2005; Lippke 2009; Puettmann and Wilson 2004]

Currently, polymers, plastics and ceramics are being reinforced with wood, flax or hemp fibres and the interest to use them for concrete as well is growing worldwide. However, so far most of the research was only focused on cementitious materials for applications such as thin sheets and non-structural building elements. For these applications a wide variety of natural fibres is used, varying from randomly distributed small single pulp fibres to long aligned fibres [Silva 2009b] in combination with mortar or concrete.

When asbestos was found to be a health hazard in the 1970´s, natural fibres came in the spotlight as a possible replacement. The aim was to develop the same light and durable material as with the asbestos for, for instance, cladding sheets, roof tiles and panels. The most common way to produce these so-called fibre cement boards is by means of the slurry dewatering process, especially when high fibre fractions are used (9% by mass or higher). In this process initially high water content is produced to achieve both high fibre content and uniform distribution. Within the slurry dewatering processes the Hatschek process [Kuder and

Shah 2003], see figure 2.1, is the most widely used method of fibre–cement production. In this process sheet is produced by the deposition of several layers of fibre–cement. The fibres are oriented preferentially in the longitudinal direction of the sheet [Savastano et al. 2009].
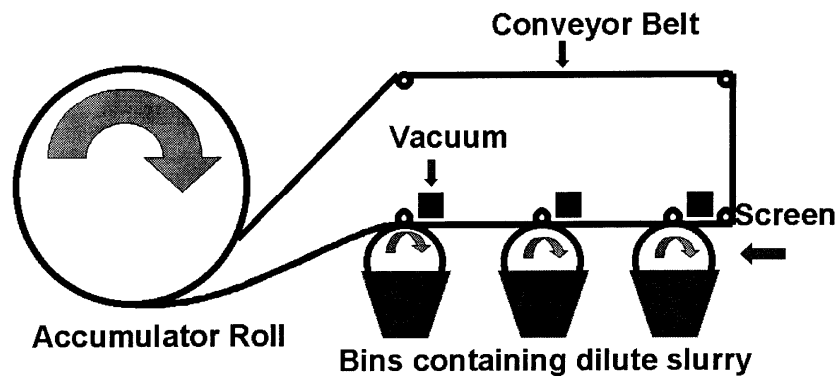

Figure 2.1: Hatschek formation machine [Kuder and Shah 2003].

During the last decades, several studies have been carried out around the world in order to analyse and develop cementitious materials with wood and other natural fibres, most of them focus in the non-structural applications (replacement of asbestos) and some of them as a material for structural applications. Though now an abundance of literature on composite mechanical properties has been published, less data is available concerning the microstructure of fibre-cement composites, and especially about wood fibre reinforced cement-based materials. This chapter gives an overview of the available data regarding natural fibres and cement-based materials.

2.2   Wood fibres

2.2.1   Wood fibre characteristics

Wood is composed mostly of hollow, elongated cells that are arranged parallel to each other along a tree. The properties of these cells or single fibres vary widely in size and structure from species to species (hardwood and softwood), but also within one species from tree to tree and even within the same tree (early-wood and late-wood fibres). For instance, the spring or early wood has cells with larger diameter and thinner walls than summer or late wood cells formed during periods of less growth [Swamy 1988].

Softwoods fall into the sub classification of gymnosperms; seed bearing plants that have their seeds exposed, usually in cones. Most species in this sub classification are conifers. The other broad sub classification, the angiosperms, includes the various orders of hardwoods. These trees have flowers; broad leaves and the seeds are enclosed in a fruit [Donath et al. 2006]. Hardwood trees have a more complex structure than softwood trees, with the additional presence of vessels or pores. Vessels are relatively large diameter cells that have the function of main arteries for the movement of sap in the tree. Sap is a fluid consisting mainly of water and nutrients. In softwood, on the other hand, the fibres perform the function of conducting

the sap longitudinally. In both hardwood and softwood, there are groups of cells horizontally oriented called rays that conduct the sap from the pith (tree core) to the bark (tree outer layer).

Softwood produces longer fibres (3-5 mm average) with diameters of 45 μm for springwood and 13 μm for summerwood. Hardwood fibres are generally shorter (1 mm average) and thinner (20 μm average). The cell wall from hardwood on the other hand is thicker and stiffer than softwood [Johnston 2001]. The difference between late wood and early wood cells as well as the rays can be seen in figure 2.2.

The main chemical components that form the physical fibre structure of wood cells are cellulose, hemicellulose and lignin (figure 2.3). Additional components that can be found in wood are for instance the extractives that are especially present in hardwood. All the chemical components are formed from the sugars produced in the leaves by photosynthesis [Swamy 1988]. Table 2.2 shows the main chemical components for wood and other natural fibres. Cellulose represents 40-50% of wood substance by weight [Kettunen 2006; Wood Handbook 1974]. It contains carbon, hydrogen and oxygen, is not affected by alkalis and dilute acids. As the amount of cellulose in the fibre increases, both the fibre tensile strength as well as the modulus of elasticity of the fibre increases as well [Young et al. 1998]. Cellulose is found in the cell walls where its hydroxyl side groups are largely responsible for the hygroscopic nature of the wood fibres [Young et al. 1998].
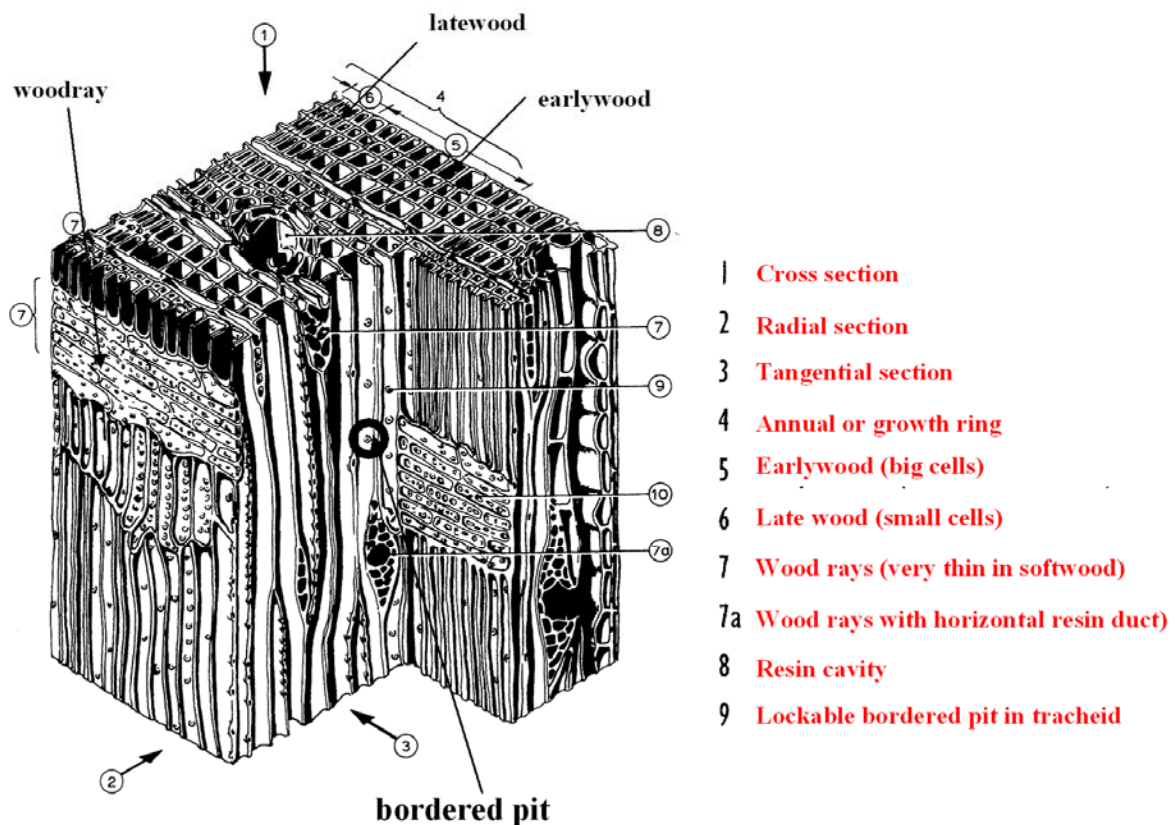

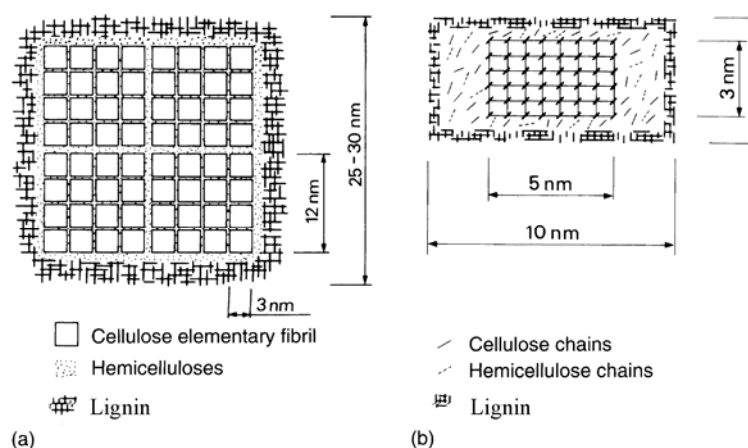*Figure 2.2: Cross section of softwood [Fraaij 2007].*

Figure 2.3: Models of the cross-section of a microfibril [Kettunen 2006].

Table 2.2: Chemical composition of some natural fibres

Fibre	Chemical Composition (%)						
	Cellulose	Hemi-	Lignin	Pectin	Wax	Ash	Moisture content (%)
Bast fibres							
Flax	71.0	18.6	2.2	2.3	1.7	1.5	10.0
Hemp	74.4	17.9	3.7	0.9	0.8	1.5	10.8
Jute	61.0	20.4	13.0	0.2	0.5	-	12.6
Ramie	68.6	13.1	0.6	1.9	0.3	-	8.0
Sugarcane	41.7	28	21.8	10	-	3.5	8.8
Bamboo	26-43	20-30	21-31	-	-	1.7-5	11.3
Hardwood	45-50	20-39	16-30	0-1	-	1.0	7.2
Softwood	40-50	30-33	23-34	0-1	-	0.7	6.9
Seed-hair fibres							
Cotton	89-99	3-6	0.5-1	2-5	0.6		10
Coir	43.0	0.3	45	4.0	-	1.1	8.0
Leaf fibres							
Sisal	78.0	10.0	8.0	0.8-2	2.0	-	11.0
Banana	25.8	17.1	24.8	3-5	-	7.0	11.7

Compiled from [Bledzki et al. 1996; Olesen and Plackett 1999; Pacheco-Torgal and Jalali 2011; Reddy and Yang 2005; Mwaikambo 2006; Rowell et al. 1997; Mansur 2000; Asukara et al. 2004; Kavelin 2005; Bilba et al. 2007; Swamy 1988]

Hemicellulose acts as a matrix for the cellulose microfibrils. It is soluble in alkalis and has a high moisture absorption capacity. Hemicelluloses are branched polymers of several non-glucose sugars [Illston and Domone 2001]. The amount of hemicellulose varies from plant to plant and so does the structure of this component [Wood handbook 1974]. Hemicellulose is easier to degrade than cellulose. The decomposition temperature of hemicelluloses is about 200 to 260 ºC, and the corresponding temperatures for cellulose are 240 to 350 ºC [Hietala et al. 2002]. Cellulose has a crystalline structure that is strong and resistant to hydrolysis. Cellulose is insoluble in water, organic solvents and alkaline solutions. Hemicellulose, on the

other hand, has a random, amorphous structure with little strength, than can be easily hydrolyzed by dilute acid and alkali [Jacobsen and Wyman 2000].

Lignin is the bonding between cells. This component is predominantly found in the fibre middle lamella but it can also be found throughout the fibre. It is vulnerable to the attack of alkalis [Johnston 2001]. Its chemical composition and amount varies in the different plant species, being more abundant in softwood than in hardwood [Swamy 1988]. Lignin accounts for 23 to 33% by mass of the softwood fibres but only 16 to 25% of the hardwood fibres [Wood handbook 1974]. Lignin has been used as a cement hydration retarder. Several chains of polymers form lignin. It cannot be divided unless it is split into more simple substances.

The extractives, finally, are organic compounds that, as mentioned before, do not form part of the fibre physical structure. They give certain properties to the wood, such as colour, odour and insect resistance. Some extractives can be incompatible with cement- based materials. Starches and tannins can inhibit cement setting, as sugar does [Vaickelionis and Vaickelioniene 2006]. Other extractives as resins and fatty acids, terpenes and terpenoids, and salts also cause problems in cement-wood compatibility [Pehanich et al. 2004].

The physical structure of a wood fibre consists of 4 distinct layers, the primary and secondary wall, the middle lamella and the lumen, as illustrated in figure 2.4. The secondary wall is a set of three sub layers S1, S2 and S3. The central and thickest secondary wall layer S2 makes up about 70-80% of the wall thickness [Sedighi Gilani 2006]. Each layer of the wood fibre wall is made of cellulose crystalline chains (microfibrils) that are located in a matrix of hemicellulose and lignin. The angle between the cellulose microfibrils and the longitudinal axis of the fibre is called the fibre-microfibril angle. These angles are related to the tensile strength and stiffness of the fibre. As the S2 layer is the thickest layer of the fibre wall, its fibre-microfibril angle plays the most important role in the mechanical properties of whole wood fibre [Sedighi Gilani 2006].
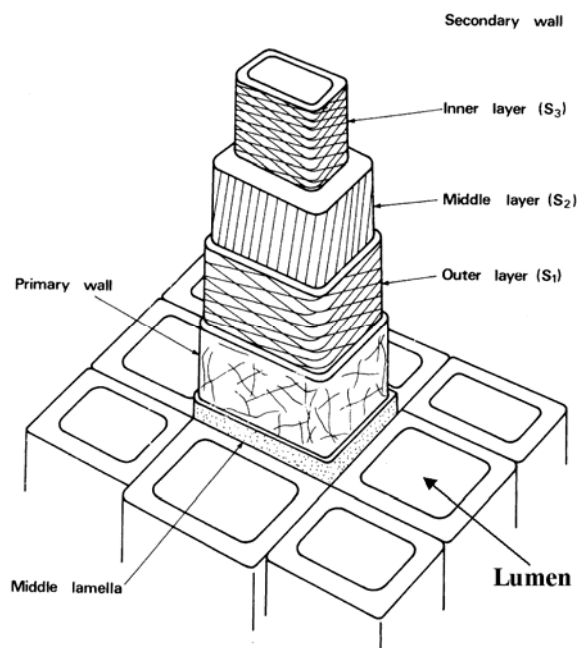

Figure 2.4: The structure of the cell wall [Fraaij 2007].

Wood changes its dimensions as it gains or loses moisture below the so-called saturation point. The saturation point in wood is the moisture content at which cell walls are completely saturated (water bound chemically within the wall cell) while no water exists in cell lumen. Above the saturation point, wood is stable in size [Wood Handbook 1974]. Regarding its shrinkage, wood is an anisotropic material: it shrinks mostly in the direction of the annual growth rings (tangentially), about half as much across the rings (radially), and only slightly along the grain (longitudinally) [Wood Handbook 1974].

Wood fibres have high tensile strength and relatively high modulus of elasticity compared to other natural fibres, as can be seen in table 2.3. Coutts [Swamy 1988] reported results from other researchers for modulus of elasticity and tensile strength. From these results it can be seen that for single fibres the modulus of elasticity varies depending on the fibril angle and the drying restraints. According to the researchers the modulus can be as low as 9 GPa for dried early wood that had no restriction when drying, or as high as 100 GPa for chemically separated fibres. Although a tensile strength of 2000 MPa was reported for spruce fibres, more realistic values are between 350 and 1000 MPa. For reasonable quality commercial wood prepared by normal methods it should be not less than 700 MPa, or around 800-900 MPa if it was carefully selected and contains late wood.

Table 2.3: Physical and Mechanical Properties of Synthetic and Natural Fibres

Fibres	Properties					
	Length (mm)	Diameter (μm)	Aspect ratio (l/d)	Tensile strength (MPa)	Modulus of elasticity (GPa)	Elongation at break (%)
Synthetic fibres						
PE	12.7	38	335	2700	120	3-80
PVA	8-12	39	255	1620	42.8	6
PP	6	12	500	770-880	11.2-13.2	17.6-25.7
Asbestos	1-5	0.02-20		700-3000	170-200	2-3
Bast fibres						
Flax	10-40	11-33	1060	345-1035	28-45	1.3-3.3
Hemp	8.5-28	15-50	560	310-1000	30-60	1-4
Jute	2-5	16-200	75	250-750	25-30	1.5-2
Ramie	60-250	40-80	2310	400-1050	60	2-4
Hibiscus, Kenaf	2-6	200	10	930	53	1.6
Sugarcane	0.8-2.8	6.6-26	115	170-290	15-19	N/A
Bamboo	2.8	10-40	280	350-500	7.3	11.3
Hardwood	0.3-2.5	10-60	35	200-1300	5-45	
Softwood	1.0-9.0	15-60	110	200-1500	40	15-40
Seed-hair fibres						
Cotton	10-65	12-20	2040	300-600	4.5-12.6	7-9
Coir	0.9-1.2	16.2-19.5	60	130-175	4-6	10-25
Leaf fibres						
Sisal	1-5	10-200	65	250-640	9-26	2-2.5
Banana	2.7-5.5	18-30	165	530-750	20-51	5.2

Compiled from [Li et al. 2002; Yang 2007; Kavelin 2005; Bledzki et al. 1996; Mwaikambo 2006; Brouwer 2000; Pacheco-Torgal and Jalali 2011; Olesen and Plackett 1999; Chand et al. 2007; Mansur 2000; Mukherjee and Satyanarayana 1984; Bowyer et al. 2007; Mueller and Krobjilowski 2003; Swamy 1988]

2.2.2 Production of wood fibres

The process for extracting the fibres from wood is called pulping. Pulping can be done mechanically, chemically or a combination of both. Chemical pulping process separates fibres from lignin by dissolving it with chemical solutions and heat. This is a very effective way to reduce the lignin, with only 3 to 8% lignin by mass remaining afterwards compared to the original 15 to 30% lignin by mass in the wood. Chemical pulping also removes the extractives from the wood fibres. There are two types of chemical pulping methods: the kraft or sulphate (alkaline) process and the sulphite (acidic) process. The most used process worldwide is the kraft process. In the mechanical process the fibres are separated either by stone groundwork or with the help of steam in a process known as thermo-mechanical pulping (TMP). Both the chemical and mechanical process have their advantages and disadvantages: on one hand any mechanical process is cheaper than the chemical process but on the other hand chemically produced fibres are strong, long and stable, as well as more flexible and easier to blend than mechanically produced fibres. Mechanical pulp has a higher yield, which is the weight of pulp per weight of wood, of 85-95% (oven dry) than chemical pulp that has only a 40-55% yield [Mohr et al. 2005b]. The specific gravity of TMP fibres is usually about 0.5 while for kraft fibres it is assumed as 1.5. This difference is caused by the open lumen found in TMP fibres compared to the collapsed lumen found within kraft fibres [Mohr et al. 2005b]. After pulping, hardwood tends to have higher fines content than softwood [Johnston 2001], and, therefore, an increased water demand in cement-based mixtures.

Pure-cellulose fibres can be obtained out of wood and other natural fibres such as cotton. From paper manufacturing one can obtain secondary wood fibres, or "wood waste". These are hardwood and softwood fibres that have been chemically processed to remove most of the hemicellulose and lignin from the cell wall. What remains in the cell wall is primarily cellulose [Blankenhorn et al. 2001]. This leads to hollow cells that can easily be flattened and laid on top of each other forming the paper [Blankenhorn et al. 1999]. In the production of newsprint, most of the hemicelluloses, lignin and cellulose remain intact in the cell wall [Blankenhorn et al. 2001].

Fibres obtained from wood are highly cost efficient. They require less production energy than other fibres conventionally used as reinforcement of cement, such as steel, glass, polyvinyl alcohol or polypropylene [Vares et al. 1997; Campbell and Coutts 1980].

2.2.3 Wood fibre-cement composites properties

2.2.3.1 Materials

Most of the research reported in literature about wood fibre-cement composites has been done with pulp; single fibres obtained by one of the pulping methods described in section 2.2.2. The average length of kraft pulp fibres (produced by chemical pulping) from softwood trees is 2 to 3 mm while pulp fibres from hardwood are shorter, up to 1 mm long. Several studies were done with recycled paper containing fibres with a maximum length of 1.5 mm. Many other reports use pure cellulose, either from wood or from other plants. However, there are three exceptions in this literature review. The research published by Soroushian and colleagues [1990, 1994, 2000] include the use of longer wood fibres of 8 mm, mechanically pulped. Coatanlem et al. in 2006 tested composites with wood chippings, which size varied from 0.5 to 10 mm. Finally, in 2005, Mohr and colleagues used kraft fibres with approximately 4-5 mm fibre length.

2.2.3.2 Fresh properties

Workability

Adding fibres to a cement-based mixture increases the surface area and therefore decreases the workability. This negative effect in the flow can be overcome by the use of superplasticizers. However, it is then necessary to take into account the effect of the superplasticizer in the early age properties of the composite: an increased setting time and decrease cohesiveness can be expected.

In praxis all fibre-reinforced concretes have a higher water/cement ratio, lower coarse aggregate content and smaller size of aggregates compared with conventional concretes [Vares et al. 1997]. Since fibres absorb water, more water is needed to maintain the consistency leading to an increased w/c ratio [Vares et al. 1997]. In order to determine the workability of fresh concrete the slump test is used. Naik et al. [2004] observe that low fibre fractions (<1% by mass) could significantly reduce the slump while using approximately the same mix proportions.

Soroushian and Marikunte [1990] measured the flow according to ASTM C230 and found that the flow slightly decreases when adding kraft pulp fibres. In this study, however, the researchers increased the water-to-cement ratio with increasing fibre mass fractions, so no definitive conclusion may be drawn here about the effect of fibres on workability.

Setting time and cement hydration

Sugar is a main inhibitor of cement setting and it is present in the chemical components of fibres, mainly in lignin and in hemicellulose. Because of its chemical composition and extractives hardwood is therefore more an inhibitor to cement setting than softwood fibres [Blankenhorn et al. 2001; Swamy 1988]. Due to the pulping process mechanical pulped fibres containing up to 30% by mass lignin can be more an inhibitor than chemical pulped fibres with less than 10% lignin. Some of the composites reported by Vares et al. [1997] show slow setting, which was caused by the hemicellulose and lignin. The wood fibre surface is the most likely place to find the inhibitory effects taking place [Pehanich et al. 2004]. Researchers have therefore chemically modified the fibres surface in order to prevent this effect [Blankenhorn et al. 2001; Pehanich et al. 2004; Coatanlem et al. 2006]. According to the predominant presence of cellulose, hemicellulose or lignin in the cell wall the reaction to the chemical surface treatments will vary [Blankenhorn et al. 2001; Pehanich et al. 2004]. The enhancement of the mechanical properties depends on chemical treatment and wood fibre type [Blankenhorn et al. 2001; Pehanich et al. 2004], as is described in section 3.2.2.3.

Since fibres may absorb/desorb water from the cement matrix or atmosphere and by doing so may effect the setting time. Soroushian and Marikunte [1990] showed that for composites with kraft pulp the initial setting time was about the same as with control samples (without fibres) and the final setting time increased with increasing fibre mass content. In the same study the composites with mechanical pulp had both longer initial and final setting times than composites with kraft fibres. The setting times also increased with increasing fibre mass content for samples with mechanical pulp.

Mohr et al. [2005b] performed calorimetric tests to evaluate the effect of wood fibres and wood powders on the rate of hydration of the cement paste. The addition of 3% kraft or TMP pulp had a negligible effect but the composites with 3% wood powder showed a slight delay in the setting time. It is necessary to highlight that during the mixing process the wood

materials were initially mixed with water as they were intended to provide internal curing to the composite.

Lin et al. [1994] on the other hand proposed to modify the cement matrix through chemical additives to accelerate the setting of cement, overcoming the unfavourable effects caused by the inhibitors in fibres. Naik et al. [2004], for instance, suggests that an excessive amount of high-range water-reducing admixture (HRWRA) used in combination with 0.6% fibres or more by mass caused delays in the setting of the concrete.

The extractives in hardwood, such as starches and tannins and other chemical constituents of wood fibres affect the exothermic hydration characteristics of Portland cement [Pehanich et al. 2004].

Wood chipping, an industrial waste product, has also been studied as reinforcement for cementitious materials. Even though the composite has good thermal and insulating properties, the high water absorption of the wood is a main difficulty. In a study by Bouguerra it was possible, by adding wood chipping, to reduce the capillary absorption inside the cement and clay mix [Coatanlem et al. 2006]. Wood chipping must be saturated before mixing in order to achieve adequate hydration of the cement.

Shrinkage

Plastic shrinkage occurs when water at the surface is lost faster than bleed water becomes available. Capillary pressure develops and cracks appear on the surface prior to final set. Therefore, the start of setting is a critical moment since only after setting the concrete will have the capacity to resist the capillary forces and thus the shrinkage. Water absorption by sub-base materials can also lead to plastic shrinkage cracking. The addition of fibres can reduce plastic shrinkage because they stop the spread of micro cracks and increase the tensile strength of concrete [Soroushian and Marikunte 1991]. Because of their hygroscopic properties wood fibres keep concrete moist for a longer time so that drying of the concrete surface starts later [Vares et al. 1997]. The incorporation of 0.06% by volume of cellulose fibres reduces the plastic shrinkage in both normal and high performance concrete [Soroushian and Ravanbakhsh 1998]. In this study, for normal concrete the average maximum crack width without fibres was 1.08 mm and with fibres was 0.58 mm. High-performance concrete samples had average maximum crack width of 0.13 mm without fibres and 0.07 mm with fibres. A later study from the same author [Soroushian 2000] points out that 0.2% pulp fibre by volume also reduced the maximum plastic shrinkage crack width of concrete from 0.14 mm to 0.02 mm.

Vares et al. [1997] reported that shrinkage of cellulose fibre concrete in the plastic stage started later than that of neat concrete without fibres, but cellulose fibres did not decrease the absolute shrinkage value (figure 2.5). For this study they used chemo-thermo-mechanical softwood pulp (CTMP).

From the moment of mixing the water with the cementitious materials until the setting the cement paste reduces in volume. The cement hydration products occupy a smaller volume than the original reactants. This reduction is known as chemical shrinkage. By the time the final set occurs, the cement paste has formed a semi-rigid skeleton. As hydration continues, if there is no influence from the surrounding environment and no external water source, self-desiccation will take place, leading to autogenous shrinkage. Autogenous shrinkage occurs at very early ages, before the cement-based material has developed sufficient structural strength. Therefore, the material is unable to resist the tensile stresses and it will experience internal cracking.
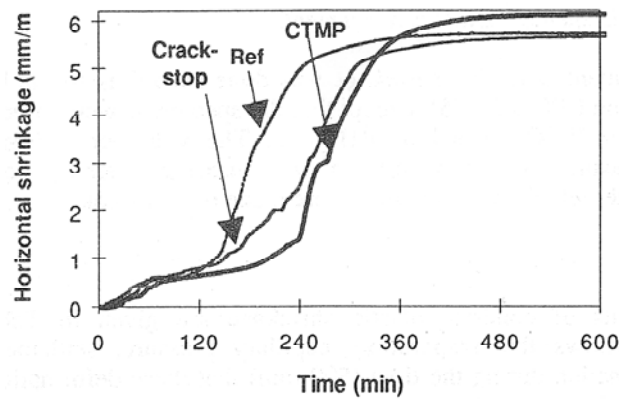
Figure 2.5: Horizontal shrinkage of tested concretes during the first 600 minutes after water addition [Vares et al. 1997].

Autogenous shrinkage should not be a problem for concretes with a high water-to-cement ratio [Neville 1995]. But if the w/c ratio decreases, as is the case for high performance concrete, then it can be considered a significant problem if the structure is prevented to deform (restrained deformation). One approach to mitigate this shrinkage is to add water-entraining materials that will release water during self-desiccation. This internal-curing will help to maintain the internal relative humidity of the cement paste and lower the capillary tension. Mohr et al. [2005b] tested cement pastes (w/c = 0.30) with additional entrained water of approx 0.050 and wood derivate materials at different fibre mass fractions. They found that 1% kraft pulp fibres (4-5 mm long) or 1% cellulose powder (10 and 700 μm) were not effective for internal curing applications. On the other hand, TMP fibres (1-2 mm) and wood powder (0.5-1 mm) reduced autogenous shrinkage of the cement paste, even to a greater extent than super absorbent polymers (SAPs). The downside is that TMP fibres have negative influence in the compressive strength, more than SAPs do.
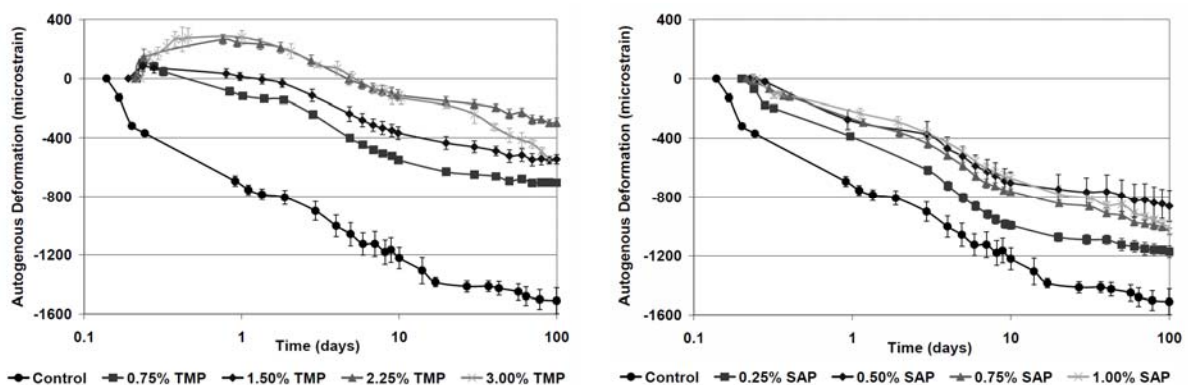

Figure 2.6: Autogenous shrinkage for pastes containing TMPs (left) and SAPs (right) [Mohr et al. 2005b].

Drying shrinkage is the volume change due to the moisture loss from concrete after setting; it is the major part of the total shrinkage for normal concrete. A high w/c ratio can lead to a high drying shrinkage [Zhou 2011]. Two ways of assessing drying shrinkage are to either measure the free shrinkage or the restrained shrinkage. To measure the free shrinkage the specimens are stored after demoulding without any restraint and later its volume changes are registered. Not much evidence is reported in literature about free shrinkage of cement-based materials with cellulose fibres [Campbell and Coutts 1980; Kawashima and Shah 2011, Mohammed and Chuan Fang 2011]. Vares et al. [1997], Soroushian and Ravanbakhsh [1998], Soroushian [2000] and Rapoport and Shah [2005] describe different studies using the restrained ring shrinkage apparatus to measure restrained shrinkage.

In the study by Mohammed and Chuan Fang [2011] the free drying shrinkage strain of samples with paper mill residues increased with increasing percentage of fibres, when compared to fibresless samples. However, the drying shrinkage was reduced, even more than for fibreless specimens, when OPC was partially replaced by FA.

According to Vares et al. [1997] the cellulose fibres did not reduce hardened concrete shrinkage and specimens with fibres shrink even more than fibreless concrete. Nevertheless the samples without fibres failed due to the restrained cracking whereas the fibre-reinforced samples did not: the cellulose fibres delay the development of the cracks. Soroushian [2000] noticed that the maximum crack width reduced from 0.2 mm (in control samples without fibres) to 0.085 mm in the samples with 0.2% pulp fibres by volume. In this study too, the onset of cracking was delayed by several days in the pulp fibre composites. Rapoport and Shah [2005] tested mortar samples with kraft pulp fibre volumes from 0.14% to 0.75%. The addition of any amount of fibres drastically reduces shrinkage crack widths. Samples with fibre volumes 0.375% and 0.75% show the same drying shrinkage performance, which indicates, according to the authors, that additional fibres above a certain amount will not provide extra reinforcement.

Fibre distribution

Following Rapoport and Shah [2005], in a cementitious matrix fibres can be distributed in three fundamental modes: uniform, random or clumped. A uniform distribution is ideal while in cast-in-place concrete a random distribution is the best that one can obtain. In their study cellulose fibres do disperse well under normal mixing circumstances. Lin et al. [1994] proposed to use high shear mixing to improve the distribution of fibres among the cement matrix. Processing the secondary fibres into fibrous form improve their dispersion in the cement matrix [Blankenhorn et al. 1999].

Pulp fibres have the tendency to clump together in water and fibre clumps become weak spots in the cement-based materials. After the observations with scanning electron microscope (SEM) in the study from Coutts and Kightly [1984], the number of fibres in a composite should not be too high so that the fibres can be evenly coated. Rapoport and Shah [2005] found that the fibre dispersion does not affect the material yield as well as the other way round; matrix yield does not affect the fibre dispersion. Changes in the yield stress do not alter drying shrinkage either. The matrix viscosity does not affect the fibre dispersion or the drying shrinkage performance.

2.2.3.3 Mechanical properties

Compressive strength

Wood reinforced cement composites have lower compressive strength than fibreless mortar or concrete [Soroushian and Marikunte 1990; Lin et al. 1994; Vares et al. 1997; Blankenhorn et al. 2001; Pehanich et al. 2004]. These results are consistent with the higher water/cement ratio of the fibre composites. Nevertheless, it is difficult to compare various research studies due to widely varying experimental procedures.

The method of producing the fibres from wood has an important effect on their mechanical and chemical properties. Therefore the pulping method also influences the fibre composite behaviour. For example, composites made with chemo-thermo-mechanical pulp from softwood have higher compressive and flexural strength and increased toughness than the fibres obtained mechanically [Vares et al. 1997]. In the same way, Soroushian and Marikunte [1990] report that adding mechanical pulp leads to lower compressive strength than using softwood and hardwood kraft. Furthermore, these researchers point out that as the fibre volume increases the composite compressive strength decreases.

The type of fibre and its inherent fibre size also plays an important role regarding the compressive strength. The larger number of shorter fibres of hardwood in a mortar sample may have helped improving the compressive strength values compared with the samples with kraft softwood. Hardwood fibres have average fibre length shorter than softwood fibres [Lin et al. 1994]. Blankenhorn et al. [2001] investigate fibre treatment methods to improve the compressive strength of pulp fibre composites without much success. With 10% alkylalkoxysilane treatment kraft softwood fibres show some improvement of compressive strength, but even then reaching only 58% of the strength of fibreless control samples. Pehanich et al. [2004] uses sodium silicate, potassium silicate and silane (aqueous silica) to treat newspaper fibres and kraft softwood and then compares the compressive test results. Without treatment the fibre-reinforced samples have about 60% of the compressive strength of control samples. With the silicate-treated kraft fibres the samples strength increased up to 90% of the compressive value of control samples.

However, the mechanism for decreased compressive strength has not yet been characterized. It may be related to the delayed strength evolution addressed in section 2.2.3.2. Another reason for strength reduction could be an increased amount of entrapped air due to presence of fibres.

Bending strength

In several studies the wood fibre reinforced composites reported higher values of flexural strength and toughness than for neat cement without fibres [Campbell and Coutts 1980; Lin et al. 1994; Vares et al. 1997; Blankenhorn et al. 2001; Pehanich et al. 2004]. These researches include samples prepared following a slurry-dewatering method as well as normal cast-in-place procedures in concrete and mortar. Rapoport and Shah [2005] reported opposite results. The cellulose-reinforced concrete beams tested show no improvement in the flexural strength compared with non-reinforced concrete beams and increase toughness late in the post-peak region (see figure 2.7).
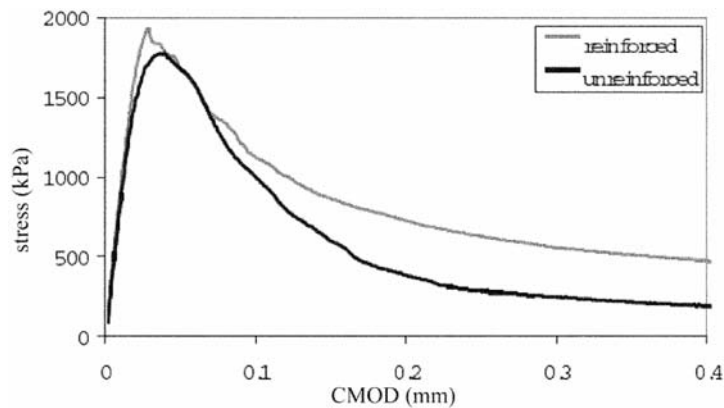
Figure 2.7: Stress-CMOD curves for unreinforced and reinforced concrete [Rapoport and Shah 2005].

The authors of that publication considered the possibility of a different behaviour either for larger values of crack-mouth-opening displacement (CMOD) or for samples not dominated by a single crack opening as in their study. The tested beams had a notch. Vares and colleagues [1997] point out that concrete with wood fibres had lower values of flexural strength than the fibreless samples, when measured at 7 days but after that age the fibres increased the concrete flexural strength to higher values than the control samples.

A higher bending strength can be achieved by replacing a certain amount of cement with silica fume [Lin et al. 1994]. The authors tested yet another improvement method by preparing the samples with high shear mixing. The samples that were prepared with 1% PVA treated kraft pulp had improved bending strength (18.2 MPa and 19 MPa after 7 and 28 days) compared to the paddle mixer samples (9.3 and 11 MPa after 7 and 28 days).

The pulping process influences the flexural strength of the reinforced composites. Samples prepared with TMP fibres have significantly lower bending strength than composites with softwood or hardwood kraft fibres [Campbell and Coutts 1980; Soroushian and Marikunte 1990; Soroushian et al. 1994] (figure 2.8). This may happen because of the lignin and extractives on the surface of TMP that slow the hydration of cement around the fibres resulting in a very weak fibre-cement matrix interface bond [Campbell and Coutts 1980].

The effect of the pulp species on the mechanical behaviour of the composites involves not only the chemical composition of the different fibres but also the inherent length of each type. On one hand, Blankenhorn et al. [2001] explain that more short fibres means more possibilities to bridge the developing microcracks but more fibres will also lead to more void space due to cell lumens in the fibres [Pehanich et al. 2004]. There is higher number of short hardwood fibres in a unit weight than of long softwood fibres. This may have contributed to slightly higher bending strength values for hardwood mortar composites compared to softwood composites. On the other hand, the research published by Campbell and Coutts [1980] and Soroushian and Marikunte [1990] show higher flexural strength for softwood fibre mortar samples than for hardwood fibre composites regardless of the fibre volume/mass fraction. These two researches were done following different mixing and casting procedures, the first one with slurry-dewatering technique (prefabricated elements) and the second one with cast-in-place.
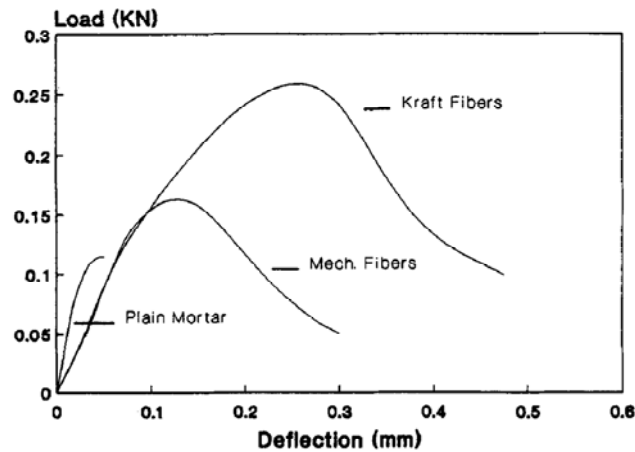
Figure 2.8: Flexural load displacement curves [Soroushian and Marikunte 1990].

From the tests done by Vares and co-authors [1997] the advantages of using new fibres instead of recycled ones is evident. Concrete reinforced with chemo-thermo-mechanical pulp from softwood has higher compressive and flexural strength and increased toughness than concrete with recycled fibres.

Morlier and Khenfer [1991] tested boards prepared by slurry-dewatering method with different fibre lengths. The load-deflection curves as seen in figure 2.9 show increased bending strength and increased flexural toughness with increasing fibre length, whereas the fibre length has practically no influence on Young's modulus.
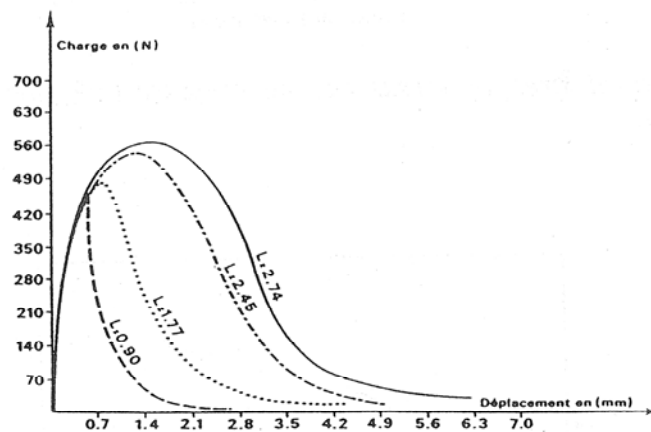

Figure 2.9: Load-deflection curves for cellulose fibre cements as a function of fibre lengths [Morlier and Khenfer 1991].

The study from Soroushian and Marikunte [1990] takes into account the effect of increasing fibre contents on the bending strength. With a 1% and 2% increasing fibre mass content for mechanically produced pulp as well as softwood and hardwood kraft, the flexural strength increased.

Aqueous chemical treatments of the fibres enhanced some of the mechanical properties of wood fibre-cement composites. The bending strength improved more with low percents of both acrylic and alkylalkoxysilane treatments [Blankenhorn et al. 2001]. The silane treated

hardwood and kraft had slightly higher average bending strength values than the silane treated newsprint. Silane is more compatible with cellulose than with hemicellulose and lignin [Blankenhorn et al. 2001].

Flexural toughness

One of the main reasons to add fibres to cement-based materials is the possibility of improving the toughness and ductility of the composite, and therefore overcome the inherent disadvantages of brittle cementitious materials. Both ductility and toughness are concepts that describe the mechanical behaviour of cement-based materials in the post-cracking stage. Ductility is the ability of a material to develop additional strain after initial cracking while sustaining the load. Hence, ductility is referred to in terms of strain. Toughness, on the other hand, is the amount of energy needed after initial cracking in order to make the material fail. Hence, toughness is referred to in terms of energy and is measured as the area underneath the load-deflection curve.

Upon cracking, while normal concrete fails, in fibre-reinforced concrete the fibres should be able to bridge the initial cracks and hold them together until the fibres are either pulled out from the cement matrix or break.

Some of the standardized methods for evaluating toughness are: ASTM C1018, ASTM C1550, JCI-SF4 and RILEM TC162-TDF [Bentur and Mindness 2007]. Unfortunately, there is still not yet an agreement on which of these methods best represents the toughness of fibre-reinforced concrete [Bentur and Mindness 2007]. So far, researchers have not agreed in one single method to quantify ductility of fibre-reinforced materials.

As reported in literature, pulp fibres significantly increase the fracture toughness. Wood fibre reinforced composites have higher values of flexural strength and toughness than fibreless cement samples [Lin et al. 1994; Vares et al. 1997; Blankenhorn et al. 2001; Pehanich et al. 2004]. The authors consider that the origin of fracture toughness comes mainly from the work dissipated in pulling out the cellulose fibres from the cement mortar matrix. Long fibres enhance even more the toughness of the composites because they have a bigger surface area in contact with the cement matrix enabling them to resist fibre pullout. Additionally, it can also make a more effective bridge of the microcracks. This behaviour was observed with kraft softwood fibres that have higher values of toughness compared with hardwood [Blankenhorn et al. 2001; Soroushian et al. 1994] and newspaper fibres [Pehanich et al. 2004]. Hardwood fibres generally have a smaller aspect ratio than softwood fibres.

Mechanical pulps are less effective than kraft pulps in increasing flexural strength and fracture toughness [Soroushian et al. 1990; 1994]. This strength reduction may be due to the presence of lignin or extractives in the surface of mechanical pulps that slow the cement hydration around the fibres leading to a weak fibre-matrix interface. The mechanical pulps used by Soroushian et al. [1990, 1994] were longer (8 mm) than the kraft pulp (below 3 mm). Even tough it is possible that with shorter fibres less fibre pullout occurs, leading to lower post-cracking toughening, it is necessary to take into account that with the same fibre mass fraction there are more small fibres per volume unit than longer fibres. Thus there may be more small fibres pulling out. Composites prepared with chemo-thermo-mechanical pulp from softwood have increased toughness compared to mixtures with recycled fibres [Vares et al. 1997] (figure 2.10).

In composites with 1% and 2% kraft fibres the toughness increased with increasing fibre mass content [Soroushian et al. 1990].

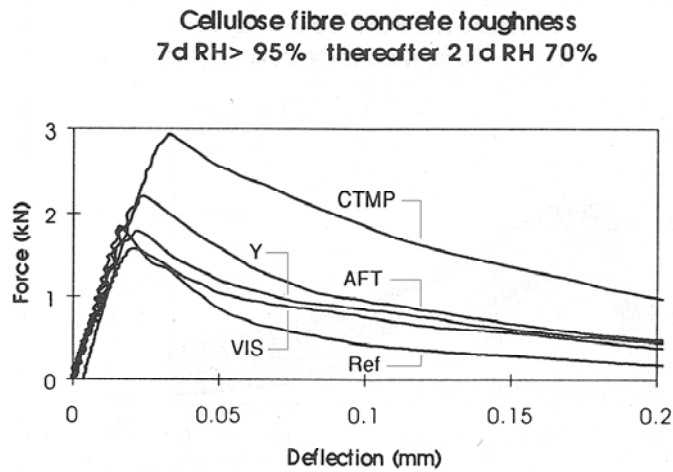Cellulose fibre concrete toughness
7d RH> 95% thereafter 21d RH 70%

Figure 2.10: Cellulose fibre concrete toughness. Concrete stored 7 days at RH>95% and thereafter up to 21 days in normal conditions (RH 70%) [Vares et al. 1997].

2.2.3.4   Interfacial bond

The mechanical behaviour of a fibre-cement composite is directly related to the bond between fibre and cement matrix. This bond depends on many factors like the physical characteristics of the fibres: geometry, type, surface characteristics, orientation, volume and distribution, the chemical composition of the fibre, but also the treatment of the fibre and additives in the cement mixture. The interfacial bond may be chemical or physical or a combination of both. In general, organic fibres are considered to be less compatible to an inorganic material, such as a cement matrix, in terms of chemically bonding [Coutts 1983a]. Therefore, wood fibre-cement bonding is typically considered to be of a physical nature. However, Coutts and Kightly [1984], in a later study, proposed chemical bonding as a means to explain composite fracture behaviour at different values of relative humidity. Since cement is an alkaline inorganic material (pH>12.5) containing surface hydroxyl groups (Ca-OH, Si-OH and Al-OH) and wood fibres contain covalent hydroxyl groups (C-OH) from either residual lignin or the cellulose component and the oxidation of end groups, the chemical bond is believed to be hydrogen bonds or hydroxide bridges between fibres or between fibres and the cement matrix. This bonding can occur during the hydration of the cement when the crystals form and interlock [Pehanich et al. 2004]. For composites that have been cured in wet conditions, Coutts and Kightly [1984] hypothesize that the hydrogen bonds are broken by insertion of water molecules between the covalent bonds. As a consequence, fibres tend to pullout during bending of the composite, rather than fracturing due to a strong fibre-cement bond. However, fibre swelling while in the wet state may present a competing effect by creating additional physical friction force with the cement matrix, in which case the composite behaviour would depend on whether this frictional force overcomes the lack of chemical bonding between the fibre and matrix.

Hachmi and Campbell, cited by Pehanich et al. [2004], described the bonding process in 3 stages: the chemical stage, which is the early wood fibre-cement hydration reactions; the chemical and physical stage when the cement begins to crystallize and form a matrix around the wood; and finally the physical stage is the one that will continue for many years. In 7 days

old samples Lin and colleagues [1994] observed hydration products on the surface of kraft fibres. In that study the authors considered that the bond between wood fibres and concrete increases with time as the matrix gets stronger but the fibres may become brittle showing different types of fibre failure. In the 7-days-old samples there is a large portion of fibre pullout, and in 1-year-old samples a large portion of broken fibres. The failure modes included failure at the cross section of the lumen, delaminating of the fibre cell wall and cracks in part of the cell wall. Partially cracked fibres consume energy, acting as crack bridging in the cement matrix [Lin et al. 1994].

Strong interfacial bond leads to a brittle material with high strength. A weak bond results in a tough material lacking high strength. This behaviour is observed in oven-dried samples: strong but brittle with fractured fibres or low post-cracking ductility, and wet samples: weak but tough with pullout fibres [Coutts and Kightly 1984]. As mentioned above, high moisture contents tend to lower the fibre-to-matrix bond strength at the same time as developing considerable frictional forces. The samples cured under ambient conditions possessed both strength and toughness; suggesting that a number of micro-mechanisms might be taking place during fracture of the sample [Coutts and Kightly 1984].

The fibre-mortar interface region in fractured composites, prepared by slurry-dewatered methods, is dense according to Coutts [1987] and show partial debonding and matrix micro cracking but without localized high porosity following Savastano et al. [2005]. In that research Energy dispersive X-ray spectroscopy (EDS) studies were done with samples reinforced either with softwood and hardwood kraft. Only one EDS spot reported the presence of calcium hydroxide close to the fibres (figure 2.11). In the study of Coatanlem et al. [2006] the microstructure of cast-in-place composites was examined using SEM. After 28 days curing the formation of ettringite needles was observed at the surface of the chipping with sodium silicate treatment and in the cement matrix close to the fibres. Since those large formations were not observed in the composite with water-saturated fibres, the authors conclude that the presence of sodium enhanced the formation of ettringite and this will improve the bond with the cement matrix [Coatanlem et al. 2006]. Since the wood fibres absorb certain amount of water when mixing with the cement paste, later the diffusion of water from their interior could lead to increased cement hydration [Lin et al. 1994].

The interfacial bond, and therefore also the behaviour, strength and failure mode of the composites, are influenced by the geometry of the fibres. Coutts and Kightly [1984] conclude that as the length of fibres embedded is increased the mode of failure changes from one of fibre pullout to one of fibre fracture. They propose that the change of failure mechanism occurs when the aspect ratio of a fibre has a value of 150±50. They mention the results of a study from 1979 by R. Andonian in which he calculated a critical length for fracture in fibres assuming that linear elastic fracture mechanics could be applied to wood fibre cement composites. This critical length was between 18 and 23 mm. But the critical length depends on the fibre and matrix characteristics. The fibres in the study of Coatanlem et al. [2006] were on average 3 mm long and fibre fracture did not take place, which suggests that the critical length should be closer to 3 mm. In a study by Savastano et al. [2005] mortar samples with pine fibres of average length 1.7 mm achieved better flexural strength and toughness than mortar with eucalyptus fibres of about 0.66 mm long.
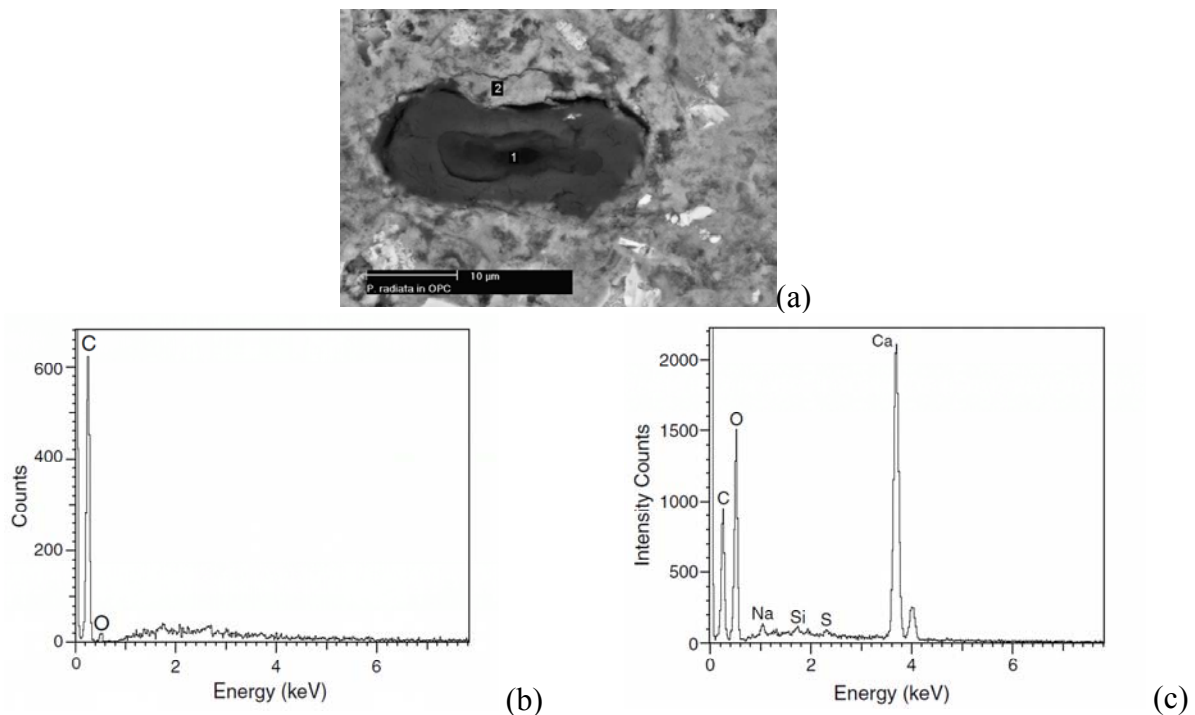
Figure 2.11: 251 days old cross-sectioned Pinus radiata in OPC.
(a) BSE image; spot 1 lumen; spot 2: hydration products at fibre surface.
(b) EDS spectrum of the internal lumen (spot 1 in figure (a))
(c) EDS spectrum of OPC interfacial region rich in calcium hydroxide (spot 2 in figure (a))
[Savastano et al. 2005].

2.2.3.5   Durability of fibres

In order to assess the durability of fibre-reinforced cement-based composites accelerated exposure testing is used in laboratories, in particular wet/dry cycling tests that replicate rain and heat conditions, and freezing/thawing cycles. The composites can also be exposed to humid environments or accelerated carbonation. Information about the durability of the composites can also be obtained by measuring the chloride-ion penetration.

Wetting-drying cycles

In the research from Soroushian and colleagues [1994] the wetting/drying cycles tend to increase the flexural strength and stiffness of both plain (fibreless) mortar and fibre-reinforced cement composites. The flexural toughness, on the other hand, decreased with the accelerated weather tests for both fibre and fibreless samples. The drop was more significant for samples with 2% than with 1% fibres. However, samples with wood fibres, with or without accelerated weathering the flexural toughness was significantly higher than for control samples without fibres, as was mentioned in section *Flexural toughness*. Microstructural studies indicated that the dominant mode of fracture in aged composites was fibre fracture, while unaged specimens showed a combination of fibre pullout and fibre fracture. In aged composites, the fibres exhibited petrification and excess bonding to the cement matrix. Blankenhorn et al. [1999] tested the dimensional stability and compressive strength after accelerated weather. Treated

and untreated fibres did enhance the ability of the mortar composite to withstand wetting/drying cycles. The alkylalkoxysilane treatment was more effective than the acrylic treatment since the average number of cycles at failure was the highest and the dimensional changes were the lowest. The compressive strength of the control samples (without fibres) decreased with the increase of temperature cycles, showing deterioration while the composite with treated fibres maintain an average compressive strength. The higher strength for treated hardwood indicates that these smaller fibres are more effective at retarding micro-crack growth than the treated kraft softwood fibres.
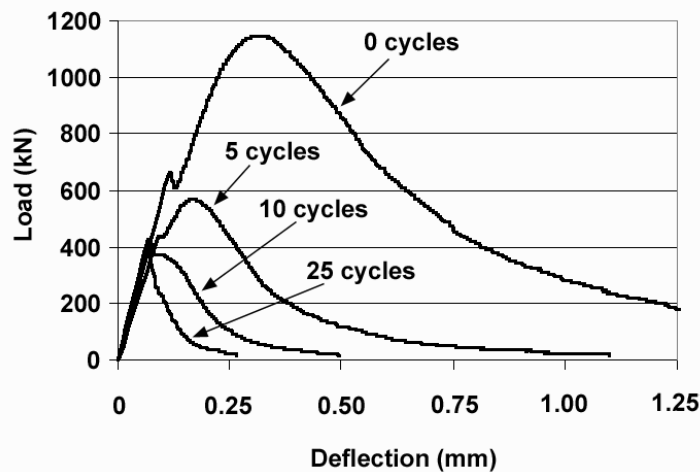
Figure 2.12: Typical load-deflection curves for kraft pulp fibre-cement composites after ageing [Mohr et al. 2005a].

Mohr et al. [2005a] obtained opposite results after wet/dry cycles. After a low number of cycles they already reported a significant loss of first crack and peak strength and a decrease in post-cracking toughness (see figure 2.12). A microscopical characterization confirmed a change in flexural behaviour; before the wet/dry cycling the fibres mainly pulled out which in this case translate into composite ductility, but after 10 or more cycles to composites exhibited brittle fracture because the fibre fractures due to mineralisation of the fibres. In this specific research the water-cement ratio was 0.60, higher than the w/c ratio used by Soroushian et al. [1994] of 0.30 to 0.43, or by Blankenhorn et al. [1999] of 0.23 and 0.37. Mohr and colleagues used 4% fibres while Soroushian and coauthors used 1 to 2%. Tonoli et at. [2009] also reported decrease of flexural toughness, deflection and modulus of rupture after 200 ageing cycles. The decrease of final deflection was bigger for untreated cellulose fibres than for treated ones. In this study the modulus of elasticity increased after the accelerated ageing as a consequence of the densification and continued hydration of the cement phase of the composite.

Freezing-thawing cycles

The dynamic modulus of elasticity of fibreless mortar samples decreased with increasing freezing and thawing cycles while the dynamic moduli of wood fibre-cement composites remained constant [Soroushian et al. 1994]. The average compressive strength values were not

significantly different after freeze-thaw intervals showing that the composite specimens did not deteriorate [Blankenhorn et al. 1999]. MacVivar and colleagues [1999] reported similar results. According to them there were no significant changes in the compression strength and porosity of sheets prepared with 8% pulp after ageing.

Humid environment

A study with wood chipping treated with sodium silicates reported loss of compressive strength after exposure to ambient (50%RH) or humid (95%RH) conditions for 16 months [Coatanlem et al. 2006]. The loss maybe evidence of deterioration of the wood fibres but that was not supported by SEM observations where a large quantity of ettingrite was observed at the surface of the wood chippings. But the presence of sodium silicate did not produce a pozzolanic effect as the researchers expected. The authors concluded that if there was any pozzolanic effect it happened while the wood was deteriorating and that was the dominant effect. The deterioration of the samples showed the high sensitivity of wood chipping mortars in humid environment, which is a limitation on the use of this fibre cement composites.

Accelerated carbonation

Air cured samples, prepared with 3.5% slash pine fibres + 2% PVA fibres, the flexural toughness decreased in 64% after 30 cycles of accelerated aging [Morton et al. 2010]. The accelerated aging program consisted of wet-dry cycles and exposure to CO_2 and it is considered to be a roughly equivalent of 7 years of natural aging in Switzerland. In this study, other combinations of synthetic fibres, PVA, PP or rayon, and slash pine lead to very different results after ageing.

MacVivar and colleagues [1999] measured a decrease in porosity in sheets with 8% pulp after accelerated carbonation. The decrease was explained as a result of the densification due to shrinkage or from continued hydration of the matrix and carbonation. They also reported an increase in compression strength due to the reduced porosity and continuing hydration.

Chloride-ion penetration

Mohammed and Chan Fang [2011] reported moderate to high chloride-ion penetrability in samples with 1 to 2% paper mill residue. The penetrability was higher than for fibreless samples. The resistance to chloride-ion penetration in samples with 1% residue improved considerably when cement was partially replaced with FA. The use of fly ash probably reduced the pore size and thickness of the transition zone between the aggregates and the surrounding cement matrix [Kuroda et al. 2000]. This resulted into a denser matrix with a higher resistance to chloride-ion penetration.

2.2.3.6   Current use

Some of the current applications of cellulose fibres are in cement boards for siding (cladding), backer board, roofing materials and non-pressure pipes, as produced by James Hardie [2011]. Buckeye Technology produces UltraFibre 500, which are used for slab on grade concrete, precast and decorative concrete.

2.3   Other natural fibres

A wide variety of natural fibres have been studied and used to reinforce cement-based materials. Based on their morphology, the fibres can be classified in four groups: stem or bast, leaf, seed-hair and wood fibres, where wood fibres were reviewed in the previous sections. Stem or bast fibres come from the stalks of plants and these fibres are usually obtained following a retting process that involves bacteria and moisture. These types of natural fibres are commonly not used as single fibres but in the form of bundles or strands, usually long ones. The most common bast or stem fibres are jute, flax and hemp.

To obtain leaf fibres one has to crush and scrap the leaves. These types of natural fibres are also used as long bundles and not as single fibre cells. Sisal, abaca and banana are typical leaf fibres. Finally, seed-hair fibres are single fibres from the surface of stems, fruits or seeds. Coir, from coconuts, and cotton are seed-hair fibres. Cotton is a popular source of pure cellulose single fibres. Typical properties of some fibres are given in tables 2.2 and 2.3. In many occasions published literature does not clearly specify if a natural fibre is a single cell fibre or a bundle of cell fibres. Therefore, a wide spectrum of properties for the same type of fibre can be found.

The microstructure of the fibres is complex and it changes from type to type. Sisal fibres, for instance, have lumen. Each fibre cell is made up of four parts, namely the primary wall, the thick secondary wall, the tertiary wall and the lumen. Within the leafs, these cells form groups with either of two distinctive shapes: horseshoe shape and arch shape. The groups of fibres are sometimes referred to as technical fibres. During the fibre-extraction process the technical fibres can adopt a third shape, twisted arch (figure 2.13).

The mechanical properties of the natural fibres will vary depending on which section of the plant they were taken from. The fibres of date palm used by Kriker et al. [2005] have weak modulus of elasticity, which can be explained by the role of the fibres in the tree, which in this case is thermal protection and not resistance.
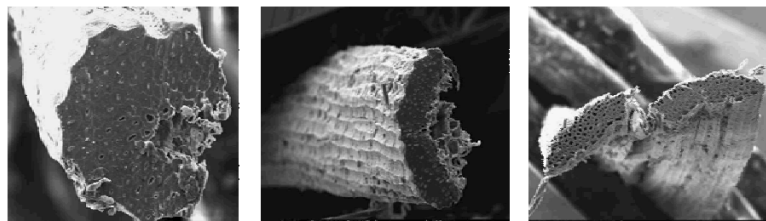

Figure 2.13: Different morphologies of the sisal fibre:
horse-shoe shape (left), arch shape (middle) and twisted arch shape (right) [Silva 2009a].

2.3.1   Mechanical properties of composites with natural fibres

As this research focuses on the use of cement-based composites reinforced with short (<30 mm) discontinuous and randomly distributed wood fibres, the review on natural fibres will also be limited to this kind of cement-based composites.

2.3.1.1   Compressive strength

As with wood fibres, the addition of other natural fibres to cementitious matrices decreases the compressive strength. In concrete reinforced with palm trees fibres the compressive

strength decreases with increasing fibre percentage and with increasing fibre length [Al-Oraimi and Seibi 1995; Kriker et al. 2005]. The compressive strength was higher for water-cured samples than for air cured specimens, but the strength was always lower than in control tests without fibres [Kriker et al. 2005]. Mortar samples prepared with coir, sisal, jute and hibiscus cannebinus also exhibit lower compressive strengths than mortar without fibres [Ramakrishna and Sundararajan 2005b]. Concrete samples reinforced with kenaf fibres (V_f 1.2%) exhibit lower compressive strength corresponding with a higher water-cement ratio [Elsaid et al. 2011]. For higher fibre content, 2.4%, the lower strength was due to the presence of the fibres.

2.3.1.2   Bending and tension strength

Some natural fibres tend to increase the bending strength of the cement-based composites. The extent of the improvement depends on the fibre content and length, curing conditions, cement-matrix composition and mixing method. Flax fibres, for example, in mortars prepared following the slurry-dewatering method, increased the Modulus of Rupture (MOR) for composites that were air or water cured [Coutts 1983b]. In this study, the air-cured samples had a higher MOR than the samples saturated in water. In both conditions the bending strength increased with increasing fibre mass percentage until reaching an optimum amount of fibres between 8 and 10%.

Reported in literature, fibres from *agave sisalana* (sisal) benefit the flexural behaviour if the composite is prepared by slurry de-watering instead of cast-in-place. Savastano et al. [2003; 2005] prepared mortar with either kraft sisal (13.5 µm width), TMP sisal (10 µm width) or sisal slivers (135 µm width) following the slurry method. These composites exhibit enhanced flexural behaviour when compared to fibreless mortar. The samples with individual sisal fibres have higher bending strength than samples with sisal slivers but lower toughness.

Tonoli et al. [2007] tested composites with sisal fibres with different degrees of refinement. The refinement causes intense fibrillation of the fibres, favouring their plastification and mechanical anchorage in the cement-based matrix. However, excessive refinement caused some decay in the mechanical performance due to the shortening of fibres.

Savastano et al. [2003; 2005] tested samples prepared with kraft sisal and two types of cementitious materials, Ordinary Portland cement (OPC) and Blast furnace slag (BFS) with gypsum and lime. The samples with OPC have lower bending strength and lower water absorption.

On the other hand, Ramakrishna and Sundararajan [2005b] reinforced OPC mortar with sisal bundles (0.10 to 0.50 mm diameter) following cast-in-place procedure and achieved lower bending strengths than plain mortar without fibres. Samples with coir, jute and hibiscus cannebius fibres report the same results. Palm fibres also, tend to reduce the flexural strength of concrete [Al-Oraimi and Seibi 1995; Kriker et al. 2005]. Flexural and splitting strength values decrease with increasing amount of natural fibres [Al-Oraimi and Seibi 1995]. The pre-cracking behaviour was not affected by the addition of date palm fibres, but it had a significant effect on the shape of the post-cracking load deflection curve. Kriker et al. [2005] report that the first crack strength (FCS) for concrete with date-palm-fibres is lower than for concrete without fibres. The behaviour in bending is elastic until the FCS. This limit is linked with quality of concrete and the matrix flaws induced by the presence of fibres.

D´Almeida and colleagues [2010] tested composites reinforced with 2 to 6% of curaua fibres in four-point bending. These fibres are extracted from leaves of Ananas erectifolius plants. The fibres had lengths of 25 and 50 mm. A cast-in-place mixing procedure was

followed. The first crack strength decreased with increasing fibre content, but the post-crack strength increased with increasing fibre content. The post-crack strength increased even more for the longer fibres (50 mm). The samples with 4% and 50 mm fibres exhibited multiple cracking prior to failure.

Silva [2009b] used long, aligned sisal fibres (volume fraction 10%) as reinforcement in thin laminates prepared with cement based mortars as well as calcium hydroxided-free (CH-free) mortars. Both materials presented multiple cracking with strain hardening behaviour under tension and bending stress. The ultimate tensile strength was 14 MPa for CH-free samples and 9 MPa for the OPC samples. The module of rupture was about 22 MPa for both composites.

The splitting tension strengths of concrete reinforced with kenaf fibres (V_f 1.2 and 2.4%) were higher than in control fibreless samples [Elsaid et al. 2011]. The flexural module of rupture and toughness, on the other hand, decreased with the presence of the fibres.

2.3.1.3 Flexural toughness

Natural fibres enhance the flexural toughness of cement-based materials, even in cases where the bending strength was lower than samples without fibres [Al-Oraimi and Seibi 1995; Kriker et al. 2005]. Savastano et al. [2003] report higher values of fracture toughness for composites with kraft banana (*Musa cavendishii*) and composites with sisal fibres that were obtained through different pulping processes. The toughening in the natural fibre-reinforced composites occurs as a result of crack bridging. When comparing the behaviour of the different sisal fibres, it is evident that the pulping process affects the fibre failure mechanism. Mechanical pulp fibres tend to pullout and have little fracture. As a consequence the mortar samples with these fibres develop higher toughness.

According to the research from Coutts [1983b] the toughness of samples made with flax fibres increase as the fibre mass percentage increases. He also compares the MOR and toughness of flax reinforced composites and mortar with softwood or hardwood pulp, all with 8% fibre mass. The MOR is about the same for all composites but the toughness with flax fibres is about half the toughness with softwood and 80% of the value estimated with hardwood. The aspect ratio of the used hardwood fibres is the lowest of the three fibres types; the flax aspect ratio is the highest. A high aspect ratio leads to fibre entanglement, poor workability and ineffectual reinforcement [Campbell and Coutts 1980; Wu 2001]. In that way, the composites with flax fibres exhibited the lowest flexural toughness, while composites with hardwood fibres (lowest aspect ratio) developed more toughness.

The flexural toughness increased with increasing fibre content of curaua fibres [d´Almeida 2010]. For the same fibre content, samples with longer fibres exhibited higher toughness.

According to Silva [2009b] the toughness of composites with long sisal fibres and a CH-free matrix under tensile load was twice as that of samples with the same sisal fibre content and OPC-based matrix.

2.3.1.4 Impact strength

The inclusion of natural fibres improves the impact resistance of cementitious materials. Al-Oraimi and Seibi [1995] report enhanced resistance with date palm fibres. Ramakrishna and Sundararajan [2005a] tested sisal, coir, jute and *hibiscus cannebinus* (kenaf) in mortar with different fibre lengths and percentages, and the impact strength was always higher than in samples without fibres, sometimes up to 18 times higher. The composites with coir absorbed the highest impact energy, twice the energy of sisal and four times more than jute and kenaf

composites. The success of coir fibre as reinforcement is explained by its behaviour: coir fibres exhibit fibre pullout whereas all the other fibres exhibit fibre fracture at ultimate failure. For all fibres the maximum crack width and length were not sensitive to fibre type or content.

2.3.1.5 Shrinkage

The addition of flax fibres at various volume fractions and lengths did not have a significantly influence on the free plastic shrinkage (within first 24 h) [Boghossian and Wegner 2008]. The total crack area reduced from 212 mm^2 for plain mortar to 30 mm^2 for 0.05% of 19 mm flax and even to 0.14 mm^2 for 0.3% of 10 mm flax. But the number of cracks was higher for the fibre-reinforced samples. In plain mortar the shrinkage is accommodated by widening of 1 or 2 dominant cracks while in the mortars with fibres a larger number of small cracks appear. Silva [2009b] reported an increase of 40% of the drying shrinkage due to the presence of sisal fibres. The porous nature of the used sisal fibres created more moisture paths into the cement matrices, which contributed to the increased drying shrinkage.

2.3.2 Microstructure

The effects of the manufacturing method and curing conditions on the microstructure of the fibre-mortar composite have been studied for sisal and date palm fibres, respectively.

For slurry de-watered sisal composites the interface region was found to be dense due to the pressure applied in this method, with no calcium hydroxide present [Savastano et al. 2003; 2005]. This method applied pressure to dewater the samples. It is possible that during this process excess water is expelled from the fibres, creating a dense interface zone. In contrast, cast in place samples have shown somewhat porous interface transition zones up to 100 μm thick containing large calcium hydroxide crystals [Savastano and Agopyan 1999]. During casting, water tends to settle around the fibres due to their hygroscopic nature, creating zones of increased water-to-cement ratio and thus, increased porosity. Calcium hydroxide is the most soluble component of cement hydration and will, therefore, preferentially migrate to porous regions where it re-crystallises during the curing of the composite.

Kriker et al. [2005] analysed the compactness and degree of voids and cracks in date palm fibre reinforced composites using the continuity index (CI). The CI of fibre-concretes decreases with increasing fibre percentage. During the first 7 days the retention of water by the fibre has a beneficial effect, especially in hot/dry curing, which is reflected in higher CI values. After this period the evaporation of water into concrete produces a slowdown of the cement hydration processes as well as shrinkage of concrete. Then the CI values for all samples with fibres were lower than the plain samples. The SEM observations show that the voids around the fibres are large for samples in hot/dry environment. Looking at the interface in water cured samples the voids between the fibres and the matrix are filled with hydration products. This finding agrees with Toledo Filho et al. [2000] and Bentur and Akers [1989] regarding the mineralisation of vegetable fibres due to migration of hydration products.

2.3.3 Durability of composites with natural fibres

Cement composites reinforced with some natural fibres show loss of bending strength after either accelerated weather tests or natural weathering. Samples prepared using a slurry vacuum de-watering technique and reinforced with 8 wt% of sisal were tested after 2 years of external exposure to tropical weather. They exhibited a considerable reduction in bending

strength since the modulus of rupture of the composite decreased to 70% [Savastano et al. 2009]. Likewise, the toughness reduced from 0.85 kJ/m^2 at 28 days to 0.62 kJ/m^2 after 2 years of external exposure. The loss in mechanical strength of the composites was attributed to the degradation of both the vegetable fibres and the cementitious matrix. Roma Jr et al [2008] reported similar degradation in composites with sisal and eucalyptus fibres exposed to natural weather for 4 months. The natural fibres degrade by embrittlement. The phenomenon of petrification can take place through the migration of hydration products to the fibre lumens and pores, as mentioned above [Savastano and Agopyan 1999; Toledo Filho et al. 2000; Bentur and Akers 1989]. Whereas the loss of strength in the matrix based on BFS, can be a consequence of carbonation.

On the other hand, Tonoli and colleagues [2007] found that after submitting composites samples with sisal pulp to wet/dry cycles, the MOR increased and the water absorption decreased. These results were due to a better packing provided by the plasticized fibres and the continued hydration of the composites subjected to wet/dry cycling, and to a gradual carbonation of the cement matrix.

Concrete samples with *agave lechuguilla* fibres were tested after exposure to accelerated weather environments [Juarez et al. 2007]. The strength of the composites decreases with exposure to wet and dry cycles, as well as to aggressive chloride and sulphate environments.

CH free mortar samples reinforced with long, aligned sisal fibres (V_f 10%) did not suffer any mechanical degradation after 6 month submerged in hot water at 60°C [Silva 2009b]. On the other hand, OPC-based mortars with the same sisal fibre reinforcement presented single-crack failure behaviour (instead of multiple cracking) after ageing. For these composites the MOR decreased in 71%. Microstructure analysis showed that the fibres in the OPC composites were mineralized and had a high concentration of calcium while the fibres in the CH free composites showed no signs of deterioration and much lower concentration of calcium inside the fibre cells.

2.4   Concluding remarks

Wood and other natural fibres are being studied as reinforcement for cement-based materials because they are non-hazardous, renewable, low cost alternative to synthetic fibres. The mechanical properties of the composites depend on the type of fibre, its physical and chemical composition, the cement matrix, the mixing procedure and the curing conditions.

As reported in literature, wood fibres enhance the flexural strength and toughness of cement composites. Other natural fibres improve the composite toughness but have not yet proved to be beneficial for the bending strength in all the manufacturing processes. All fibres reviewed in this chapter lead to lower compressive strength of the concrete or mortar they reinforced. However, the inclusion of natural fibres improves the impact resistance of cementitious materials. Adding fibres to a cement-based mixture increases the surface area and therefore decreases the workability. So far, there is not much evidence whether this affects the fibre distribution at all, or if so, which mixing method will ensure a proper fibre distribution.

The sugar present in the chemical composition of hemicellulose and lignin in the wood fibres may have unfavourable effects upon the setting time of cement. To overcome this problem the fibres can be treated and/or the cement matrix can be modified through chemical additives. Hardwood is more an inhibitor to cement setting than softwood, because of both its chemical composition and extractives.

Low percentages of cellulose fibres reduce the plastic shrinkage in both normal and high performance concrete [Sorousian and Ravanbakhsh 1998], but do not decrease the absolute shrinkage value [Vares et al. 1997]. Mechanically obtained wood fibres and wood powders reduced the autogenous shrinkage of the cement-based composites [Mohr et al. 2005b]. Chemically obtained kraft fibres and cellulose powders, on the other hand, have not been effective for internal curing applications [Mohr et al. 2005b].

During the first 24 hours of curing the formation of hydroxide bridges in-between fibres or between fibres and the cement matrix may explain the possibility of a chemical bond between fibres and matrix. However, in case after these 24 hours the matrix is water-cured some authors hypothesize that the hydrogen bonds break by insertion of water molecules between the covalent bonds. As a consequence, fibres tend to pullout during bending of the composite, rather than fracturing due to a strong fibre-cement bond that forms when the matrix is dry-cured. However, fibre swelling during water-curing may present a competing effect by creating additional physical friction force with the cement matrix, in which case the composite behaviour would depend on whether this frictional force overcomes the lack of chemical bonding between the fibre and matrix. Unfortunately there is insufficient data on mechanical properties for both wet and dry cured matrices to support the findings at the microstructure level. Finally, the interfacial bond, and therefore also the behaviour, strength and failure mode of the composites, are also influenced by the geometry of the fibres.

Regarding the durability of composites with wood and cellulose fibres, most authors agree that after ageing with wet/dry cycles the flexural stress and toughness of the composites decreased. But there were no significant differences in certain mechanical properties after freeze/thaw cycles. Cement composites reinforced with some natural fibres reported loss of bending strength after either accelerated weather tests or natural weathering.

Production of Sisal Fibres

Agave sisalana plants in Yucatan, Mexico

Decortication, leaves are crushed and beaten

Decortication, leaves are crushed and beaten

After washing, the fibres are dried
Later they will be brushed and packed

Wood and Other Natural Fibres

3.1   Introduction

In this chapter the study on a variety of natural fibres is discussed in order to determine the most suitable natural fibre for reinforcing cement based material. The natural fibres that have been studied are: spruce, larch and pine (three different types of softwood fibres) as well as sisal and abaca fibres.

In this chapter first the fibres itself and their production procedures are described. Then, the mechanical properties of these fibres will be experimentally investigated using direct tensile test. Images captured under environmental scanning electron microscope (ESEM) and with stereomicroscope are used to interpret both the fracture mode and micro-structural properties of the fibres. Additionally, the durability of the fibres in an alkaline environment such as cement-based materials is investigated by means of measuring the changes in tensile capacity and Young's modulus of the fibres. Finally, conclusions are drawn about the fibres and their suitability to be used as reinforcement in cement based materials.

3.2   Selection and production of fibres

3.2.1   Wood

Wood is generally classified in softwood and hardwood. Based upon their physical and chemical properties, softwood fibres were chosen for the present research project. Softwood cells are more uniform in size throughout the tree than hardwood fibres and softwood fibres have a more simple form without vessels. Additionally, in softwood the fibres are generally longer than 2 mm while hardwood fibres average about 1 mm long. Even more important is that hardwoods are more susceptible to attack by both acids and alkalis than softwood. Since cement-based materials exhibit an alkaline environment, this was a strong reason to prefer softwoods for this project. Finally, hardwood is more an inhibitor to cement setting than softwood is [Swamy 1988].

Single wood fibres were considered to be too short as reinforcement. Instead the author prefers naturally bonded groups of fibres, also referred to as bundles, for the research.

Two commercially available wood products, other than single fibres, were studied. Eltomation BV provides the first product: this company uses wood fibres and bundles to prepare wood cement boards. Eltomation BV supplies long continuous fibres called Wood Wool with length 250 mm, a width of 0.75 mm and a thickness varying from 0.1 to 0.5 mm. In the northern hemisphere this product is prepared mainly from pine and poplar trees, hence both softwood and hardwood, though in general they find hardwood less suitable.

The fibres are produced by cutting round wood logs into blocks of approximate 50 cm length after which the blocks are shredded into the long fibres [www.eltomation.com]. The aspect ratio of the as-delivered fibres is high, ranging between 100 and 500, but in a preliminary hand inspection the long fibres easily brake into pieces of 5 to 50 mm, reducing the aspect ratio to low values of 6 or 10. Since no information of the fibre strength was given the fibres were tested. Based on test results the estimated fibre strength is 33.3 MPa and the modulus of elasticity about 2.2 GPa. Both the strength value and the fibre aspect ratios is too low for a possible reinforcement for cement-based materials, hence these fibres were judged as unsuitable for the research here reported.

The company J. RETTENMAIER & SÖHNE GmbH + Co. KG supplies another fibre option. This company produces wood and pure cellulose fibres. The wood fibres, under the name of Lignocel, are obtained from selected conifers. For testing purposes the product Lignocel grade 3-4 that has a longer fibre length was chosen. The fibre grain size is between 1.5 and 4 mm. The sieve residue is 15 to 50% for the 2 mm mesh size and has a maximum of 3% in the 4.5 mm mesh. With a fibre width average of 3 mm and a thickness of about 0.4 mm, the aspect ratios are 1.3 and 10. These are again very low ratios. According to the material safety data sheet the fibres have approx. 50% of cellulose, 25% hemicellulose and 25% lignin. The fibres are produced with a mechanical method and are not treated. Due to the small size of the fibres and laboratory equipment constraints it was not possible to test the fibres for their strength. These fibres were not considered after testing cement composites reinforced with them.

Since the size and tensile strength of the available commercial fibres were not suitable for this research it was necessary to prepare wood bundles at the laboratory. Three different softwoods were chosen for their availability in the Netherlands as well as their properties: spruce, pine and larch. Spruce and pine, both conifers, are evergreen trees. Although a conifer larch is also a deciduous tree, it looses leaves in fall. Larch wood is tough and waterproof. Spruce is considered as suitable material for paper products because its within-ring wood density variation is small, wood density is moderate-to-low and its fibres are thin-walled [Walker 2006]. Dried spruce absorbs less water than European redwood (Pinus Sylvestus) [Fraaij 2007]. Pine, fast growing softwood, is popular for structural applications that will withstand high loads. Both spruce and pine have no insect or decay resistant qualities after logging.

Two different processes were followed to produce the bundles of fibres: A semi-chemical and semi-mechanical method for the spruce and larch fibres and a full-mechanical method for the pine fibres. In a semi-chemical pulping process wood chips were treated with chemicals at high temperatures in order to remove some lignin and hemicelluloses, after which the partially softened chips were mechanically defibred [Walker 2006]. The most commonly used semi-chemical pulping process is the neutral sulphite semi chemical (NSSC) procedure, which has high pulp yields (75-85%) as opposed to 50 to 55 percent for other chemical processes [Biermann 1996; www.epa.gov].

Small lumber blocks of spruce and larch were cooked following the NSSC process; a process developed by the U.S. Forest Products Laboratory in Madison, USA for using hardwood in the paper industry. In this process the fibres are partially delignified using less chemical and shorter cooking times than in full chemical pulping [Walker 2006]. In this thesis, for the pulping stage the cooking liquor is prepared by adding 13.5% of sodium sulphite and 4.5% of sodium carbonate anhydrous to deionised water at room temperature. The solution is then mixed for 2 to 3 min at a temperature of about 40 ℃ until all the solid parts have dissolved. The pH of the cooking liquor is between 7 and 10, hence neutral to

moderately alkaline. Small lumber blocks of spruce and larch ($1\times1\times2$ cm) are then submerged in the solution in an autoclave and placed in the oven at a high temperature (180 ºC) for 3 hours. During the cooking time sulphite ions react with the lignin in wood [www.epa.gov]. The sodium carbonate is added to neutralise wood acids released by hydrolysis of the hemicelluloses and to maintain a pH between 8 and 10. Carbohydrate losses increase considerably near the end of the process, so there is a practical limit to the extent of delignification without having a serious loss in yield and strength [Walker 2006]. Once finished the process time the blocks are washed with fresh water. Finally, the blocks were manually taken apart into bundles with an average number of 65 fibres in its cross section. Figure 3.1b shows the larch fibres produced following this procedure.

Following the NSSC process results in bundles with aligned fibres, because the bundles are taken apart in weak points where the bond between fibres was softened by the chemical process. Even though aligned fibres in a bundle will enhance the mechanical properties, there are 2 important disadvantages from using the NSSC process. In the first place, as the bundles are taken apart manually the cross sections of the bundles are not uniform in either shape or size. (figures 3.2 a, b and c). Another drawback is that the process is extremely time consuming. Therefore the author decided to use a faster way to produce bundles of wood fibres by cutting them out of commercially available veneer sheets.

(a)   (b)
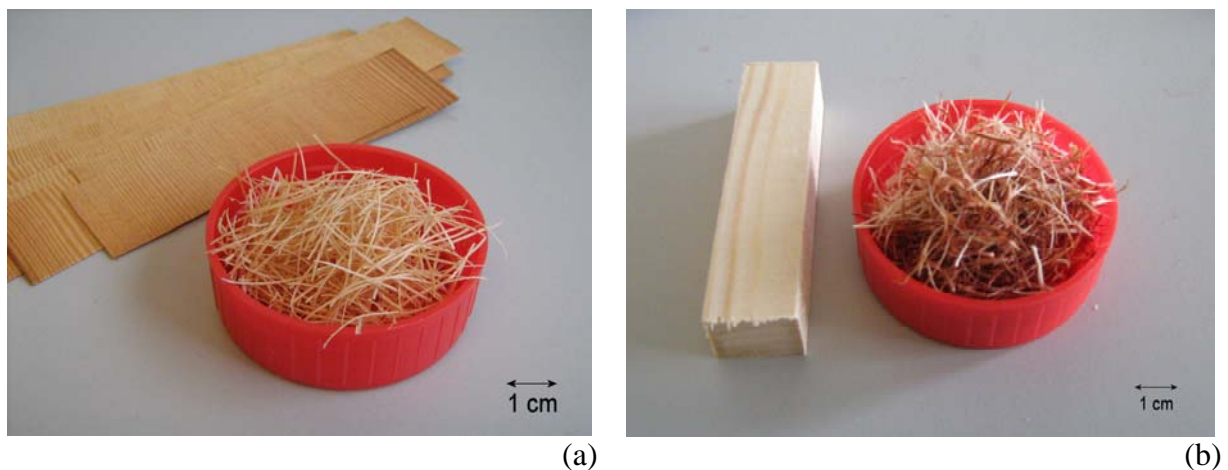
Figure 3.1: Pine fibres produced from veneer sheets (a), larch fibres produced from lumber blocks (b).

(a)   (b)   (c)
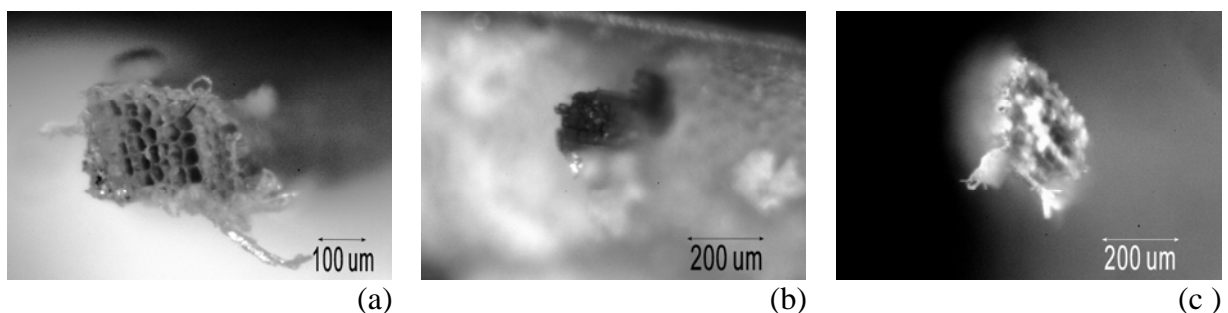
Figure 3.2: Cross sections of softwood fibres
Rectangular for Pine (a), Circular for Spruce (b) and Diamond shaped for Larch (c).

According to the literature review in section 2.2.3, composites with mechanical pulp have lower compressive and bending strength compared to composites with kraft pulp. Additionally it has been reported that mechanical pulp is less effective than kraft pulp in increasing fracture toughness. However, these studies were done with longer mechanical fibres than kraft fibres. For example, Soroushian et al. [1990; 1994] used mechanical fibres of 8 mm long and kraft fibres of 0.9 or 3 mm. Thus, cutting the bundles at the same length will neutralize the effect upon the behaviour due to fibre length.
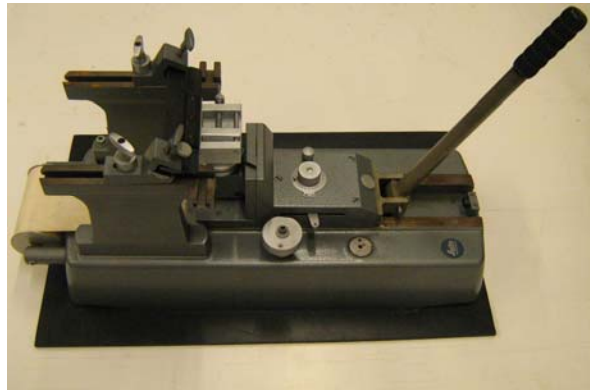
Figure 3.3: Base sledge microtome.

Veneer sheets of Oregon Pine (Douglas fir), supplied by Haagse Fijnhouthandel BV, were cut, as received, into bundles using a base sledge microtome (figure. 3.3). The bundles have a rectangular cross section, the long side being the thickness of the veneer sheet of about 0.50 millimetres and the short side was set in the microtome to be around 0.25 millimetres. These bundles have a rather constant cross section shape and size. A bundle from earlywood has a cross section with approximately 66 fibres, whereas in a cross section of a bundle from latewood there are about 120 fibres. When cutting the bundles, they were aligned as much as possible for them to have straight aligned fibres, but that was not always achieved. This is a clear disadvantage of the mechanical method: the bundles can be cut diagonal to the fibres alignment and resulting in a lower bundle tensile strength. These mechanically obtained bundles are chemically unaltered and rich in lignin [Walker 2006]. The pine fibres were all prepared from the veneer sheets. Figure 3.1a shows pine fibres and the veneer sheets. For simplicity they will be referred to as pine. For convenience the bundles will from now on be referred to as fibres.

The fibres were studied with the ESEM. All wood fibres studied have thin cell walls and, therefore, bigger lumen than the sisal fibres in which hardly any lumen can be seen. Because of the production process, the mechanically produced fibres are different from the NSSC fibres. The pine fibres have rectangular shape and a bigger and more uniform cross section than the other fibres studied. The larch and spruce fibres have a more rounded-shape cross-section, but the size and shape of it varies considerably from fibre to fibre.

3.2.2   Sisal

The company STW Schwarzwaelder Textil - Werke, supplied sisal fibres with an average length of 10 mm. The fibres were cleaned in warm tap water and let to dry before being mixed with the cement based material.

3.2.3   Abaca

The abaca plant (musa textilis) is a plant related to the banana plant. The fibre obtained from this plant is called Manila hemp. It has a long fibre length and is a versatile, all-purpose pulp that can be used for making different types of paper. [Dawson and Turner 1995]. These fibres are resistant to weathering and salt water [Barros-Cabezas 2008]. The abaca fibre used in this research was produced in Ecuador. It was cut into fibres of about 2.5 mm long and then treated with a solution of 1 part lime and 10 parts of water [Barros-Cabezas 2008]. The lime treatment serves to several purposes. In the first place it cleans the fibre from impurities from the extraction treatment. Additionally the treatment protects the abaca against deterioration because of the alkalinity of concrete paste. Finally, treated fibres may have improved roughness that leads to enhanced mechanical bond with the cement matrix.

3.3   The mechanical properties and microstructure of wood and sisal fibres

3.3.1   Mechanical properties

The use of wood fibres as reinforcement in cement-based materials first requires an understanding of the mechanical behaviour of the fibres themselves. Mechanical properties of single wood fibres are reported in literature [Sedighi Gilani 2006; Mott et al. 1995; Page et al. 1977] but there is no information available about bundles of fibres. Therefore it is first necessary to study the monotonic tensile behaviour of the proposed softwood fibres.

The fibres were tested under direct tensile strength using a micro tension-compression testing device (developed by Kammrath & Weiss). Figure 3.4 shows the setup. The fibre was glued to two steel non-rotating loading plates prior to being tested under deformation control. The glue is a two component epoxy resin. The tests were done at speed 2 μm/s while the load was measured with a 50N load cell. The displacement of the fibre is given by the displacement of the actuator (± 6 mm). All tests were conducted at laboratory conditions between 30 and 50 RH and about 22°C. The tests results are shown in table 3.1.
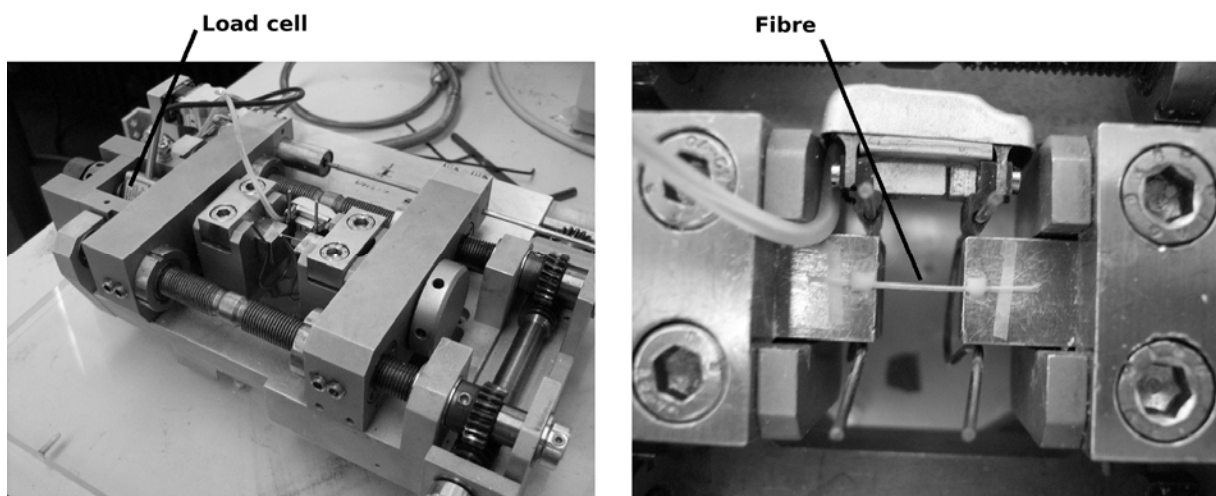
Figure 3.4: Tensile test setup.

*Table 3.1: Dimensional and mechanical characteristics of the fibres investigated.
(Standard deviations are indicated between brackets)*

Fibre	Tensile strength σ_f (MPa)	As-measured Young's modulus E_f (GPa)	Young's modulus corrected for compliance E_f (GPa)	Area (mm^2)	Strain to Failure (%)	Number of Tests
Larch	231.8 [77]	9.4 [3.3]	9.9 [3.6]	0.067 [0.026]	2.6 [0.4]	10
Spruce	169.3 [36]	7.7 [3.7]	8.1 [3.9]	0.059 [0.036]	2.4 [1.0]	10
Pine	123.9 [75]	4.5 [2.6]	4.7 [2.9]	0.106 [0.039]	3.2 [1.2]	50
Sisal	330.0 [50]	6.0 [2.8]	6.3 [3.0]	0.057 [0.045]	6.0 [1.7]	10

The mechanical properties of bundles of softwood fibres, similar to those tested for this research project, have not been found in literature. Only references to the properties of lumber or single fibres can be found. A piece of softwood lumber without defects could have a tensile strength of 70 MPa (pine) to 134 MPa (larch) [Wood handbook 1974]. The strength of the chemical bonds of cellulose, the basic molecule that makes up the wood fibres, have been estimated around 7000 MPa [Soroushian and Marikunte 1990]. In chapter 2 a summary of mechanical properties for softwood single fibres was presented and Campbell and Coutts [1980] reports results from other researchers for modulus of elasticity and tensile strength for single fibres. The modulus of elasticity can be as low as 9 GPa for dried early wood that had no restriction when drying or as high as 100 GPa for chemically separated fibres. The tensile strength has been estimated between 200 and 1500 MPa. The values reported in table 3.1 fall into these estimates, considering that the results shown here are for bundles of fibres and the values mentioned in literature are for single fibres.

When using the displacement of the actuator of the testing device to determine the extension during the test, it is necessary to take into account the compliance of the machine. The specimen is assumed to be connected in series with the load cell in the testing machine and this series connection gives the total stiffness of the system (k_{total}). For each test the total stiffness is calculated from the test results. Since the stiffness of the load cell and the machine (k_c) is known the stiffness of the specimen (k_s) can be calculated as:

$$\frac{1}{k_s} = \frac{1}{k_{total}} - \frac{1}{k_c} \tag{3.1}$$

The ratio k_s/k_{total} increases as k_t increases. For the fibres tested in this project, the values of k_{total} were between 0.01 and 0.36 N/μm.

The scattering of the tests results can be explained by three factors: the test conditions, the fibre characteristics and the area measurements. Using precise methods as is described in section 3.3.2 reduces the influence of the area measurement. The physical and mechanical properties of natural fibres exhibit an inherent variability. The effect of the fibre characteristics will be described below.

The fibres prepared following a semi chemical process have higher tensile strength than the fibres that are mechanically prepared. As can be seen from table 3.1 the tensile strength of pine fibres is 123.9 MPa, while for larch values of 231.8 MPa are found. The lower strength may be due to the fibre production process. As mentioned in section 3.2.1, spruce and larch are first cooked and later the fibres are torn from the cooked blocks along the weak points. Due to this method, the bundles have aligned fibre cells, where the mechanically prepared pine fibres may or may not have aligned cells.

Table 3.1 also illustrates other differences between the NSSC fibres (larch and spruce) and pine. The failure strains of larch and spruce are about 2.5%, while pine fibres have a failure strain of 3.2%. This higher strain capacity together with a lower strength for pine results in a lower Young's modulus. Besides having a different cross section shape, the mechanical fibres have a considerably bigger area than larch and spruce.
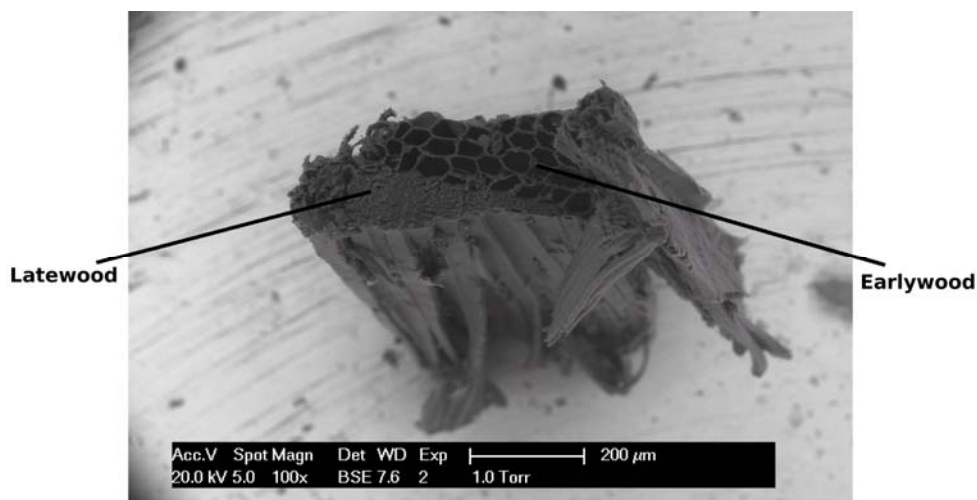
Figure 3.5: Pine fibre with earlywood and latewood.

The variability in the mechanical properties of the wood fibres studied is likely due to the variability in the microstructure of the fibres as well as from possible damage created during the production process. Independent from this process, the different types of wood fibres were prepared indistinctly from earlywood or latewood (figure 3.5). Earlywood cells have relatively large lumen and thin walls. Meanwhile cells with smaller lumen and thicker walls characterize latewood [Wood handbook 1974]. Boatright and Garret [1983] mention cell size as a dominant influence on wood fracture behaviour, in particular the different diameters and thickness in earlywood and latewood. In the study from Sedighi Gilani [2006] earlywood from softwood is characterized with Young's modulus of 2.35 GPa in contrast with latewood with a Young's modulus of 3.40 GPa.

A bundle with a very small cross section area has a little amount of fibres. The minimum will be the area of 1 single fibre cell, and the tensile strength will be as high as the values reported in literature and presented in Chapter 2: 200 to 1500 MPa for single fibres of softwood species. As the cross section area increases and therefore the amount of fibres in such a cross section, the tensile strength decreases. Apart from the tensile capacity of the single cells, the bond between cells plays an important role in the bundle composite strength. The bond between cells is weaker than the cells themselves as explained in section 2.2.1. The fibre cells and the bundles have defects either inherent to their nature or induced by the preparation process. If the amount of fibre cells increases the amount of defects and their

influence will increase as well. Figure 3.6 illustrates this relation between the tensile strength of spruce bundles and the cross sectional area. Although not statistically significant, the estimated strength values tend to decrease with increasing area, for an area smaller than 0.05 mm^2. For bigger areas the strength will increase until reaching a stable value, independent of increasing cross sections, when the bundle starts behaving as a homogeneous material. More tensile tests with bigger bundles, however, are necessary to confirm this theory.
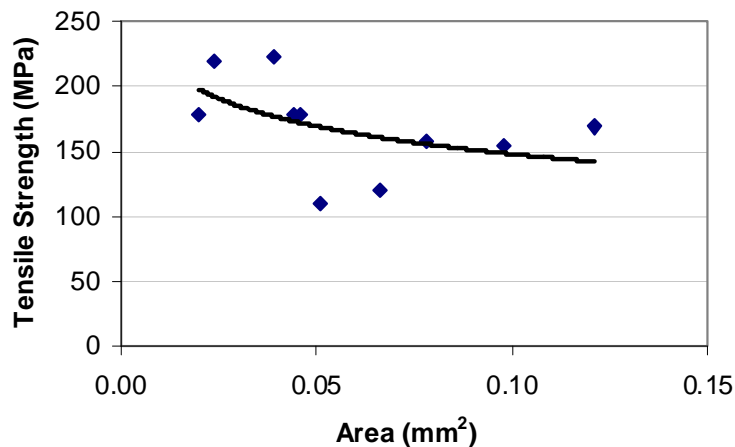
Figure 3.6: Tensile strength vs. cross sectional area for spruce fibre.s

The pine bundles have a bigger area than spruce fibres. The tensile tests show increasing strength values for increasing areas. But as is evident in figure 3.6, from the spread data, the cross section area is not the only factor affecting the tensile strength. The mechanically prepared pine bundles have a degree of alignment. The upper zone of the data in figure 3.7 must have a higher degree of alignment and therefore higher strength than the data in the lower zone. In both zones the strength increase with increasing cross section area. This fibre-orientation effect has been observed in wood as a building material. According to Bijen [1989] the tensile strength of wood varies depending on the orientation of the fibres from 100% when the fibres are parallel to the applied load to 5% when the fibres are perpendicular to the applied load.

For pine, spruce and larch the tensile strength, elastic modulus and strain to failure values were independent of the gage length.

Sisal fibres have higher tensile stength than the tested wood fibres. The calculated strain to failure for sisal was also higher. The results for sisal fibres are slightly different to the values found in literature [Silva 2009b]. The average tensile strength (330.0 MPa) and Young's modulus (6.0 GPa) are lower than the values reported by Silva [2009b] of 390 MPa and 10 GPa each. The average cross-section area of the tested fibres reported in this thesis, 0.057 mm^2, is slightly bigger than the average cross-section area of the fibres tested by Silva, 0.045 mm^2. Finally the strain to failure 6% is higher than the strains reported by Silva, 5.2% or less.

It was not possible to test abaca fibres under direct tension. The fibres slipped during the test. Attemps were made to perform pullout tests with these fibres but those tests were also not successful. Finally, the fibres were used as reinforcement in composites, and the composite samples were tested under compression and bending tests. The tests results show no improvement in the mechanical properties of the composites due to the presence of fibres,

thus the abaca fibres were discarded as possible reinforcement for the cement matrices studied in this thesis.
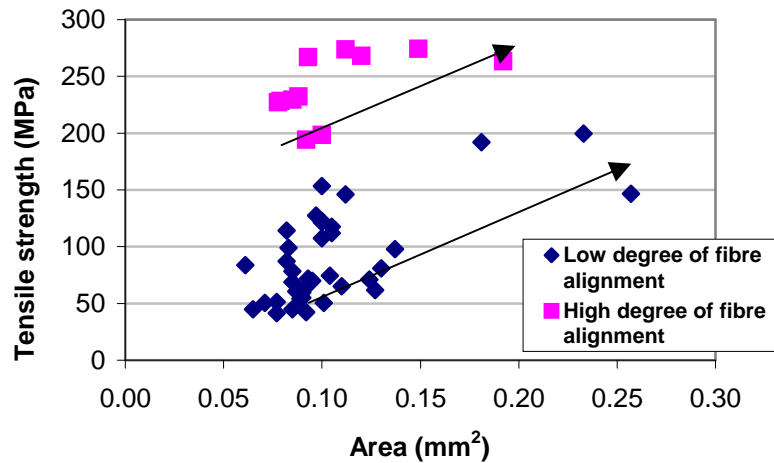

Figure 3.7: Tensile strength vs. cross sectional area for pine fibres.

3.3.2 Fibre microstructure

The fibre microstructure was investigated using a stereomicroscope and the ESEM. When possible, the fibre cross sections at the fracture were photographed as well as a cross section of an adjacent piece of the tested fibre. The obtained images were post-processed using the program ImageJ (National Institutes of Health, Bethesda, Maryland). As shown in figure 3.8 a contour line was drawn to delineate the fibre cross section after which the program computed the area. The area was calculated as an integral of the whole cross-section of the fibre, including the lumen and micro pores inside the cell walls.
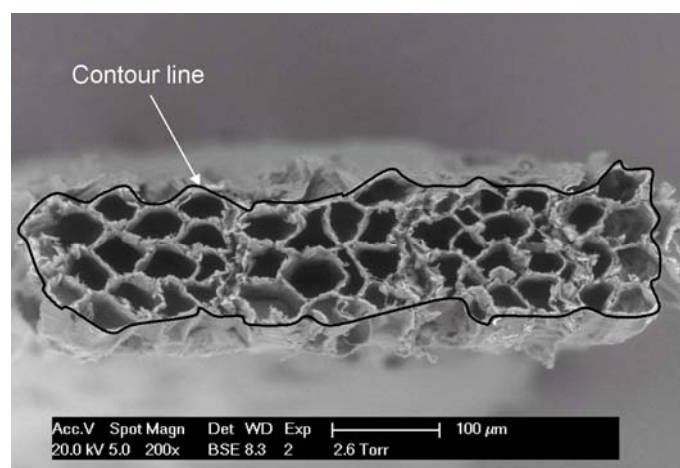
Figure 3.8: Image calculation

Softwood has groups of cells oriented horizontally in the direction from the pith toward the bark. These groups are called rays and they conduct sap radially. The presence of rays in a

fibre acts as a reinforcement or as a place where stress concentrations are introduced, as can be seen in figure 3.9, where the fibre fracture takes place just after the rays.
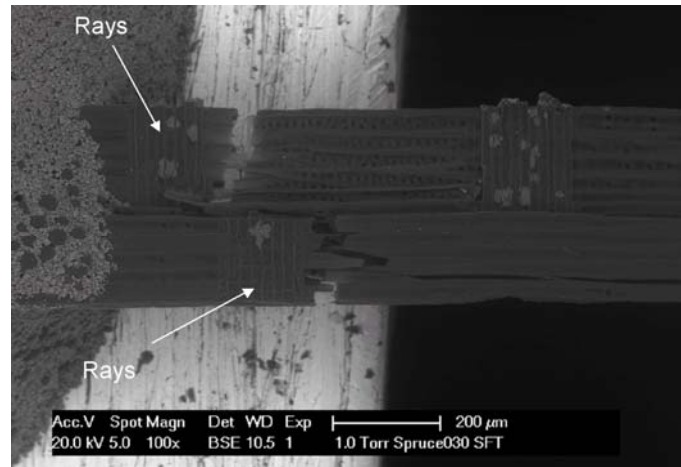
Figure 3.9: Fibre failure next to rays.

Some tensile tests were performed inside the ESEM and video recorded, which makes it possible to observe the fracture process of the fibres as well as their lateral deformation. The images were later interpreted with the aid of an image analysis system.

(a)

(b)
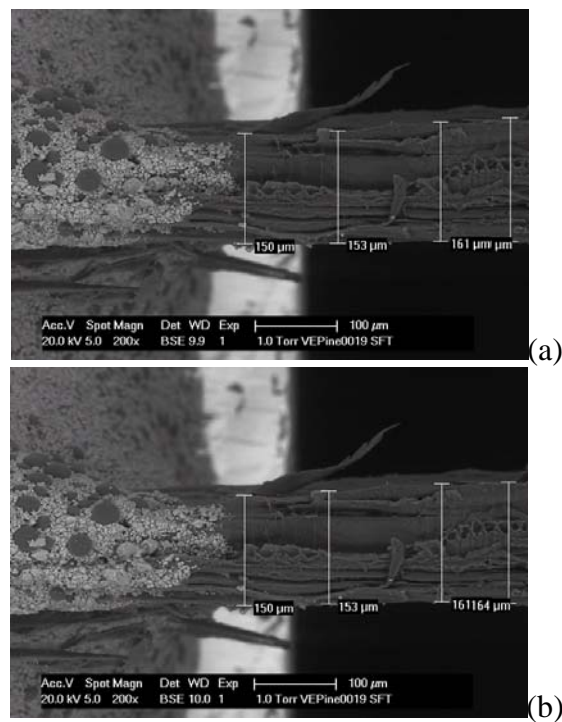
Figure 3.10: Poisson's ratio of pine fibres (null)
Fibre at the beginning of the tensile test (a) and just before failure (b).
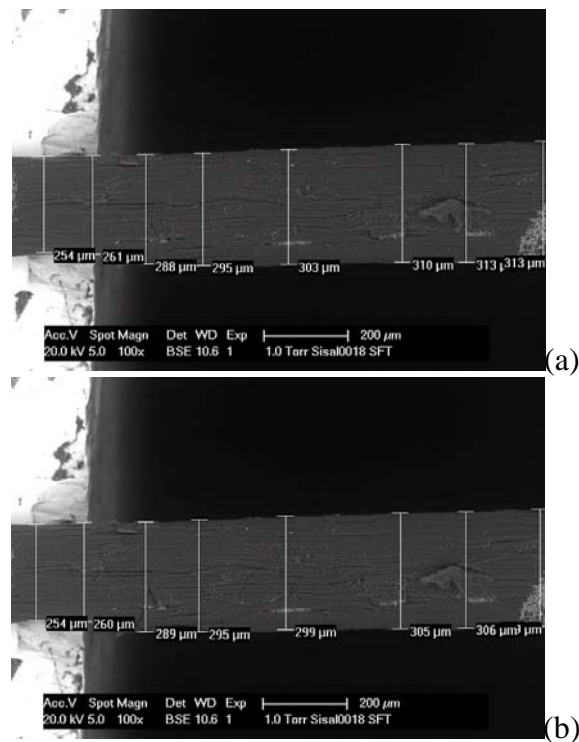
Figure 3.11: Poisson's ratio of sisal fibres = 0.37
At the beginning of the tensile test (a) and just before failure with reduced cross section (b).

The lateral deformation of the tested softwood fibres appears to be less than 1%, thus the Poisson ratio is almost zero for the wood fibres (figure 3.10). In contrast, the sisal fibres under tension show microcracking and some lateral deformation before breaking (figure 3.11). A calculated Poisson ratio of 0.37, is slightly higher than values reported in literature of 0.32 [Chandramohan and Marimuthu 2011]. The modulus of elasticity for sisal fibres reported in that study, 9 to 22 GPa, is also higher than the modulus calculated after the sisal tested for this thesis, 6 GPa. Because of this fracture behaviour the sisal fibres were discarded as possible reinforcement for the cement-based materials.

(a) Spruce   (b) Larch   (c) Pine
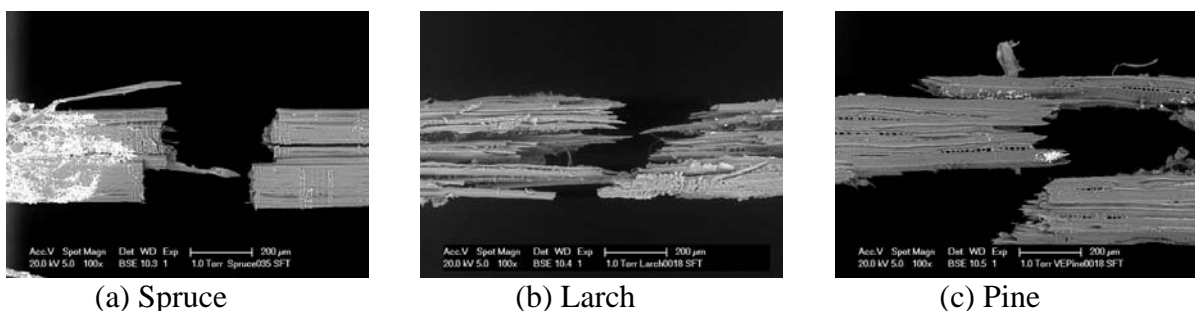
Figure 3.12: Characteristic predominant fracture behaviour for different wood fibres.

Examination of the fracture surfaces shows three different processes taking place: fracture of the fibre cells, delamination within the fibre cells and delamination between the cells. All three processes were observed in the three types of fibres tested, but each type had a

predominant behaviour, as can be seen in figure 3.12. Spruce fibres tend to undergo fracture of the fibre cells. The fracture of cells is seen at microlevel, at a magnification of at least x100. Under the stereomicroscope the fracture surface of the spruce fibres is seen as a rather sharp cut. The samples from larch under tension tend to delaminate within the fibre cell and between the cells. This behaviour takes place because of the weakening of the lignin and hemicellulose during the tension loading. Failure of the Oregon pine samples starts with delamination between groups of fibres followed by fibre fracture.

   The stress-strain curve for a given tensile test reflects the fibre fracture behaviour. In figure 3.13 the larch fibre L1 delaminated prior to failure. Due to this delamination the slope changes several times during the loading, after 1.1% and 2% strain. Another larch fibre L3 exhibits mainly fibre fracture. Figure 3.14 shows the stress-strain curves for two pine fibres, P1 and P2. For the fibre P1 the non-linear portion of the curve prior to failure is due to delamination.
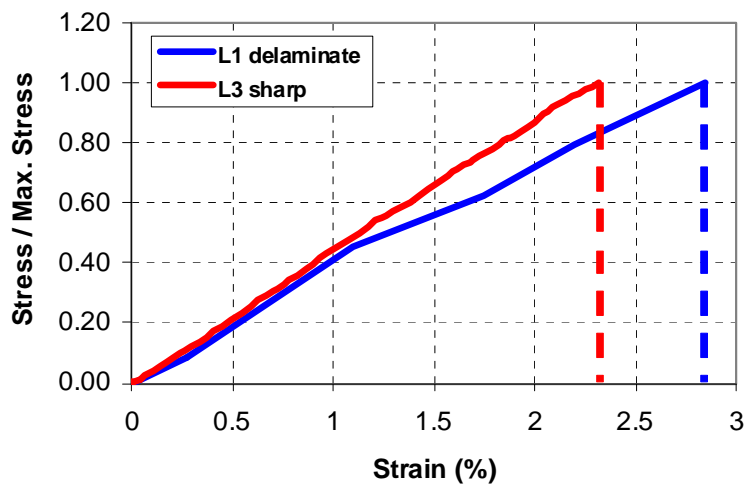
Figure 3.13: Stress-strain curves for two larch fibres.
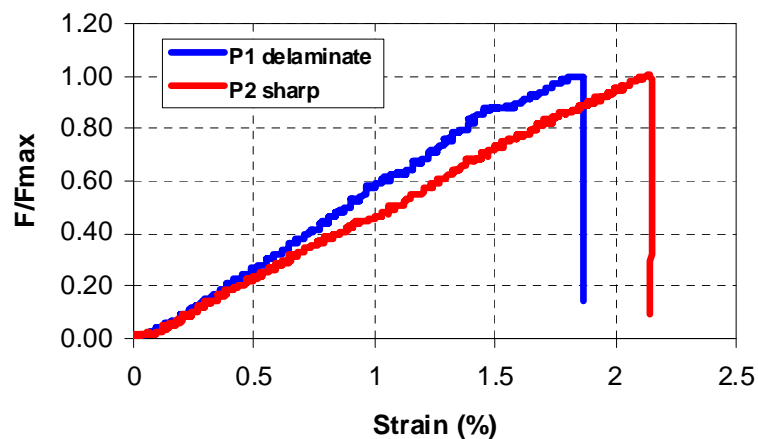
Figure 3.14: Stress-strain curves for two pine fibres.

3.4   Chemical durability of fibres

3.4.1   Introduction

When exposed to an alkaline environment, such as cement-based materials, wood can suffer serious degradation. Alkaline solutions are more destructive than acidic solutions, and hardwoods are more susceptible to attack by both acids and alkalies than softwood [Wood handbook 1974]. Two different mechanisms cause the wood to deteriorate in the cementitious materials. The first mechanism is the chemical decomposition of the lignin and hemicellulose from the middle lamella breaks the links between single fibres and, as a consequence, reducing the tensile strength. The second mechanism is the crystallization of lime from the cement matrix in the lumen and middle lamella, which leads to the decrease of flexibility and strength of the fibres [Silva 2009b]. The extent of the degradation can be determined by the strength loss after exposure to acid and alkaline environment.

3.4.2   Chemical durability test procedure

Pine fibres were submerged in solutions with pH 14, 12, 10, 8 and 6. The alkaline solutions (pH> 7) used were sodium hydroxide (NaOH) solutions. NaOH is a key component of the white liquor solution used to separate lignin from cellulose fibres in the Kraft process: while the sulphide ions break the phenol the NaOH maintains the high pH. A solution with pH 6 was prepared with hydrogen chloride HCl. The pH of the solutions was monitored along the 2 years that the fibres were kept in them and the changes were reported. The tensile strength of the fibres was tested after 6 months, 1 and 2 years.

Table 3.2: Dimensional and mechanical characteristics of the pine fibres investigated (Standard deviations are indicated between brackets)

Pine fibres	Ageing time (Months)	Tensile strength σ_f (MPa)	Young's modulus E_f (GPa)	Corrected Young's modulus E_f (GPa)	Area (mm^2)	Strain to Failure (%)	Number of Tests
Untreated		123.9 [75]	4.5 [2.6]	4.7 [2.9]	0.106 [0.039]	3.2 [1.2]	50
In pH6	6	82.7 [5]	4.3 [2.4]	4.4 [2.5]	0.078 [0.009]	3.1 [2.0]	4
In pH8	6	105.7 [88]	6.0 [3.3]	6.3 [3.6]	0.089 [0.006]	2.7 [1.5]	5
In pH10	6	76.3 [7]	4.5 [0.7]	4.6 [0.7]	0.087 [0.001]	1.6 [0.0]	4
	12	146.4 [110]	6.2 [3.6]	6.6 [4.0]	0.097 [0.032]	2.7 [1.0]	11
	24	231.2 [93]	6.6 [2.2]	7.1 [2.6]	0.087 [0.021]	4.3 [1.6]	9
In pH12	12	151.9 [108]	6.6 [4.5]	7.0 [4.9]	0.086 [0.016]	2.6 [0.8]	11
	24	66.8 [42]	2.6 [2.2]	2.7 [1.9]	0.087 [0.090]	2.6 [2.7]	9
In pH14	12	49.5 [38]	3.6 [2.3]	3.7 [2.5]	0.073 [0.015]	1.6 [0.5]	9
	24	33.4 [30]	2.3 [1.9]	2.4 [2.0]	0.085 [0.011]	1.3 [0.4]	6

The results are summarized in table 3.2 and graphed in figure 3.15. Although there are large variations in the tensile test results, the fibre average tensile strength decreases after 6 months in a NaOH solution with pH 6, 8 and 10, when compared to the average tensile

strength of untreated fibres. Fibres in higher pH solutions were not tested at this stage. After 1 year the strength of fibres exposed to pH 10 and 12 have an average strength slightly higher than untreated fibres. After 2 years in the alkaline solution the fibres in pH10 has almost double the average tensile strength, while the strength for fibres in pH12 has dropped below the average value for untreated fibres. Fibres in the solution with the higher pH 14 decrease the tensile capacity after 1 and 2 years. The longer time in the solution the more degraded the fibres are. The mechanical properties of the fibres in pH10 improve from the initial 6 months submerged in the solution, to the final ageing time of 2 years.
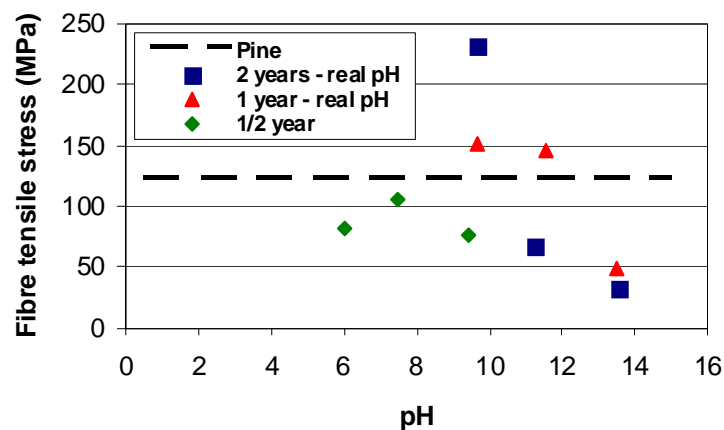
Figure 3.15: Fibre tensile strength in different pH environment

To determine whether a chemical reaction was taking place between the wood fibres and the alkaline solution some tested fibres were grinded and tested with Mid Infrared Reflectance (MIR) spectroscopy. With this technique the molecular structure of the organic compounds of a material is determined by detecting the strength of light that is absorbed by or passes through the material. Except optical isomers, each compound has its own specific IR absorption spectra [Li et al. 2010]. Mid infrared spectroscopy has been a useful tool for the determination of wood components, especially lignin [Schwanninger et al. 2004]. The wavenumber range of MIR is from 4000 to 600 cm^{-1}. This region is highly sensitive to the precise chemical composition of a material.

Mid-infrared spectra were collected at room temperature with a Spectrum 100 FT-IR spectrometer (by Perkin Elmer). FT stands for Fourier transform. The spectrum of each wood fibre sample was obtained by taking the average of 5 scans, and was corrected against the background spectrum of air. Instrument control and spectral collection were performed using Spectrum software (version 6.1, Perkin Elmer). At least 3 samples from each fibre type were tested. Mayor spectral changes were assigned to chemical bonds using published data.

Figure 3.16 presents the spectra for untreated pine and pine treated in solutions with pH10 and pH12. In the three spectrum a broad band can be observed in the region 3600-3200 cm^{-1}, attributed to stretching of the hydroxyl (OH) groups, and 3000-2800 cm^{-1} attributed to CH stretching [Poletto et al. 2011; Chen et al. 2011].

Alkali treatments change the crystal structure of cellulose from Cell I to Cell II. The original Cell I crystal structure is transformed into different Cell II lattice structure, which has been reported as thermodynamically more stable [Gwon at al. 2010]. Evidence of this shift of Cell I to Cell II can be seen in the wavenumber change from 1159 cm^{-1} (untreated pine) to

1146 cm^{-1} (pine in pH10) and 1144 cm^{-1} (pine in pH12). The band at 1159-1144 cm^{-1} is assigned to C-O-C asymmetric stretching in cellulose and hemicellulose [Smith 1999; Olsson et al. 2011]. The Cell-I band at 1430 cm^{-1} is gradually lost with increasing pH treatement. The Cell-II band at 1420 cm^{-1} remains regardless of the treatment. These wavenumbers correspond to C-OH bending in cellulose. Between 1400 and 1450 cm^{-1} there is an absorbance increase for treated fibres. These bands are assigned to –CH$_2$ symmetric bending in hemicellulose and C-H assymetric deformation of lignin [Olsson et al. 2011].
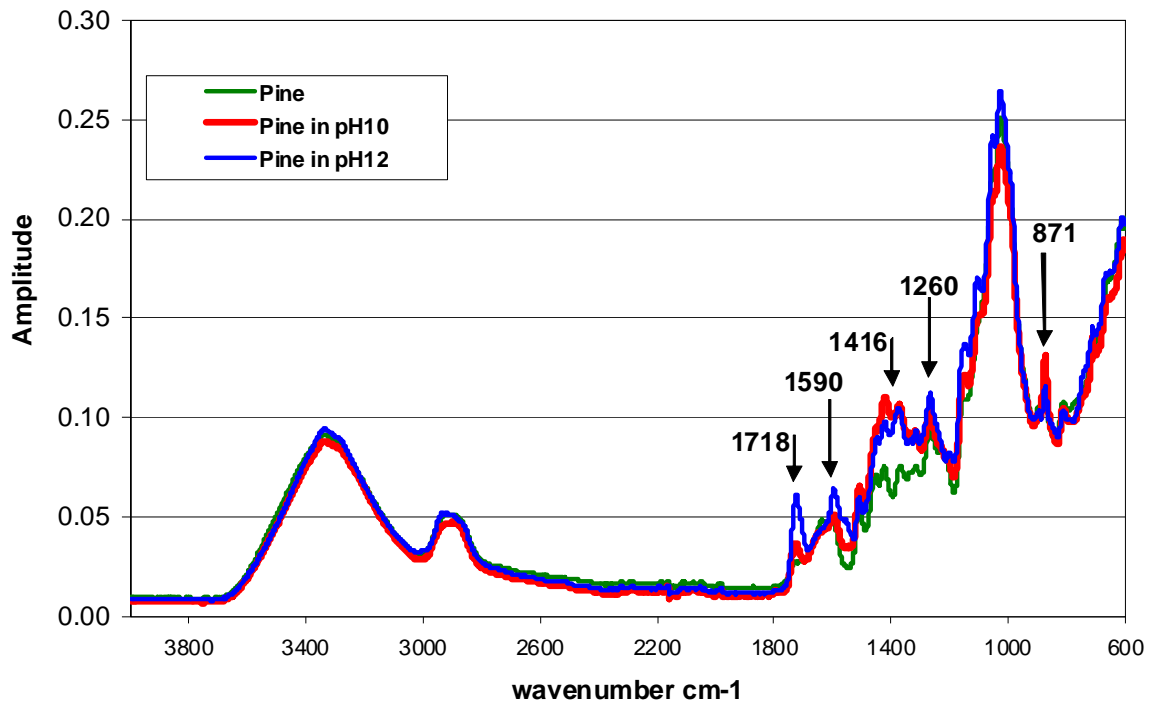
Figure 3.16: Infrared spectroscopy results for pine in different environments

The absorbance increase at wavenumbers 1730 and 1594 cm^{-1} for pine in pH12, corresponding to C=0 stretching in hemicellulose and lignin and aromatic skeletal in lignin, suggests that the alkaline solution reacted more readily with lignin and hemicellulose. Degradation of lignin would lead to a lower strength of the fibre bundles.

As reported in literature, the use of NaOH solution to treat the fibres changes the cellulose crystalline structure. Most likely, this alkaline treatment leads to Cell-II structure, which can provide high thermal stability to the fibres [Borysiak and Garbarczyk 2003; Gwon et al. 2010]. This more stable cellular lattice structure could explain the increase in fibre tensile strength for pine fibres in pH10. However, a high concentration of NaOH could cause opposite effects [Borysiak and Garbarczyk 2003]. The decrease of tensile strength in fibres in pH12 may also be related to the readily reaction of lignin in the alkaline solution.

3.5   Concluding remarks

Different fibres were studied as possible reinforcement for cement based materials. In order to be able to make a decision on the most suitable fibre the tensile strength, Poisson ratio and

durability in alkaline solutions were investigated. The experimental study leads to the following observations and conclusion:

- Two commercially available wood fibre products were not further considered for this project due to their low tensile strength and size. No other type of commercial fibres was available during the development of this thesis.
- As reported in literature, the fibres obtained following semi-chemical process have higher tensile strengths than mechanically prepared fibres. The mechanical fibres, pine, also have a lower modulus of elasticity compared to larch and spruce.
- Nevertheless, the mechanical process to prepare the pine fibres is less time consuming than the NSSC and manual defibrillation for larch and spruce and production time is considered an important factor. To take advantage of the promising results with larch and spruce fibres it is necessary to develop a more efficient production method, or to adapt an industrialized method.
- In spite of the higher tensile strength of sisal fibres the author decided not to use them as reinforcement for cement-based materials because of its strain to failure (6%) and its Poisson's ratio (0.37).
- The scattering of tensile tests results is due to the variability in the microstructure of the natural fibres as well as from possible damage created during the production process.
- Durability tests on pine fibres confirmed the deterioration of wood exposed to alkaline environments with pH above 12. However, after exposure to pH10 solution the pine fibres showed improved average tensile strength. Further research is recommended in order to avail it as a fibre treatment.

In Chapter 5 the bond mechanisms and strength between pine and spruce fibres with the cement-based materials will be studied.

Chapter 4

Low Environmental-Impact Cement Matrix

4.1 Introduction

The production of cement is an energy intensive process that is responsible for 5% of global greenhouse gas emission created by human activities [Batelle 2002]. Therefore, partially replacing cement by other binders without sacrificing mechanical properties will have the benefit of saving energy, reducing greenhouse gas release from mining, calcination and grinding of limestone [Kosmatka et al. 1998] and producing less waste. Binders are reactive particles that actively create a binding structure between inert particles, such as the aggregates, fillers and fibres. Binders can be hydraulic materials, latent hydraulic particles or pozzolanic materials. Cement, a hydraulic material, reacts with water to create an insoluble composite. Blast furnace slag is an example of a latent hydraulic particle: it will react with water in a slow way and it needs to be activated. Pozzolanic materials like fly ash, silica fume, rice husk ash and metakaolin do not react with water but with calcium hydroxide or other alkalies in the presence of moisture, to form compounds with cementitious properties. The reaction speed depends on the alkalinity of the environment and the particle fineness.

In this chapter, in order to lower the environmental impact of cement-based materials, fly ash blast furnace slag and silica fume are used to partially replace cement. First the influence of each cementitious material on the composite mechanical properties and microstructure is described after which several mix designs are discussed. The different matrices are studied to achieve a "low strength" mixture that will be compatible with the wood fibre strength calculated in the previous chapter. The particle size distribution of the aggregates is optimised and some mechanical properties of the cement-based materials are experimentally investigated.

4.2 Influence of cementitious materials other than Portland cement and fillers

4.2.1 Blast furnace slag

Blast furnace slag (BFS) is the main cement replacement used in the Netherlands. The addition of BFS improves the long-term strength of concrete as well as its durability and it lowers the heat of hydration.

BFS is a by-product of the manufacturing of pig iron in blast furnaces. BFS is formed due to the reaction of limestone with materials rich in SiO_2 and Al_2O_3 that are associated with the ore or present in ash from the coke [Taylor 1990]. Granulated BFS, produced by rapid cooling, has high latent hydraulic properties. This is a glassy material, sharp-pointed, irregular shaped

and sandy-sized. Its chemical composition is close to that of ordinary Portland cement (OPC) but with a higher SiO_2, Al_2O_3 and MgO content and lower CaO content (figure 4.1). The properties of BFS vary depending on the nature of the raw materials and the kind of iron produced. The glass content, usually between 90 and 100%, varies due to the cooling method and the temperature at which cooling was initiated [Pietersen 1993]. This glass content, due to fast cooling down, is suitable for blending with OPC, and has no significant crystalline structure. Slag that cools down slowly in air crystallizes and has, therefore, no cementitious properties; it can only be used as aggregate [Aïtcin 2008].

The addition of BFS accelerates the hydration of OPC. Escalante-Garcia and Sharp [1998] attribute this to the "effect of dilution", which means there is more water to react with OPC in the blended cement. Zhou [2006] observed that BFS accelerates the hydration of C_3S and C_3A, two phases of cement. The content of calcium hydroxide (CH), a product of C_3S hydration, decreases with increasing BFS content, which suggests that CH is consumed and this consumption is accelerated by slag. Additionally, BFS provides nucleation sites for CH.

CH probably activates the hydration of BFS as is interpreted from an additional peak in the heat evolution curve of cements blended with BFS [Zhou 2006]. This peak follows a peak usually associated with the hydration of C_3S and the formation of CH. CH activates slag because it creates a strong alkaline environment necessary for the reaction of BFS. A pH of 12 is enough to activate the hydration of BFS [Bijen 1996]. Slag should be ground finer than cement to increase its reactivity. Even though a quantitative determination of reacted slag is difficult, Battagin [1992] and Luke and Glasser [1987] report that less than half of the BFS reacts during the first month and a renewal of the hydration process has been noticed after 3 or 6 months.
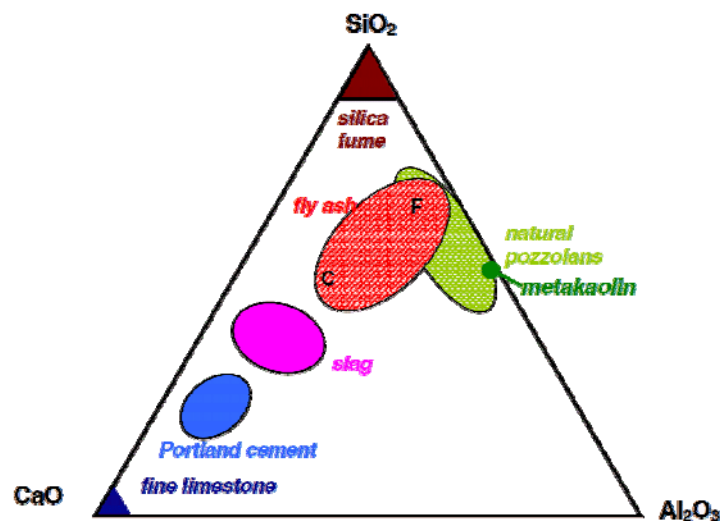
Figure 4.1: CaO–Al₂O₃–SiO₂ ternary diagram of cementitious materials [Aïtcin 2008].

Overall, BFS lowers the early age strength (first 24 hours) of the cement-based composite. It also lowers the amount of heat initially liberated. At later stage concrete with BFS has developed higher mechanical strength [Sersale et al. 1980].

A common feature of blast furnace slag cements is the low permeability. This may be caused by precipitation of Si and Ca outside the slag particle, which forms a CSH-like reaction product and densifies the cement paste [Pietersen 1993]. CSH is calcium silicate hydrate, the main hydration product of OPC and primary responsible for the cement strength. The addition of BFS leads to a fine pore system [Zhou 2006]. The low permeability improves

the durability. BFS additionally protects the material against swelling from alkali reactions and increases the resistance to sulphates and seawater [Aïtcin 2008].

BFS particles can enhance the viscosity of fresh cement paste [Kim at al. 2007]. Therefore, in fibre reinforced concrete the addition of slag leads to a more homogeneous fibre distribution. The use of slag in a cementitious material increases the ratio of tensile strength to compressive strength [Aïtcin 2008].

4.2.2   Fly ash

Fly ash is a by-product of coal-fired power generation and initially it was considered a waste material. However, in some countries, for instance the Netherlands, fly ash is nowadays considered a highly valued raw material. Since 80% of the fly ash generated worldwide still ends up in landfills, the use of fly ash as a cementitious material contributes to waste reduction. As a waste material, fly ash has a lower cost than cement. Beside this economic advantage, the addition of fly ash as a replacement of cement lowers the heat of hydration, suppresses the alkali-aggregate reaction and increases workability. However, the addition of fly ash may increase the sensitivity of concrete to carbonation [Baert 2009]. The same holds for BFS, concretes with high amounts of BFS have poor resistance against carbonation [Sisomphon et al. 2010].

The mineral and chemical composition and amount of glass in fly ash vary widely, depending on the origin, composition and particle size of the coal used as well as the burning conditions. Fly ash contains higher amounts of SiO_2, Al_2O_3 and Fe_2O_3 than what OPC or BFS have, but very low amounts of CaO (figure 4.1). Fly ash is usually classified in 2 categories according to its origin: Class F and Class C [ASTM C618 2008a]. In the Netherlands fly ash is Class F, thus in this thesis only this class will be considered. This type of fly ash, produced by burning of anthracite or bituminous coals, has low lime content and is truly pozzolanic. The content of $SiO_2+Al_2O_3+Fe_2O_3$ is above 70%. Class C fly ash, on the other hand, has a higher CaO content that gives them some hydraulic properties [Fraaij 1990]. This fly ash is produced from lignitic coal.

Fly ash (FA) consists mainly of small, spherical particles of alumina-silicate glass, together with some crystalline constitituents. The glass phase in fly ash is the most reactive part, responsible for the pozzolanic reaction in concrete. The round spheres enhance the workability as they provide a "ball-bearing" effect. The spheres can, as well, be very effective filler because of their shape only [Pietersen 1993].

When in contact with alkalies fly ash will react slowly, following a dissolution mechanism [Pietersen 1993]. For the fly ash to react it is necessary that the glass layer breaks. This breakdown of glass depends strongly on the alkalinity of the pore water, which should be of at least 13 [Fraaij 1990]. In general it will take one week for the pore water to reach pH 13 at which point the dissolution of the fly ash glass is triggered. Due to the pozzolanic reaction, fly ash will in course of time display concentric regions of relatively porous C-S-H, alternating with denser C-S-H. Ultimately, the paste will densify, resulting in a slightly increased compressive strength and a shift in the pore size distribution of the blended cement towards the very small pores [Pietersen 1993]. Erdoğdu and Türker [1998] report an increase of 91% compressive strength at 90 days when using low lime fly ash with particle size smaller than 45 μm compared to using FA with particle size bigger than 125 μm.

The particle fineness also affects the pozzolanic reaction of fly ash. Smaller particles are more reactive than larger particles [Fraaij 1990].

The hydration products in blended cements with fly ash are very similar to those precipitating in OPC. The most significant differences are a slight decrease in the Ca/Si ratio of the CSH and increased Al, Fe and K content of the paste [Pietersen 1993].

Because of the "effect of dilution" mentioned in the previous section, the addition of fly ash can decrease the water demand. The pozzolanic activity of fly ash creates a good bond between the cement paste and the fly ash by producing additional CSH gel. In long term, the compressive strength and durability of blended composites will be equal or superior to that of ordinary OPC [Pietersen 1993, Jiang et al. 2004]. Because the pozzolanic reaction needs moisture to develop, blended FA composites will show increased strength when they are water cured [Aïtcin 2008].

Regarding the increased carbonation rate for concretes with fly ash sometimes mentioned in literature, Bijen [1996] comments that concrete with a low hydration rate will carbonate faster than those with a high hydration rate if exposed to the environment at an early stage. But concretes containing slag or fly ash will also have lower lime content than Portland cement concretes. Thus the amount of material to be carbonated is lower.

4.2.3   Silica fume

Silica fume is a by-product of the fabrication of silicon metal, ferrosilicon alloys or zirconium and is a very reactive pozzolan with constant chemical composition. Used in concrete, silica fume decreases the bleeding and creates a more compact transition zone around the aggregates [Aïtcin 2008]. Unfortunately this binder is considerably more expensive than cement.

Silica fume (SF) consists of very fine particles of almost exclusively amorphous SiO_2 (figure 4.1). The content of amorphous SiO_2 is usually above 80% and sometimes up to 96% [Brandt 2009]. The particles of SF are 100 times finer than those of OPC. Silica fume is an artificial pozzolan as is fly ash. Both contain vitreous silica that reacts with the lime produced by the hydration of C_3S and C_2S of cement forming C-S-H [Aïtcin 2008]. The C-S-H will have a lower Ca/Si ratio. This consumption of lime results in a decrease of pH that will make the cementitious matrix a friendlier environment for the wood fibres (Section 3.4). Nevertheless, a value of pH above 12.5 is considered necessary as protection against corrosion of the steel reinforcement [Brandt 2009]. This high pH assures the formation of a stable passive oxide layer on the steel surface [Koleva 2007]. On the other hand, since pozzolans decrease the permeability of concrete, their use decreases the vulnerability of reinforcement steel. Blended pastes show often equal or even higher total porosities than pure OPC pastes but with a more refined pore structure [Lothenbach et al. 2011].

Due to its small particle size, the reactivity of silica fume is usually larger than that of slag or fly ash. Less than 5% of silica fume reacts during the first hours [Lothenbach et al. 2011] but afterwards the reaction speed increases and after 48 hours 20 to 80% of the SF has reacted. Since an alkaline environment is necessary for a pozzolanic reaction, an increased replacement of OPC with silica fume, which decreases the pH of the pore solution, will slow down the reaction of the silica fume. This explains why some authors found that the early strength of concrete is higher when silica fume is added [Aïtcin 2008] while others authors did not. Detwiler and Mehta [1989] compared plain concrete and 10% SF replacement and concluded that at 7 days there was no difference in compressive strength. After 28 days curing, the blended concretes had compressive strength 12 to 18% higher than plain concrete. The percentage decreased with increasing water-to-cement ratio.

4.2.4   Fillers: Limestone

Limestone powder (LP) is produced by finely grinding limestone. Limestone is used as aggregate in concrete and also as a raw material in the production of cement. The use of LP in mortars improves the early compressive strength up to 5 to 10% replacement of cement, as well as enhanced durability in LP concretes [Livesey 1991; Tsivilis et al. 2000; 2002].

Limestone consists mainly of calcium carbonate $CaCO_3$ (figure 4.1). For its use in cement the $CaCO_3$ content should be at least 75% by weight. As a natural mineral its chemical composition varies depending on the formation process and one of the possible impurities in LP is magnesium carbonate. The specification ASTM C150 limits the total magnesia content to 6% by mass. Depending upon the temperature at which the thermal decomposition from magnesium carbonate occurs, the magnesia oxide present in OPC may react with water and potentially cause expansion in the hardened cement paste [Khanna 2009].

Limestone should be considered as an inert filler material because LP does not participate in the chemical reaction. However, it does act as an accelerator during early cement hydration [Ye et al. 2007]. LP shortens the dormant period of cement, possibly because the $CaCO_3$ directly or indirectly consumes the Al in proactive membranes [Zhou 2006]. Blended limestone cements hydrate fast at the first 30 hours and an accelerated hydration forms more CH. Therefore, the CH content with limestone is higher than with BFS, but in the slag blended cements part of this CH will later be consumed by BFS. The accelerated hydration of cement due to LP results in higher early compressive strength, as mentioned above. However, since limestone powder is an inert filler a lower compressive strength will be achieved at 28 days for both mortar and concrete, if used as replacement of cement [Livesey 1991; Tsivilis et al. 2000; 2002]. Nevertheless, when LP is used as a replacement for coarse cement particles (above 30 mm) the blended samples have the same strength at 56 days as the plain samples [Bentz 2005].

The concrete with LP generally has lower porosity than pure OPC concrete, and the total porosity decreases fast at early stage [Ye et al. 2005].

4.3   Mix design

4.3.1   Materials and mix design

Fourteen different cement matrices have been studied and in each of these matrices 29% to 83% of the cement content has been replaced by either fly ash, blast furnace slag or silica fume. In all the matrices the cement type is CEM I 42.5 N. The chemical composition of the cement OPC, the blast furnace slag (BFS), pulverized fly ash (FA), silica fume (SF) and limestone powder (LP) as well as their density and mean particle size are given in table 4.1. The producers of cement and LP have provided the information presented in this table. The chemical composition of BFS, FA and SF was measured by x-ray fluorescence spectroscopy. Figure 4.2 shows the particle size distribution curves of the powder materials, measured by laser-diffraction technique.

Table 4.2 presents the mix composition for all the matrices studied. To improve the workability of the fresh cement mixtures the superplasticizer CRETOPLAST SL-01 was used. The mixes are divided into two groups: mixes starting with M have a maximum particle size of 0.250 mm and mixes starting with C a maximum particle size of 2 mm. In both groups the maximum size depends on the sand. Four different sand particle distributions were used, as is

explained in section 3.3.2. In mixes MS2, MS3, MS4, CF3 and CS3 limestone powder is considered an inert filler material. In mixes MF2 and all the C mixes, silica fume is added to improve the particle size distribution and to prevent bleeding. The last two columns of table 4.2 show the water-powder ratio ω and the superplasticizer (SP)-powder ratio. Even though not all the FA reacts as a binder, due to its high content in relation to the cement, all the fly ash is included in the ω ratio. The powder materials include limestone even though it is filler.

Table 4.1: Chemical compositions (weight %) and physical propertie of the powder materials.

Compound	CEM I 42.5	BFS	FA	SF	LP
CaO	63.3	40.8	7.1	0.4	-
SiO_2	19.5	35.4	48.4	97.2	0.3
Al_2O_3	5.6	13	31.4	0.5	0.1
Fe_2O_3	2.3	0.5	4.4	0.2	0.1
MgO	1.1	8.0	1.4	-	0.2
K_2O	0.9	0.5	1.6	1.0	-
Na_2O	0.3	0.2	0.7	-	-
SO_3	2.7	0.1	1.2	0.3	-
$CaCO_3$	-	-	-	-	98.8
Density (gr/ cm^3)	3.15	2.85	2.34	2.20	2.70
Mean particle size (μm)	16.56	10.93	21.46	0.15	7.78
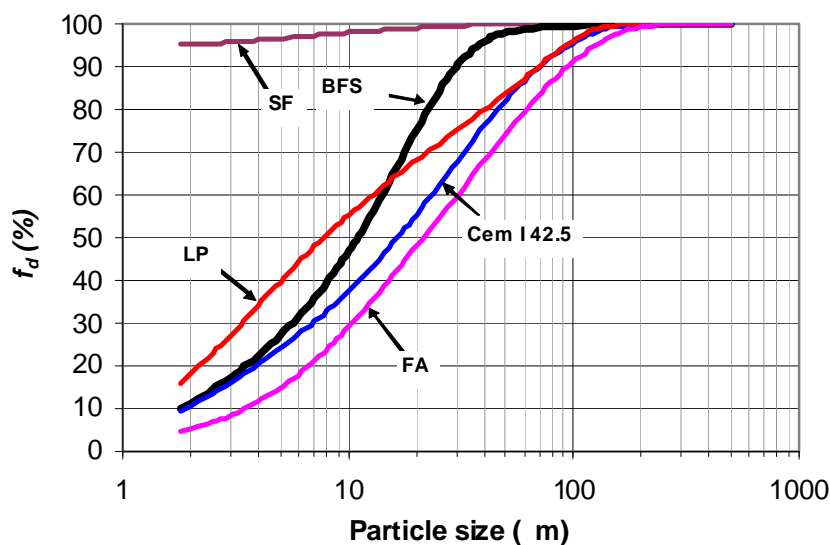
Figure 4.2: Particle size distribution for the powders: BFS, FA, SF, LP and cement.

Table 4.2: Mix compositions (weight %)

Mix ID	CEM I	FA	BFS	LP	SF	Sand	ω	SP / powder
MF1	1.00	1.20				0.80[a]	0.27	0.010
MF2	1.00	2.20			0.10	2.20[a]	0.27	0.019
MF3	1.00	2.80					0.30	0.017
MS1	1.00		1.20			0.80[a]	0.27	0.006
MS2	1.00		1.20	0.80			0.26	0.008
MS3	1.00		1.20	1.50			0.27	0.006
MS4	1.00		1.20	2.00			0.26	0.004
CF1	1.00	1.57			0.05	6.67[b]	0.45	0.005
CF2	1.00	2.00			0.05	3.00[c]	0.39	0.011
CF3	1.00	2.30		3.30	0.10	6.60[d]	0.25	0.014
CF4	1.00	5.00			0.05	3.03[d]	0.32	0.013
CS1	1.00		1.60		0.05	6.67[b]	0.44	0.005
CS2	1.00		2.00		0.05	3.00[c]	0.37	0.004
CS3	1.00		2.30	3.30	0.10	6.60[d]	0.25	0.014

[a], [b], [c], [d] are 4 sand particle size distributions, see Appendix A for the values

4.3.2   Particle size distribution

In order to achieve a closely packed dense matrix surrounding the wood fibres the particle size distribution of the combined dry materials should be controlled. The particles have to be selected in such a way that the voids between larger particles are filled up with smaller particles. In most European standards aggregate distribution is determined by optimising the mixture towards an ideal grading curve, which in practice delivers good concrete mixtures [Fennis 2011]. The original Fuller curve [Talbot and Richart 1923] that takes into account a maximum diameter D_L and an adjustment factor q to be determined experimentally was improved by Funk and Dinger [1994], who recognized that any real size distribution must have a finite lower size limit D_s. This modified equation is equation 4.1. They proposed the value of 0.37 for q for optimum packing.

$$f_d = 100 \left(\frac{D^q - D_s^q}{D_L^q - D_s^q} \right) \tag{4.1}$$

Where f_d is the cumulative percent of particles finer than D, D is the size of any particle (mm), D_s is the diameter of smallest particle in the distribution of the mix (mm) and D_L is the diameter of largest particle in the distribution (mm).

The maximum grain size of the powder materials, except FA, is 130 μm. The maximum grain size of fly ash is 180 μm, above this size only the sand contributes to the particle size distribution. The particle size distribution curves for M matrices are presented in figure 4.3. Matrix MF1 which mix proportion is based on the most common mix proportion for ECC [Li

1998; Li 2009; Lepech and Li 2008] is comparable to the Funk and Dinger optimization curve for q=0.11. Garas and Kurtis [2008] described that q values increase upon increasing the amount of coarse materials and decreases upon increasing the amount of fine materials. When increasing the percentage of sand and FA in matrix MF2 compared to MF1, the resulting particle size distribution curve adjust to an optimization curve for q=0.17, up to size 100 μm and afterwards to an optimization curve for q=0.30.

Matrices MF3, MS2, MS3 and MS4 contain no sand; therefore the maximum particle size is 180 μm. These matrices were not designed following a particle packing optimization criterion that is generally used for mortars and concrete. Similar mix proportions were used in previous studies to prepare ECC-type materials [Garcez 2009; Zhou 2011] without any problems reported for workability or self-consolidation.

For matrices CF1, CF3, CF4, CS1 and CS3 the maximum particle size is 2 mm. Two matrices were designed with maximum particle size 2.5 mm, CF2 and CS2. Figure 4.4 presents the curves for C matrices.

Matrices CF1 and CS1 were designed to adjust to an optimal curve with q=0.37. These two matrices have the higher water/binder ratio. Matrices CF3 and CS3 were designed to follow an optimal curve with q=0.17, while still meeting micromechanical requirements. These matrices have the lower water/binder ratio. As the water/binder ratio decreases the q value also decrease [Garas and Kurtis 2008]. Matrices CS2 and CF2 were designed to meet the optimal curve criterion with q=0.11.

Since the proposed optimal curves described by equation 4.1 do not take into account the influence of chemical reactivity, the model was followed only to design the sand particle size distribution and improve the particle packing. For grain sizes below 180 μm the distribution was governed by the desired paste chemical reaction.

(a)   (b)
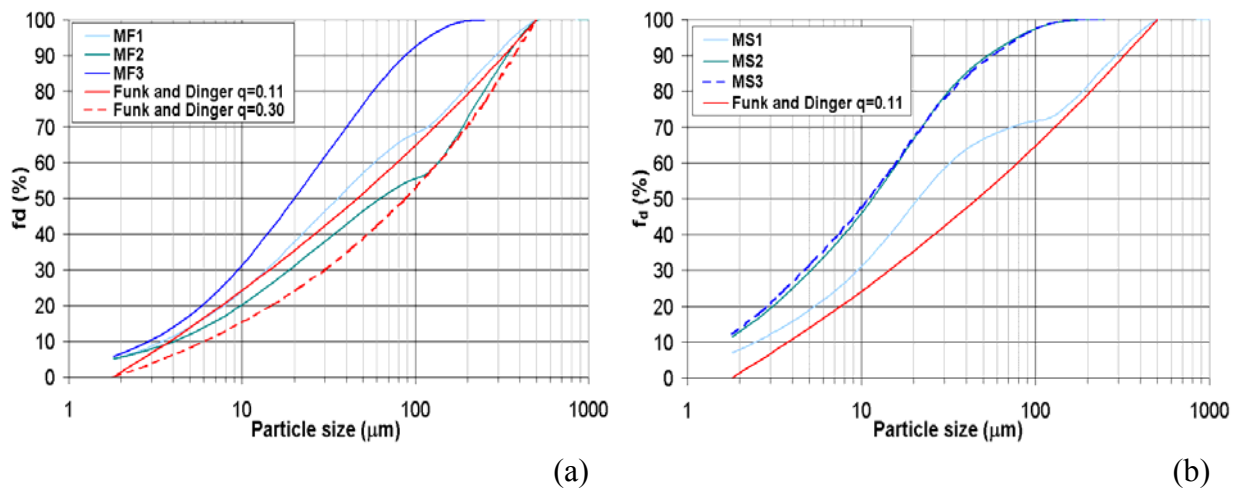
Figure 4.3: Particle distribution of the M - mixtures with FA (a) and with BFS (b).

According to Lepech et al. [2008] the Funk and Dinger curve proved to be successful in assuring a free-flowing mixture during mixing and self-consolidating during casting for strain hardening cementitious composites, when they adjusted the larger grain size proportions of their mix to be closer to the optimal curve (in the upper portion). In another study by Lepech and Li [2008] they increased the sand content of their mixtures to bring the intermediate grain size portion of their particle size distribution closer to the optimal curve. Even though they

also increased the water content of the modified mixtures, flowability tests showed a reduction of flowability as the sand content increased. This can be explained because the flowability of the fresh paste will also depend on the water/binder ratio and the amount of added superplasticizer.

(a)

(b)
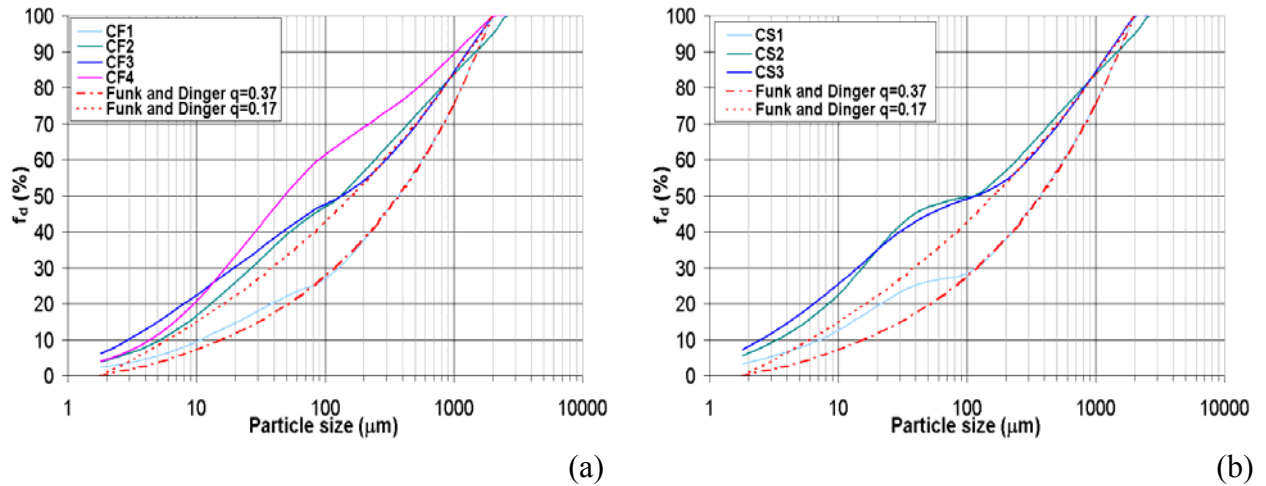
Figure 4.4: Particle distribution of the C - mixtures with FA (a) and with BFS (b).

4.3.3   Mixing and curing

The powder materials, Portland cement, silica fume, limestone powder, fly ash or BFS, were first mixed with a HOBART® mixer for 1 minute. Then water and superplasticizer were added and mixed for 3 minutes. Finally, if the mix includes sand, it was added and mixed for another 2 minutes.

The fresh mixture was cast and cured for 1 day in moulds covered with plastic. Afterwards, the samples were demoulded and cured under sealed condition at room temperature of 20°C until they were tested.

4.4   Mechanical properties

4.4.1   Compression test

Cubes with dimensions $40 \times 40 \times 40$ mm^3 were cast for compressive tests and cured for either 21, 28, 45, 60 or 90 days. Three parallel compressive measurements were done for each mixture at a predefined age. Figure 4.5 summarizes the compressive strength at 28 days. As explained in section 3.2 these mixtures prepared with supplementary cementitious materials need more time to mature than plain mortar or concrete. Therefore the compressive strength at 28 days is in some cases not more than 75% of the compressive strength at 90 days.

Comparing the compressive strength of mixtures MF1, MF2 and MF3, the increasing cement replacement with fly ash causes a decrease of strength at 28 days. The same counts for mixes MS2, MS3 and MS4, with increasing filler content. Mix MF1 and MS1 have the same materials proportions but the first one uses fly ash and the later BFS. Mix MS1 has a higher compressive strength, which is due to the fact that BFS hydrates earlier than FA. This same tendency can be seen when comparing the strength of mixtures CF1 and CS1, CF2 and CS2 or

CF3 and CS3. The mixtures with FA have lower compressive strength at 28 days than the mixtures with BFS, with the same mix proportions.

At 28 days, mix CF1 has the lower compressive strength, 20 MPa. In CF1 30% of the cement is replaced with fly ash and silica fume. The cement content of 211 kg/m^3 falls below the minimum cement content allowed by the Dutch standards, 260 kg/m^3, for concrete strength class C20/25. Thus, matrix CF1 develops the same compressive strength while using less cement. Please note than matrix CF1 is a mortar and mortars traditionally have a higher binder ratio than concrete, which is not the case for the matrices designed in this project. This fact. The stronger matrix is MS2 (69 MPa). This mixture has 41% cement replaced for a total cement content of 544 kg/m^3.
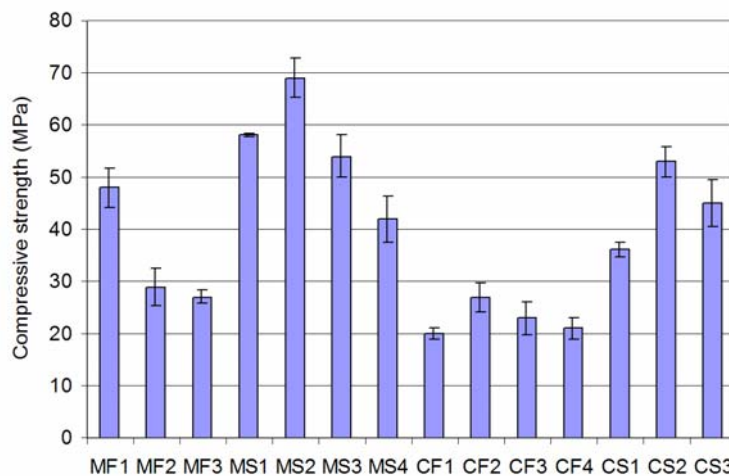
Figure 4.5: Compressive strength at 28 days
MF= matrix with fly ash, maximum particle size= 0.25 mm
MS= matrix with blast furnace slag, maximum particle size= 0.25 mm
CF= matrix with fly ash, maximum particle size= 2 mm
CS= matrix with blast furnace slag, maximum particle size= 2 mm

At water-binder ratios below 0.5, there is a relation between the particle size distribution value q (see section 4.3.2) and the compressive strength [Garas and Kurtis 2008]. For lower q values, the 28-days compressive strength increases. Within the CF matrices the matrix with the highest compressive strength (27 MPa), CF2, has a particle size distribution value q=0.11. Matrix CF3, with a q=0.17, has a strength of 23 MPa and matrix CF1 has a strength of 20 MPa and q value of 0.37. A similar tendency can be seen for the CS matrices. The highest compressive strength (53 MPa) corresponds to CS2 with the lowest q value (11), while matrix CS3 has q=0.17 and compressive strength 45 MPa, and matrix CS1 has the lowest strength 36 MPa and the highest q=0.37.

With similar q values, the compressive strength of cement matrices with FA is lower than the strengths of cement matrices with BFS. As described by Kumar and Santhanam [2003], mixes with the same overall particle size distribution but different constituents may have different strength development.

Figure 4.6 illustrates the increase of compressive strength with sample age for the C mixtures with BFS. Matrix CS1 with the higher content of sand reaches at 28 days only 70% of the strength at 90 days. On the other hand, CS2 has at 28 days a high compressive strength

(53 MPa) that remains stable with time. This mix has the lower filler content, from either sand or LP.
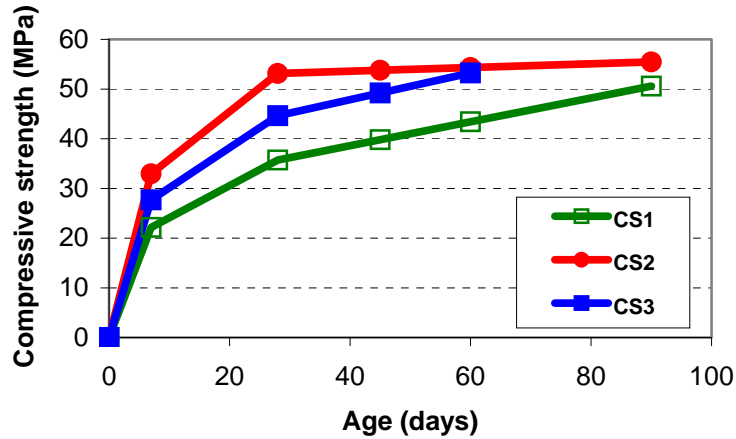
Figure 4.6: Compressive strength as function of age for C mixtures with BFS.
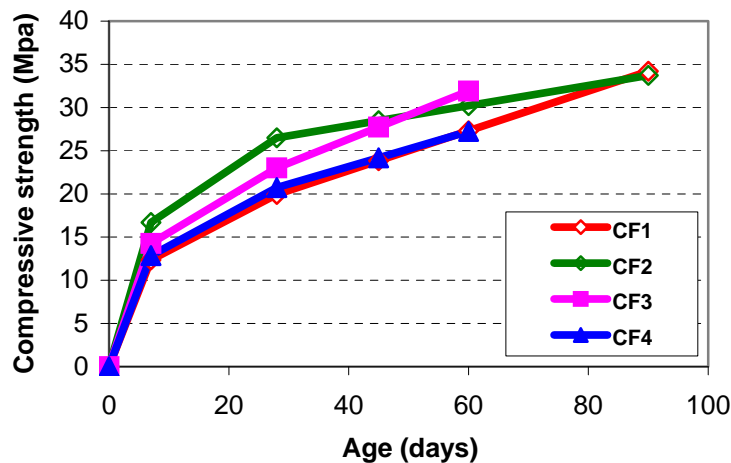
Figure 4.7: Compressive strength as function of age for mixtures with coarse sand.

All mixes prepared with fly ash gain strength with time. Figure 4.7 shows the strength development, up to 90 days, for composites with coarse sand. The most dramatic increase, 72% between 28 and 90 days, is given by mix CF1. Considering the increase of bending strength of CF3 between 28 and 60 days, this matrix would have had the higher strength at 90 days but unfortunately no tests were done at this age. After 90 days the compressive strength of mixes with fly ash is lower than for mixes with BFS, with the same percentage of cement replacement and about the same water-to-powder ratios. The lower values are due to several reasons. In the first place, eventhough FA and BFS provide nucleation sites for CH, the presence of FA has little effect on the hydration of OPC while BFS accelerates the hydration of cement [Zhou 2006]. In the second place, unreacted FA particles show a filler effect. Finally, the smaller particles of BFS are able to 'fit in' between cement particles to develop a more compact matrix with improved compressive strength, while the particles of FA are

bigger than the particles of BFS and cement. Figure 4.2 shows the particle size distribution of BFS, FA and Portland cement. In the third place, the low-calcium fly ash used in this research is less reactive than high-calcium fly ash, as ASTM Class C, and than BFS [Neville 1995]. Additionally, FA needs an alkaline environment, above pH 13 [Fraaij 1990], for the pozzolan reaction. Because of increased cement replacement with FA the pH in the mixtures is lowered, therefore inhibiting further pozzolanic activity from the FA. Normally the pH in concrete mixtures is above 13. The pH of mix CF2 was measured after age 90 days at the Institute Eduardo Torroja (Madrid) and found to be 12.55.

4.4.2   Uni-axial tensile test

Samples from the C mixes were tested under uni-axial tension using a micro tension-compression testing device (developed by Kammrath & Weiss). Figure 4.8 shows the setup.
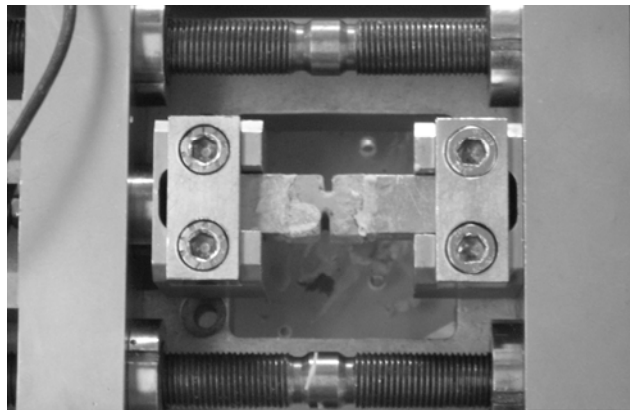
Figure 4.8: Setup of the uni-axial tension test.
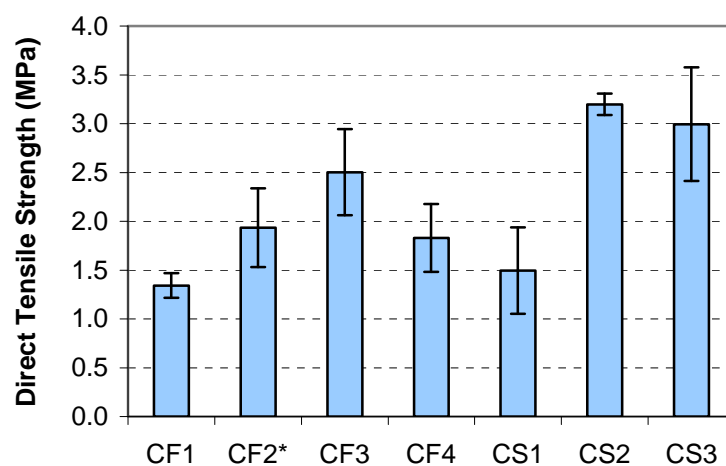
Figure 4.9: Tensile strength at 28 days.

* tested at 90 days

The sample had a cross section of about 10×10 mm^2 and a length between 10 and 15 mm. A notch was made in the block prior to testing. The sample was glued to two steel non-rotating loading plates. The glue is a two-component epoxy resin. The tests were conducted under deformation control at speed 0.5 μm/s while the load was measured with a 500N load cell. The displacement is given by the displacement of the actuator (± 6 mm). All tests were done at laboratory conditions between 30 and 50 RH and about 22°C. Figure 4.9 shows the tensile strength at 28 days, based on the test results, except for mix CF2 that was tested after 90 days.

The 2 mixes with the higher content of sand CS1 and CF1 have the lower tensile strengths. The relation between compressive and direct tensile strength is illustrated in figure 4.10. Since each matrix differs in water-to-powder ratio as well as in sand particle distribution, it is not possible to determine which factors increase or decrease the compressive/tensile strength relationship.

The correlation between direct tensile strength and average cube compressive strength given by Eurocode 2 for normal concrete, as well as the allowed scatter as applied in the Netherlands is also presented in figure 4.10 [CUR Rapport 94-12, 1994; NEN-EN 1992-1-1:2005]. The relationship of strengths for matrices CF4, CF3, CS2 and CS3 follow the tendency proposed by the Eurocode 2.

The size of the samples tested under direct tension and here reported is smaller than for the tests recommended by the Eurocode 2.
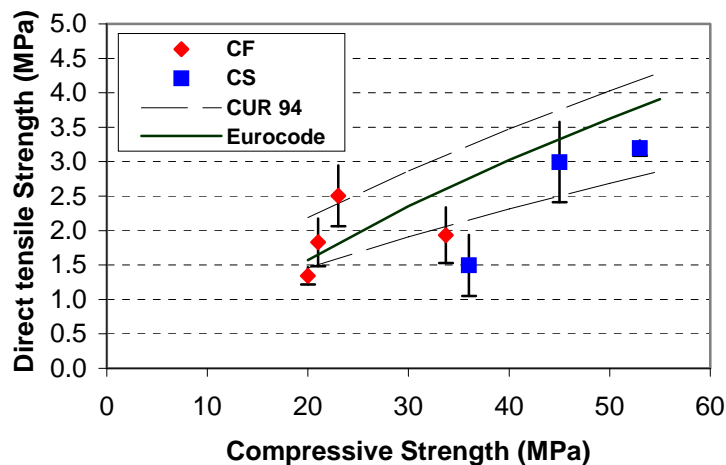
Figure 4.10: Tensile strength versus compressive strength.

4.5   Concluding remarks

Different cement matrices are proposed with low environmental impact. The cement was partially replaced and the particle size distribution optimised. The lower the strength of the matrix the more it matches with the low strength wood fibres. The following conclusions can be drawn from the experimental study:

- Improved particle size distribution leads to a more dense matrix, and may lead to a better bond with the wood fibres. The fibre and matrix interface will be study in the next chapter.

- The compressive strength of blended cement matrices increase with age, since the supplementary cementitious materials have delayed reaction times.
- The direct tensile strength of the mixtures with maximum particle size of 2 mm was evaluated. The relationship between the direct tensile strength and compressive strength for matrices CF4, CF3, CS2 and CS3 follow the tendency proposed by the Eurocode 2 for normal concrete.

In Chapter 5 the bond mechanisms and strength between pine and spruce fibres with the cement-based materials will be studied.

Fibre-Matrix Interface

5.1   Introduction

A material that shows a strain-hardening behaviour with multiple microcracking prior to failure develops enhanced ductility. To promote multiple cracking, the matrix fracture toughness should be limited and the fibre bridging stress should be enhanced. Good bonding is necessary to enable efficient stress transfer between fibre and matrix, but fibre rupture should be avoided. The pullout of the fibre rather than its rupture will favour the development of ductility in the fibre-reinforced composites [Lin and Li 1997]. To what degree the fibres enhance the mechanical behaviour of the cement matrix depends for a significant part on the fibre-matrix interaction. In this matter, three types of interactions are particularly important: the chemical adhesion, the friction and the mechanical interlocking between fibre and matrix caused by irregularities on the fibre surface or the geometry [Bentur and Mindness 2007]. The characteristics of the fibres and the matrix determine the type of interaction and therefore the strength of the interface.
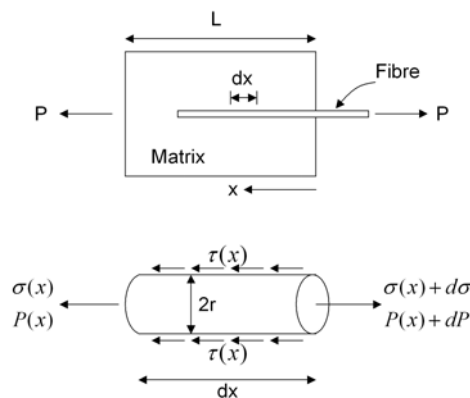
Figure 5.1: Geometry of fibre pullout.

A common way to quantify the bond between fibre and matrix is with the simple pullout geometry shown in figure 5.1. This geometry is the one used in testing in order to obtain a pullout vs. slip relation, but also in the modelling of the fibre-matrix interactions to provide a constitutive relation for the interfacial interactions by means of a characteristic curve of interfacial shear stress vs. pullout displacement.

In this chapter the fibre-matrix interface is studied by means of pullout tests and image analysis of the samples. The different pullout behaviour of each fibre type is highlighted and

the effects of curing conditions and fibre geometry are evaluated. To overcome the volume changes due to the presence of humidity the fibres were treated and the changes in pullout strength and behaviour are analysed. As a result of this study the interface properties are tailored in order to achieve the desired composite behaviour.

5.2   Experimental study

5.2.1   Pullout tests

5.2.1.1   Single fibre pullout curve and definition of bond parameters

During the pullout test the fibre is pulled out from the cement matrix while the load vs. displacement relation is recorded. The pullout behaviour depends on a number of factors, namely: the physical and chemical properties of the fibres, the matrix composition and the curing time and conditions where the nature and shape of the fibres is the most important factor. When the fibre in figure 5.1 is pulled with a constant force P, the simplest assumption would be that a constant, uniform frictional force is present on the surface between the fibre and the cement matrix [Li 1992a].
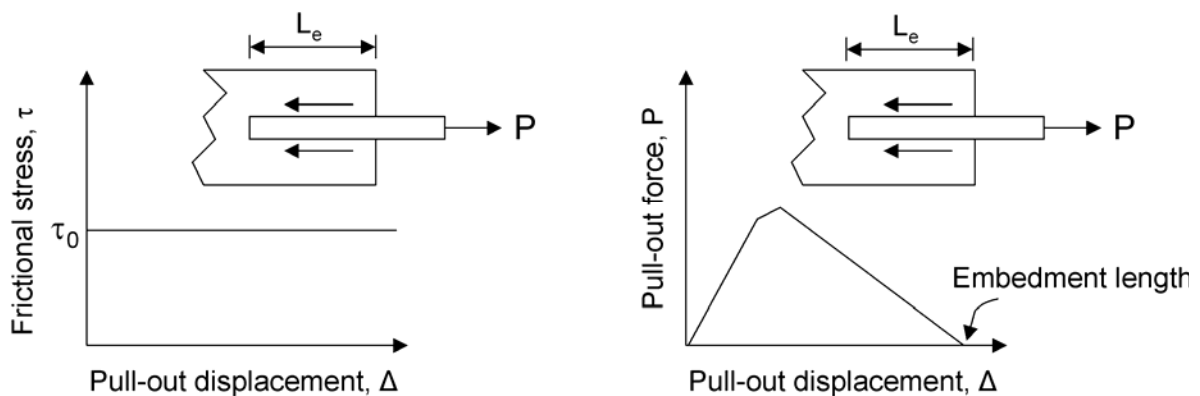
Figure 5.2: The uniform stress distribution model for pull-out (left) and the fibre pull-out response (right).

Figure 5.2 (left) presents the frictional shear stress with magnitude τ_0. If this value is independent of the embedment length of the fibre l_e, the fibre pullout response will be similar to the schematic curve in figure 5.2 (right). Deformed and smooth steel fibres [Abu-Lebdeh et al. 2011, Morrison et al. 1998], thin carbon fibres [Katz and Li 1996] and polyethylene and polyvinyl alcohol fabrics [Sueki et al. 2007] indeed exhibit this behaviour. Lin and Li [1997] observed that for certain fibres, such as polyethylene, and certain matrices the interfacial bond increased with increasing pullout displacements. To take into account this phenomenon they adjusted the model by introducing a slip-hardening coefficient β. The shear stress can then be estimated by equation 5.1. Figure 5.3 shows a schematic curve for τ.

$$\tau = \tau_0 (l + \beta \cdot \frac{\Delta}{d}) \tag{5.1}$$
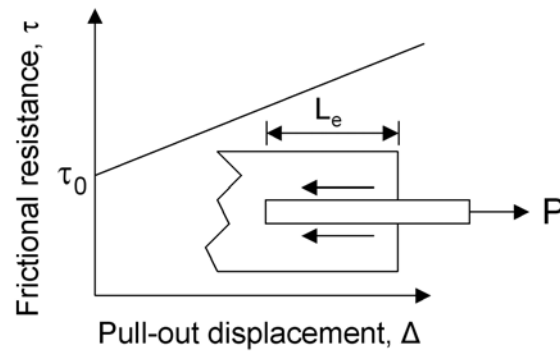
Figure 5.3: The effect of the slip hardening coefficient on the interfacial shear resistance.

According to Gray [1984] and Bartos [1981] there is, besides frictional shear, an adhesion shear bond between fibres and matrix. In the pullout curve shown schematically in figure 5.4, the frictional shear bond strength, τ_{fu}, is lower than adhesion shear bond strength, τ_{au} (0< τ_{fu} / τ_{au}<1). A force P_e is necessary to break the elastic bond between fibre and matrix. After this point the slope decreases as the debonding initiates. A maximum load is reached, corresponding to τ_{au}. Once the entire fibre is debonded the pullout load drops to a level corresponding to τ_{fu} and will continue to decline as the fibre is extracted. Steel fibres [Naaman 1991b] and sisal fibres [Silva 2009b] exhibit this behaviour.
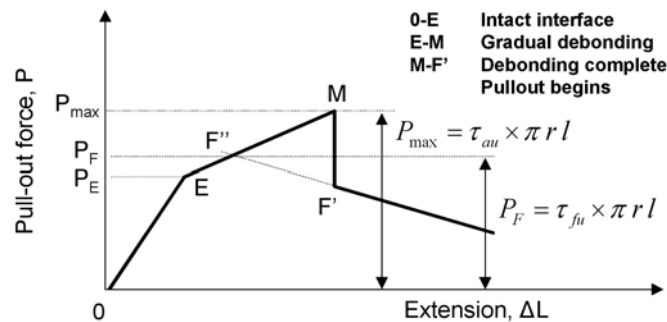
Figure 5.4: A simplified pullout force – displacement diagram.

If τ_{fu} / τ_{au} = 0, the only mechanism is elastic shear stress due to adhesion, without any debonding. After the maximum load is reached there is a sudden drop of load to zero, hence in figure 5.4 only the part 0-E exists.

For fibres that have a high chemical bond to the matrix and therefore develop adhesion shear stress, Redon et al. [2001] resume the three possible behaviours after the chemical bond is broken. In the schematic pullout load-displacement curve in figure 5.5 first a stable debonding process takes place between the fibre and the matrix, zone 1, until reaching a maximum pullout resistance P_{au} by the fibre. Then, at zone 2, the load decreases from P_{au} to the pullout frictional load P_{fr}. As explained above, if this drop of load is sudden the chemical bond between the fibre and the matrix is assumed to be broken and the fibre will be fully debonded. At the slippage zone (zone 3), frictional forces resist the pullout. Depending on the relative hardness of the fibre and the matrix as well as the curvature of the fibre in the cement matrix the fibre undergoes sliding with slip hardening, constant friction or slip softening. For instance, flexible polymer fibres often display slip-hardening behaviour [Redon et al. 2001].

P_{au} is the first peak load. In case of slip-hardening the second peak load is usually higher than P_{au} and therefore P_{max}. In case of slip softening the first peak load is the maximum load, $P_{au} = P_{max}$.
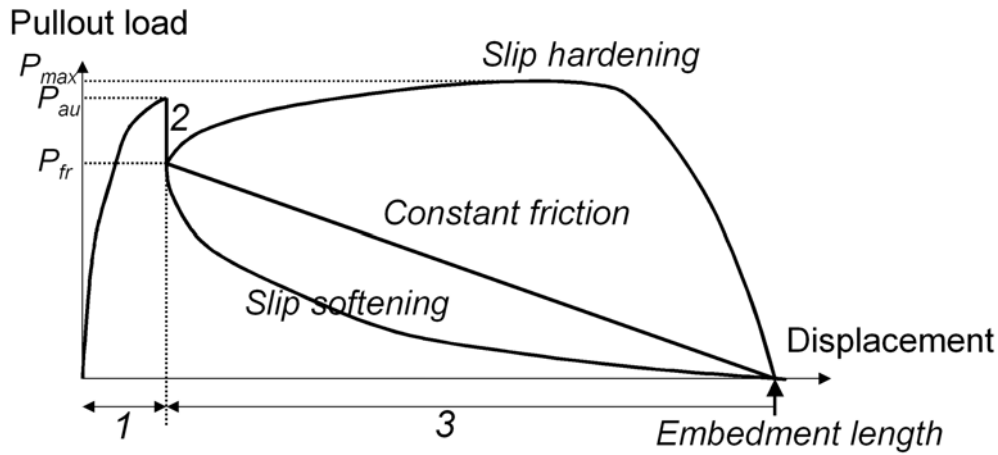
Figure 5.5: Schematic pullout load - displacement curve for 3 possible behaviours after debonding.

For constant cross section, round fibres, as for instance PVA, the chemical debonding energy value, G_d, is calculated from the P_{max} to P_{fr} difference, shown in equation 5.2 [Wang 2005]:

$$G_d = \frac{2(P_{max} - P_{fr})^2}{\pi^2 E_f d_f^3}$$ (5.2)

where E_f = fibre axial Young's modulus; and d_f = fibre diameter. From the P_{fr} value it is possible to calculate the frictional bond strength τ_{fu} at the onset of fibre slippage.

$$\tau_{fu} = \frac{P_{fr}}{\pi d_f l_e}$$ (5.3)

In the slippage regime, the slip hardening, constant friction or slip-softening effects are characterized by the coefficient β, which is, respectively, positive, zero or negative (Lin and Li 1997).

5.2.1.2 Testing techniques and materials

Two different pullout test setups have been used in this research project. The first setup is based on the test setup of Redon et al. [2001]. As shown in figure 5.6 a thin matrix specimen is glued to a metal plate attached to the load cell. The fibre free end is glued to a fibre mounting plate that is connected to the actuator. Wang [2005] found out that for PVA fibres embedded in a high strength cement matrix the embedment length should be less than 1.2 mm to ensure fibre pullout without fibre rupture. For longer embedment lengths the pullout load

exceeds the fibre tensile strength. This setup allowed them to test PVA fibres with a short embedment length.
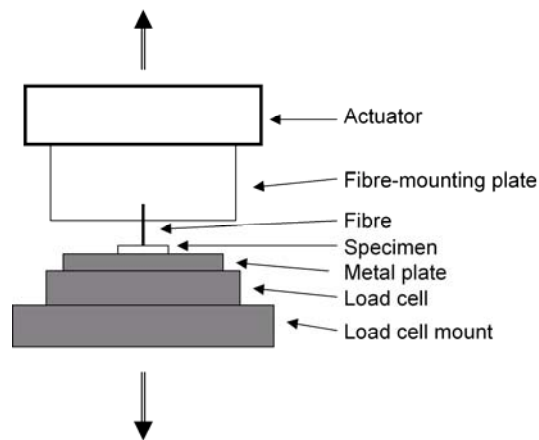
Figure 5.6: Single fibre pullout test setup according to Redon et al. [2001].

The casting setup and mould design corresponding to this test setup are based on the publication from Katz and Li [1996]. Figure 5.7 presents the cast specimen. After curing and prior to testing, each specimen was cut to dimensions 6 mm thick, 8 mm wide, and the embedment length of the fibres was chosen to be 1 mm, following the ECC guidelines [Wang 2005]. The samples were tested in a MTS 810 testing machine in which the displacement of the test is given by the displacement of the actuator (±80 mm stroke) and the load is measured with a 2 N load cell (figure 5.8). A cyanoacrylate based fast-acting adhesive (super glue) was used to attach the cement matrix to the metal plate. When gluing the cement matrix special care was taken to ensure that no glue came in contact with the end of the embedded fibre, as it can influence the pullout force.
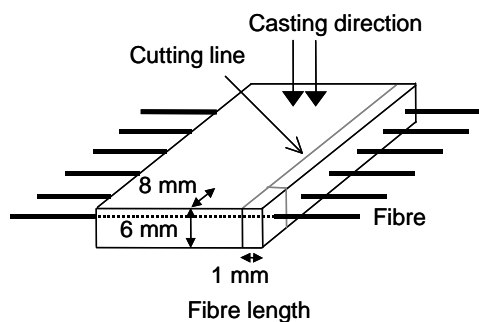
Figure 5.7: First cast specimen and cut dimensions.

A second setup for pullout tests, developed at Microlab, TUDelft, is presented in figure 5.9. For this setup the specimens were casted either 5 or 10 mm long and cut to dimensions 12 mm thick, 10 mm wide (figure 5.10). The embedment length of the fibres is 3 to 5 mm. The fibres are completely embedded and are not aligned as in the other setup. In this way the fibres are free to behave in the same way they do when randomly distributed in cement composites. The samples were tested in a micro tension-compression testing device (developed by Kammarath & Weiss) in which the load is measured with a 50 N load cell and the displacement is given by the displacement of the actuator (±6 mm). The free ends of the cement matrix sample and

of the fibre were glued to two steel non-rotating loading plates with a two-component epoxy resin.
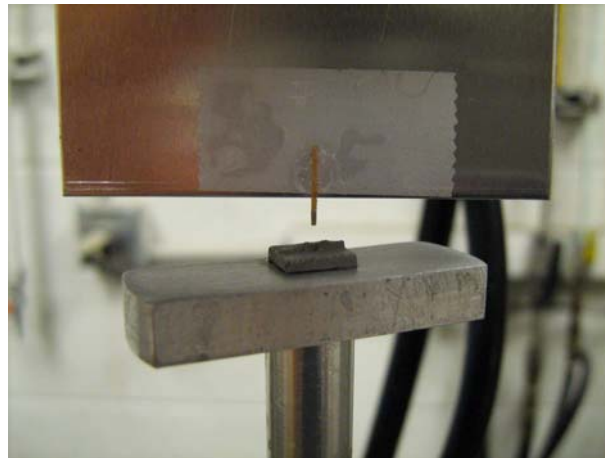
Figure 5.8: First single fibre pullout test setup.
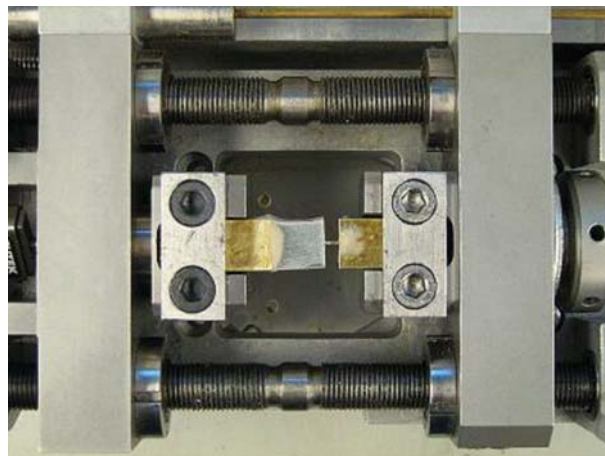
Figure 5.9: Second single fibre pullout test setup.
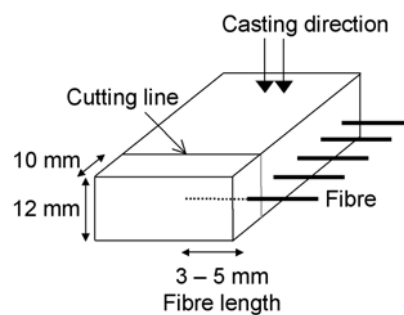
Figure 5.10: Second cast specimen and cut dimensions.

In both test set-ups a free fibre length of 1 mm is left. All the tests were conducted under deformation control at a speed of 0.002 mm/s.

All specimens were demoulded after 48 hours. Afterwards some samples were kept continuously in water (water-cured) while other samples were cured under sealed condition at a room temperature of about 22°C (air-cured). Tests were performed with samples with curing ages 28 to 130 days. The samples were cut prior to testing.

Samples were prepared with the 14 cement matrices described in chapter 4 and the three types of softwood fibres studied in chapter 2.

5.2.2 Microstructure analysis

The fibre-matrix interface microstructure was analysed by optical microscopy (Leica M26), environmental scanning electron-microscopy (ESEM, XL30 FEI) and computer tomography (CT Scan, nanotom of Phoenix X-ray systems). With the aid of these devices it is possible to study different microstructure features, such as the alignment of the fibre inside the cement matrix, the matrix penetration into the fibre and the gaps between fibre and matrix due to the different curing conditions. Additionally, the phase chemistry of the interface was determined with an EDAX energy dispersive x-ray analyser system (EDS). The microstructure characteristics have been correlated with the mechanical properties of the samples measured by the pullout tests.

For the ESEM and XDS analyses tested and untested pullout samples were impregnated with a low viscosity epoxy. After the hardening of the epoxy, the specimens were carefully cut along their length showing the fibre cross-section as well as the interface. Finally the samples surface was polished. Images of the prepared section were taken using a backscattered electron detector (BSE) with vapour mode. The acceleration voltage of 20 kV was used in order to obtain a high contrast image.

The microstructure characterization together with image analysis was also used to compute the wood fibre cross-section area of each pullout test done. The fibres were observed with the stereomicroscope or the ESEM and the obtained images were post-processed using ImageJ program.

5.3 Experimental results and discussion

Since every fibre has a different cross section area and different embedment length the pullout test results had to be normalized for comparison. Thus, the force will be expressed in terms of shear stress and the displacements will be normalized. The interface shear stress τ is obtained using equation 5.4. The maximum pullout load P is divided by the surface area of the embedded fibre that is the area in contact with the cement matrix.

$$\tau = \frac{P}{l_e C_f} \tag{5.4}$$

where C_f is the fibre cross-section contour (see figure 3.7).

The normalized displacement Δ_n is calculated with equation 5.5, dividing the displacement measured during the pullout test Δ by the embedment length l_e.

$$\Delta_n = \frac{\Delta}{l_e} \tag{5.5}$$

The displacement Δ incluides the elastic deformation of the fibre, but this deformation can be neglected.

The area under the pullout curve G_t was determined, see figure 5.11, as a measurement of the total energy released during the whole pullout. Additionally the area under the curve up to a displacement of 1 mm, G_1, was also determined.
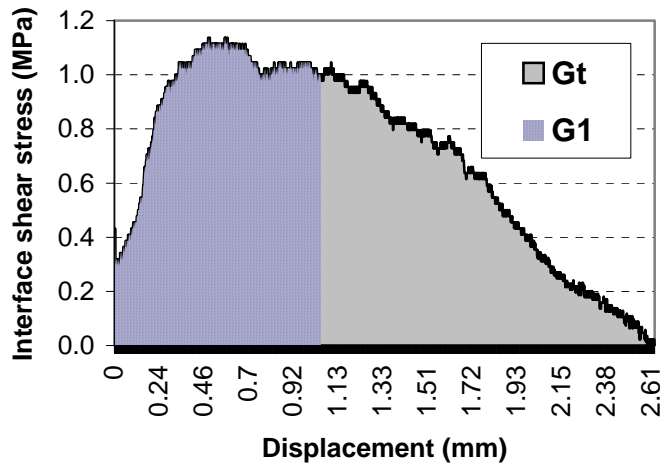

Figure 5.11: Energy as area below the pullout curve.

Pullout testing of natural fibres embedded in cement matrices is not a straightforward task. The test results vary significantly, even for fibres having the same cross section area and similar embedment length [Jun et al. 2009]. Pullout tests results with wood fibres also have scattered results. The pullout loads are low, for wood fibres the loads registered are below 10 N; therefore an accurate test setup is necessary.

Several factors influence the interface properties, but the main factors are the fibre type and interface geometry, the cement matrix composition and the curing conditions. The following sections discuss the pullout tests and microstructure analysis accordingly, but since all the factors interact and influence the results, it is not easy to isolate one factor at a time. The effort is made, however, in order to better understand the fibre and matrix interface.

5.3.1 Fibre type: larch, spruce and pine

When comparing the test results for the three types of wood, larch fibres show higher interface shear stress compared to the pine and spruce fibres. In every case the comparison is made for the same cement matrix, curing age and curing condition. Only very few tests were done with larch fibres and all of them were water-cured. Larch fibres were very labour intensive to produce and so the decision was made not to have both water-cured and air-cured samples, as there would not be enough samples of both curing types to obtain conclusive results. Since water-cured samples behave better than air-cured samples for both pine and spruce fibres, it was decided to only make water-cured samples from the larch fibres available. For air-cured samples, pine fibres have a slightly higher average interface shear stress than spruce fibres.

Figure 5.12 shows the maximum interface shear stress τ_{max}, at 28 days of pine and spruce fibres with most of the cement matrices under air-cured conditions, and figure 5.13 present the

results for water curing including larch fibres. τ_{max} is calculated as the maximum shear resistance over the original embedment interfacial area.
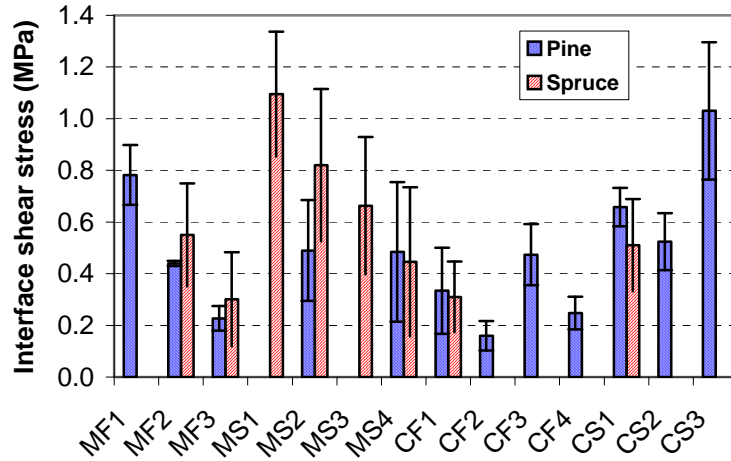

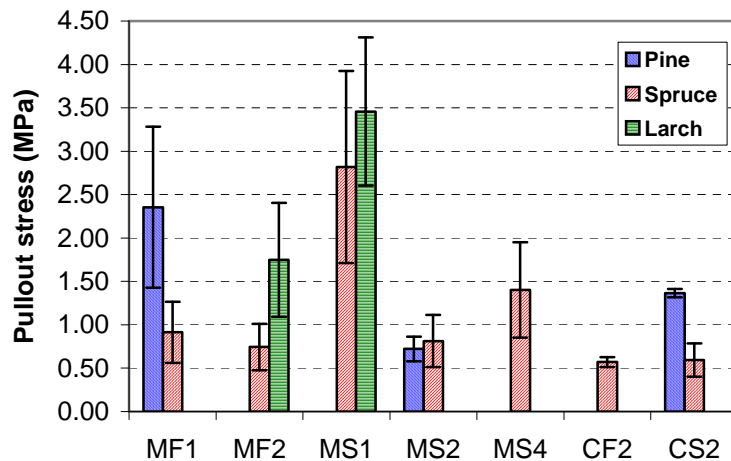*Figure 5.12: Maximum interface shear stress at 28 days, air-cured samples.*

Figure 5.13: Maximum interface shear stress at 28 days, water-cured samples.

Beside the pullout stress values, the performed tests also give important information about the behaviour in the interface when the fibre is pulled out. It is precisely the pullout behaviour that is the most noticeable difference between mechanically prepared pine fibres and the semi-chemically prepared spruce and larch. About 65% of the pine fibres that were pulled out, without breaking, had an interface bond mainly governed by friction. This behaviour can be seen in figure 5.14 where a stress-displacement pullout curve recorded for a pine fibre embedded in MF3 is presented. In this curve there is no sudden drop from the adhesional stress τ_{au}, corresponding to P_{au}, to the friction stress τ_{fu}, corresponding to P_{fr}. On the other hand, spruce and larch fibres have a strong adhesional bond. For these types of fibres the most frequent pullout behaviour was slip softening, 66% of the pulled out spruce fibres and 43% of larch. This typical behaviour for spruce fibres is shown in figure 5.14.
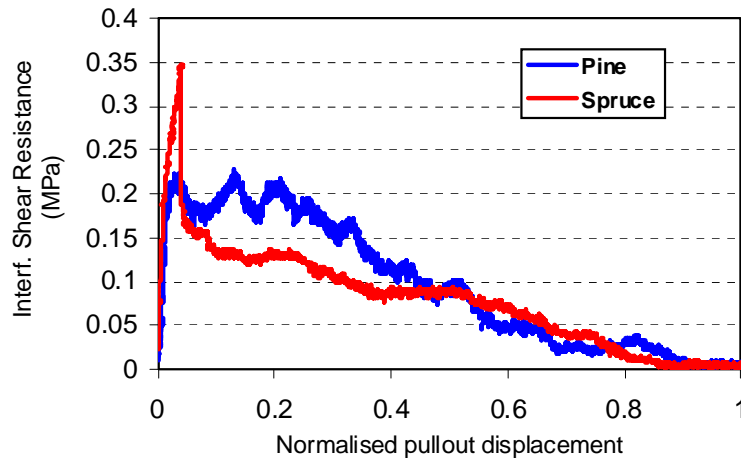
Figure 5.14: Typical pullout behaviour of pine and spruce, MF3 samples.

About a third of all the pullout tests with pine fibres broke during the tests, while only 18% of the other types of fibres undergo sudden rupture. A strong adhesion bond between fibre and matrix could explain the high percentage of fibre rupture, but judging from the results of the tests that did not break, pine fibres do not have such a strong adhesion bond. Therefore other mechanisms should be producing the fibre rupture, as is explained in the next sections.

Even tough fibre rupture is not a desirable behaviour for the pullout of fibres; when comparing the behaviour of pine fibres vs. spruce fibres, it is important to notice that the amount of energy released by a pine fibre in a full-friction pullout test is higher than that released by a spruce fibre sliding with slip softening. For example the energy G_t / L_e estimated from the pullout curves in figure 5.14 is 0.08 N/mm^2 for the spruce fibre test and 0.096 N/mm^2 for the pine fibre test. The total energy G_t is divided here by the embedment length L_e to be able to compare different pullout tests. The average energy G_t / L_e for all pullout tests with pine fibres (air-cured conditions at 28 days) is 0.18 N/mm^2. The total energy for pullout tests with spruce fibres in the same conditions is slightly lower, 0.17 N/mm^2. Additionally the energy released during the first millimetre of pullout displacement G_1 give information about the expected behaviour of the fibres in the composite when bridging a crack that grows up to 1 mm wide. For all pine tests the average energy G_1, estimated as the area under the pullout curve until displacement 1 mm, is 0.39 N/mm and for spruce tests is 0.24 N/mm.

The influence of the maximum interface shear stress on the fibre critical length can be calculated using an equation proposed by Kelly [1988]:

$$L_c = \frac{r\sigma_f}{\tau} \quad (5.6)$$

where L_c = fibre critical length, r = fibre radius, σ_f = fibre ultimate tensile strength, and τ = fibre bond strength. This equation is rephrased in equation 5.7 to take into account the rectangular cross section of the wood fibres:

$$L_c = 2\frac{A_c\sigma_f l}{P_{max}} \quad (5.7)$$

where A_c is the fibre cross-section area, P_{max} is the maximum pullout load and l is the embedment length corresponding to P_{max}. Using eq. 5.7 the critical length for pine fibres is 3.6 mm and 3.2 mm for spruce fibres.

5.3.2 Cement matrix

When comparing the overall results for the fourteen cement matrices, fibres embedded in matrices with BFS show higher interface shear stress than with FA mixtures (figures 5.12 and 5.13). Spruce fibres, in water or air-cured conditions, achieved higher shear stresses with M matrices (maximum particle size 0.25 mm) than with C matrices (maximum particle size 2 mm). The highest stress was estimated for spruce fibres in mix MS1 for both curing conditions. Pine fibres, on the other hand, show a different tendency when air-cured than when dry cured, as will be explained in section 5.3.3, when the effect of curing condition is analysed. For air-cured pine samples the highest stress was achieved with mix CS3 while in water-cured samples the highest stress happened with mix MF1. When directly comparing pullout results for mixes that have the same percentage of cement replacement, samples with BFS have higher shear stress than samples with FA, as for example CS1 samples have higher stress values for both pine and spruce fibres, than CF1 samples.

The FA mixes have the lowest compression strength as well as the lowest interface shear stresses. There is a clear tendency to improve the pullout stress if the compression strength increases as can be seen in figure 5.15.
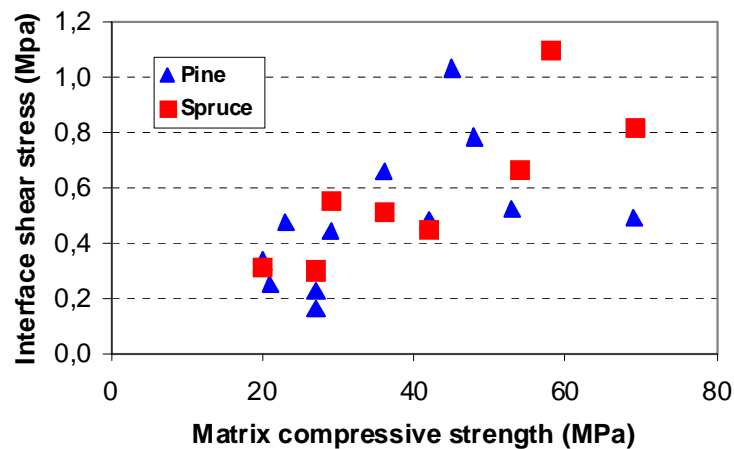
Figure 5.15: Interface shear stress versus compressive strength.

The pullout behaviour is analysed for each cement matrix, starting with the ones in which the fibres developed higher interface shear stresses. Pine fibres in matrix CS3 achieved on average an interface shear stress of 1.03 MPa. For this matrix, 60% of the fibres broke during the pullout test. Fibres that were successfully pulled out exhibited behaviour governed by friction and were able to release a high amount of energy G_t, compared to the other tests, as is presented in figure 5.16. Nevertheless, the fact that such a high percentage of fibres undergo rupture when pulled out is a negative behaviour for this cement matrix. The same occurred for mix MF1, which developed an interface stress, in average 0.78 MPa in air-cured condition and 2.36 MPa in water-cured condition. With this mix, a higher percentage of fibres broke during the pullout tests for samples that were air-cured (71%) than for samples that were water-cured

(33%). 50% of the pine fibres pulled out from air-cured cement matrices CF1 and CF2 broke, 40% out of MF2 and 30% from CS2, MS4 and MF3. On the other hand, no pine fibres embedded in CF3; CF4 and CS1 undergo rupture when pulling them out. The average interface shear stress for these matrices is 0.47, 0.24 and 0.66 MPa, respectively. The pullout behaviour of these fibres is also governed by friction, with a special remark for fibres in CS1, in which 25% tests had slip softening behaviour and 25% tests have slip hardening.
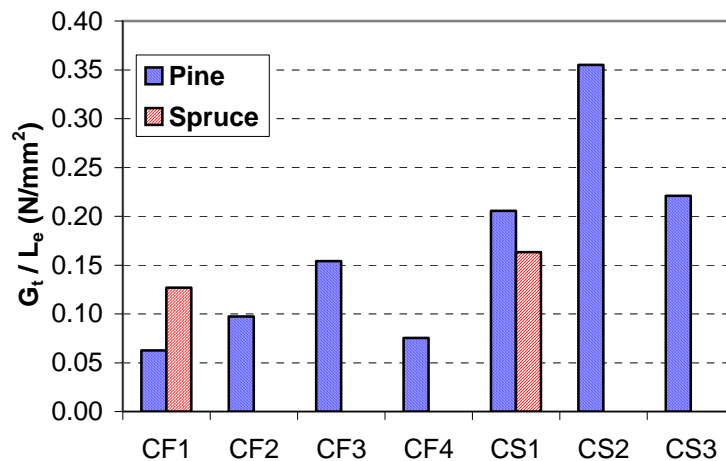
Figure 5.16: Area under the curve G_t normalized with embedment length L_e for C mixes.

Spruce fibres in MS1 have the higher pullout stresses for both curing conditions. In air-cured conditions they release the higher amount of energy, in part because 17% of the tests exhibited slip-hardening behaviour, but 44% of the fibres broke during the test. Even though in water-cured conditions no fibre broke, the most frequent behaviour was slip softening and smaller energy release was estimated. Spruce fibres seem to have a strong adhesion bond with this cement matrix MS1, so strong that often fibres broke, and additionally once the adhesion bond is broken, the fibre can easily be pulled out. Spruce fibres embedded in matrix MF1 exhibited the best pullout behaviour for both curing conditions. These samples had the highest percentage of slip hardening behaviour. In dry curing condition, spruce fibres in CF2 either broke or slipped with slip softening. The same counts for spruce embedded in MF2 and water-cured. When comparing the estimated energy G_t for some C mixes (see figure 5.16) the fibres in CS2 have the higher energy and, even better, no fibre rupture.

The densification of the matrix improves the fibre-matrix interfacial zone, thus leading to a better bond. This effect can easily be seen when comparing the pullout test results of spruce fibres embedded in CF2 and in a CF2 mix without silica fume. The CF2 mixture contains cement, FA, sand and 14.2 kg/m³ of silica fume (0.05% per weight). The maximum interface shear stress in the samples without silica fume was 0.33 MPa, while for the samples with SF was 0.57 MPa. Beside the stress increase also the pullout behaviour improved. To compare the pullout behaviour, considering that for both mixtures the behaviour was slip softening, the total energy G_t was computed and normalized by the fibre embedment length and by the maximum shear stress. The fibres embedded in CF2 with SF have on average a normalized total energy of 0.39 MPa/N versus 0.11 MPa/N computed for the fibres in CF2 without SF.

5.3.3   Curing condition

The curing conditions have a strong influence on the pullout behaviour. The interface shear stress is higher for samples that were constantly kept under water than for dry samples. Figures 5.17 and 5.18 show the interface shear stress for some cement matrices with wood fibres that were cured under the two conditions. In the case of pine fibres and mix MF1, the difference regarding the curing condition may be explained because the pozzolanic reaction needs moisture to develop blended FA composites will show increased strength when water-cured [Aïtcin 2008]. A further pozzolanic reaction lead to a less porous cement matrix and this promotes a better adhesion between matrix and fibre. For mix MF1 the increase in compressive strength at 28 days due to the constant presence of water is not dramatic, from 48 MPa for dry samples to 49.5 MPa for wet samples. Therefore this is not the only factor responsible for the higher interface shear stress in water-cured samples.
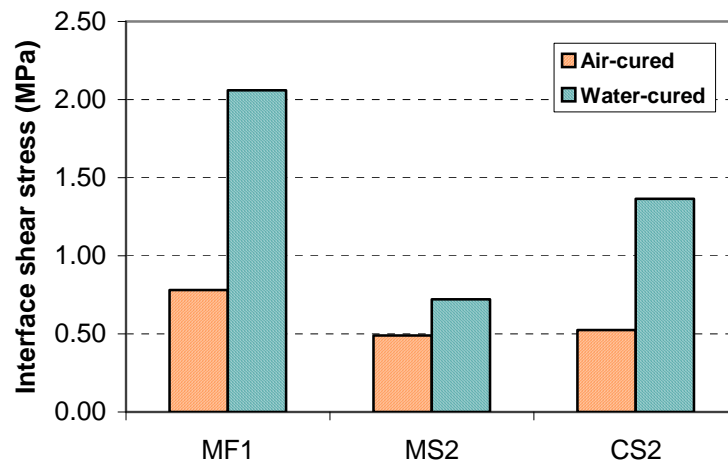
Figure 5.17: Maximum interface shear stress for pine fibres under both curing conditions.
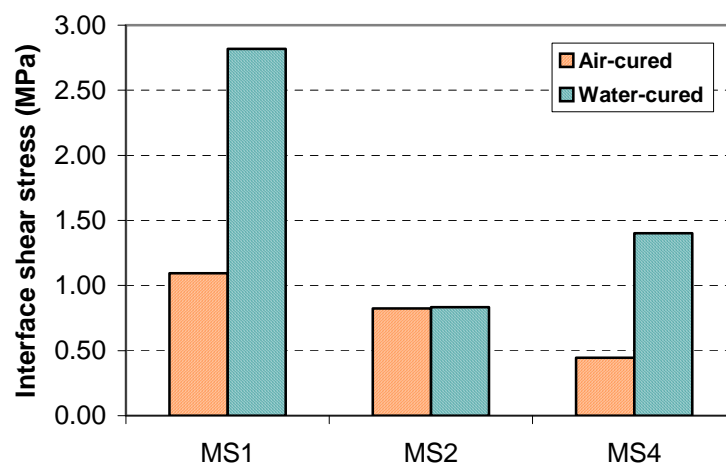
Figure 5.18: Maximum interface shear stress for spruce fibres under both curing.

The pullout behaviour of the pine fibres in mix MF1 that were cured submerged in water differs from the behaviour of fibres pulled from air-cured samples. For the first group, 12% of the samples had full friction behaviour while in the second group all samples had adhesion bond. The same tendency was seen with pine fibres in matrix MS2. Every dry sample tested exhibited friction behaviour. Meanwhile half the wet samples had friction behaviour and half had adhesion bond that once lost slipped with constant friction.

As mentioned in previous sections the most frequent pullout behaviour of spruce fibres is slip softening. These fibres show strong adhesion bond in most of the tests. When comparing the test results for both curing conditions in MS4 samples, 33% of spruce fibres pulled from air-cured samples showed friction behaviour (see figure 5.19). The remaining 67% had either slip hardening or slip softening. The behaviour changed for water-cured samples, among which no friction behaviour was observed. Of the specimens tested, 12% had slip-hardening behaviour and 88% slip softening.
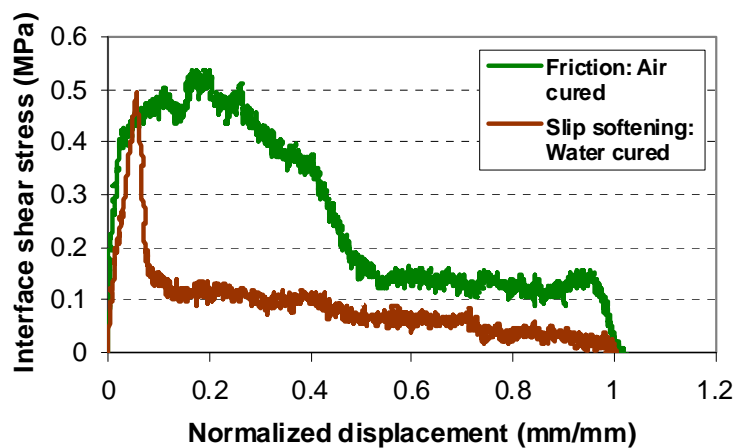
Figure 5.19: Pullout behaviour of spruce fibres in MS4 under both curing conditions.
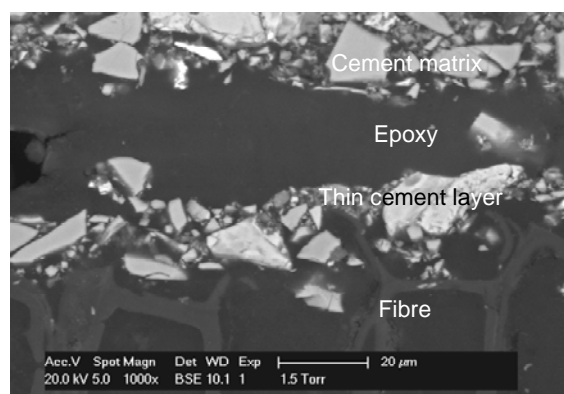
Figure 5.20: Esem image of pine fibre – MF1 interface at 28 days under air-cured condition.

In order to understand the behaviour depending on the curing conditions untested samples have been analysed with the ESEM. Wood fibres have the characteristic to undergo volume changes in the presence or absence of water. The same phenomenon is observed in the fibres embedded in cement matrices: fibres swell in the fresh paste stage, while later they shrink

during the hydration of cement. The fibres swell with the water present in the cementitious mixture. In this initial stage the cement paste directly next to the fibre hydrates, thus creating the thin layer of reacted paste shown in figure 5.20. This layer is weak due to a high water/cement ratio. Later as the cement hydration continues and if the curing conditions do not provide additional water (as with air curing) the fibre shrinks and breaks the young cement paste leaving a gap that was filled with epoxy when preparing the sample for the ESEM images. When the fibre shrinks the adhesion bond with the cement matrix is lost. From the samples observed the gap width ranges between 3 and 30 μm. In images of tested fibres and videos of pullout tests done in the ESEM patches of cement matrix covering the fibres have been observed (figure 5.21). Those patches are these thin layers of reacted paste. ESEM images of water-cured specimens reveal a sound and intimate contact between the fibres and cement matrix, as presented in figure 5.22. In the air-cured samples the fibre has internally cracked and that crack is now also filled with epoxy. In the ESEM, under BSE mode, the epoxy looks dark gray because it has a lower atomic number than the fibre or the cement matrix.
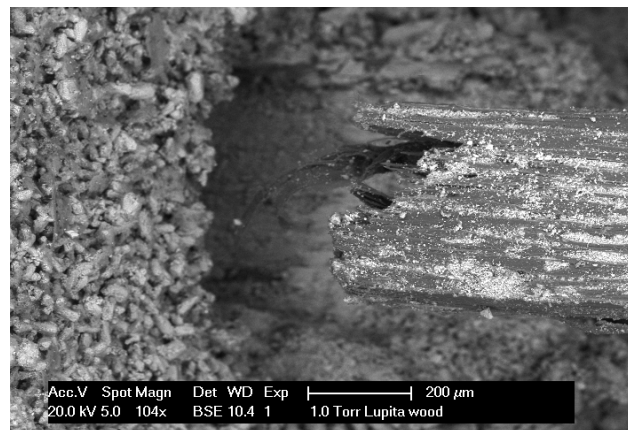
Figure 5.21: Esem image of fibre pulled out of matrix.

(a)   (b)
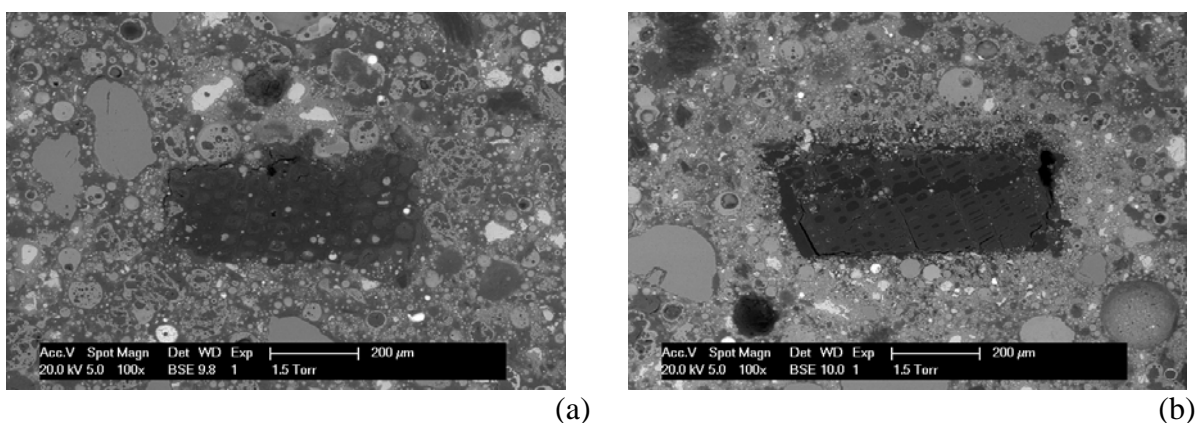
Figure 5.22: Esem images of pine fibres embedded in MF1 under
a) water-cured condition and b) air-cured condition.

However, the phenomenon is not uniform in all the fibres since the volumetric changes in the fibres will vary according to their cross section shape, their chemical composition, the

water/cementitious materials ratio, the pH of the cementitious composite and the temperature and relative humidity during curing. As can be seen in figure 5.23 the swelling is not uniform in every direction of the cross section of this spruce fibre embedded in air-cured CF2 material. In the central segment the fibre that once was attached to the cement matrix has shrunk and there is a gap between the cement matrix and the fibre. On the right side of the image the fibre-matrix interface remains sound. This behaviour will explain the tendency of the tested spruce fibres to undergo a slip softening behaviour. During the pullout test, once the chemical bond is completely broken, the fibre is loose inside the cement matrix and it is easy to pull out, therefore the pullout load decreases rapidly. On the other hand, if from the beginning there is no chemical bond at all, for instance due to uniform shrinkage of the fibre, there may still be frictional behaviour during pullout if the fibres has an irregular shape, rough surface or curvature along its length. This can be seen with fibres embedded in MF3, MS2, MS3 and MS4. Figure 5.19 presents different pullout behaviours for spruce fibres in MS4.
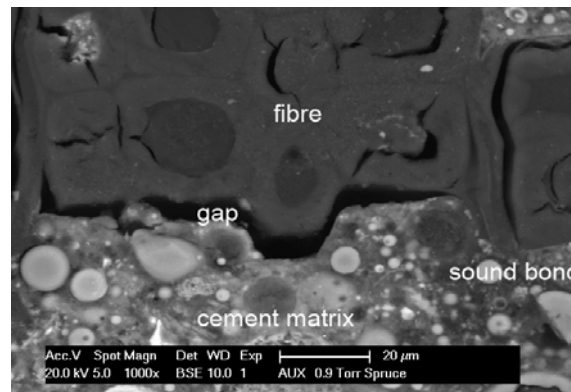
Figure 5.23: Esem image of spruce fibre – CF1 interface at 28 days under air-cured condition.

Surface chemical composition analysis via energy dispersive detector (EDS) of untested samples with spruce fibres also showed the differences in the fibre-matrix interface depending on curing conditions. The atomic elements of the cement matrix were analyzed at two zones: 1) at the interface, immediately next to the fibre; 2) at 250 μm away from the fibre. The chemical analyses of samples with matrix CS2 are presented in figure 5.24. In the sample that was air-cured the two measurements have very similar results. There are only small differences in the weight percentage of carbon, slightly higher when close to the fibre, and oxygen, slightly lower when close to the fibre. Other small differences are neglectable. These results suggest that in air-cured samples there is very little influence of the fibre in the chemical composition of the interface. On the contrary, the sample that was water-cured presents noticeable differences in the weight percentages of carbon, oxygen and calcium between the measurements done next to the fibres vs. the measurements at 250 μm away (figure 5.24b). In the interface the percentage of carbon is higher than in the bulk matrix, due to the presence of the fibre. The percentage of carbon in the bulk matrix is about the same for air-cured and water-cured samples. The percentage of calcium is lower at the interface than in the bulk matrix. Beside carbon, the dominant elements are calcium, silicon and oxygen, which are typical for hardened cement gel, CSH. The percentages of chemical elements in the matrix are similar for both curing conditions.

The high percentage of carbon in the interface may be carbon from the fibre itself or carbon from the epoxy than fills in the voids during the preparation of the sample for the ESEM. If the sample is more porous in the fibre-matrix interface, there will be a higher presence of epoxy and therefore a higher percentage of carbon. The origin of the carbon that has been measured is not clear. In the ESEM, the X-ray information comes from a region below the surface. The X-ray emission penetration depths depend on the applied acceleration voltages and the atomic number of the element. At the acceleration voltage of 20 kV, the penetration depths for the elements mentioned in figure 5.24 are: Carbon (C) 4 μm, aluminium (Al) 3.4 μm, silicon (Si) 3.7 μm and calcium (Ca) 5.8 μm [Dijkstra 1998]. The image observation was done in backscattered electrons (BSE) mode, for which the interaction depth is 1 to 2 μm. As the position for the EDS-measurements was chosen based on BSE images (1-2 μm deep) it is possible that below the depth of the BSE images, pieces of wood fibres or epoxy were measured with the X-Ray (3 to 5 μm deep). Similar results were observed in other untested samples with spruces fibres. More tests are necessary to confirm the influence of the fibres in the fibre-matrix interface chemical composition.

In order to keep the intimate contact between fibre and matrix the fibres were treated to reduce the swelling and shrinkage, as will be discussed in section 5.4.

(a)   (b)
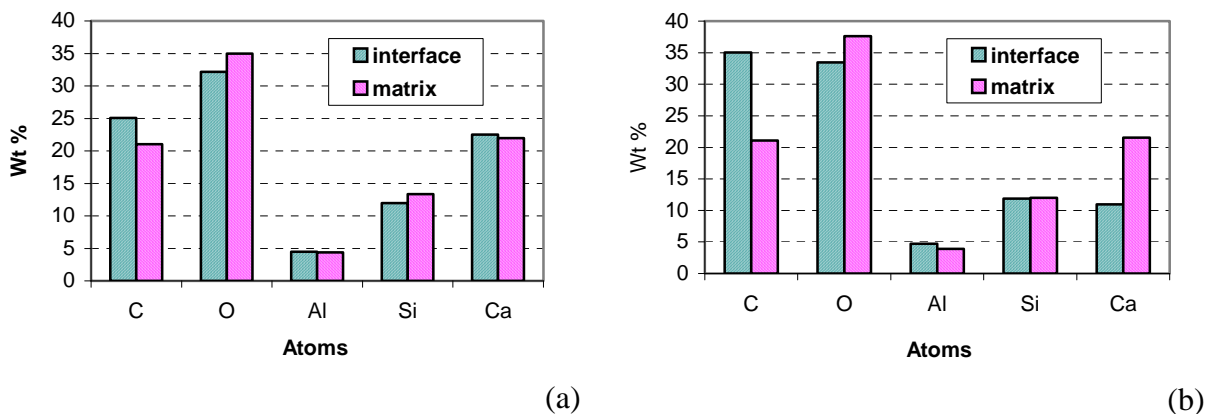
*Figure 5.24: EDS chemical analysis of CS2 samples with spruce fibre, under
a) air-cured condition and b) water-cured condition.*

5.3.4   Interface geometry

The wood fibre is a natural mini-composite by itself with naturally bonded filaments. The shape of the fibres, made either partially or completely mechanically, is not uniform. The fibres have a rough surface with short filaments coming out which may help the adherence, the mechanical bond and increased friction when pulled out, resulting in an effective reinforcement for a cement matrix composite as long as the fibres do not shrink. Along the length of the fibres the mechanical bond may also be increased due to the tendency of the fibres to curve. The fibres naturally curve, even inside the cement matrix.

The curving of the fibres can increase the mechanical bonding, but only until a certain degree. Beyond this level of curvature the bending moment necessary to pullout the fibre is higher than the fibre strength, leading to fibre rupture. Images produced by a CT-scan of single fibres embedded in a cement matrix reveal the importance of the curvature of the fibres

inside the matrix and its influence in the behaviour during the pullout. It can be seen that a tested pullout sample that had undergone fibre rupture has a sharper curvature inside the cement matrix than a tested sample that shows any other pullout behaviour. For example: A pine fibre in matrix MF1 with 5 mm embedment length that showed a constant friction effect when pulled out has a curvature angle of 3.6°, while a fibre that broke during the test had an angle of 11.6° (figure 5.25). The fibre-matrix interface shown in figure 5.25(a) has cracks and spalling as a result of pulling the fibre out. In figure 5.25(b) it is noticeable that the embedment end has slipped inside the fibre tunnel before rupture.

(a) (b)
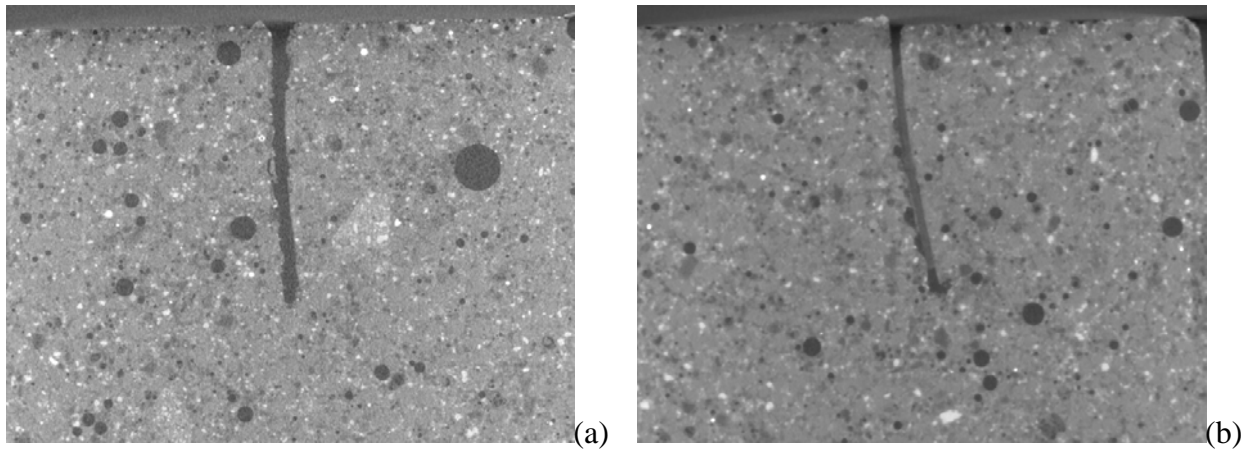
Figure 5.25: CT Scan of pine and MF1 air-cured samples: a) constant friction b) fibre rupture.

(a) (b)
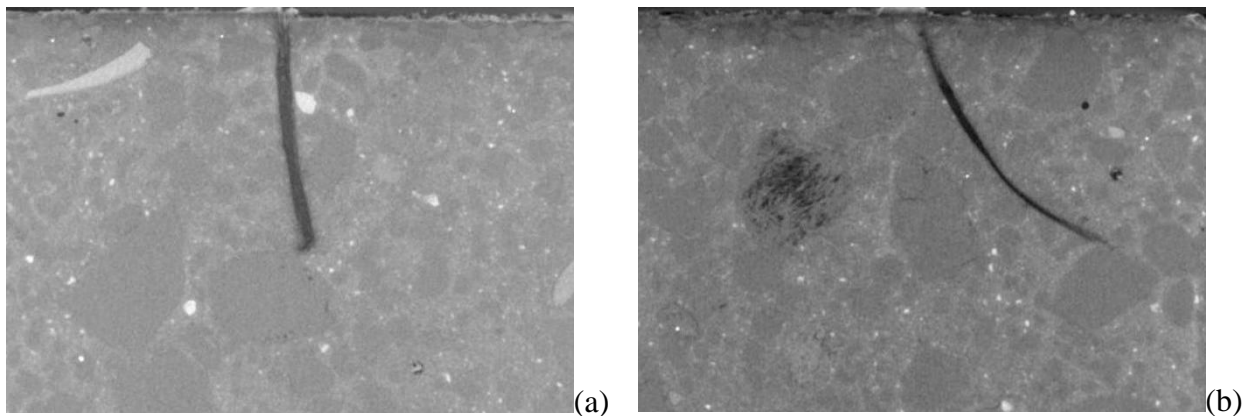
Figure 5.26: CT Scan of spruce and CS2 air-cured samples: a) constant friction b) fibre rupture.

In figure 5.26 CT scan images of the trace of two spruce fibres that have been pulled out of blocks of CS2. The first sample had constant friction behaviour (figure 5.26(a)). Here the curvature angle was about 12°. The second sample had a significant curvature and an angle bigger than 30°. This fibre broke during the test. For samples of MF3 matrix the angle of a spruce fibre that shows slip softening behaviour is smaller (6.9°) than for a fibre that shows slip hardening (8.2°). Also larch fibres embedded in MF3 were scanned and from the images an angle of 27° was estimated for a fibre that broke before being pulled out while for a fibre that was fully pulled out with behaviour governed by friction the angle was 15°.

Does the maximum interface shear stress depend on the embedment length? Since the natural fibres vary in cross section area, instead of just looking at the embedment length, in this research the embedment area of the fibre, which is the fibre cross section contour times the embedment length, is taken into account. For every tested fibre, using the program ImageJ, the contour is measured from photographs made of the part of the fibre that remained outside the cement matrix prior to the test, the part of the fibre that was inside the cement matrix prior to the test and the cement matrix that hosted the fibre. During the pullout the cross section of some of the fibres decreased due to the pulling action, as can be seen in figure 5.27. Special care was taken in such cases to measure the embedded area accurately. Spruce fibres, which were semi-chemically produced and showed overall adhesion bond with the different cement matrices, have a clear tendency to decrease the interface shear stress with increasing embedment area.

(a)   (b)
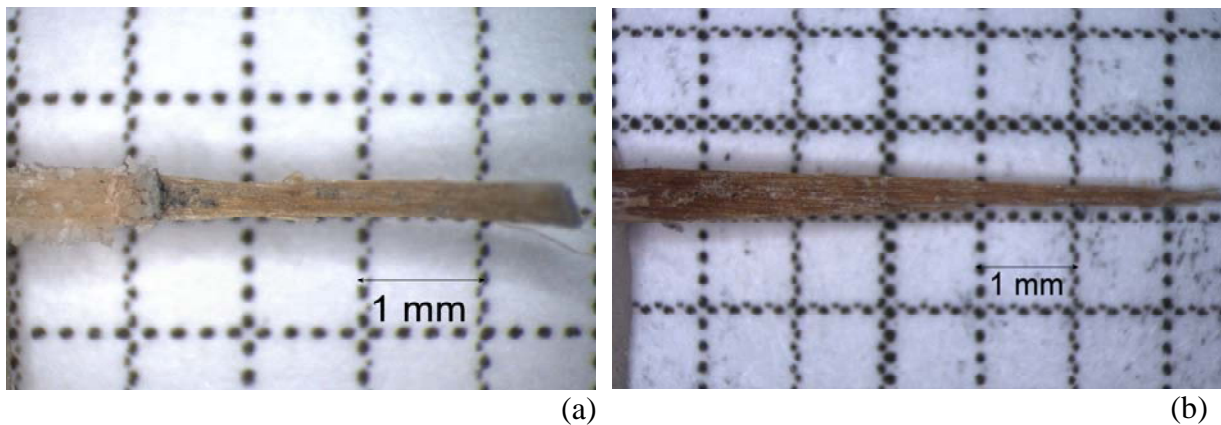
Figure 5.27: Cross section reduction in the fibre after been pulled out: (a) spruce and (b) pine.

Figures 5.28 and 5.29 present the relation between embedment area and interface shear stress for spruce fibres under air-cured and water-cured conditions respectively. This same tendency was observed in PVA fibres embedded in cement and fly ash based material [Boshoff 2007], polypropylene thin sheets embedded in conventional mortar [Singh et al. 2004], steel fibres embedded in conventional mortar matrices (1.4 MPa) as well as steel fibres embedded in mortar with optimized particle packing (4.4 MPa) [Shannag et al. 1997], and sisal fibres in mortar with metakaolin and waste crushed clay brick [Silva 2009a;b]. On the other hand, the interface shear stress tendency to decrease with increasing embedment area is not as clear for pine fibres as for spruce fibres (figure 5.30). This may be because the most frequent pullout behaviour of pine fibres is governed by friction and not by adhesion. The friction developed as the fibre slips will increase and decrease due to other factors, such as the curvature angle, as previously explained.
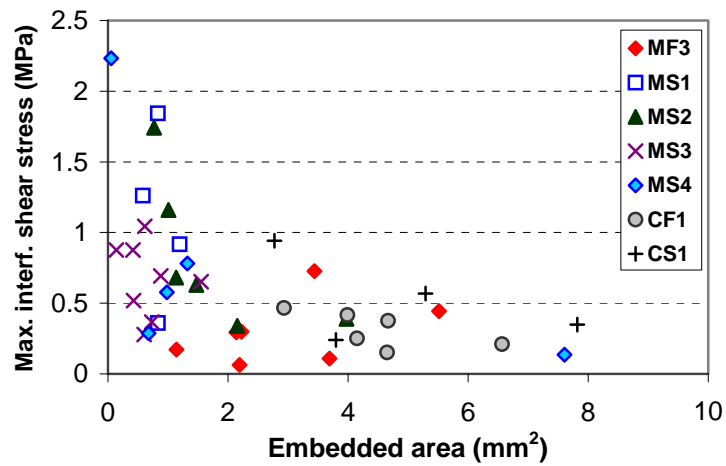
Figure 5.28: Embedment area vs. interface shear stress (spruce fibres, air-cured)
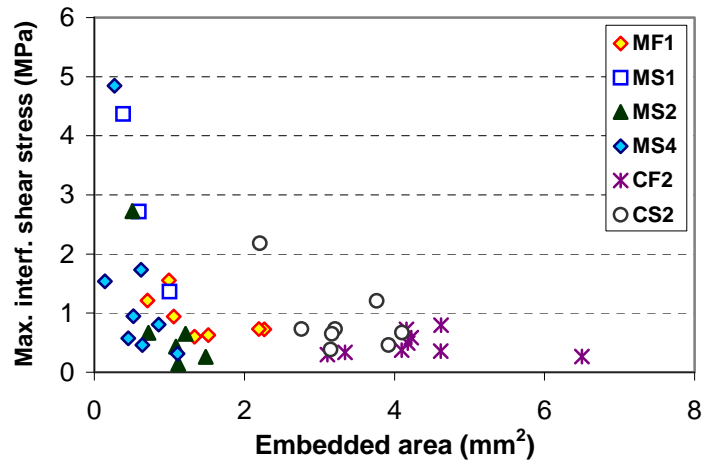

Figure 5.29: Embedment area vs. interface shear stress (spruce fibres, water-cured)
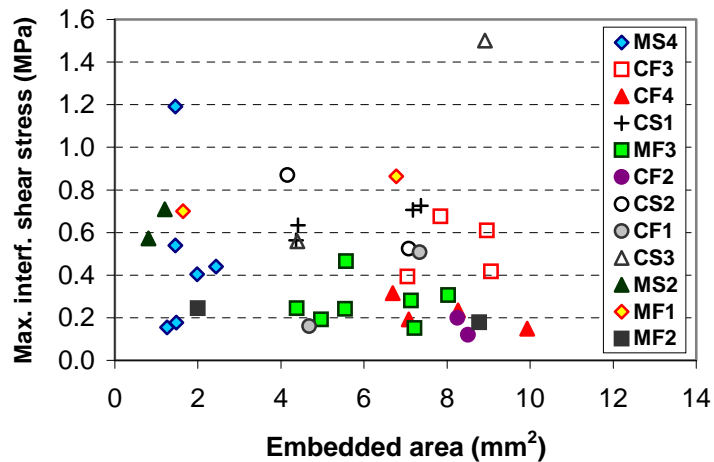

Figure 5.30: Embedment area vs. interface shear stress (pine fibres, air-cured)

5.4   Fibre treatments

Wood changes dimensions as it gains or loses moisture below the saturation point. The fibres shrink when losing moisture from the cell wall and swell when gaining moisture in the cell wall. Tangential, radial and volumetric shrinkage values are higher for hardwood than for softwood [Wood handbook 1974; Schroeder 1972]. Hardwood and softwood have about the same amount of cellulose, but different amounts of lignin and hemicellulose. Hardwood has about 5% more hemicellulose than softwood has and hemicellulose is the chemical component that exhibits the highest absorption capacity. From measurements presented by Schroeder [1971] the volumetric shrinkage ranges between 10 and 12% for different types of spruce and between 8 and 12% for different types of pine. Inside the cement matrix the wood fibres also swell and shrink in the presence or absence of water. These volumetric changes affect the bond between the fibre and the matrix. To overcome this problem the fibres were treated to decrease the volumetric changes.

Chemical modification of wood to improve both dimensional stability and decay protection has been extensively studied and successfully applied. Some of the chemicals used to modify wood fibres include anhydrides, acid chlorides, carboxylic acids, isocyanides, aldehydes, esters and epoxides [Rowell et al. 1986]. Commercially available water repellents can also change the long-term properties of wood. The most studied chemical modification process is acetylation. For the present research project simple and practical fibre treatment methods are preferred, thus a simplified acetylation process will be tested with spruce and pine fibres as well as a short treatment with commercially available silane systems.

5.4.1   Silane treatment

Silanes are silicon compounds with the general formula Si_nH_{2n+2}. These compounds are chemically less stable than their carbon counterparts and are inflammable on contact with air [Donath et al. 2006]. Silane groups include compounds in which organic or inorganic groups, such as alkyl, alkoxy or chloride groups substitute the hydrogen atoms [Ullmann 2011]. Silanes can provide the basis for hydrophobation of ceramics and concrete, and can also promote the adhesion between organic and inorganic materials, as in this case, between organic fibres and inorganic cement-based matrix. Silanisation of natural fibres increases the adhesion between fibres and polymer matrices, thereby upgrading the composite strength [Kozlowski et al. 2004]. The dimensional stability of wood chips treated with alkoxysilane improved [Schneider and Brebner 1985]. Donath and colleagues [2006] proved that the water uptake of wood treated with commercially available oligomeric silane systems, Dynasylan[®] HS2909 and Dynasylan[®] F8815, reduced considerably. In their research they dilute the functional silanes in tap water to a specific concentration and later dip the wood in this solution and cure it at 60ºC. Following this procedure the treatment with Dynasylan[®] HS2909 resulted in more stable protection against water. Explained by the authors, silanes, in general, form hydrogen bonds to hydroxyl groups of the wood cell-wall via siloxane but Dynasylan[®] HS2909 showed higher affinity with the hydroxyl groups because of the additional amino groups. X-Ray mapping of pine samples with this multifunctional silane revealed accumulation of silicon in cell lumina and bordered pits. The plugging of pits, ray cells and tracheids, main penetration paths for water intake, explains the reduction in water intake in fibres treated with this silane.

Following the experience from these researchers, two commercially available products where chosen for fibre treatments in the present thesis: Dynasylan[®] HS2909 and Dynasylan[®]

HS2627. According to the manufacturers, both products have equal functionalities within a wide pH-range. Dynasylan® HS2909 has a pH of 4 while Dynasylan® HS2627 a pH of 11. The silanes were diluted with tap water to obtain concentrations of 20% and 5%. The fibres were dipped in the solution for 30 min, then drained and placed in a pre-heated oven at 60ºC to be cured there for the next 16 hours. Donath et al. [2006] pointed out that although higher temperatures lead to higher completion of the silane reaction, a maximum temperature of 60ºC was chosen to reduce the risk of superficial cracking. The fibres were stored at room temperature and 50% RH until testing or casting with cement matrices.

5.4.2   Acetic acid treatment

Pine and spruce fibres were treated according to a simplified rapid acetylation method developed by Rowell et al. [1986]. The wood fibres were placed in a stainless steel mesh container and then dip in the acetic anhydride for 1 min, after which they were removed from the container with acid and drained for 3 min. The dipping and draining was done at room temperature of around 22ºC. Later the fibres were placed in a pre-heated oven at 60ºC for 2 hours. After this reaction time the fibres were placed in a vacuum device for 2 hours at room temperature. Finally the fibres were oven dried at 60ºC for another 16 hours. The short vacuum cycle helps to quickly remove the chemicals from the fibres after the reaction. This is necessary because of the small size of the fibres being acetylated.

Rowell and colleagues [1986] proved that with this simplified method of 1-minute dipping in acetic anhydride and 3-minutes draining time, southern pine flakes absorbed about 100% in weight and that a longer dipping did not increase the weight gain. The flake boards prepared with treated pine flakes absorbed less water and swelled at a lower rate and to a lower extent than boards made with fibres without treatment. Nevertheless, after the draining the reference followed a slightly different drying procedure: the reaction time and temperature were 1 hour and 120ºC, the vacuum was applied also at 120ºC and the fibres were oven dried for 105ºC for 12 hours. But considering that the reference used wood flakes of dimensions 0.5x64 mm and a random width, implying bigger wood pieces than the fibres used in this research, it is necessary to reduce the oven temperature to minimise the risk of surface crack formation. Also due to a laboratory constraint, it is not possible to apply a temperature of 120ºC to the vacuum chamber, it was judged necessary to reduce the temperature variations in the fibres if they were first placed in the oven at 120ºC for the reaction time, then at room temperature (22ºC) for the vacuum and later at 105ºC to oven dry.

After curing the fibres were stored at room temperature and 50% RH until testing or casting with cement matrices.

5.4.3   Fibre mechanical properties and microstructure (and chemical changes)

Some randomly selected spruce and pine fibres treated with the simplified acetic acid and silane treatments described above were tested under direct tensile strength. The test details were given in Chapter 3. Table 5.1 presents the results for spruce fibres. The average values of the tensile strength and the Young's modulus are lower for treated fibres. The lowest strength was registered for fibres treated in a solution with 20% Dynasylan® HS2909. Since this solution has low pH (4) pine fibres were treated with 5% Dynasylan® HS2627 which has pH11. The results for pine fibres are shown in table 5.2. For both acid and silane treatments the tensile strength average values are about the same as for non-treated fibres, taking into account the wide variation of the results expressed by means of the standard deviations.

Tensile tests results for acid treated spruce showed that the tensile strength decreases with increasing cross-section area, up to an area of 0.1 mm². This is the same tendency observed for non-treated spruce fibres. Fibres with bigger cross-section were not tested.

Table 5.1: Characteristics of treated and untreated spruce fibres
(Standard deviations are indicated between brackets)

Spruce fibre	Tensile strength σ_f (MPa)	Corrected Young's modulus E_f (MPa)	Area (mm²)	Strain to Failure (%)	Number of Tests
20% HS2909	70.6 [12]	3.3 [1.4]	0.067 [0.025]	2.2 [0.3]	5
Acetic acid	91.8 [26]	2.9 [0.5]	0.060 [0.020]	3.2 [0.6]	7
Untreated	169.3 [36]	8.1 [3.7]	0.059 [0.036]	2.4 [1.0]	10

Table 5.2: Characteristics of treated and untreated pine fibres
(Standard deviations are indicated between brackets)

Pine fibre	Tensile strength σ_f (MPa)	Corrected Young's modulus E_f (MPa)	Area (mm²)	Strain to Failure (%)	Number of Tests
5% HS2627	103.2 [86]	4.6 [3.1]	0.104 [0.024]	2.6 [1.3]	19
Acetic acid	156.9 [74]	10.2 [4.7]	0.094 [0.068]	1.7 [0.3]	8
Untreated	123.9 [75]	4.7 [2.6]	0.106 [0.039]	3.2 [1.2]	50

Figure 5.31 shows the longitudinal section of a pine fibre treated with 5% HS2627. The rectangles 1 and 2 in the micrograph indicate the target regions of 2 EDS analyses that follow in figures 5.32 and 5.33. The EDS analyses show the presence of Si in the surface of the fibres, and in the cell wall and lumen close to the surface (figure 5.32) and in fewer amounts in the cell wall in the centre of the fibre (figure 5.33). The chemical analysis by EDS of a non-treated pine fibre, presented in figure 5.34, indicates no presence of Si, only C and O as is expected.
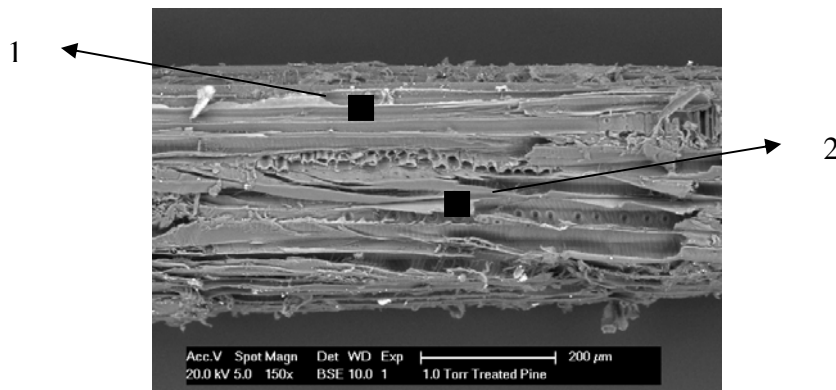

Figure 5.31: Esem image of longitudinal section of pine fibre treated with 5% HS2627, EDS target regions indicated as (1) and (2).
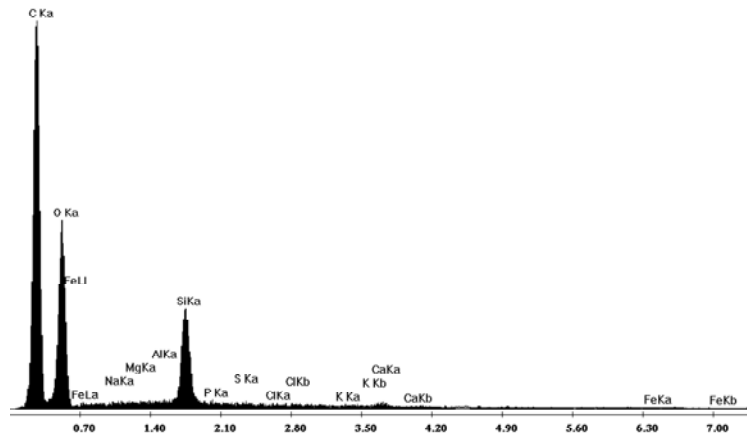
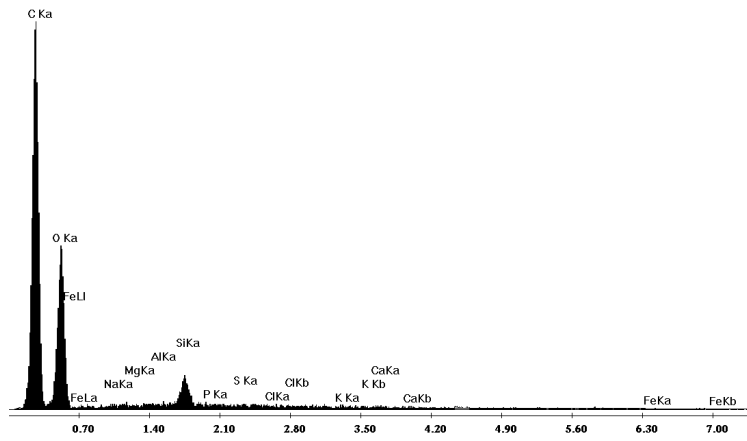*Figure 5.32: EDS spectrum of treated pine fibre surface [1].*

Figure 5.33: EDS spectrum of treated pine fibre, cell wall in the centre of the fibre [2].
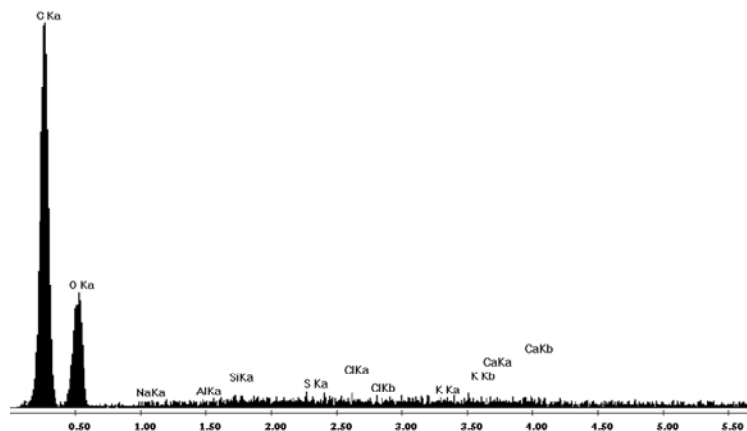

Figure 5.34: EDS spectrum of untreated pine fibre.

5.4.4 Improvements on fibre-matrix interface

The effect of the fibre treatment upon the fibre-matrix interface was studied by means of microscopic images, IR spectroscopy tests and pullout tests. Untested pullout samples were prepared according to the method described in section 5.2.2 and observed in the ESEM. As can be seen in figure 5.35 the contact between a spruce fibre treated with acetic acid and the cement matrix remains sound after 73 days under air-cured conditions (30% - 50% RH). The fibre cross-section dimensions have not changed and there is no gap between the fibre contour and the matrix. Similar observations with pine fibres show that treated fibres do not shrink when cured in dry conditions. Figure 5.36 presents ESEM images of pine fibres treated with acetic acid embedded in mix G2 and cured with and without additional water. These fibres show no apparent volumetric changes.
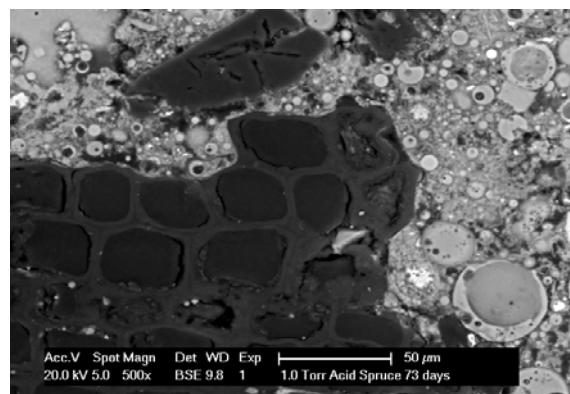
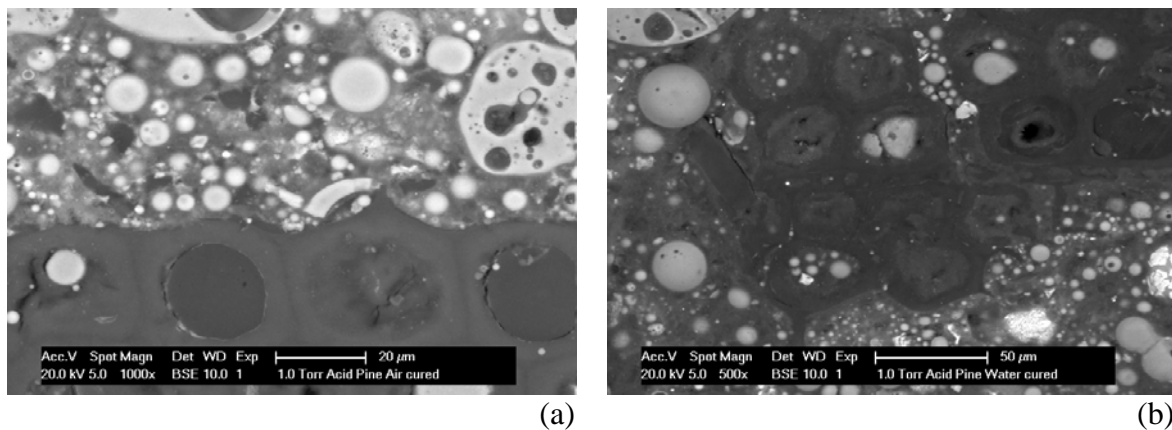*Figure 5.35: ESEM image of an acid spruce fibre embedded in MF1.*

(a)   (b)

Figure 5.36: ESEM images of acid pine fibres embedded in CF4
a) air-cured and b) water-cured.

EDS analysis of the interface between matrix F1 and treated and untreated pine fibre showed differences in the chemical composition of the interface depending on the fibre treatment. The results are summarized in figure 5.37. The highest percentage of carbon was measured in the interface with fibres treated with 20% HS2909. In this interface the percentage of oxygen is the lowest. Measurements done at the interface with untreated pine and at 250 μm from the fibre are similar, indicating that there is almost no influence of the

fibre on the chemical composition of the surrounding matrix. The main chemical elements present in the bulk matrices are oxygen, silicon and calcium. These are typical elements for cement gel (CSH).
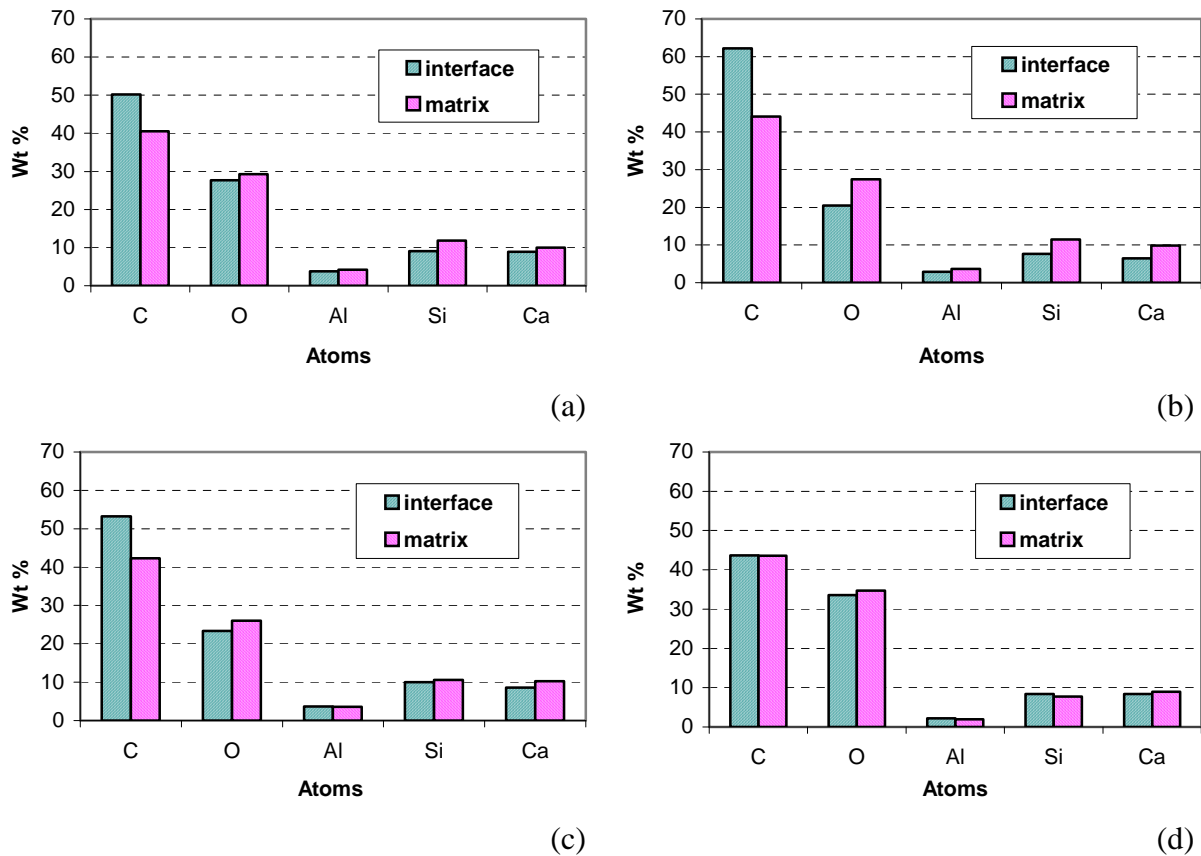

(a)

(b)

(c)

(d)

Figure 5.37: Chemical analyses on different zones of pullout samples of cement matrix MF1 and a) 5% HS2909 pine, b)20% HS2909 pine, c) acetic acid pine and d) untreated pine.

The chemical analyses of pullout samples with treated and untreated spruce fibres and matrix MF1 show variations between the interface and the matrix at a distance of 250 μm from the fibre, for all the samples. The variations are more noticeable for untreated spruce and spruce treated with acetic acid. Figure 5.38 presents the measurements. For all the samples, in the interface the weight percentage of carbon is higher, while the percentage of oxygen, silicon and calcium are lower.

As explained in section 5.3.3 the high content of carbon may be due to the fibre itself since the fibre is basically carbon, or due to a higher porosity as consequence of the presence of the fibre. During the preparation of the samples the pores are filled with epoxy and the epoxy is also, mainly carbon.

Treated pine fibres were pulled out of three C matrices, CF1, CF2 and CS2. When comparing the maximum interface shear stresses achieved by untreated pine, pine fibres treated with 5% HS2627 (Silane Pine) and pine treated with acetic acid (Acid Pine), embedded in CF1, the highest values were estimated for silane pine, as shown in figure 5.39.
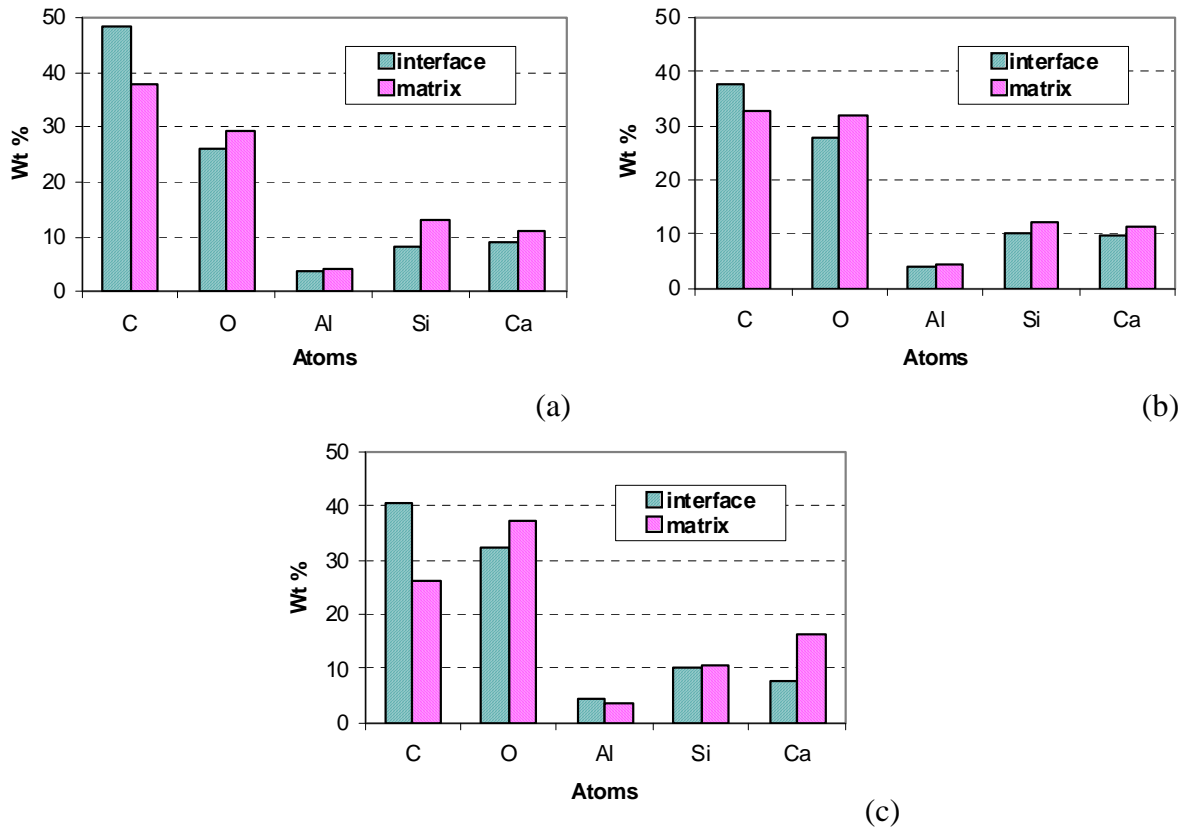
(a)

(b)

(c)

Figure 5.38: Chemical analyses on different zones of pullout samples of cement matrix MF1 and a) acetic acid spruce, b)5% HS2909 spruce and c) untreated spruce.
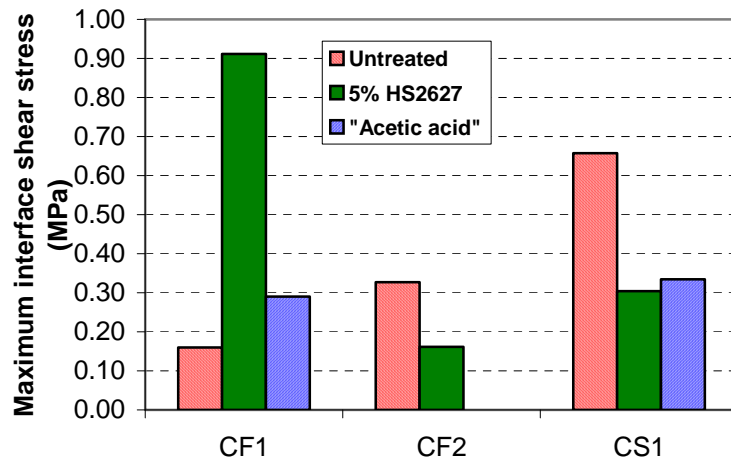

Figure 5.39: Average maximum interface shear stress for treated and untreated pine fibres in C matrices.
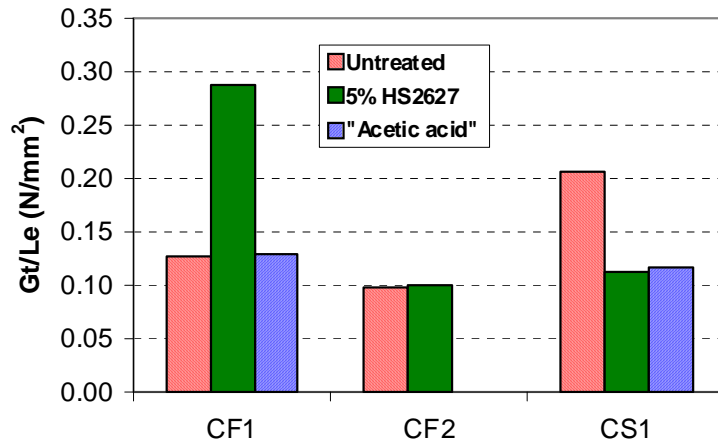
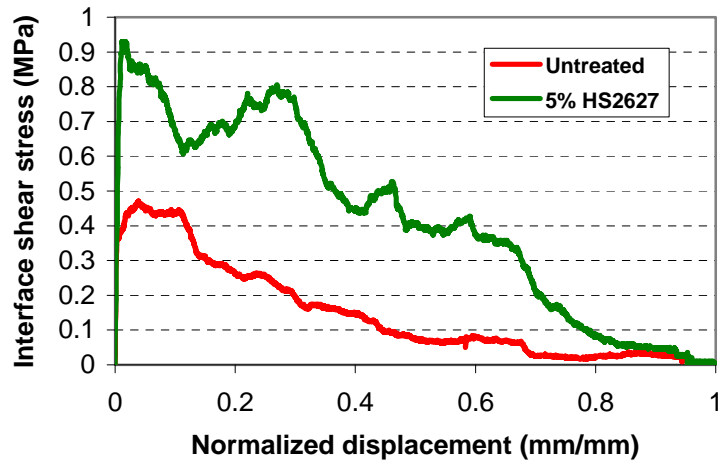*Figure 5.40: Pullout energy for treated and untreated pine.*

Figure 5.41: Pullout curve of untreated pine and silane pine in CF1 matrix.

The pullout energy, G_t / L_e, for silane pine was also high (figure 5.40) and this represents the improvement in pullout behaviour. The pullout curves plotted in figure 5.41 illustrate this improvement. The silane fibre reaches a higher interface shear stress and additionally releases more energy during the pullout. Silane pine in matrix CF2 have about the same shear stress as untreated pine and slightly higher G_t energy but when pulled from CS1 matrix, a mix with BFS and cement both shear stress and energy values were the lowest compared to acid and untreated pine. It is interesting to notice that the pullout results for silane pines are more stable, with lower values of standard deviation, than for acid or untreated pine.

Acid pine pulled out of CS1 and CF1 matrices develop low values of shear stress, below 0.35 MPa, see figure 5.39, and limited amounts of energy as presented in figure 5.40.

Figure 5.42 presents the average maximum interface shear stress for treated and untreated spruce fibres in C matrices and figure 5.43 the pullout energy calculated for treated and untreated spruce.
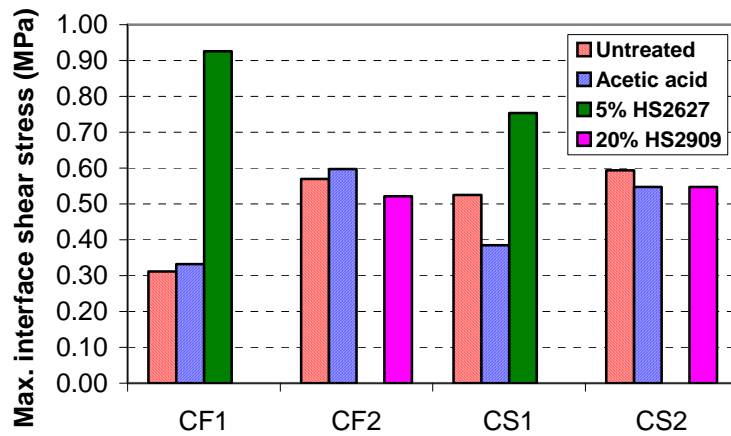
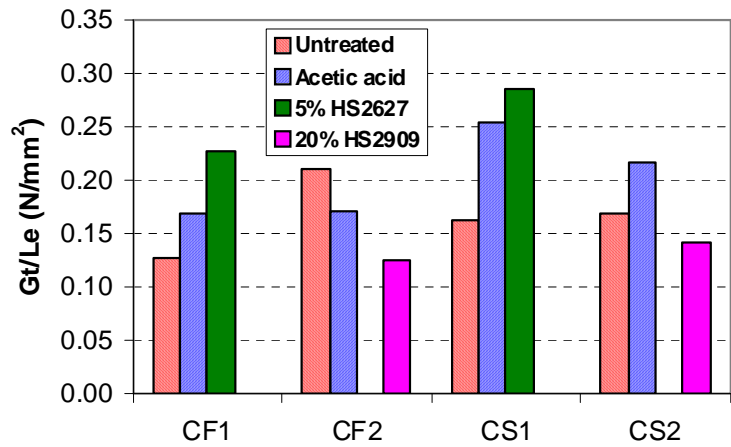*Figure 5.42: Average maximum interface shear stress for treated and untreated spruce fibres in C matrices.*

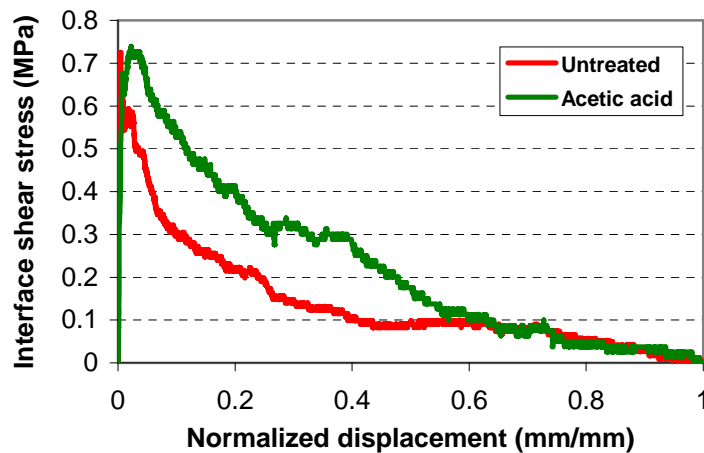*Figure 5.43: Energy for treated and untreated spruce.*

Figure 5.44: Pullout curve of untreated pine and acid spruce in CS2 matrix.

Spruce fibres treated with acetic acid (Acid spruce) achieved about the same average interface shear stress with mixes CS2 and CF2 as other treated spruce and non-treated spruce but with both mixes, the acid spruce have higher pullout energy and therefore the best pullout behaviour. This improvement is more noticeable with mixes CS2 than with CF2. Pullout tests of acid spruce in CS2 exhibited mainly slip hardening behaviour, in comparison with the predominant slip softening behaviour of untreated spruce in CS2, as can be seen in figure 5.44.

All the pullout samples of CF2 and CS2 were water-cured. This condition explains the uniformity of interface shear values registered for treated and untreated spruce. In the permanent presence of water the untreated spruce fibres do not experience volumetric changes. For air-cured conditions, acid spruce fibres pulled out of CF1 matrices have higher interface shear stress and pullout energy G_t than untreated fibres. On the other hand, in CS1, acid spruce fibres had lower shear stress than untreated fibres, but higher G_t due to better behaviour.

Spruce fibres treated with 20% HS2909 and embedded in CF2, have the same shear stress and energy G_t than acid and non treated spruce. These silane spruce fibres in CS2, yield about the same shear stress but lower energy than acid and untreated spruce. Spruce fibres treated with 5% HS2627 and pulled from mixes CF1 and CS1 have the highest interface shear stress and pullout energy G_t. Since the shear stress and pullout energy for both acid spruce and untreated spruce decrease from CF2 to CF1 and from CS2 to CS1, as well as the matrix compressive stress, also for spruce fibres treated with HS2909 lower values of stress and energy were expected for CF1 than for CF2. Instead, fibres were treated with HS2627 and higher stress and energy values were registered, after which the author concludes that this fibre treatment, with pH11, does improve the fibre-matrix interface to a larger extent than the silane treatment HS2909 with pH4. Unfortunately, the bond of fibres with HS2909 to the cement matrices improves to such a level that the bond shear strength is higher than the fibre tensile strength. Therefore the fibre itself is weaker than the bond to the cement matrix, and fibre rupture happens during the pullout test.

5.5   Analytical model

There are several analytical models for fibre pullout force vs. pullout displacement relationship. For most researchers, fibre debonding governs the ascending stage of the load-displacement curve. The existing models can be classified into two groups, depending of the basic assumption of the condition for debonding. One group includes strength-based models [Gopalaratnam and Shah 1985; Naaman et al. 1991a,b; Sueki et al. 2007; Jun et al. 2009] while the other group are energy/fracture-based models [Stang and Shah 1986; Gao et al. 1988; Lin et al. 1999; Jun et al. 2009]. Leung and Li [1990] discuss the suitability of these approaches.

The strength-based models reviewed here were developed for steel fibres embedded in cement matrices and Sueki et al. [2007] adapted the model for textile yarns. In this model the characteristic pullout curve can be divided into three zones based on the various stages of shear stress distribution in the fibre, see figure 5.45. The initial slope of the pullout curve, in stage I, corresponds to a linear elastic behaviour due to perfect bonding between fibre and matrix. After a certain point the response becomes non-linear due to initiation of debonding (stage II). The stiffness of the curve will decrease as the debonding propagates along the embedment length until reaching a maximum load P_{max}. The debonding continues in the post peak region until the whole fibre length is debonded. After this point, the fibre slides out dynamically (stage III). This model seems to be suitable for the pure-friction pullout

behaviour exhibited by pine fibres in the present thesis because of several reasons. In the first place, the shape of the curve in the model (figure 5.45) corresponds to the pullout curves of pine fibres (figure 5.14). Additionally, two basic assumptions of the model, which are that beyond the interface bond strength τ_{max} purely frictional conditions prevail and that the chemical adhesion between matrix and fibre is negligible shape of the curve, fully describe the experimental results.
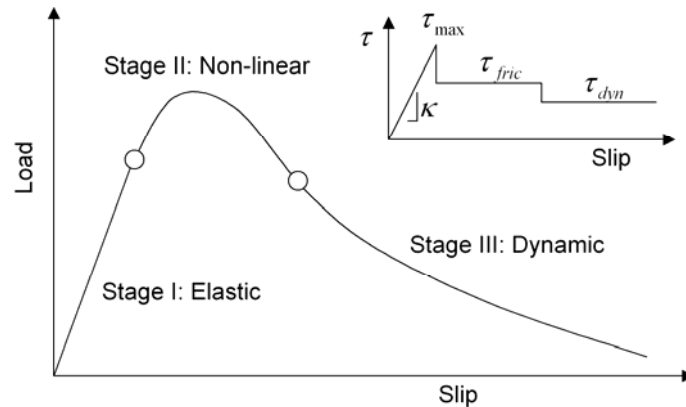

Figure 5.45: Pullout-slip response and shear strength diagram.

The model by Sueki et al. [2007] was derived for boundary conditions where the front of the matrix was fixed so that the matrix is under compression during the pullout test and therefore shortens. However, the test setup as shown in figures 5.8 and 5.9 has a boundary condition where the bottom of the cement matrix sample is fixed leading to the cement matrix being in tension.

In spite of taking into account this difference between the used setup and the mathematical model, the model does not reproduce the phenomena observed during the pullout of pine fibres. The initial slope of the pullout tests reported here does not correspond to the elastic deformation of just the fibre free length, but to the elastic deformation of the entire fibre, as can be seen in figure 5.46, before showing displacements that are even larger than the elastic deformation of the entire fibre. The results shown in figure 5.46 could be explained by assuming that the fibre in the pullout test almost immediately debonds or may not be bonded at all from the beginning. In the case shown in figure 5.46a the fibre is still connected to the matrix for a short while so that it shows near elastic behaviour before starting to slip out while in the case shown in figure 5.46b the fibre immediately starts to slip. This is in contradiction to the mathematical model that assumes there is first a fully bonded elastic domain followed by a gradual debonding with the increase of force.

The application of this analytical model to the pine fibre pullout tests is described in detail in Appendix B.

The energy-based models also take into account initial elastic stretching of the fibre free length [Lin et al. 1999]. A stable debonding stage follows the fibre stretching. The debonding process is viewed as crack propagation along the interface tunnel from the matrix free end toward the embedded end. The debonding continues until reaching a maximum load, and then there is a sudden load drop, interpreted as the loss of adhesion or chemical bond. After this point the fibre will slide with the only resistance of friction forces (figure 5.6). The pullout behaviour described by this model corresponds to the pullout behaviour exhibited by most of the spruce fibres.
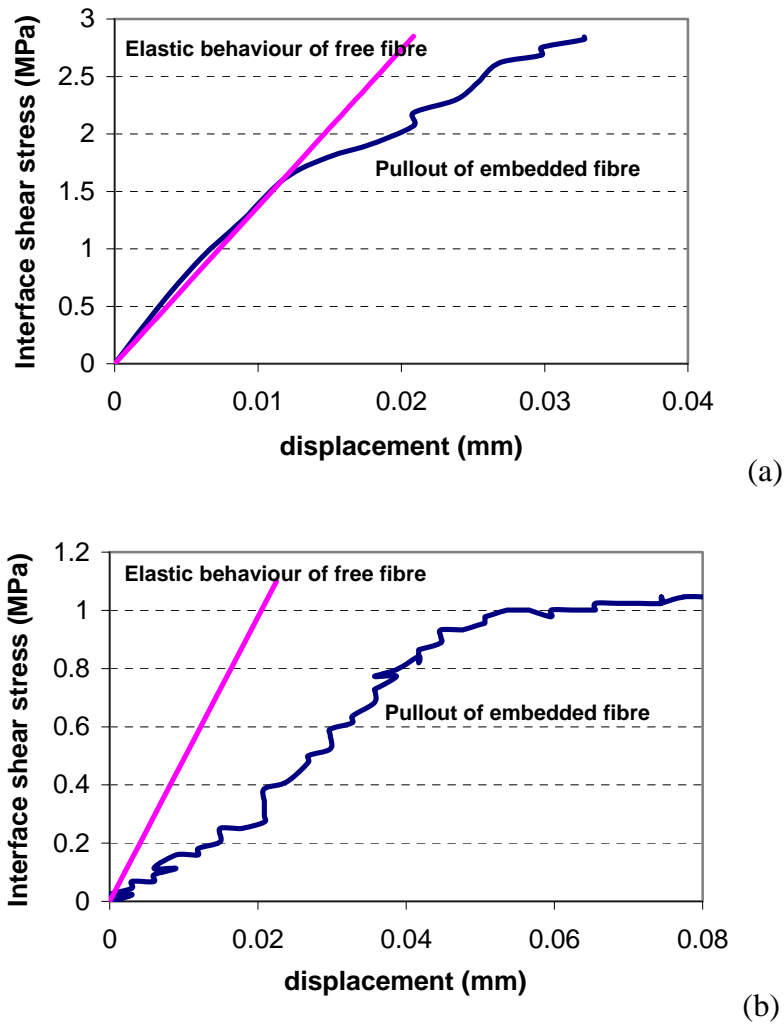
Figure 5.46: Elastic curve for fibre and for pullout test
a) near elastic behaviour b) immediate slip.

5.6   Numerical model

In the previous paragraph the assumption was made that during the pullout test the fibre undergoes a rapid debonding followed by slip. Based on this assumption a numerical model has been proposed in order to see if it is possible at all to produce curves equal to the measured curves. Therefore, the pine pullout curves, with realistic boundary conditions, were modelled using the finite element software Plaxis [Brinkgreve et al. 2010].

The finite element model is a 2D axisymmetric model representing the matrix as a cylinder with the same cross sectional area as the matrix used in the test (which has a square cross section), and a fibre with circular cross section such that the circumference of the fibre in the model equals the circumference of the real rectangular fibre in order to get the same frictional surface. Both the matrix and the fibre are assumed to behave linear elastic while the matrix-

fibre interface is modelled as linear elastic perfectly-plastic with constant shear strength. The details and results of this model are described in Appendix C.

The fibre is pulled out displacement controlled until the shear strength is fully mobilised in the matrix-fibre interface and the fibre is fully debonded. From this moment on the fibre will slip and the shear strength of the matrix-fibre interface is decreased as function of the pullout displacement. Figure 5.47 shows the pullout force as function of the pullout displacement (slip) for both the test and the Plaxis model.

It can be seen that the numerical model can indeed produce the pullout behaviour as measured in the real pullout test based on the assumption of rapid debonding and slip, though the numerical model has a more sudden start of the slip phase than the tests do. This can be explained by the fact that the numerical model assumes a fibre of constant cross sectional area that indeed will slip instantaneously when the full shear strength of the matrix-fibre interface is mobilised, whereas the real fibre has an irregular cross section and therefore during slip may still develop some additional friction during slip.
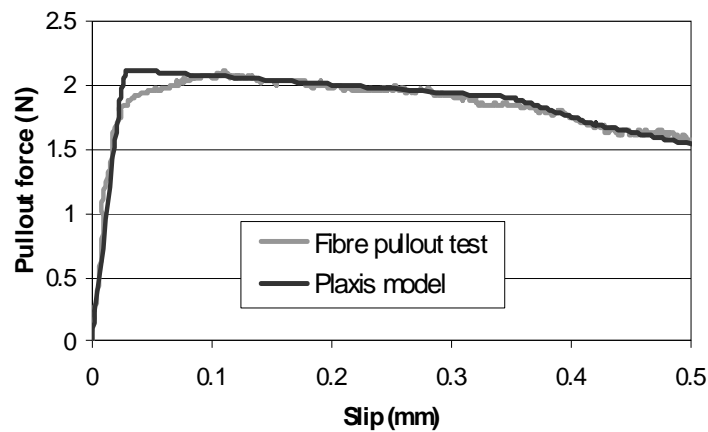

Figure 5.47: Pullout behaviour of the test vs. results of the numerical model.

5.7   Concluding remarks

This chapter explores the effect of the cement matrix composition, the curing conditions and the fibre type and geometry on the interface behaviour between softwood fibres and cement-based matrices. Among these factors it is necessary to highlight the loss of interface bond due to the volume changes of the fibres in the presence of water. To minimize this effect the wood fibres have been treated in different ways. The following conclusions are drawn from the experimental results:

- Two simple and practical treatments for wood fibres probed to reduce the volumetric changes of the fibres and, as a direct consequence, improved the pullout behaviour. A constant and sound interface bond was observed between treated fibres and the cement matrices.
- The natural curving from the fibres increases the mechanical bond. However, it is necessary to take into account that excessive curving will lead to fibre rupture when the fibre is pulled out.

- The interface shear stress tends to increase with increasing cement matrix compressive strength.
- For most of the tested cement matrices, both pine and spruce fibres yielded about the same maximum interface shear stress. The pullout behaviour, on the other hand, is remarkably different, spruce fibres tend to show slip softening while pine fibres exhibit behaviour governed by friction.
- The analytical model for synthetic fibres, assuming gradual debonding of the fibre and later fibre slide, is not applicable for wood fibres.
- The numerical model for fibre pullout fits the laboratory test results, hence its assumption of volume loss due to internal damage of the wood fibre during pullout is plausible.
- From the pullout tests results it can be seen that the best pullout behaviour of pine fibres was in combination with matrices CF3, CF4 and CS1. Therefore, in Chapter 6, pine fibres will be used as reinforcement for cement matrices with these matrices.

In chapter 6 the physical and mechanical properties of cement-based material reinforced with wood fibres are presented. In order to obtain a ductile material with wood fibres, the ratio of the stiffnesses of the matrix and the fibres should be as low as possible. Thus, regarding the use of pine fibres, in Chapter 6, they will be used as reinforcement for cement-matrices with low compressive strength and low interface shear stress. The matrices that fall under these criteria are CF2, CF3 and CF4.

Chapter 6

Wood fibre-cement matrix composites

6.1   Introduction

This chapter deals with the link between the fibre properties studied in Chapter 3, the matrix properties described in Chapter 4 and the fibre-matrix interface analysed in Chapter 5 in order to develop wood-fibre cement composites. The composites are designed to exhibit a deflection-hardening behaviour. "Deflection-hardening" describes the behaviour of a ductile composite that exhibit multiple cracking in bending. In this thesis ductility is understood as the ability of a material to develop additional strain after initial cracking while sustaining the load.

The first part of this chapter describes preliminary laboratory tests conducted with composites consisting of one single type of cement matrix but prepared with all the possible wood fibres. These laboratory tests were conducted to serve as input for a micromechanic-based model for the composite behaviour as well as to evaluate the suitability of each fibre type as reinforcement for a cement-based composite. Additionally, information on fibre properties and fibre pullout behaviour has been used in the micromechanics model. The micromechanics model provides the amount of fibres necessary to develop multiple cracking before failure under bending stress, which is the aim of this research. Based on the results of the preliminary tests and the micromechanics model the most suitable type of fibres is chosen for further investigation of the composite material using different cement matrices. The results of this further investigation are presented in sections 6.4 and 6.5.

6.2   Preliminary laboratory tests

6.2.1   Materials and mix design

Preliminary tests were conducted with cement matrix MF1 reinforced with 2% softwood fibres. In this matrix 55% of the cement content has been replaced by fly ash. Matrix MF1 has been chosen for the preliminary tests because it has the same mix design as was used for ECC, Engineered Cementitious Composites. ECC is a material developed by the University of Michigan [Li 1998] and forms the bases of the micromechanics model used in this research. ECC is material reinforced with short discontinuous artificial fibres (<10 mm long) and it shows enhanced ductility achieved by multiple cracking prior to failure. This is the behaviour expected from the material with wood fibres being designed in this thesis. ECC.

The mix composition of MF1 is given in table 4.3 of chapter 4, with the addition of 2% per volume wood fibres. The chemical composition of the cement OPC and pulverized fly ash (FA) as well as the density and particle size distribution are given in Chapter 4. The cement

type is CEM I 42.5 N. The river sand used has a maximum particle size of 250 μm and a minimum size of 125 μm. To improve the workability of the fresh cement mixtures the superplasticizer CRETOPLAST SL-01 con. 35% has been used.

6.2.2 Mixing and curing

The powder materials, Portland cement and fly ash, and the river sand were first mixed together, for 1 minute at low speed, with the sand using a HOBART® mixer. Then water and superplasticizer were added and mixed for another 3 minutes. Finally, the fibres were added and mixing continued for 2 more minutes.

The fresh mixture was cast and cured for 1 day in moulds covered with plastic after which the samples were demoulded and cured submerged in water at room temperature of 20°C until they were tested.

6.2.3 Laboratory tests

6.2.3.1 Four point bending test

Specimens with dimensions $240 \times 60 \times 10$ mm^3 were cured for 28 days. Prior to testing the specimens were cut into four samples with dimensions $120 \times 30 \times 10$ mm^3. These samples were used for four-point bending tests. Figure 6.1 shows the test set-up. The support span is 110 mm and the load span is 30 mm. Two LVDTs were fixed on both sides of the test set-up to measure the flexural deflection of the specimen. The average of these two measurements was used as feed back signal. The tests were conducted under deformation control at a speed of 0.01 mm/s. At least three tests were done for each mixture.
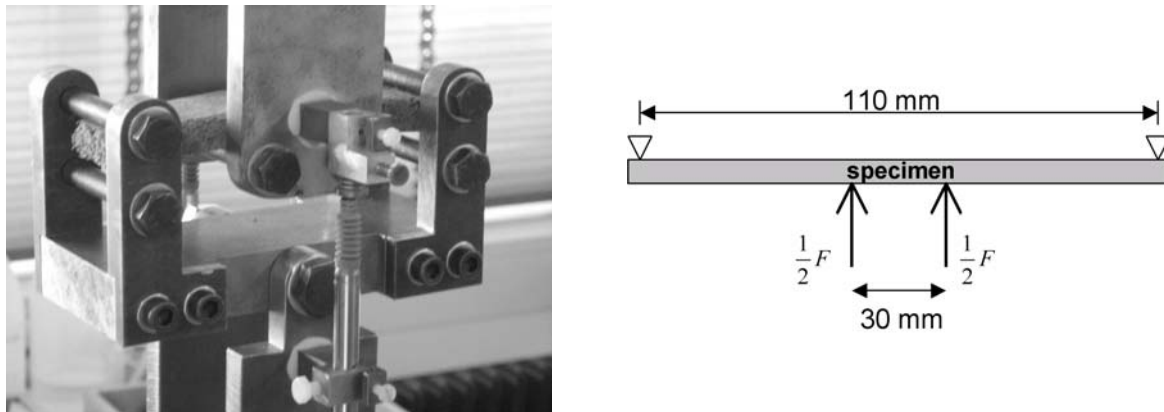

Figure 6.1: Four-point bending setup.

6.2.3.2 Uni-axial tensile test (with a notch)

Deformation controlled tensile tests were conducted on notched specimens to measure the composite fibre-bridging behaviour relation $\sigma(\delta)$ over a single crack. The notched specimen has a thickness of 10 mm, a width of 45mm and a height of 175 mm. Prior to testing the samples were cut from bigger samples with dimensions $240 \times 60 \times 10$ mm^3, and the notch was drilled. The notch is 6 mm deep (figure 6.2). The resulting reduced cross section is 33 mm $\times$ 10 mm. Two LVDTs were glued to both sides of the specimen, at the edge of the

notches. The testing gauge length is 70 mm. The loading rate used was 0.00002 mm/s to simulate a quasi-static loading condition. The crack opening was calculated from the average displacement across the crack measured by the 2 LVDTs. The test setup is shown in figure 6.2.
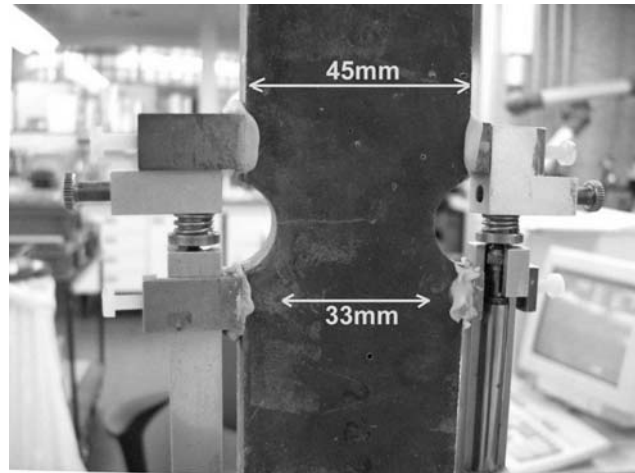

Figure 6.2: Setup of uniaxial tensile test for preliminary determination of σ(δ) curve.

6.2.4   Results and discussion

Under four-point bending load all the composites exhibit a single crack within the load span prior to failure. When comparing the results of samples tested after curing for 28 days submerged in water, and removed from the water tank just before the test, the samples prepared with pine fibres have the lowest bending stress: 2.8 MPa. The specimens with spruce fibres have the highest bending stress, 4.38 MPa, as can be seen in figure 6.3. The slope in the elastic range is about the same for all the composites.
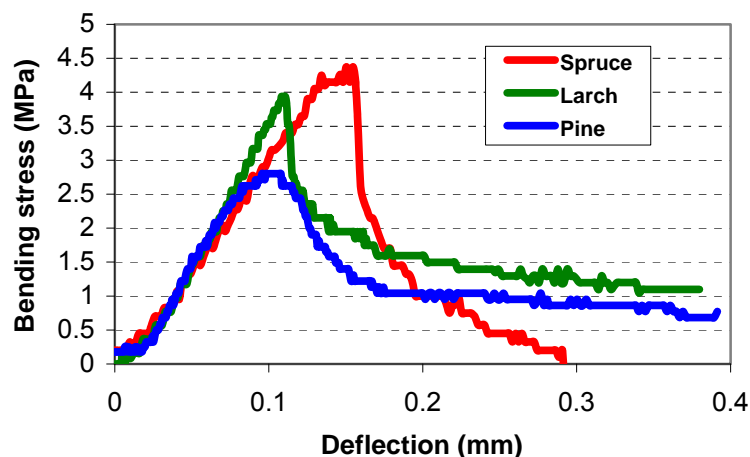

Figure 6.3: Flexural load-deflection curves for composites with 2% spruce, larch and pine fibres, at 28 days cured in water.

For the samples prepared with pine and larch the failure was not completely brittle. The width of the single crack kept increasing with the loading. There was visible fibre bridging within the crack that prevents the sample from exhibiting completely brittle failure. Figure 6.4 shows the fibre crack bridging.

Figure 6.4: Larch fibre-crack-bridging in a sample tested under flexural load.

Under uniaxial tensile load the samples had, as expected due to the presence of a notch, a single crack. The first crack strength was measured from these tests. Table 6.1 summarizes the average results.

Table 6.1: Properties of MF1 with V_f = 2% softwood fibres

Fibres	Bending strength (MPa)	First crack strength σ_{fc} (MPa)
Spruce	4.4	3.2
Larch	4.6	3.3
Pine	2.8	2.0

The first crack strength σ_{fc} is determined by matrix fracture toughness. Flaws in the matrix contribute to lower the matrix toughness and thus lower the first crack strength [Wang 2005; Li 2009]. Therefore, the first crack strength of the cement matrix was expected to be more or less the same for the three composites reinforced with different wood fibres, but the presence of the different fibres changed the matrix fracture toughness (table 6.1). The lower first crack strength is for composites with pine fibres, which have a considerably larger average cross section area (0.106 mm^2) than spruce (0.059 mm^2) or larch fibres (0.067mm^2). Since the fibre content of 2% per volume in all the tested composites is a too low percentage to develop a fibre bridging strength higher than the first crack strength of the matrix, the fibres are acting as fillers or flaws and not as reinforcement. At the same fibre volume content, there are less pine fibres than spruce or larch fibres due to the bigger cross section area of the pine fibres. Considering the fibres as flaws, in the composites with pine there are less flaws but the flaw size is bigger. Bigger size flaws lead to lower cracking strength [Wang 2005].

To understand the influence of the degree of saturation on the bending properties of the composites, four-point bending tests were conducted with samples that were cured under water and then left to dry in laboratory conditions (20°C and 50% RH) for increasing amounts of time. The samples of the first group were tested immediately after taking them from the water while the surface was dried with a towel. This condition is labelled "wet". Other groups were placed out of the water for 3, 6 and 24 hours prior to testing. The last group was kept outside the water for 3 days. This group is labelled as "dry"; even though there is still a moisture gradient, and possibly a stress gradient too. Figures 6.5 and 6.6 present the bending

stress for composites with larch and pine, respectively. The bending stress increases as the drying time increases. There is a moisture gradient within the sample that leads to different behaviour. When the samples were dried for 3 days, the samples behaved brittle and after failure it was not possible to continue the data registry.
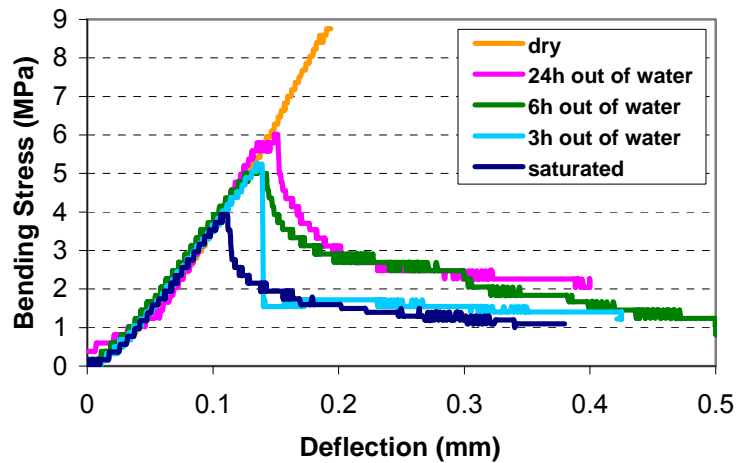

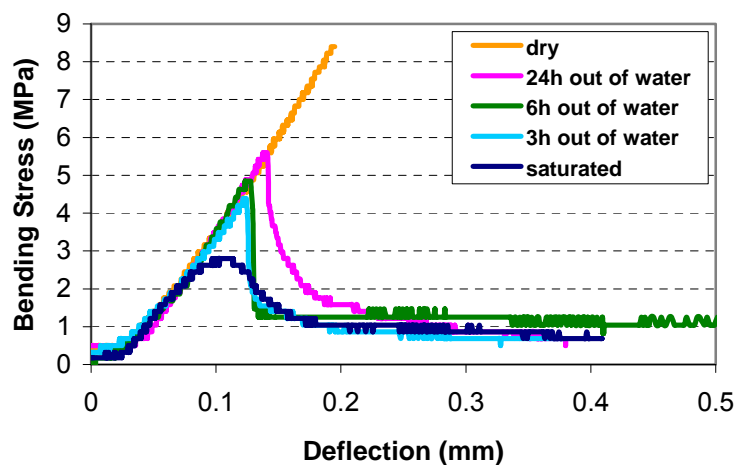*Figure 6.5: Influence on bending behaviour of drying time of water cured samples with 2% larch fibres.*

Figure 6.6: Influence on bending behaviour of drying time of water cured samples with 2% pine fibres.

6.3   Micromechanics-based design

6.3.1   Micromechanics model

Micromechanics models based on fracture mechanics and deformation mechanisms make it possible to tailor the material by controlling the failure mode, the tensile strength and the ultimate tensile strain [Li 1998]. In cement-based composites reinforced with fibres, such a

model will predict the tensile strength by calculating the maximum fibre bridging stress. Lin et al. [1999] described the composite performance by 11 micromechanics properties of the fibre-matrix system:

- Fibre parameters: fibre length (L_f), fibre diameter (d_f), fibre stiffness (E_f), fibre tensile strength (σ_f), fibre volume fraction (V_f)
- Matrix parameters: matrix stiffness (E_m), matrix fracture toughness (K_m), initial flaw size (c).
- Fibre-matrix interaction parameters: interfacial frictional bond strength (τ_{fu}), interfacial chemical bond energy (G_d), snubbing coefficient (f)

The snubbing coefficient (f) takes into account an increase of bridging force P due to an inclination angle ϕ relative to the crack plane. Fibres that are not perpendicular to the crack plane are subjected to additional frictional stress when being pulled out due to the interaction to the matrix at the exit.

A material that shows a strain-hardening behaviour with multiple microcracking prior to failure develops enhanced ductility. Two criteria must be satisfied in order to achieve strain-hardening behaviour: a strength-based criterion and an energy-based criterion. The strength-based criterion, also referred to as the first-crack stress criterion; states that the first crack strength σ_{fc} should not exceed the maximum fibre bridging strength σ_o [Wu 2001]:

$$\sigma_{fc} \leq \sigma_0 \tag{6.1}$$

When a cement-based matrix is subject to tension stress it cracks in its weakest cross-section. If there are fibres reinforcing this matrix, the fibres crossing the crack will then take over the tensile load. This strength criterion determines the initiation of cracks.

As the tensile load increases the fibres will slip out of the matrix at the first crack and the crack will progressively open. With unstable Griffith type cracks, the fibres break and the crack opens leading to the failure of the material with a localized single crack [Li 2008]. On the other hand, if the energy-based criterion is fulfilled, a steady-state type crack will develop. This is a flat crack extending indefinitely through the matrix, properly bridged by a sufficient number of fibres [Li and Leung 1992]. Figure 6.7 presents both types of cracks. To clarify the energy-based criteria, the bridging stress versus crack opening relation $\sigma(\delta)$ is plotted in figure 6.8. As illustrated in this figure the steady state crack criterion will assure the presence of multiple cracking if the complementary energy $J_b{'}$ is equal to, or greater than the matrix crack tip toughness J_{tip}:

$$J_{tip} \leq J_b{'} \tag{6.2}$$

According to Wang and Li [2007], $J_b{'}$ depends on the fibre and fibre matrix interface parameters, while J_{tip} is estimated as K_m^2/E_m, where K_m = matrix fracture toughness and E_m = matrix stiffness. The steady state crack stress σ_{ss} must satisfy:

$$\sigma_{ss}\delta_{ss} - \int_0^{\delta_{ss}} \sigma(\delta)d\delta = J_{tip} \tag{6.3}$$

The condition that steady state cracks can occur can then be expressed as:

$$J_{tip} \leq \sigma_0 \delta_0 - \int_0^{\delta_0} \sigma(\delta) d\delta \equiv J_b' \tag{6.4}$$

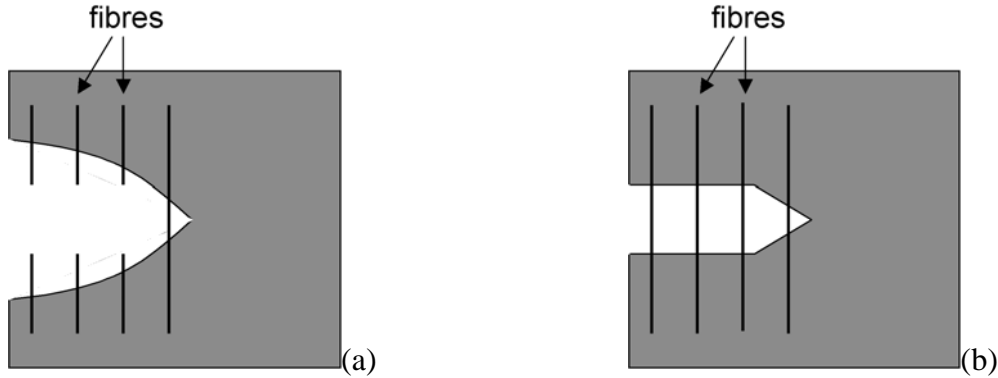where δ_0 is the crack opening corresponding to maximum bridging stress σ_0.

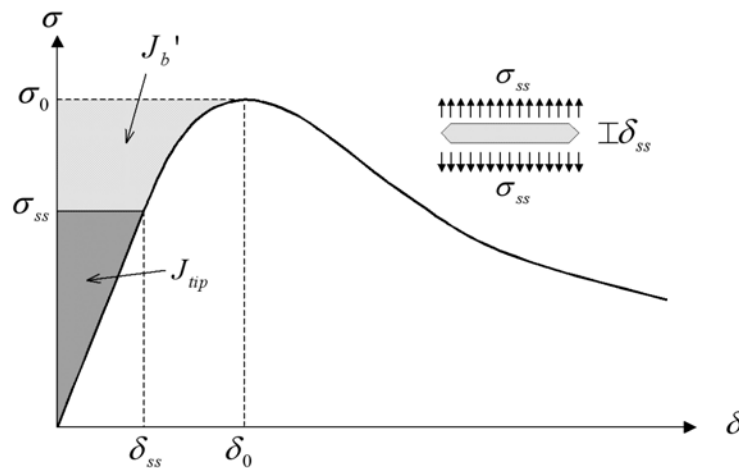*Figure 6.7: Growth of a Griffith type crack (a) and a steady-state crack (b).*

Figure 6.8: Typical $\sigma(\delta)$ curve for strain-hardening composite.

The relation in figure 6.8 describes the fundamental material property that rules the mechanical performance of fibre-reinforced composites beyond the first crack. The stress σ as function of the crack opening δ can be formulated (Eq. 6.5) by integrating the contributing effects of the individual fibres bridging the crack with the use of probabilistic density functions [Wu 2001]. It takes into account probability density functions of orientation angle $p(\phi)$ and centroidal distance of fibres from crack plane $p(z)$. Equation 6.5 represents the bridging law where no rupture occurs during debonding. The pullout load-displacement relation $P(\delta)$ is modelled at a single fibre level.

$$\sigma(\delta) = \frac{4V_f}{\pi d_f^2} \int_{\varphi=0}^{\pi/2} \int_{z=0}^{(L_f/2)\cos\varphi} P(\delta) p(\varphi) p(z) dz d\varphi \tag{6.5}$$

Equation 6.6 shows $\sigma(\delta)$ relation for a special case where short fibres are aligned to tensile direction and no fibre rupture is considered [Wang and Li 2007].

$$\sigma(\delta) = \begin{cases} 2V_f \sqrt{(2G_d + \tau_{fu}\delta)\dfrac{E_f}{d_f} - \dfrac{V_f E_f \delta}{L_f}} & \delta \leq \delta_c \\[4mm] \dfrac{4V_f \tau_{fu}}{L_f d_f}\left(\dfrac{L_f}{2} - \delta\right)^2 & \delta_c \leq \delta \leq \dfrac{L_f}{2} \end{cases} \tag{6.6}$$

where δ_c is the crack opening when all fibres, regardless of the embedded length, finish debonding. After this simplification the complementary energy can be calculated as:

$$J_b' = \frac{V_f \tau_{fu}^2 L_f}{6 d_f^2 E_f} - \frac{2V_f G_f L_f}{d_f} + \frac{8V_f G_d}{3\tau_{fu}}\sqrt{\frac{2E_f G_d}{d_f}} - \frac{2V_f E_f G_d^2}{\tau_{fu}^2 L_f} \tag{6.7}$$

Considering that the last two terms in this equation have relatively small values, it can be further simplified to:

$$J_b' = V_f \frac{L_f}{d_f}\left(\frac{\tau_{fu}^2 L_f^2}{6 d_f E_f} - 2G_d\right) \tag{6.8}$$

6.3.2 Application to wood fibre cement composites

The pullout tests described in Chapter 5 and the preliminary tests results reported in section 6.2 provide enough information to apply the micromechanics model to wood fibre cement composites.

From the pullout tests conducted with wood fibres embedded in cement matrix MF1 the chemical debonding energy (G_d) and the frictional bond strength (τ_{fu}) were calculated according to equations 5.2 and 5.3. The results are presented in table 6.2.

Table 6.2: Estimated values of τ_{fu} and G_d for wood fibres-MF1 interface

	Spruce fibres	**Larch fibres**	**Pine fibres**
G_d **(N/m)**	0.244	0.144	0.0
τ_{fu} **(MPa)**	0.362	0.819	0.686

It is known that a strong chemical bond promotes fibre rupture: the fracture energy is reduced while the tensile strength of the composite increases; hence the material becomes strong but brittle. Since cement is an alkaline inorganic material (pH>12.5) containing surface hydroxyl groups [Coutts and Kightly 1984; Pehanich et al. 2004] and wood fibres contain covalent hydroxyl groups from either residual lignin or both the cellulose component and the oxidation of end groups [Coutts and Kightly 1984] the chemical bond is believed to be either

hydrogen bonds or hydroxide bridges between fibres or between the fibres and the cement matrix. There was "chemical debonding" between the semi-chemically produced larch and spruce fibres and the cement matrices during the pullout tests. But the values of G_d estimated from the pullout tests (table 6.2) are low compared to values reported for PVA fibres and the same cement matrix MF1 of 1.2 N/m [Yang et al. 2007]. Pine fibres exhibited pullout behaviour governed only by friction therefore, thus G_d is zero.

The micromechanical model described above assumes a 1-D fibre orientation. In the $\sigma(\delta)$ relation (equation 6.6), this model only takes into account the contribution of short fibres aligned in the testing tensile direction. A 1-D assumption is applicable to wood-fibre composites casted into thin sheet samples where the thickness, 10 mm, is the same as the fibre length. The casting process for this type of samples also contributes to the fibre layering.

For the proposed cement matrix MF1 Wang and Li [2007] determinated the matrix fracture energy J_{tip} by wedge splitting tests. They reported a value of $J_{tip} =15$ J/m^2. For the composites tested with 2% wood fibres, the crack opening δ_0 is calculated for a maximum fibre bridging strength, that is when the derivate $\partial\sigma/\partial\delta = 0$:

$$\delta_0 = \frac{\tau_{fu}L_f^2}{d_f E_f} - \frac{2G_d}{\tau_{fu}} \tag{6.9}$$

The maximum fibre bridging strength σ_o is then calculated with equation 6.6 for the crack opening δ_0. The complementary energy $J_b{}'$ is calculated with equation 6.8 taking into account the fibre length of 10 mm. Table 6.3 presents the results for each fibre type.

Table 6.3: Estimated values of crack width, bridging strength and complementary energy

Fibre type	Spruce fibres	Larch fibres	Pine fibres
δ_0 (mm)	0.02	0.03	0.04
σ_0 (MPa)	0.29	0.57	0.37
$J_b{}'$ (N/m)	0.40	2.59	2.59

To fulfil the requirements for strain-hardening, σ_o should be higher than σ_{fc} and $J_b{}'$ higher than J_{tip}. Due to the random nature of flaw size and fibre distribution in cement composites, materials with a larger margin between $J_b{}'$ and J_{tip} and σ_o and σ_{fc} have a better chance of multiple cracking. Kanda [1998] experimentally demonstrated that composites with polyethylene (PE) with relations $J_b{}'/J_{tip} > 3$ and $\sigma_o /\sigma_{fc} > 1.2$ exhibited pseudo-strain-hardening behaviour with multiple cracking. The same ratios are applied in this section.

Comparing the strength values from table *6.3* and 6.1 it is evident that the fibre bridge strength is too low for the present conditions. This means that after the first crack no more load is transferred and the load drops due to fibre rupture or pullout. This is the behaviour observed during the preliminary bending tests. The estimated values of complementary energy are in all cases lower than the crack tip toughness J_{tip} of 15 N/m.

Based on the present calculations several actions can be undertaken to assure a strain hardening behaviour. The fibre diameter has a strong influence in the estimation of $J_b{}'$ Therefore; a logical first assumption would be to lower the diameter of the fibres in order to be able to develop a ductile behaviour. However, this may not be possible due to production constraints. Fibre volume fraction and fibre length also have a strong impact in $J_b{}'$, but high

fibre percentage or longer fibres will decrease the rheology of the composite, affecting the workability and the uniform dispersions of the fibres. Since the fibre aspect ratio is low (<100) there may be end effects on the total debonding load. The matrix contribution J_{tip} could be made lower by either increasing the water-to-binder ratio, reducing the size of aggregate particles or by the use of inert filler.
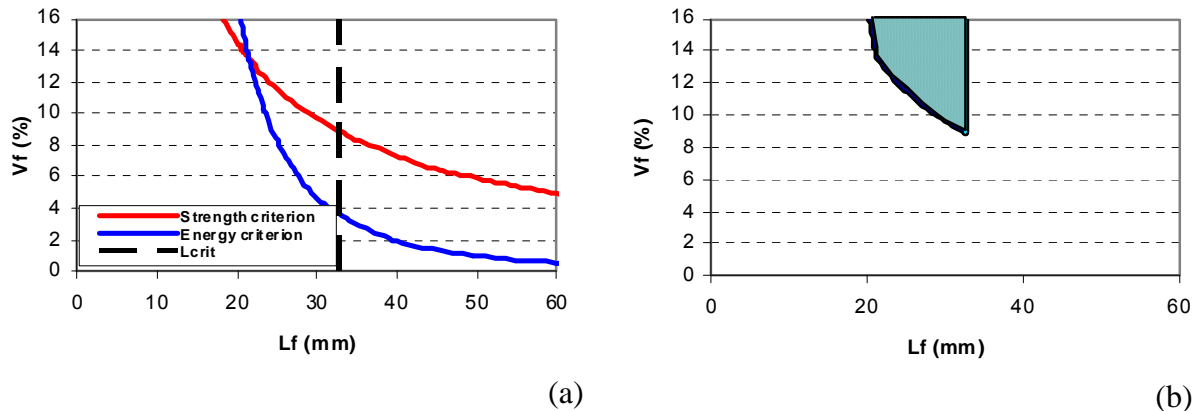

(a)

(b)

Figure 6.9: Micromechanical model calculated V_f and L_f of spruce fibres (a) fulfilling all criteria (b) combined effect.

Figure 6.9a shows the relation between fibre volume and fibre length to achieve saturated multiple cracking and tensile pseudo-strain-hardening behaviour of spruce fibres-MF1 matrix, based on the micromechanics model. The graphic includes the value of critical length, calculated in Chapter 5, which will ensure fibre pullout instead of fibre rupture. L_{crit} is 32.6 mm for spruce. Figure 6.9b shows the combined effect of the strength and energy criterion and the critical fibre length. Only combinations of volume fraction and fibre length that fall into this area will ensure multiple cracking. It is also necessary to take into account a maximum amount of fibres that can be properly distributed within the cement matrix. The author considers 10% as the maximum volume percentage. Therefore for spruce fibres and mix MF1, an optimum amount of 9% per volume fibres of 30 to 32 mm long will ensure the desired composite behaviour.

For larch and pine fibres there are more possible combinations of fibre length and volume fractions that fulfil both criteria, as can be seen in figures 6.10 and 6.11. For larch fibres a minimum of 5% fibres will be necessary with 30 mm length. Fibres down to 15.2 mm can be used, in 9.5% per volume, which is a high percentage of fibres. The results for pine fibres, however, are more interesting from a practical point of view. Only 4% fibres will ensure multiple cracking, if fibres are 35 mm long. For shorter fibres, between 20 and 25 mm long, 5.5 to 7% fibres are necessary for this cement matrix, MF1. As shown in Chapter 4, MF1 is a strong matrix. Matrices with a lower first crack strength σ_{fc} will need lower fibre percentages to ensure multiple cracking.

Considering how time demanding it is to prepare fibres following the semi-chemical procedure and preparing them by hand, the decision was taken to not continue working with them. Larch fibres show promising results but only with a more efficient extraction procedure these fibres could be used as reinforcement in cement-based matrices. From now on only pine

fibres, mechanically cut from veneer sheets, will be used as reinforcement for cement-based composites.
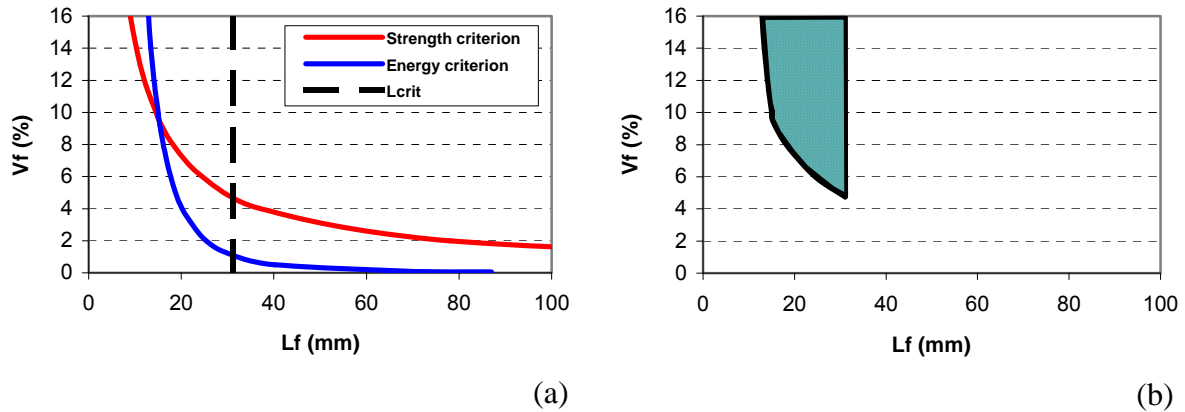

(a)

(b)

Figure 6.10: Micromechanics model calculated V_f and L_f of larch fibres
(a) fulfilling all criteria (b) combined effect.
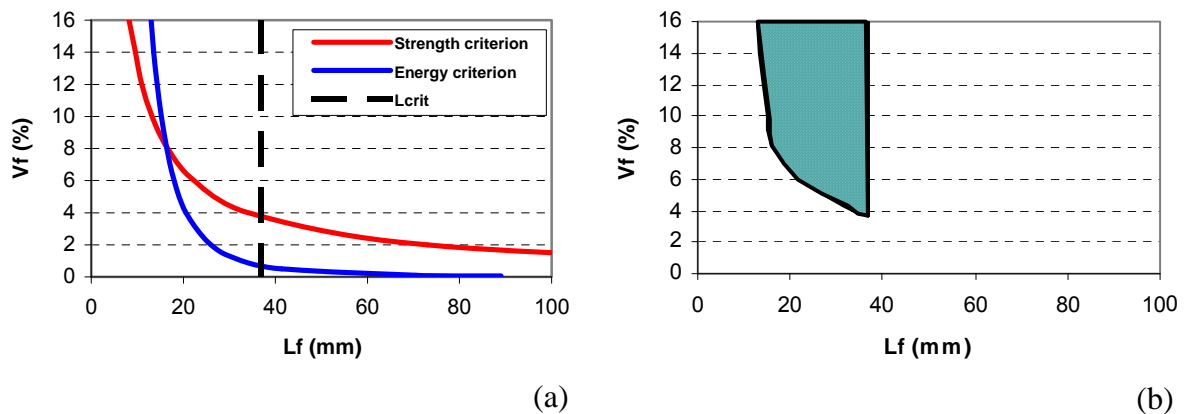

(a)

(b)

Figure 6.11: Micromechanics model calculated V_f and L_f of pine fibres
(a) fulfilling all criteria (b) combined effect.

6.4   Experimental study

6.4.1   Materials and mix design

Different composites were prepared using five different cement matrices with treated and untreated pine fibres or PVA fibres. PVA fibres are the synthetic fibre most commonly used as reinforcement in ECC materials. The cement matrices used are CF2, CF3, CF4, CS2 and CS3. For these matrices the mix composition is the same as presented in table 4.3, except for the water-powder material ratio that was adjusted depending on the amount and nature of the fibres. Pine fibres were cut to length 10 and 25 mm. Some pine fibres were treated with 5% HS2627, according to the procedure described in Chapter 5. The wood fibre content was either 4% or 5% by volume.

Composites were also prepared with 1% or 0.5% PVA fibres. The tensile strength of these fibres is 1600 MPa and the density is 1300 kg/m^3. The diameter of the fibres is 40 μm and the length is 8 mm. The surface of the fibres is coated with 1.2% oil by weight to reduce the bond between the fibre and the matrices. Hybrid composites were prepared with 0.5% PVA and 3% treated or untreated 10 mm long wood fibres.

6.4.2   Mixing and curing

The mixing procedure from section 6.2 was reviewed in order to ensure a proper fibre distribution of a higher percentage of fibres. In this new mixing sequence, the powder materials (Portland cement, silica fume, limestone powder, fly ash or BFS) were first mixed with a HOBART® mixer for 1 minute. Next, part of the water and superplasticizer were added and mixed for another 2 minutes. The amount of water and SP is such that the liquefied paste mix reaches a consistent and uniform state before adding fibres. The consistency is checked visually. When the fibres are added to a paste with the proper consistency the fibres do not float. The water-powder ratio β and the SP-powder ratio for some of the composites are presented in Table 6.4. In the next step the fibres were slowly added while mixing continued until all fibres were evenly distributed. After this, the sand was added together with the remaining water and an adjusted amount of superplasticizer to ensure the correct workability. Finally, after 2 more minutes of mixing, the mixture was cast.

By mixing the fibres with the fresh paste without sand a better coverage of the fibres with the paste and a proper fibre distribution was reached. The fibre distribution will be discussed in section 6.5.

The fresh mixture was cast and cured for 1 day in moulds covered with plastic. Afterwards, the samples were demoulded and cured under sealed condition at room temperature of 20°C until they were tested. To emulate curing conditions similar to engineering conditions the samples were no longer cured submerged in water.

6.4.3   Compression test

Cubes with dimensions $40 \times 40 \times 40$ mm^3 were cast for compressive tests and cured for 28 days. Three parallel compressive measurements were done for each mixture at a prefixed age.

6.4.4   Bending test

Three different setups were used for bending tests, and two sizes of samples. Thin samples, with dimensions $120 \times 30 \times 10$ mm^3, were tested using the same four-point bending setup used for the preliminary tests (Section 6.2.3). The samples were cured for 7, 21, 28, 45, 60 or 90 days prior to testing.

To understand the behaviour of the composites with a 3D distribution of fibres, beam samples with square cross section 40×40 mm^2 and length 160 mm were tested under three-point and four-point bending. Figure 6.12 shows both set-ups for beams samples. In the three-point bending setup the support span is 107 mm. In the four-point bending setup the support span is 120 mm and the load span is 40 mm. In both setups two LVDTs fixed on both sides of the test set-up measured the flexural deflection of the specimen.

All the tests were conducted under deformation control at a speed of 0.01 mm/s using the average of the two LVDT´s as feed back signal. For each mixture at each age three measurements were done, unless indicated otherwise.
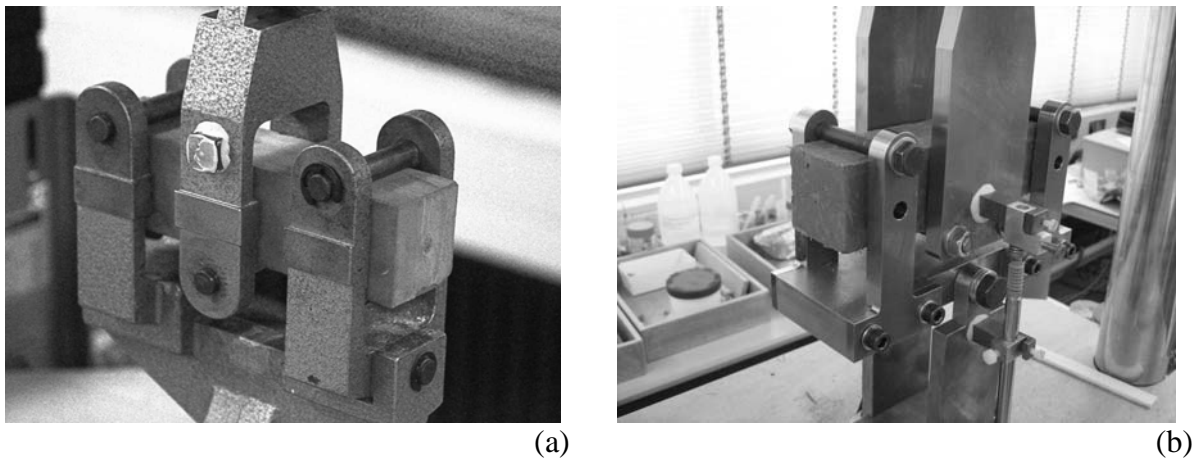
(a) (b)

Figure 6.12: Bending setups for beam samples
a. Three-point bending - b. Four-point bending.

6.4.5 Esem observations

The microstructure of the composites was investigated by means of ESEM observations and XDS analyses. Some observations were done on fracture surfaces of tested samples, without any treatment or coating in order to see the predominant failure mode of the fibres in the fracture surface. Other tested samples were first placed in the vacuum chamber under low vacuum and impregnated with a low viscosity epoxy. After the hardening of the epoxy, the sample surface was polished. The samples were placed in the ESEM and images were taken using a backscattered electron (BSE) detector with vapour mode. The acceleration voltage of 20 kV was used in order to obtain a high contrast image.

6.4.6 CT Scan and image analysis

Landis and Nagy [2000] and Schlangen [2008] related the microstructure of concrete to the fracture behaviour and other properties using CT scans. In a similar way, the fibre distribution is analysed by means of computer tomography CT Scans and later image analysis. The CT Scanner is a nanotom of Phoenix x-ray Systems. The resolution changed depending on the size of the samples, the voxel-size varies between 8 and 28 μm.

6.5 Experimental results and discussion

6.5.1 Compression stress

Table 6.4 summarizes the compressive strength at 28 and 45 days for composites with cement matrices CF2, CF3 and CF4 and different fibres. In this table the tests results of composites with CF2 mix with the same water-powder ratio ω are reported. The ratio is 0.33-0.34. The ratio for samples with CF3 is 0.25-0.286. For matrix CF4, on the other hand, the only available results are for 2 composites with different ω ratio. The samples without fibres have a ω= 0.32, lower than the ratio for composites with 4% long pine fibres, of 0.346.

Table 6.4: Compressive strength at 28 and 45 days (MPa) and water-powder ratio ω for composites with CF2, CF3 and CF4 and different fibres

Mix ID	Fibre type	Compressive strength [MPa]		ω [-]	SP / powder [-]	ρ [kg/m³]
		28 days	45 days			
CF2	1.0% PVA	40.1	43.9	0.336	0.015	1819
	0.5% PVA	40.6	43.5	0.336	0.013	1864
	0.5% PVA + 2% T	41.0	44.9	0.347	0.013	-
	4.0% T	-	44.4	0.330	0.014	1899
	4.0% U	-	28.2	0.336	0.013	1820
	no fibres	40.4	43.4	0.330	0.011	-
CF3	0.5% PVA	18.6	22.3	0.286	0.014	1981
	4.7% LT	13.1	-	0.267	0.014	1752
	no fibres	23.0	28.6	0.246	0.014	-
CF4	5.0% LU	12.9	-	0.346	0.013	1615
	no fibres	20.7	24.2	0.317	0.013	-

All fibres percentages are by volume. T stands for treated pine of 10 mm long, U for untreated pine fibres of 10 mm long, LT for long treated fibres of 25 mm and LU for long untreated pine fibres of 25 mm.
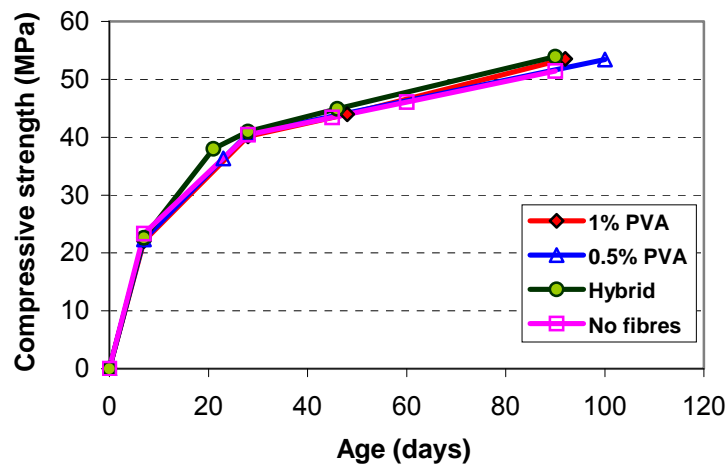

Figure 6.13: Compressive strength development of composites with CF2 and different fibres (β=0.33).

As summarized in table 6.4 and figure 6.13, the compressive strength for the CF2 composites with and without fibres is about the same. The only exception is for composites with 4% pine fibres, for which the compressive strength at 45 days is 36% lower than the average for the other tested composites. The increase of PVA fibres, from 0.5% to 1% per volume, and even the addition of 2% treated pine fibres have no effect on the compressive strength. The same can be said for the composite with 4% treated pine fibres. The effect on

the compressive strength of the addition of fibres varies depending on the type and amount of fibres [Li 1992b]. Composites with 2% PVA has exhibit very little variation in the compressive strength compared with fibreless samples. Composites with wood fibres, on the other hand, have lower compressive strength than fibreless specimens, as reported in section 2.2.3.3.

The fly ash in these composites contributes to an additional strength gain in the long term. The compressive strength at 28 days is about 72 to 78% of the compressive strength at 90 days.

The effect of the total amount of cement in composites with CF2 and 0.5% PVA can be seen in figure 6.14. The amount of cement decreases from 293 to 258 kg/m^3, leading to a decrease in compressive strength of 10% at 28 days and 16% at 90 days.
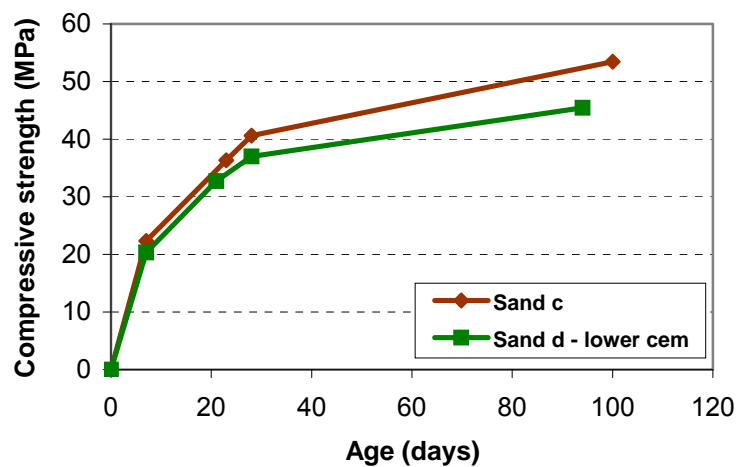

Figure 6.14: Effect of the amount of cement in composites with CF2 and 0.5% PVA.

The coupled effect of decrease of cement, increase of amount and length of the fibres is shown in figure 6.15. In hybrid composites the compressive strength decreased when the amount of pine fibres increased, from 2% per volume to 3%, the length of the fibres increase from 10 to 25 mms and the cement decrease from 283 to 242 kg/m^3. Beside wood fibre, the hybrid composites have 0.5% PVA fibres. To isolate the effect of the fibre increase, figure 6.14 and figure 6.15 are compared. The upper curves in each of these figures are almost the same; they were also drawn in figure 6.13. If the compressive stress will decrease only due to decrease of cement, as in figure 6.14, at 28 days it should be 36.2 MPa and at 90 days, 44 MPa. These values are presented in figure 6.15 as "projection". Instead, the compressive strength is even lower due to the addition of more and longer pine fibres. The same effect is seen with composites with CF3 and CF4. As presented in Table *6.4* the addition of 4.7% or 5% long pine fibres considerably decrease the compressive stress when compared to samples without fibres.

The density of the composites decreases with increasing amount of fibres, as is indicated in table 6.4. Both PVA fibres and wood fibres are lighter than any of the other components of the composites. The density of PVA and wood fibres are 1.3 and 0.59 g/cm^3 each. The sand used in the composites has a density of 2.64 g/m^3. The density of the other components range between 2.2 g/cm^3 for silica fume and 3.15 g/cm^3 for cement, as is indicated in Chapter 4. The addition of fibres in the fresh mix increases the voids volume [Bentur and Mindness 2007]

and, therefore, decreasing the density. The effect of voids can be beneficial for promoting ductility in fibre-reinforced materials [Yang 2007], but has a negative effect on the compressive strength, as is demonstrated by the data in table *6.4*. The composites with the lower compressive strength, CF3+4.7%LT and CF4+5%LU, also have the lower densities.
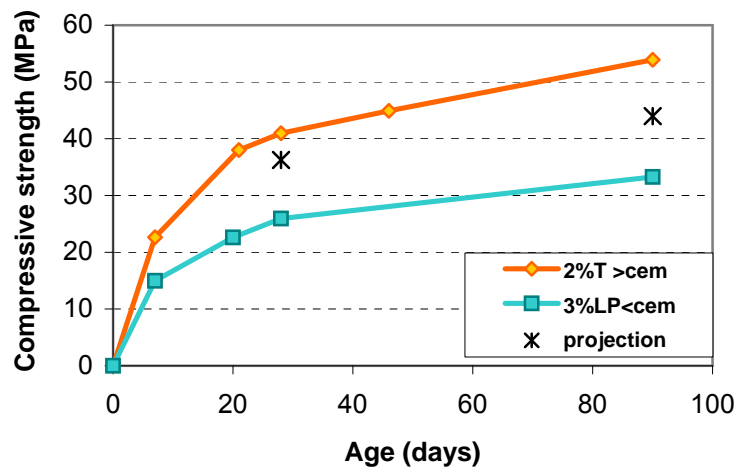

Figure 6.15: Effect of the amount of cement and increased amount of wood fibres in hybrid composites with CF2.

6.5.2 Bending strength

6.5.2.1 Composites with cement matrix CF2

Under four-point bending load, the thin samples prepared with either treated or untreated 10 mm long pine fibres and a fibre volume of 4%, do not exhibit multiple-cracking behaviour. Figure 6.16 shows typical flexural load-deflection curves for these tests and for bending tests done with samples without fibres. Even though the samples with fibres do not behave as brittle as a sample without fibres, it is evident that the fibre reinforcement is not enough for these composites to develop multiple cracking. Either because the fibre volume is too low or the fibre length to short, but the fibre bridging strength is lower than the first crack strength, thus after the first crack the fibres are not able to sustain any more load and the material failed. When reinforced with 4% treated pine the bending strength increased considerably compared to the samples with 4% untreated pine or without fibres. The samples with untreated pine have more voids, as explained in the previous section, and the voids represent weaker sections where the crack can initiate. The bending stress increased with the age of the samples, for both treated and untreated fibres, as can be seen in figure 6.17. The increase of bending strength with age corresponds to the increase of compressive strength described in Chapter 4. Measurements were done up to 105 days.
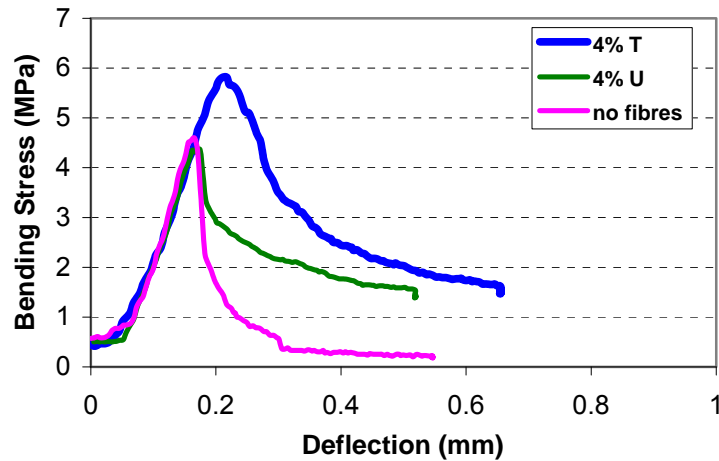
Figure 6.16: Flexural load-deflection curves for composites with V_f 4% treated and untreated fibres 1 mm long (Age 45 days.)
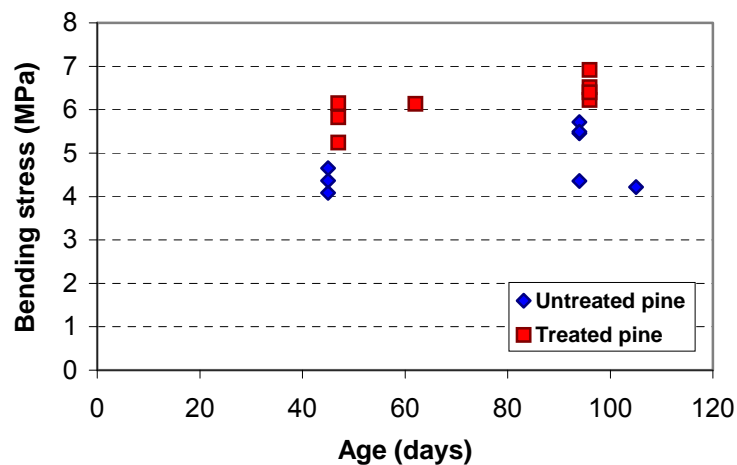

Figure 6.17: Bending strength development for composites with V_f 4% treated and untreated fibres 10 mm long.

In order to achieve a multiple-cracking behaviour the fibre volume increased from 4 to 5% and the fibre length from 10 to 25 mm. Under four-point bending load samples prepared with untreated pine exhibit multiple-cracking behaviour as shown in figure 6.18. Figure 6.19 shows representative load-deflection curves for samples tested after 7 and 21 days curing. When tested at 7 days the fibre bridging strength was higher than the first crack strength, thus after the matrix cracked for the first time the bending stress increased due to the fibres bridging action. New cracks developed until fibre failure at a localized crack. At 21 days the matrix has increased its compressive and bending strength. At that age the fibre-matrix interface friction has increased too, but to a lower extent. Therefore, after the first crack, the fibres cannot sustain the load. With increasing deflection, a few more cracks develop, but as the interface fails the composite load capacity decreases rapidly and the localized crack opens leading to the composite failure.

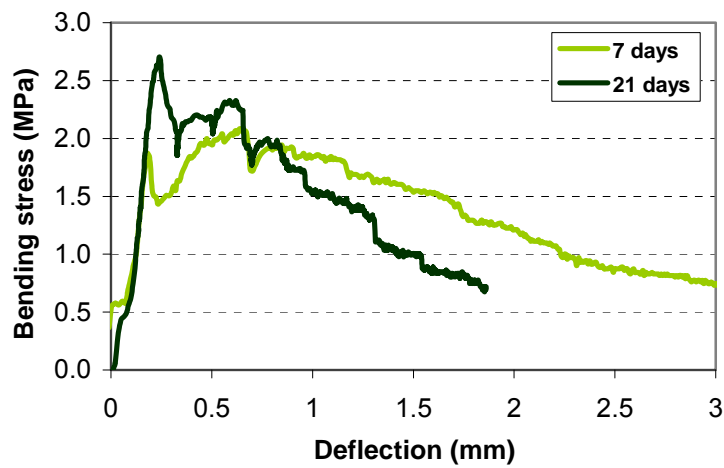*Figure 6.18: Multiple cracking of the samples under four-point bending load.*

Figure 6.19: Flexural load-deflection curves for composites with
V_f 5% untreated pine fibres 2.5 mm long.

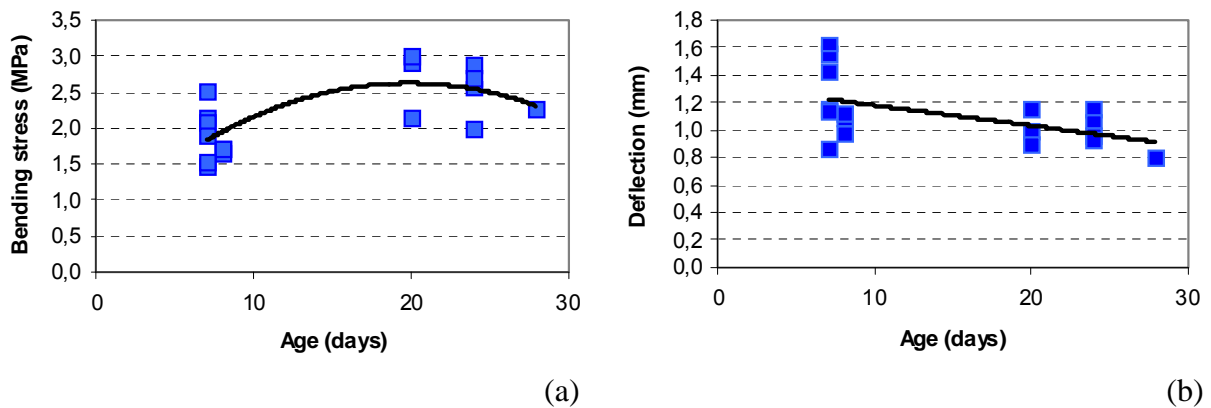(a)   (b)

Figure 6.20: Bending strength (a) and deflection (b) development for composites with
V_f 5% untreated pine fibres 25 mm long, thin sheet specimens.

The development of bending strength with age is shown in figure 6.20a and the decrease of the deflection capacity is shown in figure 6.20b. The composite exhibits some ductility at early age, and with time behaves more brittle.

Composites reinforced with PVA fibres, fibre volumes 0.5 and 1%, showed multiple-cracking behaviour. The composites with 1% PVA fibres have larger deflection capacity, but for both composites type the deflection capacity decreased with increasing specimen age, as can be seen in figures 6.21b and 6.22b. This is a characteristic of ECC type materials [Yang et al. 2007, Lepech and Li 2006]. The deflection at 28 days is estimated as 2.72 mm for composites with 1% PVA and 2.42 mm for composites with 0.5% PVA.
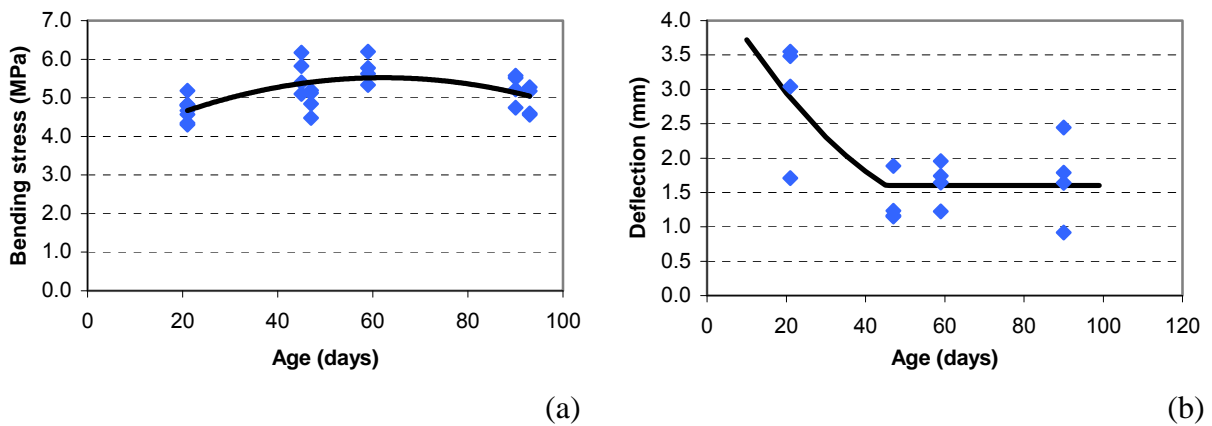

(a)   (b)

Figure 6.21: Bending strength (a) and deflection (b) development for composites with
V_f 0.5% PVA fibres.

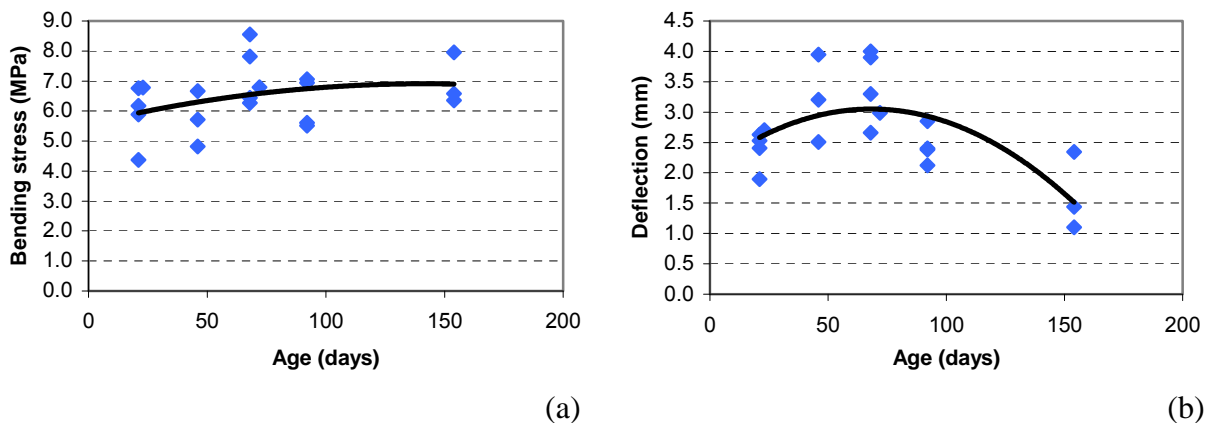(a)   (b)

Figure 6.22: Bending strength (a) and deflection (b) development for composites with
V_f 1% PVA fibres.

The estimated bending strength at 28 days is 6.1 MPa for composites with 1% PVA and 4.9 MPA for 0.5% PVA. The development of bending strength for CF2 with PVA fibres is presented in figures 6.21a and 6.22a. The bending strength of composites with 1% PVA increases with age. Measurements were done up to 154 days. On the other hand, according to the test results from composites with 0.5% PVA a maximum bending strength is reached at age of about 62 days. This maximum bending strength is measured as 5.5 MPa. At 21 days the

first crack strength is 4.5 to 5 MPa and the fibre-bridging stress in the weakest section is also about 4 to 5 MPa. With age the matrix first crack strength increases to values 5.1 to 6.1 MPa. The fibre matrix interface properties also improve to reach fibre-bridging stress at the weaker section ranging between 4.6 and 5.2 MPa. After 90 days the fibre-matrix properties maintain the same fibre-bridging strength, but the matrix first crack strength has decreased to values 4 to 5.1 MPa. When the composite has its maximum bending stress, age 45 to 60 days, and its deflection capacity is lower compared to earlier or later ages. This corresponds to a more brittle behaviour, in which after the first crack (5.1 to 6.1 MPa), the fibres can only sustain loads up to 5.2 MPa.
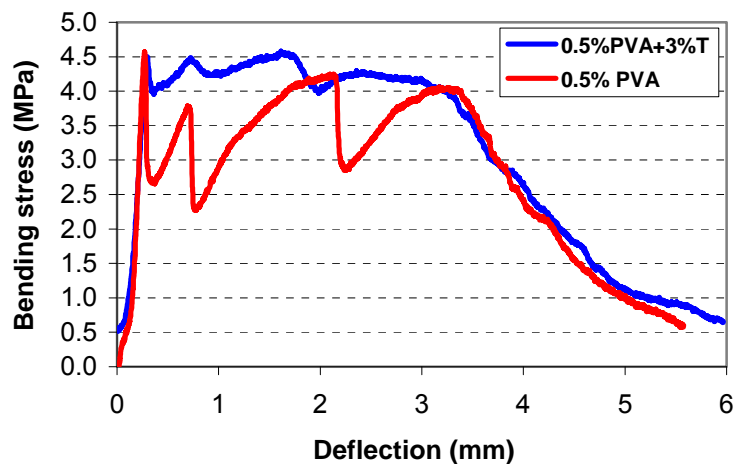

Figure 6.23: Flexural load-deflection curves for composites with V_f 0.5% PVA and hybrid reinforcement V_f = 0.5% PVA + 3% treated pine fibres at 21 days.

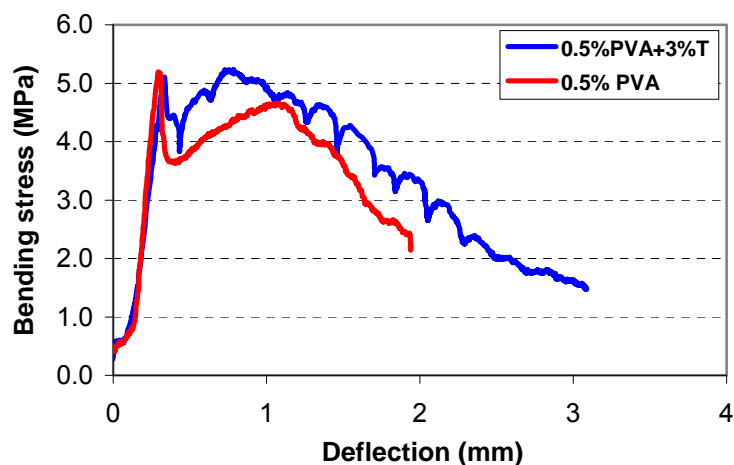*Figure 6.24: Flexural load-deflection curves for composites with V_f 0.5% PVA and hybrid reinforcement V_f = 0.5% PVA + 3% treated pine fibres at 45 days.*

The flexural behaviour of composites with 0.5% PVA is compared to the behaviour of composites with hybrid reinforcement, 0.5% PVA + 3% treated pine in figures 6.23 and 6.24. The addition of fibres improved the behaviour by improving the overall fibre bridging

capacity. At each testing age, both composites exhibit the same first crack strength and also failed after about the same deflection. But during the test, with increasing deflection, the hybrid composites developed more small cracks than the composites with only PVA, which had just a few localized bigger cracks. After the first crack, the hybrid composites reached a higher bending strength than the 0.5% PVA composites.
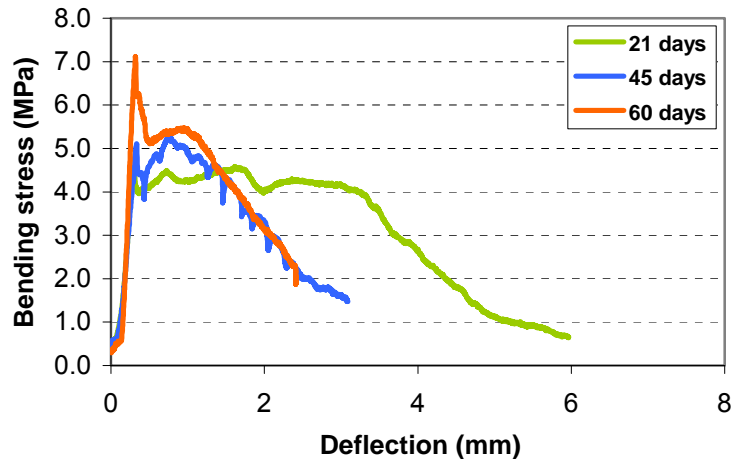

Figure 6.25: Flexural load-deflection curves for hybrid composites with
V_f = 0.5% PVA + 3% treated pine fibres at different ages.

The first crack strength of hybrid composites increased with age (figure 6.25). After 60 days the strength is above 7 MPa. The fibre bridging capacity, on the other hand, increased to a lower extent and after 45 days it seems to have reached its maximum. The second load peak, after the first crack, for samples cured for 45 days, is at 5.23 MPa and for samples cured 60 days is 5.48 MPa.

For hybrid fibres composites the addition of 3% treated pine instead of only 2%, improved the deflection capacity considerably, as can be seen in figure 6.26.
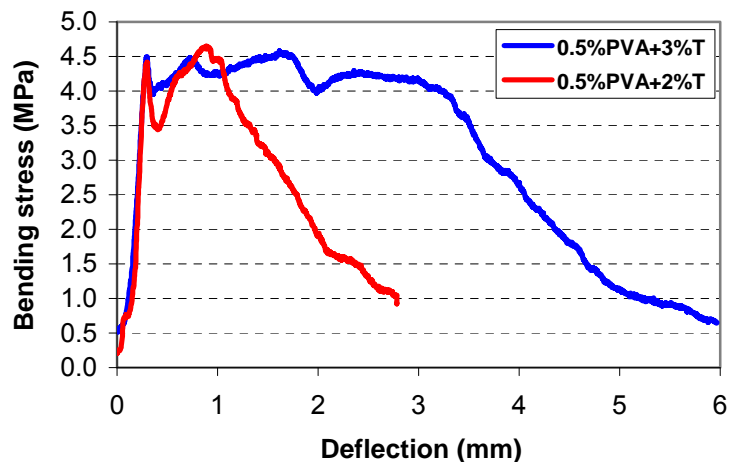

Figure 6.26: Flexural load-deflection curves for hybrid composites with V_f = 0.5% PVA+3%
treated pine and V_f =0.5% PVA + 2% treated pine fibres at 21 days.

Observations in the ESEM showed a good bonding between treated pine fibres and the surrounding cement matrix, as well as between untreated pine fibres and the cement matrix. Figure 6.27 presents ESEM images focusing on the interface between a treated pine (a) and an untreated pine (b) and matrix CF2. Even though the fibre surface is not regular; the bond with the matrix is sound in both cases. In some segments of the interface the matrix is more porous, which may lead to lower pullout shear stress when the fibre is pulled out. The bonding between untreated pine and the cement matrices will be further discussed in section 6.5.3, after image analysis of 3-D CT scans done to investigate if the sound interface happens in the whole perimeter of the fibre.
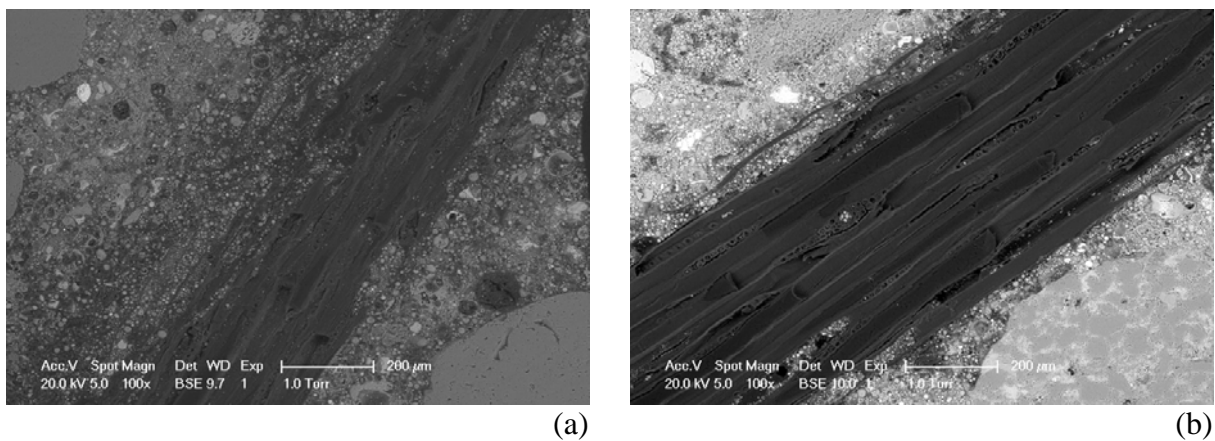

(a)   (b)

*Figure 6.27: ESEM images of CF2 composites with
treated pine fibres (a) and untreated pine fibres (b).*

6.5.2.2 Composites with cement matrix CF3

The bending strength for composites made with CF3 and 5.3% long pine fibres is lower than the other composites with long fibres. The test results are summarized in table 6.5. At these low strength values, the ultimate deflection is higher than for the other composites. The composites with CF3 also have the lowest cement content, 147 kg/m^3, compared to composites with CF2 (283 kg/m^3) or CF4 (178 kg/m^3). Mix CF3 has the highest content of sand, 971 kg/m^3, and additionally, it is the only mix prepared with limestone powder (485.5 kg/m^3). Taking into account that limestone powder is an inert filler, the binder content is only 22% per weight of the composite. This mix was chosen because of its lower compression strength compared to that of matrix CF4 (table 6.4) and enhanced ductility, for applications in which a non-brittle material with deflection capacity is necessary as for instance for temporary filling during drilling operations.

Table 6.5: Flexural properties of wood fibres composites (thin sheets) at 21 days.

Mix ID	Fibre type	Bending strength (MPa)	Ultimate deflection (mm)
CF2	5.0% LU	2.7	1.02
CF3	4.7% LT	0.2	1.75
	5.3% LU	0.6	1.80
CF4	5.3% LU	1.6	1.34

The thin sheet composites with both the long treated and untreated pine fibres exhibited multiple-cracking behaviour under four point bending load. As is summarized in table 6.5 and graphed in figure 6.28, the bending strength of composites with treated fibres is lower than the strength of composites with untreated pine. The bending strength for these composites increases with the sample age and the deflection decreases, similar to the composites with mix CF2. The development with age for thin sheet samples is shown in figure 6.29.
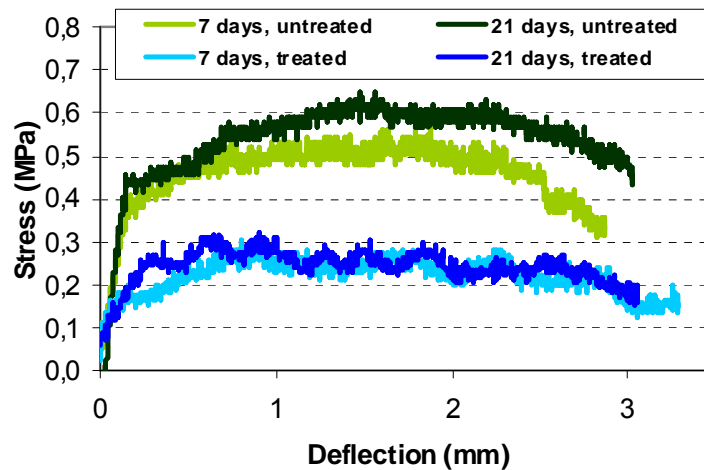

Figure 6.28: Flexural load-deflection curves for treated and untreated pine – CF3 composites at different ages, thin sheet specimens.

The flexural strength of beam samples with dimensions $40 \times 40 \times 160$ mm^3 was higher than for thin sheet samples with dimensions $60 \times 30 \times 10$ mm^3 (figures 6.30 and 6.28) for composites with treated and untreated pine. The flexural behaviour of composites with treated pine was similar for beam samples as well as for thin sheets. These composites had multiple cracking prior to failure. Beam samples with untreated pine, on the other hand, behave less ductile than thin sheet samples (figures 6.30 and 6.28). Similar results were obtained with CF3 and 0.5% PVA fibres. The beam specimens had higher bending strength and reduced deflection capacity when compared to thin sheet specimens (figure 6.31). The bending strength in the beam samples is higher for two reasons. The beam specimens have a depth of 40 mm, 30 mm more than the thin sheet samples. In a higher cross section the shear stress path is longer. Therefore, increasing the load capacity before the first crack occurs.

The deflection capacity depends on the fibre distribution, which has been explained in detail in section 6.1.2. The beam samples have a 3-D fibre distribution while the thin sheet samples have a 1-D fibre distribution (for $L_f = 25$ mm). Thus, for the same fibre volume V_f the samples with 3-D fibre distribution have less fibres perpendicular to a given fracture surface while the samples with a preferential 1-D fibre distribution will have more fibres perpendicular to a given fracture surface. The lower amount of fibres available to bridge the crack will lead to the excessive crack opening (Griffith type crack instead of steady-state crack), and failure without developing multiple cracking nor ductile behaviour.
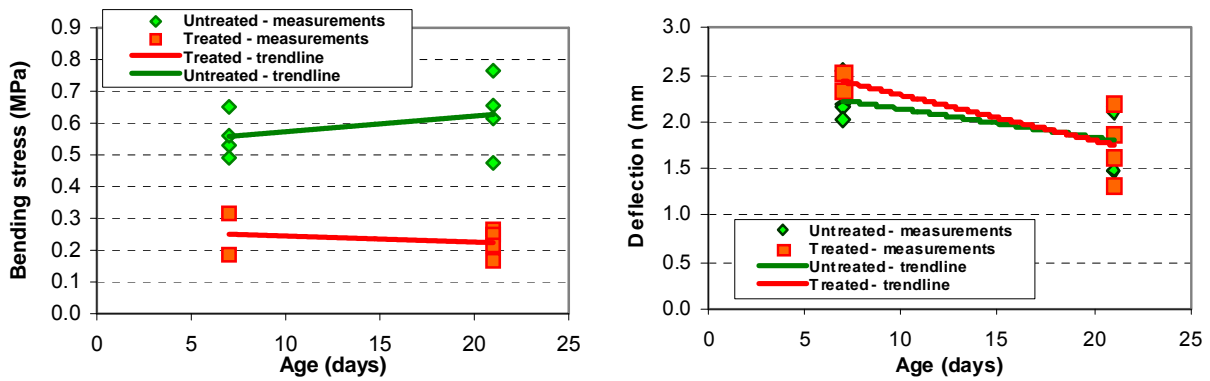
Figure 6.29: Bending strength and deflection development for composites with treated and untreated pine fibres and CF3, thin sheet specimens.
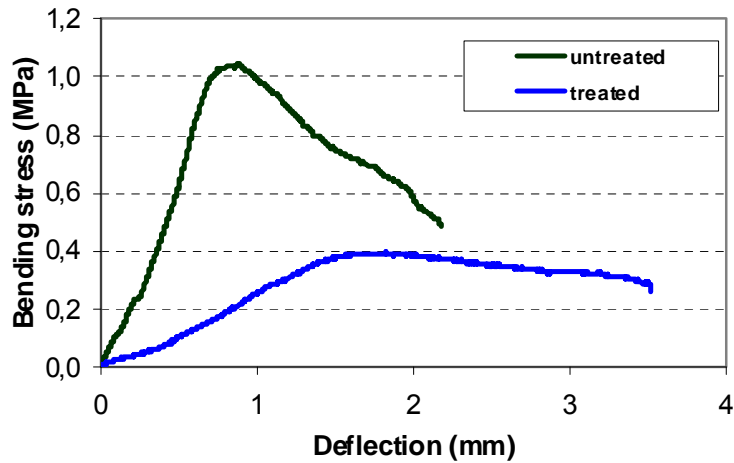

Figure 6.30: Flexural load-deflection curves for treated and untreated pine –CF3 composites at 21 days, beams specimens.
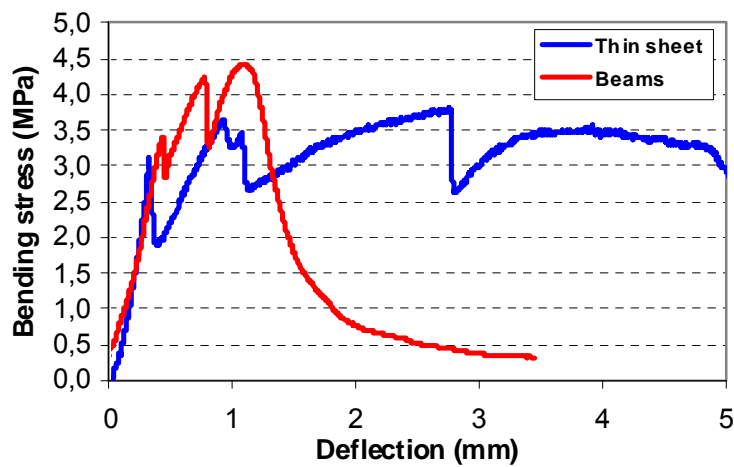

Figure 6.31: Flexural load-deflection curves for CF3- 0.5% PVA composites 21 days and different specimen geometries.

6.5.2.3 Composites with cement matrix CF4

Matrix CF4 has a lower compressive strength (21 MPa), a lower content of sand (539 kg/m^3) and a higher content of fly ash (891 kg/m^3) than matrices CF2 and CF3. As can be seen in table 6.5, the bending strength for composites with 5.3% long pine fibres and CF4 matrix is in average 1.59 MPa. This value is lower than for composites with 5% long pine fibres and CF2. The ultimate deflection for composites with CF4 is 1.34 mm, a higher value compared to the deflection for composites CF2 (1.02 mm). These results can be explained by the increased amount of FA in this cement matrix. The presence of FA reduces the fibre/matrix interface bond and additionally lowers the matrix toughness. These two trends improve the strain-hardening potential of the composites, and explain the increased deflection capacity of composites with CF4, as well as the lower compressive, tensile and bending strengths.

Similar tendency is observed in ECC composites with an increasing FA/cement relation, which has an increasing tensile strain capacity (%) [Wang and Li 2007], and decreasing flexural strength [Sahmaran et al. 2009].

A typical flexural load-deflection curve for thin sheet samples with long pine can be seen in figure 6.32. With age the bending strength increases (figure 6.33a) while the maximum deflection decreases (figure 6.33b).

Beam shaped samples tested under four-point bending exhibited multi-cracks before failure. This is an improved behaviour when compared to beam samples with CF3, which failed after a single crack opening.

The deflection capacity was lower for beam specimens of CF4 and untreated pine than for thin sheet specimens. The bending strength for beam samples was higher than the bending strength for thin sheet samples (figure 6.32).

Composites with CF4 and untreated pine developed higher bending strengths for both thin sheet and beam samples, than composites with CF3 matrix. The ultimate deflection for composites with CF4 was slightly lower than for the composites with CF2 matrix, but they all developed multiple cracking prior to failure. Beam specimens of CF4 composites also exhibited multiple cracking prior to failure, which was not the case for beam specimen with other cement matrices.
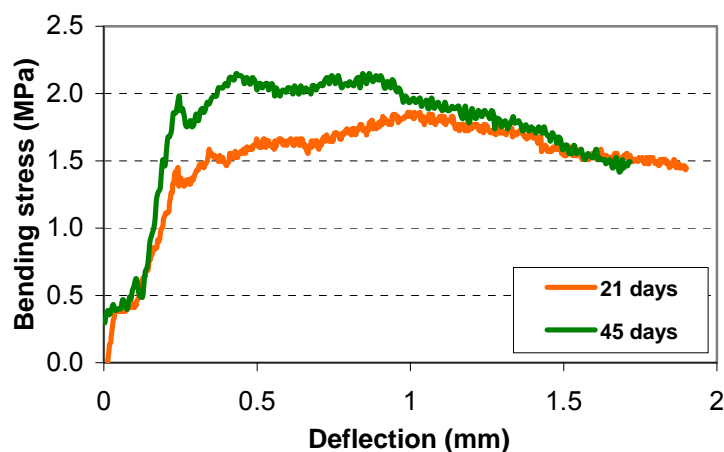

Figure 6.32: Flexural load-deflection curves for long pine - CF4 composites at different ages, thin sheet specimens.
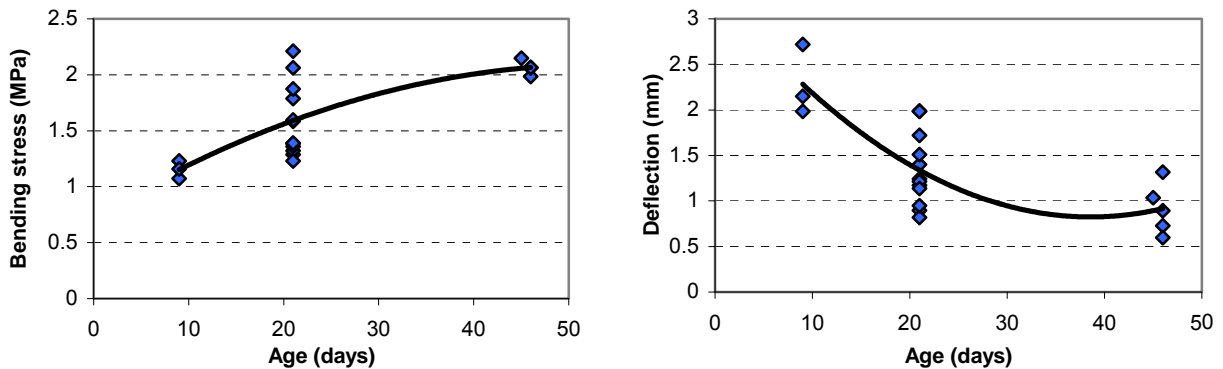
Figure 6.33: Bending strength and deflection development for composites with long pine fibres and CF4, thin sheet specimens.

Figure 6.34: Flexural load-deflection curves for CF4 - 5% untreated pine composites, 21 days and different specimen geometries.

The composites with 5.3% long pine fibres and cement matrix CF4 exhibited a ductile behaviour with multiple cracking prior to failure when tested at ages 21 and 45 days, independent from the sample geometry. Control samples, without fibres, had a modulus of rupture of 2.3 MPa at age 21 days. The failure mode for these samples was brittle.

According to the standards ASTM C78, traditional concrete that has a compressive strength of 13 MPa, similar to matrix CF4 with 5% LU fibres, the flexural strength at age 28 days should be 2.5 MPa. This strength is comparable to the flexural strength of beam samples with 5% LU, which behaviour is shown in figure 6.34.

6.5.2.4 Composites with cement matrix CS3

The cement matrix CS3 has a high compressive and tensile strength, 45 MPa and 3 MPa, compared to matrices CF2, CF3 and CF4, for which the compressive strength is below 35 MPa and the tensile strength below 2.5 MPa. With a strong cement matrix as CS3, the pine

fibres developed a high interface shear stress of 1 MPa at 28 days. This was the highest interface shear stress of pine fibres developed during the pullout tests.
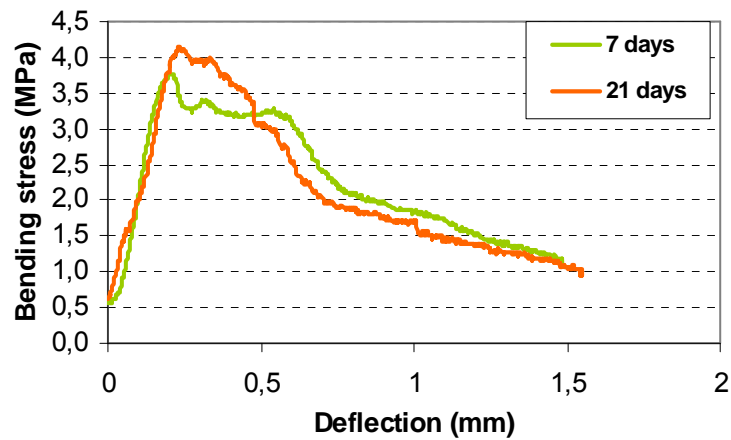
Figure 6.35: Flexural load-deflection curves for long pine - CS3 composites at different ages, thin sheet specimens.

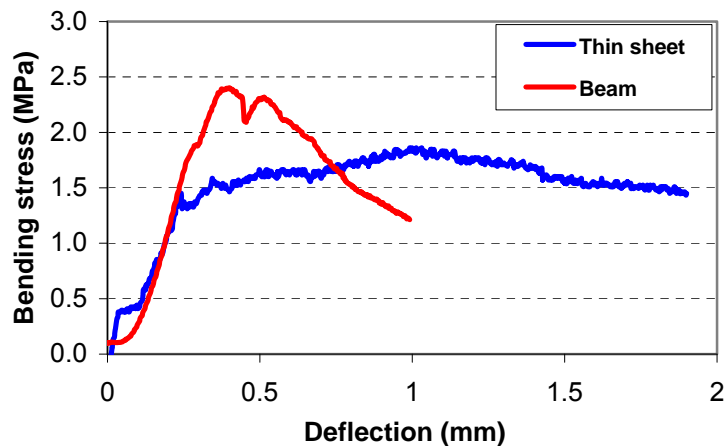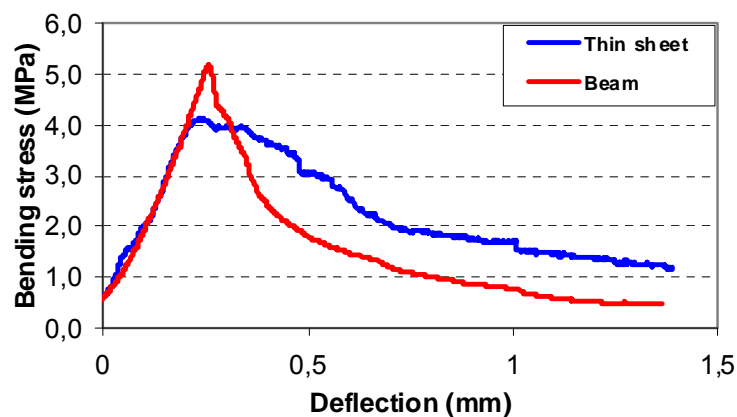*Figure 6.36: Flexural load-deflection curves for CS3- 5.7% untreated pine composites, 21 days and different specimen geometries.*

In composites reinforced with 5.7% long pine fibres and tested under four point bending (thin sheets), the fibre-bridging strength is not higher than the first crack strength. As can be seen in figure 6.35, at age 7 days after the first crack in the cement matrix the fibres bridge the crack to avoid brittle failure, but the fibres cannot sustain a specimen deflection beyond 0.7 mm. At age 21 days, both the cement matrix tensile strength as the fibre-matrix shear stress have increased, but the first crack strength remained higher than the fibre bridging strength and the composite failed without developing multiple cracks. Beam specimens show higher bending strength than thin sheet samples, as with other cement matrices described above. The failure is brittle, with one crack opening (figure 6.36).

6.5.3   Fibre distribution

The fibre distribution of tested and non-tested samples was analyzed by means of CT scans and image analysis. It can be seen that even though the fibres are lighter (in weight) than the

other materials in the cement-based composites they do not float. Instead, in all samples, the fibres are evenly distributed on the depth. The geometry of the two types of samples used for four-point bending tests is shown in figure 6.37. Thin sheets samples (thickness 11 mm) from materials containing pine fibres with length 10 mm have a 3-D fibre distribution. The fibres just shorter than the smaller dimension of the specimens allow them to distribute tri-dimensionally. There is a tendency to be orientated parallel to the two other specimen dimensions. Figure 6.38 shows a tomography image of a thin sheet sample of matrix CF2 with untreated pine fibres ($l = 10$ mm). Here one can see fibres in parallel to the y direction as well as the trajectory of fibres in xy direction. There are also a few fibre cross-sections from fibres that are parallel to the z direction of this sample.
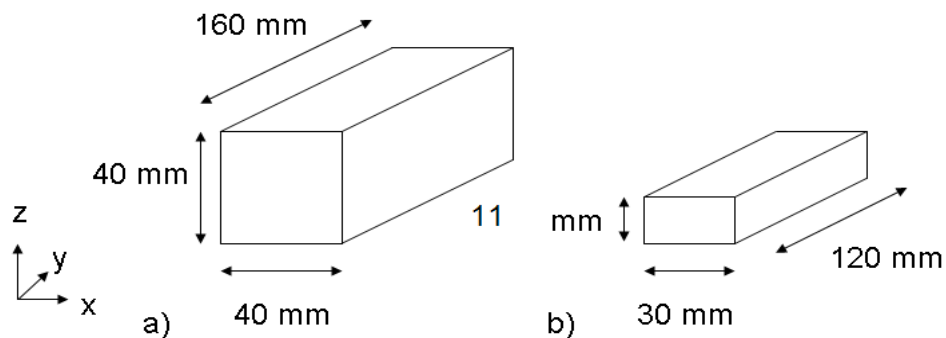
Figure 6.37: Geometry of samples for four-point bending tests a) Beam sample b) Thin sheet sample.
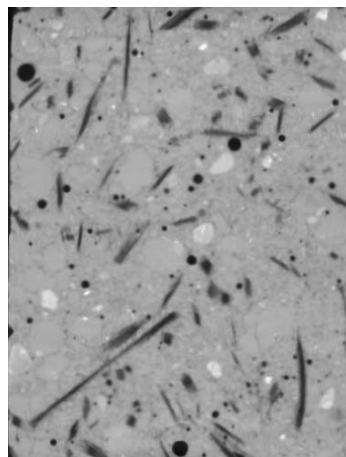
Figure 6.38: CT scan of a thin sheet sample of matrix CF2 with untreated pine fibres (l0 mm).

Thin sheet specimens from materials containing pine fibres with length 25 mm show a preferential orientation along the longer dimension of the sample (figure 6.39). This preferential orientation is due to the casting procedure: the fresh material is first placed in the centre of the sample and then distributed in the length direction.

Pine fibres with length 25 mm in beam samples (cross section 40×40 mm^2) have a 3-D distribution, with a tendency to align in the x and y directions. Figure 6.40 shows tomography images in each direction and the same images after processing showing only the fibres.
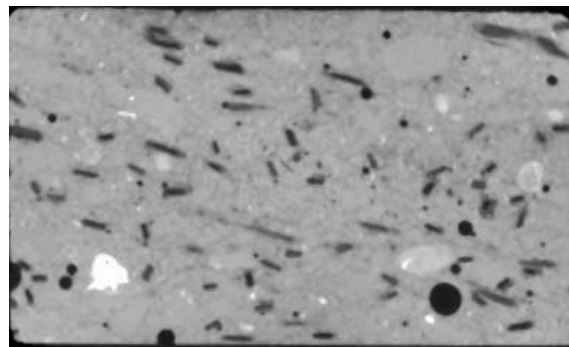
Figure 6.39: CT scan of a thin sheet sample of matrix CF2 with untreated pine fibres (25 mm)
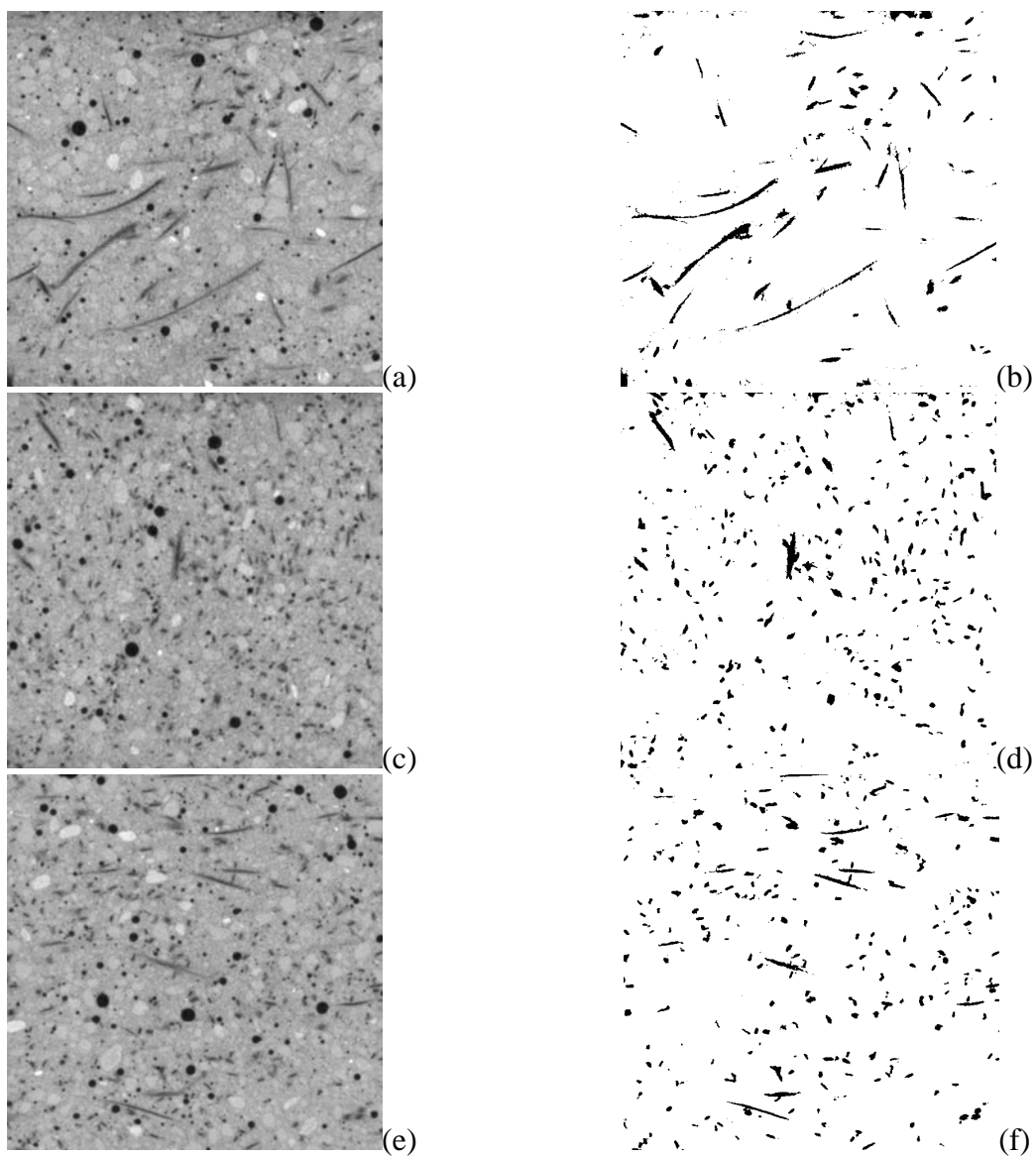
Figure 6.40: CT scan of a beam sample of matrix CF2 with untreated pine fibres (25 mm)
(a) XY-plane; (b) XY-plan, only fibres; (c) XZ-plane;
(d) XZ-plane, only fibres; e) YZ-plane; (f) YZ-plane, only fibres.

In a tomography image of a beam sample from matrix CF4 and untreated pine fibres tested under four-point bending is possible to see fibres bridging the crack (figure 6.41). Some fibres were pulled out; some fibres broke as the crack width increased. The bond between untreated pine and cement matrix is sound. Thus, when the crack passes at the tip of any fibre, this tip is pulled out breaking a piece of matrix. Inside the composite untreated fibres seem to keep a sound bond with the matrix, even though the specimens were air-cured. This was not the behaviour observed in pullout specimens with 1 fibre; as explained in Chapter 5. Due to its small dimensions of the pullout specimen, $10 \times 10 \times 10$ mm^3, it is possible that it completely dries while in the composite specimens there will remain some moist.

The flexural deflection curve of the sample in figure 6.41 is shown in figure 6.32.
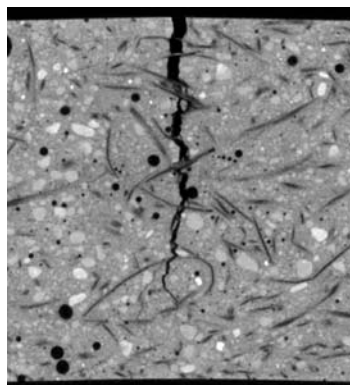
Figure 6.41: CT scan of a beam sample of matrix CF4 with untreated pine fibres (25 mm) showing fibre crack bridging.

6.6   Concluding remarks

Preliminary experimental tests with a high strength cement matrix (MF1) and a low fibre volume percentage (2%) together with micromechanical-based modelling show the need to lower the cement matrix strength and to increase the fibre volume in order to develop a material with multiple-cracking behaviour prior to failure. A material with increased deflection capacity was developed with 5% untreated pine fibres and cement matrices (CF3 and CF4) with a cement replacement between 70 and 83.5%. Composites with sand and limestone, two fillers, have a low bending strength (CF3).

The following conclusions can be drawn:
- CT Scans showed that wood fibres are evenly distributed in the composites. Even though the fibres are lighter they do not float because of a proper viscosity of the fresh cement paste.
- The fibres showed preferential orientation in thin sheets (10 mm thick), which lead to an improved deflection capacity.
- Beam samples, dimensions $40 \times 40 \times 160$ mm^3 have a 3-D fibre distribution with a preferential orientation along the specimen length.
- Under four-point bending load the composites with 5.7% untreated pine and cement matrix CF4 developed improved deflection capacity independent from the specimen geometry, both thin sheet and beam samples.

Chapter 7

General Conclusions

7.1　Highlights of this thesis

In order to turn a brittle cement matrix into a ductile composite different types of man-made fibres such as steel, glass and polyvinyl alcohol are currently used as reinforcement, as well as some natural fibres. Compared to synthetic fibres, natural fibres are more easily available worldwide and they are friendlier to the environment since less energy is needed to produce them. They are also a renewable resource. However, the properties of natural fibres are not as constant as those of artificial fibres and natural fibres have a lower tensile strength.

Some studies using natural fibres in cement-based materials have shown several benefits: reduction of plastic shrinkage and improvement of the bending behaviour and tensile-hardening with multiple-cracking behaviour in pre-cast, thin elements. While synthetic fibres are used for both pre-cast and cast-in-place applications, the use of natural fibres has been limited to pre-cast elements. The main goal of this project is to develop and mechanically characterize a cement-based composite reinforced with natural fibres from wood that will show an enhanced ductile capacity and that can be cast-in-place. In order to achieve this goal the three constituents of the composite, fibre, matrix and fibre-matrix interface were studied.

From a variety of available natural fibres, wood was chosen. Within wood, softwood fibres were selected over hardwood fibres because softwood single fibres are bigger and more uniformly distributed. Fibres were obtained from three different softwood species: larch, spruce and pine. Even tough larch fibres showed promising results regarding the fibre tensile strength and the fibre-matrix interface, due to production constraints they were ruled out as possible reinforcement for this research.

Cement matrices using partial cement replacement with other binders were studied to achieve a low environmental-impact matrix as well as a matrix with a tensile strength compatible with the chosen wood fibre's strength.

This thesis contributes to a better understanding of the wood fibre-matrix interface properties. Pullout test results and the microstructure analysis showed that the bond depends on the fibre type, the cement matrix composition, the curing conditions and the fibre geometry. Among these factors it is necessary to highlight the loss of interface bond due to the volume changes of the fibres in the presence of water. By treating the fibres the volumetric changes due to humidity were controlled. This leads to improved pullout behaviour for both spruce and pine fibres. A numerical model that assumes volume loss due to internal damage of the wood fibre during pullout, fits the laboratory test results.

A micromechanics model using information from the fibres, the cement matrix and the interface provided the amount of fibres necessary to develop multiple cracking prior to failure

under bending stress. The model showed the need to lower the cement matrix strength and increase the fibre content to 5%.

Proper viscosity of the fresh mix allows the fibres to evenly distribute in 2D or 3D arrangements, depending on the geometry of the samples casted. Fibres do not float even though they are lighter than any other composite ingredient.

A lightweight cement-based composite reinforced with pine fibres was designed to exhibit deflection hardening behaviour. This material can be cast-in place as well as pre-cast. The designed material can be considered for applications such as low-budget housing in countries subject to seismic risk, where ductility and low weight are desirable characteristics of the building material.

7.2   General conclusions

The following conclusions were drawn:

- As reported in literature, the fibres obtained following semi-chemical process have higher tensile strengths than mechanically prepared fibres. Due to process constraints and the extensive amount of time consumed by the semi-chemical procedure, only mechanically obtained fibres were used as reinforcement in cement-based composites.

- The slip behaviour of natural fibres during pullout is, in contrast to the slip behaviour of synthetic fibres, not determined by gradual debonding of the fibre-matrix interface. The slip behaviour of natural fibres during pullout seems to be determined by degradation of the fibre and its irregular shape.

- Numerical modelling of the pullout tests and ESEM observations during the tests showed that the pine fibres slip from the beginning of the pullout. If there is a very fast debonding or no debonding stage at all still has to be studied.

- Volumetric changes of the fibres, due to humidity, in pullout samples were controlled by means of two simple and practical fibre treatments. The pullout behaviour improved for the treated fibres.

- Inside cement-based composites that were cured without extra water, the untreated pine fibres showed less volumetric changes than in single-pullout samples. By maintaining a good fibre-matrix bond in air-cured conditions, it was possible to achieve a ductile material reinforced with wood fibres, that can be mixed and cast-in-place and then cured without any special requirement.

- In accordance to the literature review in Chapter 2, the wood fibre-composites studied in this thesis have enhanced flexural toughness than control matrices without fibres. The bending strength did not increase but deflection hardening was achieved giving the material ductility capacity. The compressive strength, as in literature, decreased due to the presence of fibres.

- This thesis demonstrates the feasibility of designing a more sustainable fibre-reinforced composite, when compared to currently used materials, which contain high percentage of cement and synthetic fibres. Even though the bending strength and ductility is lower than some other fibre-reinforced materials, the material presents several advantages such as lower environmental-impact, production costs and weight as well as the higher sustainability of the materials.

- The design path followed in this research can be applied to any other fibre-reinforced cement-based material.

7.3   Further research

This thesis presents promising results for the use of bundles of wood fibres as reinforcement in cement based materials for specific ductility requirements. Further research can focus in different aspects of the material properties as well as the durability assessments to improve and optimize the use of wood bundles in cement-based materials.

- Larch fibres have a higher tensile strength than spruce and pine fibres, as well as good interface properties. In order to take advantage of these promising results, it is necessary to develop a more efficient production method than the semi-chemical semi-manual method followed in this thesis.
- After evidence of improved tensile strength of pine fibres exposed to solutions with pH 10, further research is recommended in order to avail this as a fibre treatment.
- Further research should be done into the precise slip behaviour of natural fibres. Insight in the most important factor for pullout behaviour can lead to an improved choice of natural fibres or an improved processing method for natural fibres.
- The durability of wood fibre- reinforced cement-based materials needs to be evaluated in detail. The fibres that are in the exterior of the composites may exhibit volumetric changes due to changes in the humidity conditions and these changes will affect the fibre-matrix bonding. Additionally these fibres, in the exterior, may act as easy paths for chloride ingress.
- The tensile properties and impact resistance of the composites with wood fibres needs to be evaluated.
- The setting delay in composites with fly ash and wood fibres could be overcome by the proper use of chemical additives. The influence of such additives in the fibre-matrix interface needs to be studied.
- A numerical tool, which can simulate the mechanical behaviour of the composites reinforced with wood fibres as well as the change in properties with age, will lead to a better understanding of the behaviour and improvements in the material design.
- Life cycle analysis of the wood fibre-reinforced cement-based materials is needed. This analysis will quantify the economical and environmental benefits of using wood fibres in cement-based composites.
- The variability of the mechanical properties of the wood fibres can be improved by developing an automatic production process.

References

Abu-Lebdeh, T., Hamoush, S., Heard, W. and Zornig, B. (2011), Effect of matrix strength on pullout behavior of steel fiber reinforced very-high strength concrete composites, *Construction and Building Materials* 25: 39-46.

Aïtcin, P.C. (2008), *Binders for durable and sustainable concrete*, Taylor and Francis, New York.

Al-Oraimi, S.K. and Seibi, A.C. (1995), Mechanical characterization and impact behaviour of concrete reinforced with natural fibres, *Composite Structures* 32: 165-171.

Asakura, R., Morita, M., Maruyama, K, Hatori, H. and Yamada, Y. (2004), Preparation of fibrous activated carbons from wood fiber, *Journal of Materials Science* 39 (1): 201-206.

Baert, G. (2009), *Physico-Chemical Interactions in Portland Cement – (High Volume) Fly Ash Binders*, PhD thesis, Ghent University, Belgium.

Balaguru, P.N. and Shah, S.P. (1992), *Fibre-reinforced cement composites*, Mc Graw-Hill, Auckland.

Barros Cabezas, J. (2008), *Hormigón reforzado con fibras vegetales* (In Spanish), BSc thesis, Universidad Católica de Santiago de Guayaquil, Ecuador.

Bartos, P. (1981), Review paper: bond in fibre reinforced cements and concretes, *International Journal of Cement Composites and Lightweight Concrete* 3: 159-177.

Battagin, A.F. (1992), Influence of degree of hydration of slag on slag cements, *Proc. of the 9th International Congress on the Chemistry of Cement*, pp. 166-172.

Battelle (2002), *Climate Change, Toward a Sustainable Cement Industry*, World Business Council on Sustainable Development (WBCSD), available from: http://www.wbcsd.org/web/publications/batelle-full.pdf [Cited on January 2011].

Bentur, A. and Akers, S.A. (1989), The microstructure and aging of cellulose fibre reinforced cement composites cured in a normal environment, *International Journal of Cement Composites and Lightweight Concrete* 11 (2): 99-109.

Bentur, A. and Mindness, S. (2007), *Fibre reinforced cementitious composites*, 2nd edition, Concrete Technology 15, Taylor and Francis, New York.

Bentz, D.P. (2005), Replacement of "coarse" cement particles by inert fillers in low w/c ratio concretes; II: Experimental validation, *Cement and Concrete Research* 35: 185-188.

Biermann, C.J. (1996), *Handbook of Pulping and Papermaking*, 2nd edition, Academic Press.

Bijen, J. (1989), *Class notes from Course Materiaalkunde I: Organische Materialen*, Delft University of Technology, The Netherlands.

Bijen, J. (1996), Benefits of slag and fly ash, *Construction and Building Materials* 10(5): 309-314.

Bilba, K., Arsene, M.A. and Ouensanga, A. (2007), Study of banana and coconut fibers botanical composition, thermal degradation and textural observations, *Bioresource Technology* 98 (1): 58-68.

Blankenhorn, P.R., Silsbee, M.R., Blankenhorn, B.D., DiCola, M. and Kessler, K. (1999), Temperature and moisture effects on selected properties of wood fibre-cement composites, *Cement and Concrete Research* 29: 737-741.

Blankenhorn, P.R., Blankenhorn, B.D., Silsbee, M.R. and DiCola, M. (2001), Effects of fibre surface treatments on mechanical properties of wood fibre-cement composites, *Cement and Concrete Research* 31: 1049-1055.

Bledzki, A.K., Reihmane, S. and Gassan, J. (1996), Properties and modification methods for vegetable fibers for natural fiber composites, *Journal of Applied Polymer Science* 59(8): 1329-1336.

Boatright, S.W.J. and Garrett, G.G. (1983), The Effect of Microstructure and Stress State on the Fracture Behaviour of Wood, *Journal of Materials Science* 18(7): 2181-2199.

Boghossian, E. and Wegner, L.D. (2008), Use of flax fibres to reduce plastic shrinkage cracking in concrete, *Cement and Concrete Composites* 30: 929-937.

Borysiak, S. and Garbarczyk, J. (2003), Applying the WAXS method to estimate the supermolecular structure of cellulose fibres after mercerisation, *Fibre and Textiles in Eastern Europe*, 11(5): 104-106.

Boshoff, W.P. (2007), *Time-Dependant Behaviour of Engineered Cement-Based Composites*, PhD thesis, University of Stellenbosch, Stellenbosch, South Africa.

Bowyer, J.L., Shmulsky, R. and Haygreen, J.G. (2007), *Forest products and wood science: An introduction*, 5th edition, Blackwell Publishing, Oxford.

Brandt, A.M. (2009), *Cement-Based Composites*, 2nd edition, Taylor and Francis, New York.

Brinkgreve, R.B.J., Swolfs, W.M. and Engin, E. (2010), *Plaxis finite element code manual*.

Brouwer, W.D. (2000), Natural Fibre Composites in Structural Components: Alternative Applications for Sisal?, *Common Fund for Commodities - Alternative Applications for Sisal and Henequen - Technical Paper* 14, Available from: http://www.fao.org/DOCREP/004/Y1873E/y1873e0a.htm [cited on January 2011].

Campbell, M.D. and Coutts, R.S.P. (1980), Wood fibre-reinforced cement composites, *Journal of Materials Science* 15: 1962-1970.

Chand, N., Dwivedi, U.K. and Acharya, S.K. (2007), Anisotropic abrasive wear behaviour of bamboo, *Wear* 262 (9-10): 1031-1037.

Chandramohan, D. and Marimuthu, K. (2011), Characterization of natural fibres and their application in bone grafting substitutes, *Acta of Bioengineering and Biomechanics* 13 (1): 77-84.

Chen, W., Yu, H. Liu, Y. Chen, P., Zhang, M. and Hai, Y. (2011), Individualization of cellulose nanofibers from wood using high-intensity ultrasonication combined with chemical pretreatments, *Carbohydrate Polimers* 83: 1804-1811.

Coatanlem, P., Jauberthie, R. and Rendell, F. (2006), Lightweight wood chipping concrete durability, *Construction and Building Materials* 20: 776-781.

Coutts, R.S.P. (1983a), Wood fibres in inorganic matrices, *Chemistry in Australia* 50(5): 143-148.

Coutts, R.S.P. (1983b), Flax fibres as a reinforcement in cement mortars, *International Journal of Cement Composites and Lightweight Concrete* 5 (4): 257-262.

Coutts, R.S.P. (1987), Fibre-matrix interface in air-cured wood-pulp fibre-cement composites, *Journal of Materials Science Letters* 6: 140-142.

Coutts, R.S.P. and Kightly, P. (1984), Bonding in wood fibre-cement composites, *Journal of Material Science* 19: 3355-3359.

CUR Rapport 94-12 (1994), Beoordeling van de constructieve consequenties van het toepassen van grindvervangende toeslagmaterialen, Gouda.

D´Almeida, A., Toledo Filho, R. and Melo Filho, J. (2010), Cement composites reinforced by short curaua fibers, *Revista Materia* 15(2): 153-159.

Dawson, S. and Turner, S. (1995), *A Hand Papermaker´s Sourcebook*, Design books, New York.

Detwiler, R.J. and Mehta, P.K. (1989), Chemical and physical effects of silica fume on the mechanical behavior of concrete, *ACI Materials Journal* 86 (6): 609-614.

Dijkstra, H. (1998), *EDAX Operator´s School Course manual*.

Donath, S., Militz H. and Mai, C. (2006), Creating water repellent effects on wood by treatment with silanes, *Holzforschung* 60: 40-46.

Elsaid, A., Dawood, M., Seracino, R. and Bobko, C. (2011), Mechanical properties of kenaf fiber reinforced concrete, *Construction and Building Materials* 25: 1991-2001.

Erdoğdu, K. and Türker, P. (1998), Effects of fly ash particle size on strength of portland cement fly ash mortars, *Cement and Concrete Research* 28 (9): 1217-1222.

Escalante-Garcia, J.I. and Sharp, J.H. (1998), Effect of temperature on the hydration of the main clinker phases in Portland cements: Part II, blended cements, *Cement and Concrete Research* 28 (9): 1259-1274.

Fennis, S.A.A.M. (2011), *Design of Ecological Concrete by Particle Packing Optimization*, PhD thesis, Delft University of Technology, The Netherlands.

Forest Products Laboratory, Forest Service, US Department of Agriculture (1974), *Wood handbook*, Agriculture Handbook 72.

Fraaij, A. (1990), *Fly ash a possolan in concrete*, PhD thesis, Delft University of Technology, The Netherlands.

Fraaij, A. (2007), *Class notes from Course Durability of Concrete*, Delft University of Technology, The Netherlands.

Frybort, S., Mauritz, R., Teischinger, A. and Muller, U. (2008), Cement bonded composites - A mechanical review, *BioResources* 3(2): 602-626.

Funk, J.E. and Dinger, D.R. (1994), *Predictive Process Control of Crowded Particulate Suspensions – Applied to Ceramic Manufacturing*, Kluwer Academic Publishers, Boston.

Gao, Y.C., Mai, Y.W. and Cotterell, B. (1988), Fracture of fiber-reinforced materials, *Journal of Applied Mathematics and Physics* 39: 550-572.

Garas, V.Y. and Kurtis, K.E. (2008), Assessment of methods for optimising ternary blended concrete containing metakaolin, *Magazine of Concrete Research* 60 (7): 499-510.

Garcez, E.O. (2009), *Investigacao do Comportamento de Engineered Cementitious Composites Reforcados com Fibras de Polipropileno como Material para Recapeamento de Pavimentos*, PhD thesis, Universidade Federal do Rio Grande do Sul, Brazil.

Gopalaratnam, V.S. and Shah, S.P. (1985), Tensile Failure of Steel Fiber-Reinforced Mortar, *Journal of Engineering Mechanics* 113(5): 635-652.

Gray, R.J. (1984), Analysis of the effect of embedded fibre length on fibre debonding and pull-out from an elastic matrix, Part 1: review of theories, *Journal of Material Sciences* 19: 861-870.

Gwon, J.G., Lee, S.Y., Doh, G.H and Kim, J.H. (2010), Characterization of Chemically Modified Wood Fibers using FTIR Spectroscopy for Biocomposites, *Journal of Applied Polymer Science* 116: 3212-3219.

Hietala, S., Maunu, S.L., Sundholm, F., Jämsä, S. and Viitaniemi, P. (2002), Structure of thermally modified wood studied by liquid state NMR measurements, *Holzforschung* 56 (5): 522–528.

Illston J.M. and Domone P.L.J. (2001), *Construction Materials: Their Nature and Behavior*, Spon Press, New York.

Jacobsen, S.E. and Wyman, C.E. (2000), Cellulose and Hemicellulose Hydrolysis Models for Application to Current and Novel Pretreatment Processes, *Applied Biochemistry and Biotechnology* 84-86: 81-96.

Jiang, L., Liu, Z. and Ye, Y. (2004), Durability of Concrete Incorporating Large Volumes of Low-Quality Fly Ash. *Cement and Concrete Research* 34 (8): 1467-1469.

Johnston, C.D. (2001), *Fibre-reinforced Cements and Concretes*, Gordon and Breach Science Publishers.

Juarez, C., Duran, A, Valdez, P., and Fajardo, G. (2007), Performance of "Agave lecheguilla" natural fiber in Portland cement composites exposed to severe environment conditions, *Building and Environment* 42: 1151-1157.

Jun, P., Mechtcherine, V. and Kabele, P. (2009), Derivation of a multi-scale model for Strain-Hardening Cement-based Composites (SHCC) under monotonic and cyclic tensile loading, *Advances in Cement Based Materials*, pp. 245-253.

Kanda, T. (1998), *Design of engineered cementitious composites for ductile seismic resistant elements*, PhD thesis, University of Michigan, Ann Arbor, USA.

Katz, A. and Li. V.C. (1996), A Special Technique for Determining the Bond Strength of Carbon Fibers in Cement Matrix by Pullout Test, *Journal of Materials Science* Letters 15: 1821-1823.

Kavelin, K.G. (2005), *Investigation of natural fibre composites heterogeneity with respect to automotive*, PhD thesis, Delft University of Technology, The Netherlands.

Kawashima, S. and Shah, S.P. (2011), Early-age autogenous and drying shrinkage behaviour of cellulose fiber-reinforced cementitious materials, *Cement and Concrete Composites* 33: 201-208.

Kelly, A. (1988), *Strong solids*, Clarendon press, Oxford.

Keoleian, G.A., Kendall, A., Dettling, J.E., Smith, V.M., Chandler, R.F., Lepech, M.D. and Li, V.C. (2005), Life Cycle Modeling of Concrete Bridge Design: Comparison of Engineered Cementitious Composites Link Slabs, *ASCE Journal of Infrastructure Systems* 11(1): 51-60.

Kettunen, P.O. (2006), *Wood: Structure and properties*, Trans Tech Publications, Ltd, Zurich.

Khanna, O.S. (2009), *Characterization and Utilization of Cement Kiln Dusts (CKDs) as Partial Replacements of Portland Cement*, PhD thesis, University of Toronto, Canada.

Kim, J.K., Kim, J.S., Ha, G.J. and Kim, Y.Y. (2007), Tensile and fiber dispersion performance of ECC (engineered cementitious composites) produced with ground granulated blast furnace slag, *Cement and Concrete Research* 37 (7): 1096-1105.

Koleva, D.A. (2007), *Corrosion and protection in reinforced concrete. Pulse cathodic protection: an improved cost-effective alternative*, PhD thesis, Delft University of Technology, The Netherlands.

Kosmatka, S. and Panarese, W.C. (1998), *Design and Control of Concrete Mixes*, 13th edition, Portland Cement Association, Skokie.

Kozlowski, R., Wladyka-Przybylak, M.H. and Kurzydloski, K. (2004), Composites Based on Lignocellulosic Raw Materials, Molecular Crystals and Liquid Crystals 418 (1): 131-151.

Kriker, A., Debicki, G., Bali, A., Khenfer, M.M. and Chabannet, M. (2005), Mechanical properties of date palm fibres and concrete reinforced with date palm fibres in hot-dry climate, *Cement & Concrete and Composites* 27: 554-564.

Kuder, K.G. and Shah, S.P. (2003), Effects of Pressure on Resistance to Freezing and Thawing of Fiber-Reinforced Cement Board, *ACI Materials Journal* 100 (6): 463-468.

Kumar, S.V., Santhanam, M. (2003), Particle packing theories and their application in concrete mixture proportioning: A review, *Indian Concrete Journal* 77 (9): 1324-1331.

Kuroda, M., Watanabe, T. and Terashi, N. (2000), Increase of bond strength at interfacial transition zone by the use of fly ash. *Cement and Concrete Research* 30(2): 253-258.

Landis, E.N. and Nagy, E.N. (2000), Three-dimensional work of fracture for mortar in compression, *Engineering Fracture Mechanics* 65 (2-3): 223-234.

Lepech, M.D. and Li, V.C. (2006), Long term durability Performance of Engineered Cementitious Composites, *International Journal for Restoration of Buildings and Monuments* 12 (2): 119-132.

Lepech, M.D., Li, V.C., Robertson, R.E. and Keoleian, G.A. (2008), Design of Green Engineered Cementitious Composites for Improved Sustainability, *ACI Materials Journal* 105 (6): 567-575.

Lepech, M.D., Li, V.C. (2008), Large-Scale Processing of Engineered Cementitious Composites, *ACI Materials Journal* 105 (4): 358-366.

Leung, C.K.Y. and Li, V.C. (1990), Strength-based and fracture-based approaches in the analysis of fibre debonding, *Journal of Materials Science* Letters 9: 1140-1142.

Li, D., Li L. and Zhou, J. (2010), Applications of Infrared Spectroscopy in the study of Wood Plastic Composites, *Advanced Materials Research* 113-114: 2003-2006.

Li, M. (2009), *Multi-scale design for durable repair of concrete structures*, PhD thesis, University of Michigan, Ann Arbor, USA.

Li, V.C. (1992a), Post-Crack Scaling Relations for Fiber-Reinforced Cementitious Composites, *ASCE Journal of Materials in Civil Engineering* 4 (1): 41-57.

Li, V.C. (1992b), A Simplified Micromechanical Model of Compressive Strength of Fiber-Reinforced Cementitious Composites, *Cement and Concrete Composites* 14: 131-141.

Li, V.C. (1998), Engineered Cementitious composites – Tailored composites through micromechanical modelling, in N. Banthia, A. Bentur and A. Mufti (ed.), *Fiber Reinforced Concrete: Present and the Future*, Montreal: Canadian Society for Civil Engineering, pp. 64-97.

Li, V.C. (2008), *Class notes from CEE650,* University of Michigan, Ann Arbor, USA.

Li, V.C. and Leung, C.K.Y. (1992), Theory of steady state and multiple cracking of random discontinuous fiber reinforced brittle matrix composites, *ASCE Journal of Engineering Mechanics* 118 (11):2246-2264.

Li, V.C., Wu, C., Wang, S., Ogawa A. and Saito, T. (2002), Interface Tailoring for Strain-hardening PVA-ECC, *ACI Materials Journal* 99 (5): 463-472.

Lin, X., Silsbee, M.R., Roy, D.M., Kessler, K. and Blankenhorn, P.R. (1994), Approaches to improve the properties of wood fibre reinforced cementitious composites, *Cement and Concrete Research* 24 (8): 1558-1566.

Lin, Z. and Li, V.C. (1997), Crack bridging in fiber reinforced cementitious composites with slip-hardening interfaces, *Journal of the Mechanics and Physics of Solids* 45 (5): 763-787.

Lin, Z., Kanda, T. and Li, V.C. (1999), On interface property characterization and performance of fiber-reinforced cementitious composites, *Concrete Science and Engineering* 1: 173-174.

Lippke, B. (2009), *Impact of Carbon Accounting on Green Building*, available from: http://www.corrim.org/presentations/2009/Lippke_UNECE.pdf [Cited on October 2011].

Livesey, P. (1991), Strength characteristics of Portland-limestone cements, *Construction and Building Materials* 5 (3): 147-150.

Lothenbach, B., Scrivener, K. and Hooton, R. D. (2011), Supplementary cementitious materials, *Cement and Concrete Research* 41: 217-229.

Luke, K and Glasser, F.P. (1987), Selective dissolution of hydrated blast furnace slag cements, *Cement and Concrete Research* 17 (2): 273-282.

MacVivar, R., Matuana, L.M. and Balatinecz, J.J. (1999), Aging mechanisms in cellulose fiber reinforced cement composites, *Cement and Concrete Composites* 21: 189-196.

Mansur, A. (2000), *Analysis of Calcutta bamboo for structural composite materials*, PhD thesis, Virginia Polytechnic Institute and State University, USA.

Mohammed, B.S. and Chuan Fang, O. (2011), Mechanical and durability properties of concretes containing paper-mill residuals and fly ash, *Construction and Building Materials* 25: 717-725.

Mohr B.J, Nanko, H. and Kurtis, K.E. (2005a), Durability of Kraft Pulp Fiber-cement Composites to Wet/Dry Cycling, *Cement and Concrete Composites* 27(4): 435-448.

Mohr, B.J., Premenko, L., Nanko, H. and Kurtis, K.E. (2005b), Examination of wood-derived powders and fibers for internal curing of cement-based materials, *Proc. of the 4th International Seminar on Self-Desiccation and its importance in concrete technology*, pp. 229-244.

Morlier, P. and Khenfer, M.M. (1991), Effet de la longuer des fibres sur les propriétés mécaniques des ciments renforces de fibres cellulosiques, *Matériaux et Constructions*, 24: 185-190.

Morrison, J.K., Shah, S.P. and Jenq, Y.S. (1998), Analysis of fiber debonding and pullout in composites, *Journal of Engineering Mechanics* 114 (2): 227- 294.

Morton, J.H., Cooke, T. and Akers, S.A.S. (2010), Performance of slash pine fibers in fiber cement products, *Construction and Building Materials* 21:165-170.

Mott, L., Shaler, S.M., Groom, L.H and Liang, B.H. (1995), The tensile testing of individual wood fibers using environmental scanning electron microscopy and video image analysis, *Tappi Journal* 78 (5): 143-148.

Mueller, D. H. and Krobjilowski, A. (2003), New Discovery in the properties of Composites Reinforced with Natural Fibres, *Journal of Industrial Textiles* 33 (2): 111-130.

Mukherjee, P.S. and Satyanarayana, K.G. (1984), Structure and properties of some vegetable fibres, *Journal of Materials Science* 19: 3925-3934.

Mwaikambo, L.Y. (2006), Review of the history, properties and application of plant fibres, *African Journal of Science and Technology: Science and Engineering Series* 7 (2): 120-133.

Naaman, A.E, Namur, G.G, Alwan, J.M. and Najm, H.S. (1991a), Fiber Pullout and Bond Slip. I: Analytical Study, *Journal of Structural Engineering* 117(9): 2769-2790.

Naaman, A.E, Namur, G.G, Alwan, J.M. and Najm, H.S. (1991b), Fiber Pullout and Bond Slip. II: Experimental Validation, *Journal of Structural Engineering* 117(9): 2791-2800.

Naik, T. R., Friberg, T.S. and Chun, Y. (2004), Use of pulp and paper mill residual solids in production of cellucrete, *Cement and Concrete Research* 34: 1229–1234.

Neville, A.M. (1995), *Properties of Concrete*, 4th ed., Longman, Harlow.

Olesen, P.O. and Plackett, D.V. (1999), Perspectives on the performance of natural plant fibres, *Natural Fibres Performance Forum* (available online: http://www.ienica.net/fibresseminar/fibresindex.htm), Denmark.

Olsson, A.M., Bjurhager, I., Gerber, L., Sundberg, B. and Salmen, L. (2011), Ultra-structural organization of cell wall polymers in normal and tension wood of aspen revealed by polarisation FTIR microspectroscopy, *Planta* 233: 1277-1286.

Pacheco-Torgal, F. and Jalali, S. (2011), Cementitious building materials reinforced with vegetable fibres: A review, *Construction and Building Materials* 25 (2): 575-581.

Page, D.H., El-Hosseiny, F., Winkler, K. and Lancaster, A.P.S. (1977), Elastic modulus of single wood pulp fibers, *Tappi* 60 (4): 114-117.

Pehanich, J.L., Blankenhorn, P.R. and Silsbee, M.R. (2004), Wood fibre surface treatment level effects on selected mechanical properties of wood fibre-cement composites, *Cement and Concrete Research* 34: 59-65.

Pietersen, H.S. (1993), *Reactivity of fly ash and slag in cement*, PhD thesis, Delft University of Technology, The Netherlands.

Poletto, M., Pistor, V., Zeni, M. and Zattera, A.J. (2011), Crystalline properties and decomposition kinetics of cellulose fibers in wood pulp obtained by two pulping processes, *Polymer Degradation and Stability* 96: 679-685.

Puettmann, M and Wilson, J. (2004), Forest to Product: Cradle-to-Gate Life Cycle Investories of Structural Wood Products, available on: http://www.corrim.org/presentations/2004/Puettmann_LCI.pdf [Cited on October 2011].

Ramakrishna, G. and Sundararajan, T. (2005a), Impact strength of a few natural fibre reinforced cement mortar slabs: a comparative study, *Cement and Concrete Composites* 27: 547-553.

Ramakrishna, G. and Sundararajan, T. (2005b), Studies on the durability of natural fibres and the effect of corroded fibres on the strength of mortar, *Cement and Concrete Composites* 27: 575-582.

Rapoport, J.R. and Shah, S.P. (2005), Cast-in-Place Cellulose Fibre-Reinforced Cement Paste, Mortar, and Concrete, *ACI Materials Journal* 102 (5): 299-306.

Reddy, N. and Yang, Y. (2005), Biofibers from agricultural byproducts for industrial applications, *Trends in Biotechnology* 23(1): 22-27.

Redon C., Li. V.C., Wu, C., Hoshiro, H., Saito, T. and Ogawa, A. (2001), Measuring and Modifying Interface Properties of PVA Fibers in ECC Matrix, *ASCE Journal of Materials in Civil Engineering* 13(6): 399-406.

Reis, J.M.L. (2006), Fracture and flexural characterization of natural fibre-reinforced polymer concrete, *Construction and Building Materials* 20: 673-678.

Roma Jr., L.C., Martello, L.S. and Savastano Jr., H. (2008), Evaluation of mechanical, physical and thermal performance of cement-based tiles reinforced with vegetable fibers, *Construction and Building Materials* 22: 668-674.

Rowell, R.M., Tillman, A-M and Simonson, R. (1986), A Simplified procedure for the acetylation of hardwood and softwood flakes for flakeboard production, *Journal of Wood Chemistry and Technology* 6(3): 427-448.

Rowell, R.M., Young, R.A. and Rowell, J.K. (1997), *Paper and composites from agro-based resources*, CRC/Lewis Publishers: Boca Raton.

Sahmaran, M., Lachemi, M., Hossain, K.M.A., Ranade, R. and Li, V.C. (2009), Influence of Aggregate Type and Size on Ductility and Mechanical Properties of Engineered Cementitious Composites, *ACI Materials Journal* 106 (3): 1-9.

Savastano Jr., H. and Agopyan, V. (1999), Transition zone studies of vegetable fibre-cement paste composites, *Cement and Concrete Composites* 21: 49-57.

Savastano Jr., H., Warden, P.G. en Coutts, R.S.P. (2003), Mechanically pulped sisal as reinforcement in cementitious matrices, *Cement and Concrete Composites* 25: 311-319.

Savastano Jr., H., Warden, P.G. en Coutts, R.S.P. (2005), Microstructure and mechanical properties of waste fibre-cement composites, *Cement and Concrete Composites* 27: 583-592.

Savastano Jr., H., Santos, S.F., Radonjic, M. and W.O., Soboyejo (2009), Fracture and fatigue of nature fiber-reinforced cementitious composites, *Cement and Concrete Composites* 31: 232-243.

Schlangen, E. (2008), Crack Development in Concrete, Part 1: Fracture Experiments and CT-scan Observations, *Key Engineering Materials* 385-387: 69-72.

Schneider, M.H. and Brebner, K.I. (1985), Wood-polymer combinations: The chemical modification of wood by alkoxysilane coupling agents, *Wood Science and Technology* 19: 67-73.

Schroeder, H.A. (1972), Shrinking and swelling differences between hardwoods and softwoods, Wood and Fiber Science 2 (1): 20-25.

Schwanninger, M., Hinterstoisser, B., Gradinger, C., Messner, K. and Fackler, K. (2004), Examination of spruce wood biodegraded by Ceriporiopsis subvermispora using near and mid infrared spectroscopy, *Journal of Infrared Spectroscopy* 12: 397-409.

Sedighi Gilani, M. (2006), *A Micromechanical approach to the behaviour of single wood fibres and wood fracture at cellular level*, PhD thesis, École Polytechnique Fédérales de Lausanne.

Sersale, R., Marchese, B. and Frigione, G. (1980), Microstructure and properties of hydrated cements with different slag content, *Proc. of the 7th International Congress on the Chemistry of Cement*, pp. 63-68.

Shannag, M.J., Brincker, R. and Hansen, W. (1997), Pullout Behavior of Steel Fibers from Cement-Based Composites, Cement and Concrete Research 27 (6): 925-936.

Sierra Beltran, M.G. and Schlangen, E. (2008), Wood fibre reinforced cement matrix: a micromechanical based approach, *Key Engineering Materials* 385-387: 445-448.

Silva, F. (2009a), Bond mechanisms in sisal fibre reinforced cement composites, *Proc. of the 11th International Conference on Non-conventional Materials and Technologies*.

Silva, F. (2009b), *Durability and mechanical properties of cement composites reinforced with sisal fibres*, PhD thesis, Federal University of Rio de Janeiro, Brazil.

Smith, B. (1999), *Infrared Spectral Interpretation: A systematic approach*, CRC Press LLC, Boca Raton.

Simonson. R. and Rowell, R.M. (2000), A new process for the continuous acetylation of lignocellulosic fiber, *Proc. of the 5th Pacific Rim Bio-Based Composites Symposium*, pp 190-196.

Singh, S., Shukla, A. and Brown, R. (2004), Pullout behavior of polypropylene fibers from cementitious matrix, *Cement and Concrete Research* 34: 1919-1925.

Sisomphon, K., Copuroglu, O. and Fraaij, A.L.A. (2010), Durability of blast-furnace slag mortars subjected to sodium monofluorophosphate application, *Construction and Building Materials* 25: 823-828.

Soroushian, P, and Marikunte, S. (1990), Reinforcement of cement-based materials with cellulose fibers, *Thin-section fiber reinforced concrete and ferrocement*, SP-124, American Concrete Institute, Detroit: 99-124.

Soroushian, P and Marikunte, S. (1991), Moisture sensitivity of cellulose fiber reinforced cement. *Durability of Concrete* V. 2, SP-126, American Concrete Institute, Detroit: 821-835.

Soroushian, P, Marikunte, S., and Won, J.P. (1994), Wood Fiber Reinforced Cement Composites under Wetting-drying and Freezing-thawing Cycles, *Journal of Materials in Civil Engineering* 6 (4): 595-611.

Soroushian, P. and Ravanbakhsh, S. (1998), Control of plastic shrinkage cracking with specialty cellulose fibers. *ACI Materials Journal* 95 (4): 429-435.

Soroushian, P. (2000), Reinforcing effects on processed cellulose fibers in mortar (stucco), thin sheet products and concrete, *High-performance fiber-reinforced concrete thin sheet products*, SP-190, American Concrete Institute, Detroit: 203-214.

Stang, H. and Shah, S.P. (1986), Failure of fibre-reinforced composites by pull-out fracture, *Journal of Materials Science* 21(3): 953-957.

Sueki, S., Soranakom, C., Mobasher, B. and Peled, A. (2007), Pullout-Slip of Fabrics Embedded in a Cement Paste Matrix, *Journal of Materials in Civil Engineering* 19 (9), 718-727.

Swamy, R.N. (Ed.) (1988), *Natural Fibre Reinforced Cement and Concrete*, Concrete Technology and Design Vol. 5, Blackie: London.

Talbot, A.N. and Richart, F.E. (1923), The strength of concrete in relation to the cement, aggregates and water, *University of Illinois Engineering Experiment Station, Bulletin No. 137*.

Taylor, H.W.F. (1990), *Cement Chemistry*, Academic Press, London.

Toledo Filho, R.D., Srivener, K., England, G.L. and Ghavami, K. (2000), Durability of alkali-sensitive sisal and coconut fibres in cement mortar composites, *Cement and Concrete Composites* 22(2): 127-143.

Tonoli, G.H.D., Joaquim, A.P., Arsene, M.A., Bilba, K. and Savastano Jr, H. (2007), Performance and Durability of Cement Based Composites Reinforced wth Refined Sisal Pulp, *Materials and Manufacturing Processes*. 22: 149-156.

Tonoli, G.H.D., Rodrigues Filho, U.P., Savastano Jr., H., Bras, J., Belgacem, M.N. and Rocco Lahr, F.A. (2009), Cellulose modified fibres in cement based composites, *Composites: Part A, Applied Science and Manufacturing* 40: 2046-2053.

Tsivilis, S., Batis, G., Chaniotakis, E., Grigoriadis, Gr. and Theodossi, D. (2000), Properties and behavior of limestone cement concrete and mortar, *Cement and Concrete Research* 30: 1679-1683.

Tsivilis, S., Chaniotakis, E., Kakali, G. and Batis, G. (2002), An analysis of the properties of Portland limestone cements and concrete, *Cement and Concrete Composites* 34: 371-378.

Ullmann (2011), *Ullmann's Encyclopedia of Industrial Chemistry*, online edition: http://eu.wiley.com/WileyCDA/Section/id-410176.html

Vaickelionis, G. and Vaickelioniene, R. (2006), Cement hydration in the presence of wood extractives and pozzolan mineral additives, *Ceramics – Silikaty* 50 (2): 115-122.

Vares, S., Sarvaranta, L. and Lanu, M. (1997), *Cellulose fibre concrete*, VTT Publication 296.

Walker, J.C.F. (2006), Pulp and paper manufacture, *Primary wood processing principles and practice*, Springer, Houten.

Wang, S. (2005), *Micromechanics based matrix design for Engineered Cementitious Composites*, PhD thesis, University of Michigan, Ann Arbor, USA.

Wang, S. and Li, V.C. (2007), Engineered Cementitious Composites with High-Volume Fly Ash, *ACI Materials Journal* 104 (3): 233-240.

Wolfe, R.W. and Gjinolli, A. (1999), Durability and strength of cement-bonded wood particle composites made from construction waste, *Forest products Journal* 49 (2): 24-31.

Wu, C. (2001), *Micromechanical tailoring of PVA-ECC for structural applications*, PhD thesis, University of Michigan, Ann Arbor, USA.

Yang, E.H. (2007), *Designing added functions in Engineered Cementitious Composites*, PhD thesis, University of Michigan, Ann Arbor, USA.

Yang, E.H., Yang, Y. and Li, V.C. (2007), Use of High Volumes of Fly Ash to Improve ECC Mechanical Properties and Material Greenness, *ACI Materials Journal* 104 (6): 303-311.

Ye, G., Poppe, A.M., De Schutter, G., van Breugel, K. and Liu, X. (2005), Microstructure of self-compacting concrete: experimental study and numerical simulation, *Proc. of the 4th international RILEM Symposium on Self-Compacting Concrete*.

Ye, G., Liu, X., De Schutter, G., Poppe, A.M. and Taerwe, L. (2007), Influence of limestone powder used as filler in SCC on hydration and microstructure of cement pastes, *Cement and Concrete Composites* 29: 94-102.

Young, J.F., Mindness, S., Gray, R.J., and Bentur, A. (1998), *The science and technology of civil engineering materials*, Prentice Hall, Saddle River, NJ.

Zhou, J. (2006), *Microstructure and Permeability of Portland cement blended with Blast furnace slag, Fly ash and Limestone powder*, MSc thesis, Delft University of Technology, The Netherlands.

Zhou, J. (2011), *Performance of Engineered Cementitious Composites for Concrete Repairs*, PhD thesis, Delft University of Technology, The Netherlands.

Standards

ASTM C150 (2000), *Standard Specification for Portland Cement*, American Society for Testing and Materials ASTM

ASTM C230/230M (2008), *Standard Specification for Flow Table for Use in Tests of Hydraulic Cement*, ASTM Subcommittee C01.22

ASTM C78 (2010), *Standard Test Method for Flexural Strength of Concrete (Using Simple Beam with Third-Point Loading)*, ASTM Subcommittee C09.61

ASTM C618 (2008a), *Standard Specification for Coal Fly Ash and Raw and Calcinated Natural Pozzolan for use in Concrete*, ASTM Subcommittee C09.24

NEN-EN 206-1:2001. Concrete – Part 1 : Specification, performance, production and conformity

NEN-EN 1992-1-1:2005. Eurocode 2: Design of concrete structures – Part 1-1: General rules and rules for buildings.

Websites

http://www.jameshardie.com/ [Cited on January 2011]
http://www.eltomation.com/Eng/Folders/Brochure%20Properties,%20Applications%20WWCB%20etc%20NEW.pdf [Cited on January 2011]
http://www.epa.gov/ [Cited on January 2011]

Sand Particle Size Distributions

River sand from the Maas River was used in this research. The particles sizes ranged from 0.125 mm to 2.5 mm. For size fractions above 0.25 mm the particles were evaluated as round. Filcom Papendrecht, from the Netherlands supplied the sand, classified by sizes. Table A.1 presents the cumulative size distribution.

Table A.1: Cumulative size distribution of sand (%).

Sieves	0.125-0.25	0.25-0.5	0.5-1	1-2	2-4
C4	0	0	0	0	8.29
2 mm	0	0	0	1.45	98.88
1 mm	0	0	1.4	98.17	99.92
500 μm	0.34	3.34	93.08	99.9	99.96
250 μm	49.33	94.45	99.95	99.97	99.96
125 μm	99.66	99.64	99.95	99.97	99.96
Rest	100	100	100	100	100

Table A.2: Sand combinations (%).

Distribution	0.125-0.25	0.25-0.5	0.5-1	1-2	2-4*
a	100.0	0.0	0.0	0.0	0.0
b	38.0	4.5	24.0	25.5	8.0
c	40.0	1.0	23.0	36.0	0.0
d	26.5	10.0	31.5	32.0	0.0

* used sand only up to 2.5 mm

Four sand combinations were prepared with different particle size distributions. Each sand combination was design to achieve, together with the powder materials, an optimal particle size distribution for dry materials. The combinations are presented in Table A.2 and the curves for the 4 combinations are presented in figure A.1.
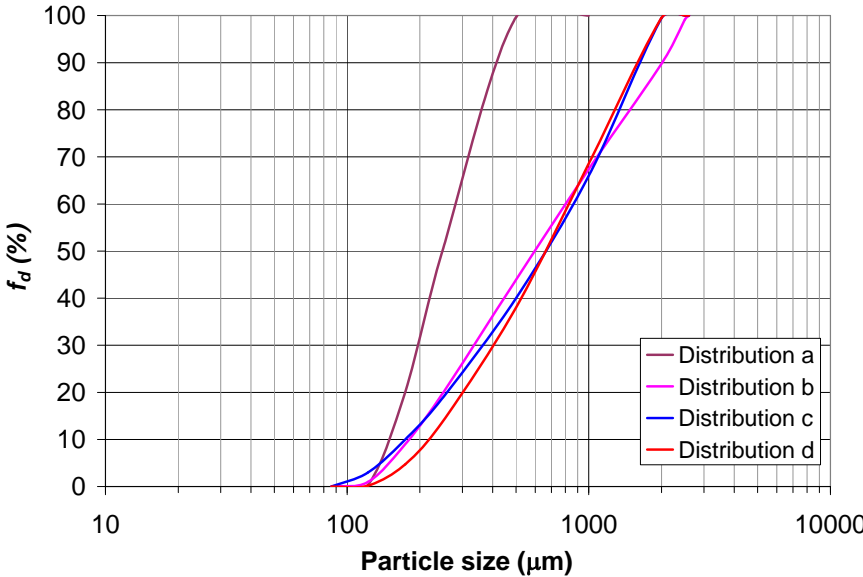
Figure A.1: Particle size distribution for 4 sand combinations.

Analytical Model of Fibre Pullout

B.1 Introduction

A pullout-slip response model has been derived by Sueki et al. [2007] in order to model pullout behaviour for several different artificial fibres in two different mix designs.

In chapter 5 it was shown that the pullout behaviour of the natural fibres used in this thesis is comparable with the pullout behaviour of artificial fibres and therefore it was assumed that the analytical model by Sueki et al. can be used as a basis for an analytical model of pullout-slip response of natural fibres in a cement matrix.

B.2 Model

The analytical model assumes that the fibre pullout distinguishes 3 different stages for the behaviour of the fibre-matrix interface, a so-called elastic stage, a non-linear stage and a dynamic stage, see figure B.1: . The behaviour of the fibre and matrix itself is assumed to be fully elastic at all times.
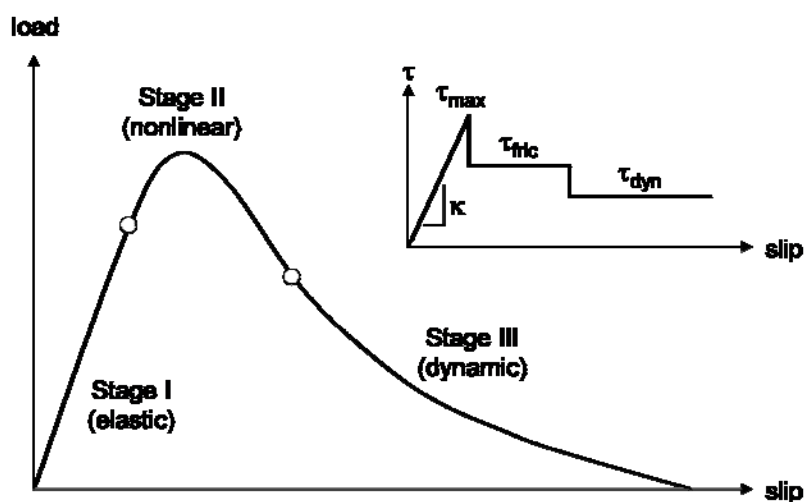

Figure B.1: Pullout-slip response and shear strength diagram.

In the elastic stage the shear stress in the fibre-matrix interface increases, but remains smaller than the fibre-matrix shear resistance τ_{max} and therefore the fibre-matrix interface behaves elastically. The elastic stage ends when the maximum shear stress in the fibre reaches τ_{max}. In the non-linear stage the fibre-matrix interface debonds there where the maximum

shear stress has reached τ_{max}. Due to redistribution of shear stresses the debonding propagates along the fibre until the fibre is completely debonded. This latter situation marks the end of the nonlinear stage. At any moment during the nonlinear stage the fibre has a bonded part and a debonded part. In the debonded part the shear resistance has reduced to τ_{fric}. Finally, in the dynamic part the fibre is completely debonded and will slide out. During sliding the shear resistance will reduce even further to τ_{dyn}. See figure B.2: for shear stress and force distribution in the 3 stages.
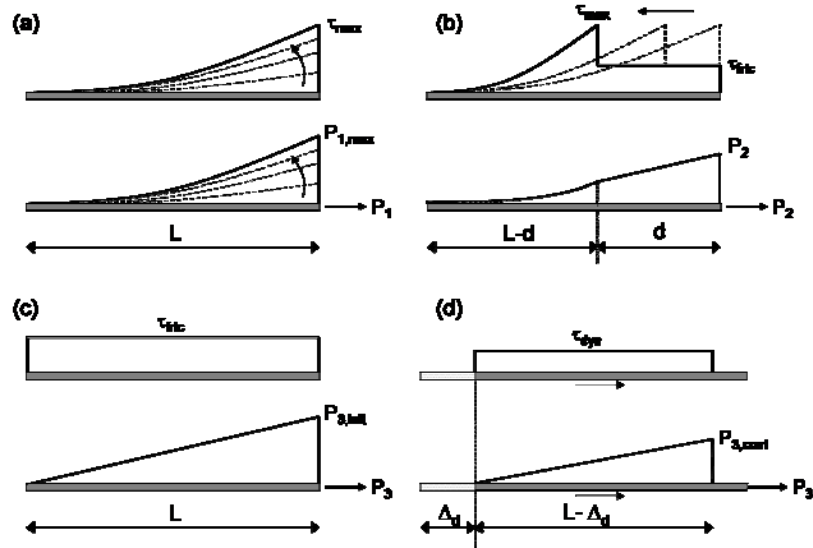

Figure B.2: Shear stress and force distribution along the fibre
(a) elastic stage; (b) nonlinear stage;
(c) beginning of dynamic stage; (d) during dynamic stage.

From the equilibrium between tensile forces in the fibre and matrix through the fibre-matrix interface the axial force and shear stress distributions are derived in Sueki et al. [2007] for the bonded part of the fibre:

$$F(x) = P\frac{\sinh(\beta x)}{\sinh(\beta L)}$$

(B.1)

$$\tau(x) = \frac{P\beta}{\psi}\frac{\cosh(\beta x)}{\cosh(\beta L)}$$

where ψ is the equivalent circumference of the fibre, $\beta^2 = \psi\kappa Q$ and Q is a measure for the combined axial stiffness of fibre and matrix defined as $Q=(1/E_fA_f) + (1/E_mA_m)$.

B.2.1 Elastic stage

In the elastic stage the fibre is still fully bonded and so the distribution of shear stress and tensile force along the complete fibre is described by equation B.1. The slip of the fibre at the

location where the force is applied can be calculated as the sum of the strains in the fibre and matrix, integrated over the length of the fibre, see equation B.2.

$$S(L)_1 = \int_0^L (\varepsilon_f + \varepsilon_m)\, dx = \int_0^L \left(\frac{F(x)}{E_f A_f} + \frac{F(x)}{E_m A_m} \right) dx = \frac{P_1 Q}{\beta \sinh(\beta L)} \left(\cosh(\beta L) - 1 \right) \qquad \text{(B.2)}$$

At the end of the elastic stage the shear stress in the fibre reaches the maximum value τ_{max} for a maximum bonded load equal to:

$$P_{1b,max} = \frac{\tau_{max} \psi}{\beta} \tanh(\beta L) \qquad \text{(B.3)}$$

B.2.2 Nonlinear stage

In the nonlinear stage the fibre changes gradually from fully bonded to fully debonded. The stage ends when the fibre is just fully debonded. At any stage of debonding where the length of the debonded part is d and the remaining part of the fibre $L\text{-}d$ is still bonded the slip of the fibre can be determined by integrating the strains over the length of the fibre, similar to the elastic stage, taking into account separately the bonded and debonded part.

$$
\begin{aligned}
S(L)_2 \quad &= \int_0^{L-d} (\varepsilon_{f,b} + \varepsilon_{m,b})\, dx + \int_{L-d}^{L} (\varepsilon_{f,d} + \varepsilon_{m,d})\, dx \\
&= \int_0^{L-d} \left(\frac{F_b(x)}{E_f A_f} + \frac{F_b(x)}{E_m A_m} \right) dx + \int_{L-d}^{L} \left(\frac{F_d(x)}{E_f A_f} + \frac{F_d(x)}{E_m A_m} \right) dx \\
&= \frac{Q \cdot P_{2b,max}}{\beta} \frac{\left[\cosh(\beta(L-d)) - 1 \right]}{\sinh(\beta(L-d))} + \frac{1}{2} Q d \cdot (\psi \tau_{fric} d + P_{2b,max})
\end{aligned}
$$

During the debonding stage with the increase of debonded length from zero to the full length of the fibre, the pullout force will first increase and after reaching a maximum decrease again until the end of stage II. At the end of the nonlinear stage the fibre is fully debonded but not sliding out yet. In this situation the maximum possible slip that can occur is when the friction along the fibre is zero but the tip of the fibre can transfer all pullout force P to the matrix along the last infinitesimal small part that is still bonded. In this case the fibre is simply stretched up linearly and the slip will be

$$S(L)_{2,max} = \frac{P}{E_f A_f} L$$

In following sections this maximum slip will be referred to as the full elastic slip.

B.3   Model fitting on pullout results

Figure B.3 shows typical result for a pullout test on a spruce, pine and larch fibres. In figure A.4 the same results are shown, but now more zoomed in on the first part of the test. In this figure additional lines are drawn that are the full elastic slip as explained in the previous section. This fill elastic slip is the maximum slip that can occur at the end of stage II according to the analytical model. Though the exact amount of slip at the end of stage II depends on many factors stage II does not end until at least the highest pullout force has been reached. This can be concluded as in the dynamic phase, when the fibre slides out, the pullout force will only decrease according to the analytical model.
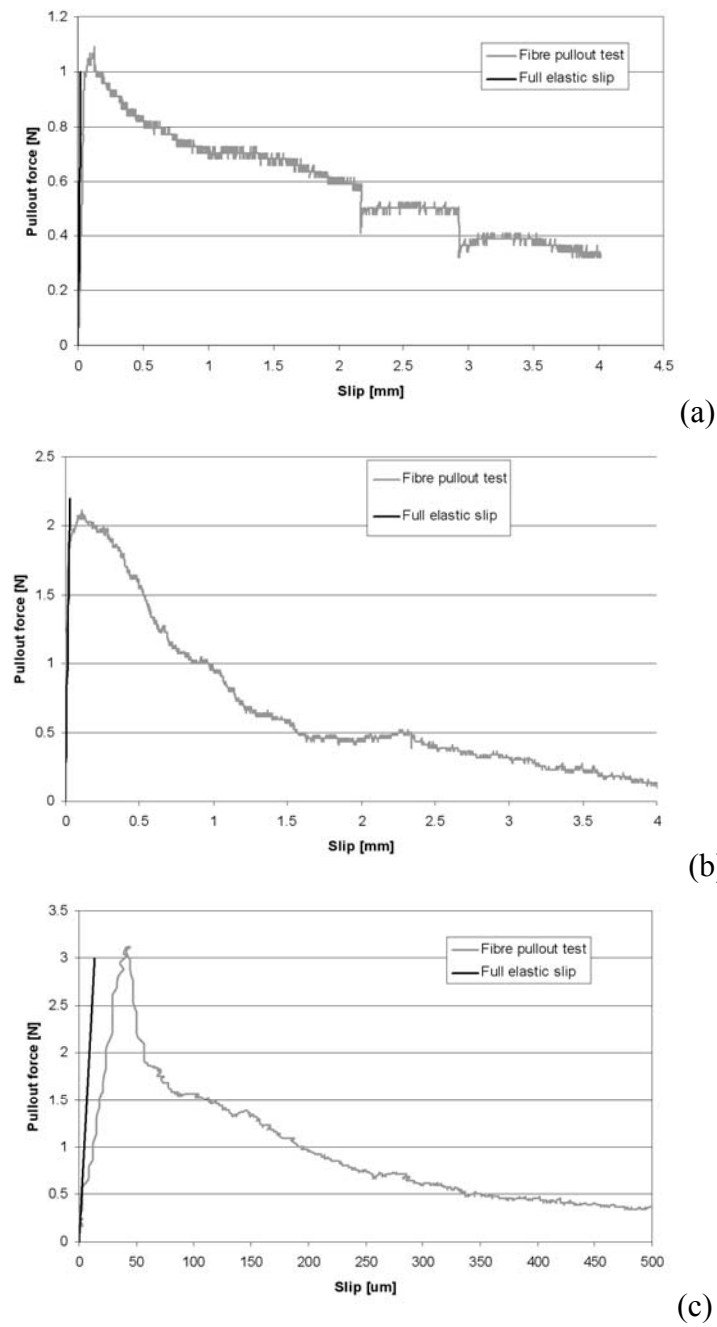

(a)

(b)

(c)

Figure B.3: Typical fibre pullout test results for spruce (a), pine (b) and larch (c).

As can be seen from figure B.4 the slip measured in the pullout test at the highest force is far higher than the free fibre slip for the all three types of fibres. This can only mean that the fibre is already sliding out. This violates the basics of the analytical model according to Sueki et al. [2007] as in this model sliding does not occur until stage III. Therefore the model proposed by Sueki et al. [2007] cannot be applied to pullout of the pine, spruce and larch fibres investigated in this thesis.
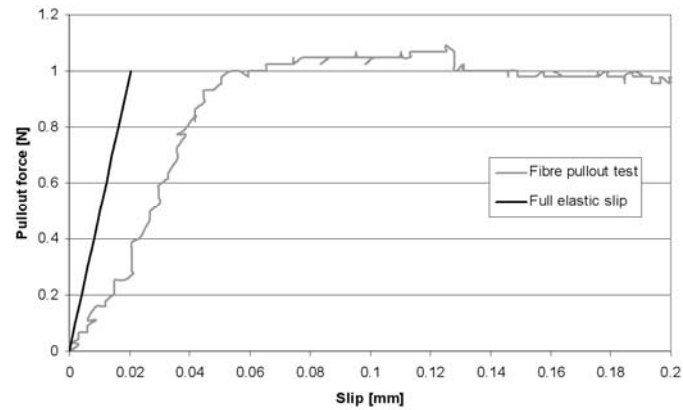
(a)
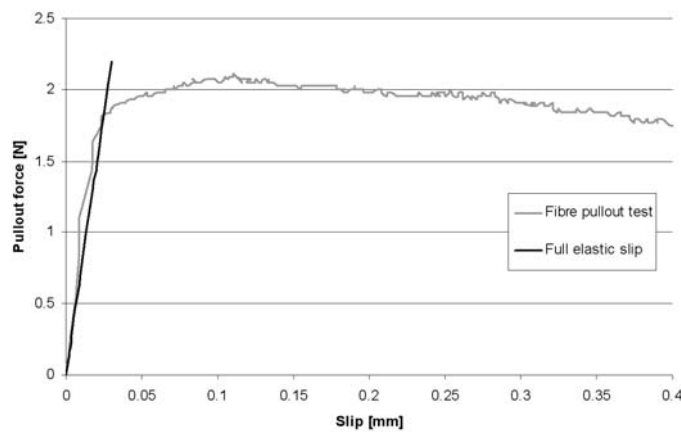
(b)
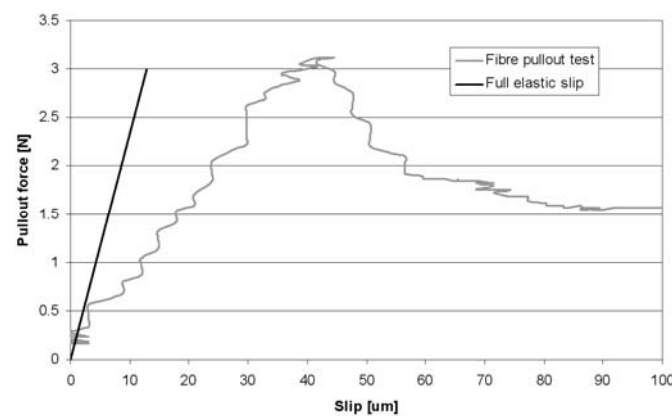
(c)

Figure B.4: Typical fibre pullout test results for spruce (a), pine (b) and larch (c) in the first stages of the pullout test.

Numerical Model of Fibre Pullout

C.1   Introduction

In Appendix A a mathematical model was described that assumes pullout behaviour consists of 3 phases, an elastic phase, a debonding phase and a slip phase with constant maximum shear stress. It was also shown that this three-phase model could not explain some of the features of the pullout curves obtained from laboratory tests, and so an alternative two-phase model was proposed consisting of a rapid debonding phase followed by a slip phase in which the maximum shear stress decreases with increasing slip.

In order to see if the pullout curves obtained from the laboratory tests can result from the proposed two-phase behaviour a numerical model was made using the finite element software Plaxis. Though Plaxis is in principle for geotechnical application it offers enough possibilities to model fibre pullout.

C.2   Model

Pullout was performed on fibres embedded in concrete cubes of $10\times10\times10$mm. Considering the nature of the test it was decided that the pullout can be modelled using a 2D axisymmetric model taking into account that an axisymmetric model assumes a round cross sectional area for both matrix and fibre, while in reality the cross section of the matrix is square and the cross section of the fibre is rectangular.

For the matrix the radius of the cylinder in the axisymmetric model is chosen such that the cross sectional area used in the model is equal to the cross sectional area in the laboratory test. For the fibre, however, the radius in the axisymmetric model is chosen such that the circumference of the fibre in the model equals the circumference of the real fibre, as the model should have the same surface area for slip as the real fibre.

The test will be simulated as displacement controlled test. To do so, Plaxis offers the possibility to define a prescribed displacement at the head of the fibre. The change of displacement at the head of the fibre will be set after which the program calculates the necessary force to reach this displacement.

C.2.1   Material properties

Material properties of the matrix, fibre and fibre-matrix interface are taken from a representative pullout test performed in the laboratory. The matrix will be modelled as linear

elastic with a modulus of elasticity E = 21 GPa and a Poisson's ratio $\nu = 0.2$. The influence of the weight of the matrix is considered negligible; hence no weight is taken into account.

The fibre is also modelled as linear elastic with a modulus of elasticity E = 4.5 GPa and a Poisson's ratio $\nu = 0$.

The fibre-matrix interface is considered to be linear elastic-perfectly plastic, hence it will behave linear elastic until some strength criterion is reached from where the fibre-matrix interface will behave perfectly plastic. In order to do so, Plaxis offers the Mohr-Coulomb constitutive model for which the strength criterion, when using it in an interface, is defined as:

$$\tau_{max} = c + \sigma_n \tan(\varphi) \tag{C.1}$$

As this model is meant to model soil, in this equation c represents the cohesion of the soil, φ is the angle of internal friction and σ_n is the normal stress acting on the fibre-matrix interface. As the normal stress acting on the fibre-matrix interface is not assumed to change significantly during the pullout test it is chosen to discard this effect completely by selecting $\varphi = 0$ so the maximum friction in the fibre-matrix interface found in laboratory tests can be entered directly into the model as "cohesion". The modulus of elasticity of the fibre-matrix interface is unknown, but will be determined when calibrating the numerical model with the pullout results from laboratory tests.
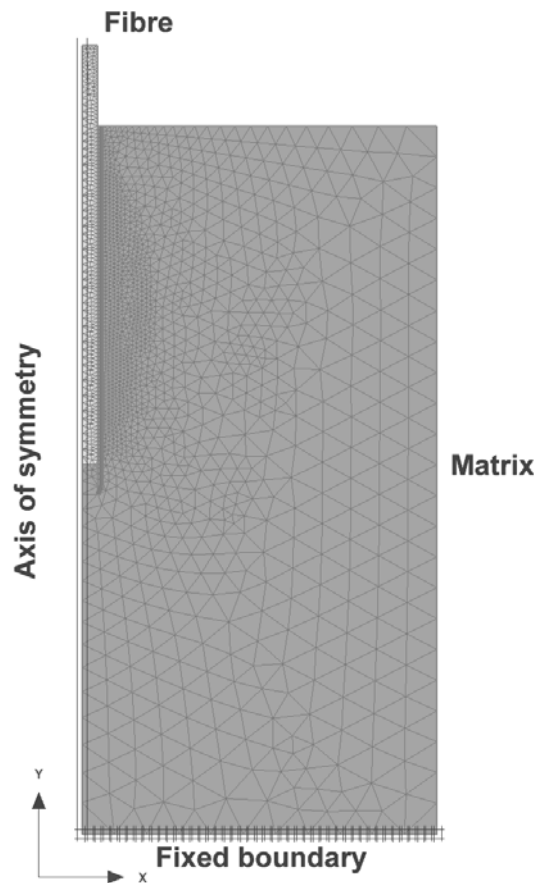

Figure C.1: Finite element mesh for simulating fibre pullout.

C.2.2 Mesh

Plaxis only offers isoparametric triangular elements of either 2nd order or 4th order. To obtain the best accuracy 4th order elements have been chosen, and additionally the mesh elements have been made very small close to the fibre. This leads to the mesh as shown in figure C.1.

C.3   Simulation procedure

C.3.1   Simulation of pullout

Beforehand the assumption was made that the resistance of the fibre-matrix interface is fully mobilized before the fibre dynamically pulls out, while during dynamic pullout the quality of the fibre-matrix interface deteriorates leading to a reduction of its resistance. This implies that the maximum force during the complete pullout process is reached when resistance of the fibre-matrix interface is just completely mobilized and before the dynamic pullout starts.

From the laboratory tests it is known at what level of pullout slip the maximum force is reached, and those data are used to calibrate the model. Initially the stiffness of the fibre-matrix interface is assumed to be equal to the stiffness of the fibre, after which the stiffness of the fibre-matrix interface is decreased to calibrate the slip at maximum pullout force. It appears that the stiffness of the fibre-matrix interface has to be E = 1.5 MPa in order to obtain the correct pullout slip at the maximum pullout force.

After this, the fibre is pulled out further while the maximum shear resistance of the fibre-matrix interface is reduced to 90%, 80% etc. until a residual shear resistance is reached. As it is not possible in Plaxis to make the maximum shear resistance automatically dependent on the slip, the shear resistance had to be manually changed every time after a certain amount of slip. The amount of slip at the moment that the maximum shear resistance changes is taken from the laboratory test results. Figure C.2 shows the results of the original pullout test as well as the results from the numerical simulation.
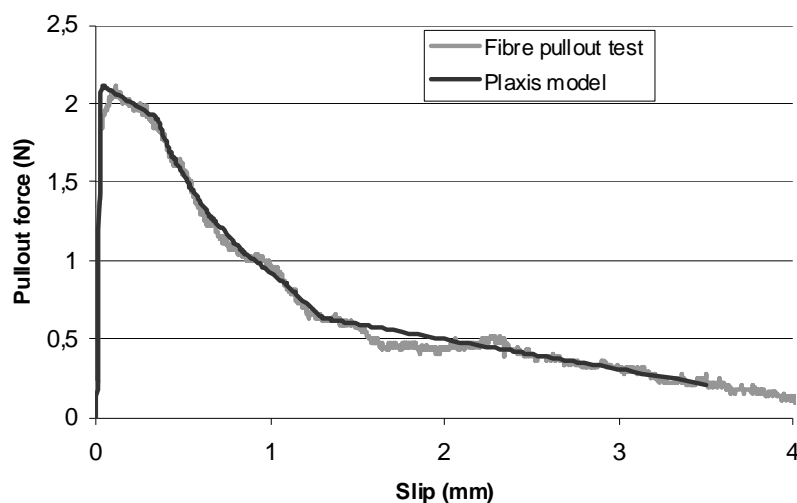

Figure C.2: Results of the numerical model and the laboratory pullout test.

C.3.2 Influence of boundary conditions

The original mathematical model fixed the matrix at the front so that during the test the plane where the fibre was pulled out has zero displacement while the matrix is under compression. However, the test setup used in Microlab fixes the rear of the matrix, leading some deformation of the matrix directly next to the fibre at the plane where the fibre is pulled out while the matrix will be under tension. Though it was assumed that the influence of this difference in boundary condition is small due to the high stiffness of the matrix compared to the stiffness of the fibre and fibre-matrix interface, in the numerical model described above the same pullout test has been performed with both boundary conditions to confirm this.

As can be seen from figure C.3 the influence of the boundary conditions is indeed very small as the pullout curves of both the Microlab setup and the setup according to the mathematical model coincide. Closer investigation learns that the deformation of the matrix close to the fibre in the setup as used in Microlab is about 3 μm.
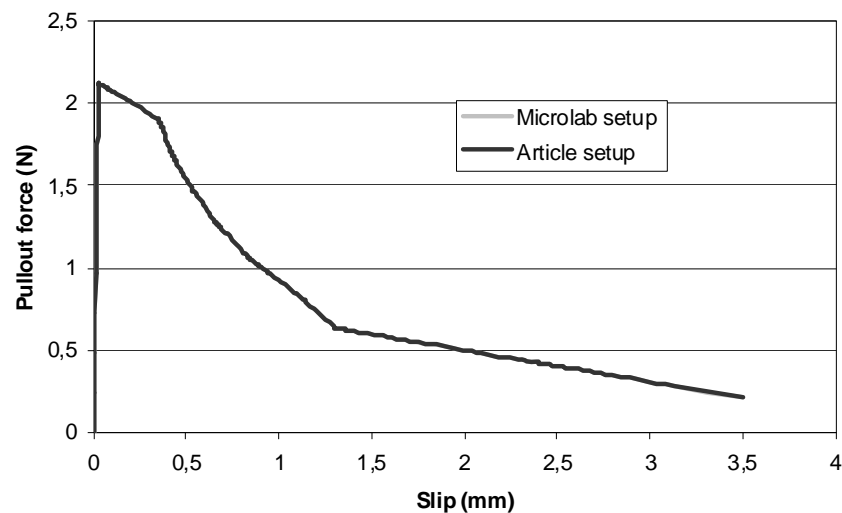
Figure C.3: Influence of the boundary conditions on the pullout results of the numerical model.

Curriculum Vitae

Name: Mercedes Guadalupe Sierra Beltrán

Date of Birth: 19 August 1973

Place of Birth: Mexico City, Mexico

Email: m.g.sierrabeltran@tudelft.nl

2011 -	Post-Doc Researcher, Delft University of Technology, Faculty of CiTG, Microlab, Delft, The Netherlands.
2006 - 2010	PhD researcher, Delft University of Technology, Faculty of CiTG, Microlab, Delft, The Netherlands.
2002 - 2006	Structural Project Manager, Stark+Ortiz S.C., Mexico City, Mexico.
1999 - 2002	Master of Science (MSc.) in Civil Engineering, National Autonomous University of Mexico, UNAM, Mexico City, Mexico.
1996 - 1999	Structural Engineer, Sinecuanon Co., Guayaquil, Ecuador.
1992 - 1997	BSc. Degree in Civil Engineering, Catholic University of Santiago de Guayaquil, Guayaquil, Ecuador.

Publications

Sierra Beltran, M.G. (2010), Wood fibres as reinforcement in a low environmental-impact cementitious material, *Proc. of the 6th International Conference on Concrete under Severe Conditions*, Merida, Mexico, pp. 1037-1044.

Sierra Beltran, M.G. (2010), Fibre-matrix interface properties in a wood fibre reinforced cement matrix, *Proc. of the 7th International Conference on Fracture Mechanics of Concrete and Concrete Structures*, Jeju, Korea, pp. 1425-1430.

Garcia, A, Schlangen, E, van de Ven, M, and **Sierra-Beltran, G.**, (2010), Preparation of capsules containing rejuvenators for their use in asphalt concrete, *Journal of Hazardous Materials* 184(1-3): 603-611.

Zhou, J. , Qian, S. , **Sierra-Beltran, M.G**. , Ye, G. , Van Breugel, K. and Li, V.C. (2010), Development of engineered cementitious composites with limestone powder and blast furnace slag, *Materials and Structures* 43(6) 803-814.

Sierra Beltrán, M.G. and Schlangen, E. (2009), Desarrollo de materiales cementicios dúctiles con fibras de Madera, *Revista Cemento Hormigón* 934: 4-13 (In Spanish).

Sierra Beltran, M.G. and Schlangen, E. (2009), Interface bond characteristics between wood fibres and a cement matrix, *Proc. Of the 9th International Symposium of Brittle Matrix Composites*, Warsaw, Poland, pp. 43-51.

Schlangen, E., Qian, Z., **Sierra-Beltran, M.G**. and Zhou, J. (2009), Simulation of fracture in fibre cement based materials with a micro-mechanical lattice model, in *Proceedings of the 12th International Conference on Fracture*, Ottawa, Canada, pp. 1-10.

E. Schlangen, H. Prabowo, M.G. **Sierra-Beltran M.G.**, and Z. Qian (2009), A model for building a design tool for ductile fibre reinforced materials, *Proc. Advanced Concrete Materials*, Stellenbosch, South Africa, pp. 307-312.

Sierra Beltran, M.G. and Schlangen, E. (2008), Wood fibre reinforced cement matrix: A micromechanical based approach, *Key Engineering Materials*, 385-387 445-448.

Sierra Beltran, M.G. and Schlangen, E. (2008), Development of ductile cementitious materials with wood fibres, *Proc. of the 11th International Inorganic-Bonded fiber Composites Conference*, Madrid, Spain, pp.11-18.

Sierra Beltran, M.G. and Schlangen, E. (2008), Wood and other natural fibres as reinforcement in cementitious materials, *Proc. of the 7th International RILEM Symposium on Fibre Reinforced Concrete: Design and Applications*, Chennai, India, pp.51-61.

Zhou, J., Qian, S., **Sierra Beltran, M.G.**, Ye, G., and van Breugel, K., Engineered Cementitious Composite with Blast furnace slag and limestone powder, in *Proceedings of the Workshop on the 50-year Teaching and Research Anniversary of Prof. Sun Wei*, 2008. Nanjing, China.

Acknowledgements

Working on this PhD project has been a great pleasure. Not only because I had the unique opportunity to develop my own idea: to design a ductile material for poor countries with earthquakes, but also because during this journey I met amazing people, I learned about concrete and fibres and I learned about myself, I changed my country of residence, I got married and I am learning a new language. As much as it is true that a PhD is a lonely job, during the past five years I was never alone, not in my work, nor after work. Many people contributed to my project in sometimes completely different ways, and I am sincerely grateful to all of them. At these final pages of my thesis, I would like to mention some of them in particular.

I thank Professor Klaas van Breugel for the trust in my project that he expressed from the first day until the end. Even on days where I truly believed I wouldn't obtain any stable laboratory results he stayed confident I would sort it out.

I express my gratitude to my advisor, Erik Schlangen, who pointed out in which direction to go in moments I wanted to solve more problems than can reasonably be done in a single PhD research. I admire his confident and relax way of handling situations. I am thankful for all his advice and for his invaluable help in setting up some of the laboratory equipment.

I am grateful with the committee members that gave me their trust, allowing me to defend my thesis, and for their numerous improvements to this dissertation.

I thank Professor Victor C. Li from the University of Michigan at Ann Arbor, for allowing me to work in his group and using the laboratory equipment.

To Professor Gideon van Zijl from Stellenbosch University for his warm welcome in South Africa and his help on the analytical model for fibre pullout, my gratitude.

I acknowledge Drs. Wolfgang Gard, who guided me to the wood world, and made it a very interesting world to explore.

To the Microlab technicians: Gerard Timmers, Jon van der Weg, Gerrit Nagtegaal and Arjan Thijssen, for sharing with me their practical experience and keep giving me brilliant solutions for my laboratory problems. And a special word for Arjan, who also helped me with practicing my Dutch.

To all the Microlab colleagues, thank you for some memorable lunch and coffee break chats. You made Microlab a very nice place to work!

Special thanks to Sonja Scher, Alvaro Garcia Hernandez, Jon Einarsson, Virginie Wiktor and Ying Wang, dear friends and colleagues, for all their help in the lab or discussing about my project. And a special word for Ayda Agar Ozbek, who shared with me the ups and downs of research while keep inspiring me to do research in the best way possible.

I am grateful with Henk Jonkers, who at the end of last year invited me to join him and Virginie Wiktor in a challenging and very interesting new subject for me, self-healing with bacteria in concrete. While I slowly grow into the matter of bacteria, I finish writing my thesis. I am very thankful with both of them for their patience and support in all those days when my head was split between wood fibres and bacteria.

To all the friends in USA, Brazil, South Africa, Mexico and Ecuador that have shared their knowledge with me and help me with this research, thank you. My gratitude goes to my non-engineer friends on both sides of the Atlantic, who kept cheering me and showing me how wonderful life is outside the laboratory.

My sincere thanks to my in-laws, who, since I arrived in the Netherlands, made me feel as their daughter.

My love, respect and gratitude go to my parents and my brother, who always believed that I should do a PhD, and keep pushing me towards it. Thank you for your love and faith, that reach me no matter how far away we are.

Finally, a very special recognition to my husband Dennis. It all happened because of you! Thank you for convincing me of doing the PhD in Delft, for helping me out when needed and cheering me up whenever I was overwhelmed with work, and, not important, for your editing work on this thesis report.

I was born and raised in ever-green countries, but I lived most of my life there in cities, far away from the ever-green nature. Working in this project help me understand the impact that our human activity puts on the environment. That, together with my husband endless love for outdoors, has made me appreciate nature beyond words. I am grateful for that.